2022

Endoplasmic Reticulum membranes are continuously required to maintain mitotic spindle size and forces

Margarida Maria Mimoso Reis Araújo

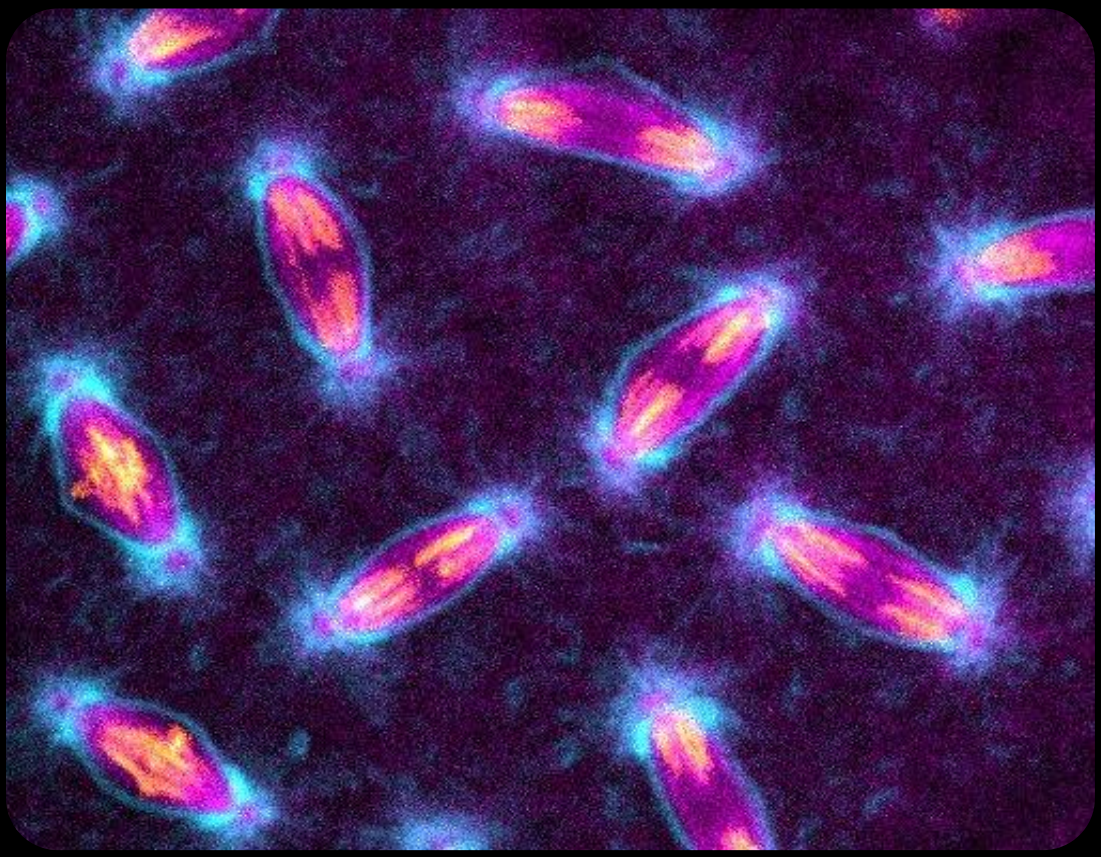

Dissertation presented to obtain the **Ph.D degree in**

Integrative Biology and Biomedicine

Oeiras, November, 2022

INSTITUTO DE TECNOLOGIA QUÍMICA E BIOLÓGICA ANTÓNIO XAVIER | UNIVERSIDADE NOVA DE LISBOA

Endoplasmic Reticulum membranes are continuously required to maintain mitotic spindle size and forces

Margarida Maria Mimoso Reis Araújo

Dissertation presented to obtain the Ph.D degree in Integrative Biology and Biomedicine

Instituto de Tecnologia Química e Biológica António Xavier | Universidade Nova de Lisboa

Research work coordinated by: INSTITUTO GULBENKIAN DE CIÊNCIA

Oeiras, November, 2022

List of publications:

Margarida Araújo, Alexandra Tavares, Diana V. Vieira, Ivo A. Telley, Raquel A. Oliveira, Endoplasmic Reticulum membranes are continuously required to maintain mitotic spindle size and forces (2022) https://doi.org/10.1101/2022.05.14.491942, (preparing re-submission to Life Science Alliance).

Catarina Carmo, **Margarida Araújo**, and Raquel A. Oliveira, Microinjection Techniques in Fly Embryos to Study the Function and Dynamics of SMC Complexes (2019) *Methods in Molecular Biology*, 2004, 252-568.

Declaration: This dissertation is the result of my own research carried out between January 2017 and September 2022 in the laboratories of Dr. Raquel A. Oliveira and Dr Ivo A. Telley, at the Instituto Gulbenkian de Ciência in Oeiras, Portugal, within the PhD Programme in Integrative Biology and Biomedicine (2017 edition).

Declaração: Esta dissertação é o resultado do meu próprio trabalho desenvolvido entre Janeiro de 2017 e Setembro 2022 nos laboratórios da Doutora Raquel A. Oliveira e do Doutor Ivo A. Telley, no Instituto Gulbenkian de Ciência em Oeiras, Portugal, no âmbito do Programa de Doutoramento em Integrative Biomedical Sciences (edição 2017).

Financial support: This dissertation had the financial support from Fundação para a Ciência e a Tecnologia and European Social Found, through grant PD/BD/128431/2017 awarded to Margarida Araújo, and Fundação Calouste Gulbenkian.

Apoio financeiro: Esta dissertação teve o apoio financeiro da Fundação para a Ciência e a Tecnologia e do Fundo Social Europeu no âmbito do Quadro Comunitário de apoio através da bolsa de doutoramento PD/BD/128431/2017 Margarida Araújo e da Fundação Calouste Gulbenkian.

I dedicate this thesis to my niece Isabel

Summary

Dynamic spindle microtubules bind to, align, and move chromosomes to opposite sides of the cell, ensuring that each daughter cell gets precisely one copy of the genetic material at each division round. Mitosis has often been studied in the context of these isolated and alluring events, although changes in other intracellular compartments occur in parallel. In fact, membrane organelle function, localization, and proper partitioning upon cell division depend on interactions with the cytoskeleton. Whether, reciprocally, membrane organelles also impact the function of cytoskeletal elements remains less clear. Therefore, investigating the reorganization and interaction between several intracellular structures during mitosis may elucidate why and how such an incredibly efficient process takes place.

The initial aim of this project was to uncover additional forces acting on mitotic chromosomes besides the ones generated by the microtubule-based spindle. Chapter 2 describes our results in this quest. I found that dispersed sister chromatids unexpectedly move to the center of the nuclear space upon the removal of spindle microtubules. Although I cannot exclude that the kinetics of spindle disassembly could drive clustering of sister chromatids, my results indicated that additional factors could also be involved. These findings prompted me to focus on external organelles and how they may influence the mitotic apparatus. I observed that the ER is highly dynamic during mitosis, and it undergoes deformation after microtubule depolymerization, concomitantly with the clustering of sister chromatids. ER deformation may contribute to the initial stages of chromatid clustering, but its deformation does not accompany centromere clustering the entire time this phenomenon is observed. Nevertheless, I observed a tight association between the ER and the spindle during mitosis that was functionally elusive, which prompted us to study this in more detail.

Chapter 3 describes several tested strategies to induce acute ER membrane disruption. I focused on the ER-shaping protein called Atlastin, known to fuse ER membranes. In my experiments, ectopic addition of the cytoplasmic domain of Atlastin (cytATL) into *Drosophila* embryos arrested at metaphase led to substantial disruption of ER membranes-proximal to spindle poles.

In Chapter 4, I utilized the cytATL protein to investigate the role of ER membranes on mitotic spindle shape and function. Upon cytATL-mediated disruption of the ER, I observed a significant reduction in spindle size and detachment of spindle poles from the spindle body. Yet, spindle microtubule dynamics were unaffected by cytATL-mediated disruption of the ER. These results suggested that ER membranes-proximal to spindle poles are essential to maintain spindle size and architecture. Finally, I investigated whether the changes in spindle morphology due to ER disruption influenced spindle function. I found that although the smaller spindles could pull sister chromatids apart, the separation efficiency was reduced compared to the control condition. Moreover, after mitotic exit, nuclear spacing was affected by cytATL-driven disruption of the ER.
This work unveiled a novel role for ER membranes throughout metaphase, even after unperturbed spindle assembly. Our findings emphasize that the mitotic spindle should not be viewed as an isolated organelle providing a more integrated view of cell division.

Sumário

Os cromossomas são alinhados e segregados para lados opostos da célula através de uma máquina composta por microtúbulos chamada fuso mitótico. Isto garante que cada célula-filha recebe precisamente uma cópia do material genético a cada ronda de divisão. A mitose tem sido estudada frequentemente no contexto destes eventos isolados e cativantes, porém, alterações noutros compartimentos intracelulares ocorrem em paralelo. A função, localização e distribuição adequadas de organelos membranares dependem de interações com o citoesqueleto. Contudo, se estes organelos membranares influenciam a função de elementos do citoesqueleto reciprocamente ainda é incerto. A investigação da reorganização e interação entre as várias estruturas intracelulares durante a mitose pode elucidar como e porque é que este processo é incrivelmente eficiente e sincronizado.

O objetivo inicial deste projeto era descobrir que outras forças atuam nos cromossomas mitóticos para além daquelas geradas pelos microtúbulos do fuso. O Chapter 2 descreve os nossos resultados a esta pergunta. Descobrimos que cromatídeos-irmãos dispersos se movem inesperadamente para o centro do espaço nuclear após a remoção dos microtúbulos do fuso. Apesar de não podermos excluir que a aglomeração dos cromatídeos-irmãos pode ser causada pela cinética de desagregação do fuso, os nossos resultados indicam que outros fatores adicionais possam estar envolvidos. Estas descobertas direcionaram o nosso foco para organelos externos e como estes podem influenciar o aparelho mitótico. Descobrimos que o Retículo Endoplasmático (RE) é muito dinâmico durante a mitose e que, simultaneamente com a aglomeração dos cromatídeos-irmãos, o RE sofre uma deformação após a despolimerização dos microtúbulos. A deformação do RE pode contribuir para a aglomeração dos cromatídeos-irmãos numa fase inicial, mas parece não acompanhar a aglomeração durante todo o tempo que

este fenómeno é observado. No entanto, a associação próxima entre o RE e o fuso mitótico que observei encontrava-se inexplorada ao nível funcional até então, o que me levou a querer explorá-la em maior detalhe.

O Chapter 3 descreve as diferentes estratégias que testámos para induzir uma perturbação imediata nas membranas do RE. Neste contexto, foquei-me na proteína Atlastin, cuja função é a fusão de membranas do RE. Ao adicionar ectopicamente o domínio citoplasmático da Atlastin (citATL) a embriões de *Drosophila* em metafase, induzimos uma forte perturbação nas membranas do RE que rodeiam os polos do fuso.

No Chapter 4, utilizei a citATL para investigar o papel das membranas do RE na morfologia e função do fuso mitótico. A perturbação no RE mediada pela citATL levou a uma redução significativa do tamanho do fuso, assim como a separação dos polos do fuso. Porém, a dinâmica dos microtúbulos do fuso manteve-se inalterada sob a perturbação mediada pela citATL. Estes resultados sugeriram que as membranas do RE próximas dos polos do fuso são importantes para manter o tamanho do fuso e a sua arquitetura. Finalmente, averiguei se as alterações na morfologia do fuso influenciavam a sua função. Verifiquei que os fusos mais pequenos mantêm a capacidade de segregar os cromatídeos-irmãos, mas com uma eficiência menor em comparação com a condição controlo. Além disso, descobri que o espaçamento entre os núcleos fica afetado ao induzir a saída da mitose sob o efeito da citATL.
Este trabalho revelou um novo papel das membranas do RE durante a metafase, mesmo quando a formação do fuso mitótico não é perturbada. As nossas descobertas realçam a função das membranas do RE na arquitetura do fuso proporcionando uma perspetiva mais integrada do processo de divisão celular.

Acknowledgements

I started my scientific life at IGC and got the opportunity to work and learn with amazing people. Ever since my Master's, I worked here, jumping around from lab to lab, and I will take a lot of good memories with me.

This Ph.D. would not be possible without so many people with whom I discussed my work and life along this very long way.

First, I want to thank Raquel and Ivo, for accepting me in their labs after many meetings and for all their patience during the writing of this thesis. Thank you for your support when I needed the most and when I was filled with doubt.

I really need to thank all the past and present members of the CHR lab. To Sara, Mihailo, Ewa, Gaston, João, Abha, Catarina Carmo, Xana, Inês, Ana, Salma, Laura, Catarina Pedro, Carolina, Paola, Mia, thank you. I learned a lot with all of you every day in the lab, during beer hours, flipping stocks in the fly room, during dinners, and so on. I'm glad I had the opportunity to meet you all.

To all the past and present members of the PND lab, Catarina Nabais, Jorge, Diana, Ojas, Ana, Amid, Gustavo, and Leonor, for all the discussions, help with experiments, and advice.

To all the friends from IGC that are also my peers, Catarina Nunes, Filipe Vieira, André Barros, Marília Pereira, and Nuno Santos, I hope we keep in touch and wish you all the success in your endeavors!

To my classmates from IBB 2017, it was so nice to share this journey with you and I'm proud of all of you.

To all the ladies from Sofia's team at the canteen, Sandra, Margarida, Rute, Ana (and the ones backstage), who during lunch time always smiled and made my days easier.

To all the facilities at the IGC, especially to the motivated people that make things work around here: Liliana, Sandra, and Raquel that

always took care of my orders and last-minute requests; to the imaging facility, past and present members – Gaby, Nuno Pimpão, Zé, Patrícia, Mariana, Alexandre – who always helped with my apparent curse when using microscopes.

Above all people, I want to thank my boyfriend Gonçalo, that supported me and believed more in me as a scientist than I did. You were always there (even if far away at times) to comfort me in the good and bad moments during the last 6 years of my life. You make me want to be not only a better scientist but also a better person every day, thank you for that. Without you, this big experiment would have been much more difficult.

To my best friends Joana, Maria, Teresa, and Vera for always supporting me. We have a long-lasting friendship (25 years and counting) and I feel I can always count on you.

To my entire family, especially to my mom, dad, and sister. Mãe, pai e mana, even without understanding exactly what I do, you always supported me and celebrated all my achievements. To my sister Joana, for being one of my role models and the person I look up to ever since I was a kid. You taught me to always go after what I want and to not look back. And, of course, thank you for giving me the best thing in the world, my niece Isabel! Being her godmother is a big responsibility and watching her grow is an incredible and wonderful experience. I hope I can influence her and empower her in one way or another.

To my dear grandparents, avó Manelinha and avô Raúl, which also raised me and whom I love so much. I will never forget all my birthday parties in your garden and will carry them as the happiest memories of my childhood. To my grandma Manelinha, the biggest example of strength, kindness, and generosity I have.

Finally, to my dog Darwin. A fierce water lover and the best beach companion that I will always take with me. Tenho muitas saudades.

Table of Contents

Chapter 1

General Introduction

1.1. The cell cycle

Cell cycle regulation and what keeps it going forward

The cell cycle is essential for life, as it is a conserved process that allows for genome duplication and its equal distribution into two identical daughter cells. This ensures that the genetic information is faithfully propagated from one generation to the next.

Broadly, the cell cycle can be divided into interphase and mitosis. Interestingly, and certainly not by chance, the cell spends most part of the cycle preparing to divide. Transitions between these phases are under the regulation of the usual suspects – Cyclins and Cyclin-dependent kinases (CDKs). CDKs, only activated upon Cyclin binding, are serine/threonine protein kinases that promote phosphorylation of crucial substrates to uphold DNA synthesis and progression into mitosis (Malumbres 2014). In eukaryotic cells, division starts with activation of CDK1 (Nasa et al. 2018). Other kinases including Aurora A, Aurora B and Polo-like kinase 1 (PLK1), facilitate entry and progression through the cell cycle (Figure 1.1.) (H. T. Ma and Poon 2011; Nasa et al. 2018). Degradation (proteolysis) of cell cycle proteins guarantees that the cycle is unidirectional. When cells terminate division, now phosphatase activity becomes predominant allowing cells to transition to interphase (Nasa et al. 2018; Huguet, Flynn, and Vagnarelli 2019).

In depth, there are four distinct phases of the cell cycle: G0/G1, S, G2 and M (Suryadinata, Sadowski, and Sarcevic 2010). In G1 phase, the cell grows, prepares everything necessary for the duplication of the genome, and upregulates transcription and translation necessary for subsequent stages. Then, after passing the G1-S checkpoint where cell size is controlled, the DNA undergoes replication in S phase. With two identical copies of the genome, now the cell transitions to G2 phase, where it also grows and resumes metabolic activity. At the end of G2, the cell passes

the G2-M checkpoint prior to entry into mitosis, upon the dispute between Cyclin B-Cdk1 activation and its inhibitors. Once the cell is committed to enter the mitotic phase, it cannot go back. During mitosis, the cell follows a succession of stages that culminate in the symmetric division of the genetic material, cytoplasmic components, and organelles into two daughter cells. Each of these newly formed cells will then undergo their own cell cycle progression.

1.2. Mitosis: an extraordinary orchestra

Mitosis has been studied for more than a century. Even before Walter Sutton's and Theodor Boveri's first hand-drawn sketches of meiotic divisions came about, Alexander Flemming had already been interested in chromosome movements during animal cell division in 1882. This intriguingly choreographed process keeps mesmerizing all cell biologists to this date, including me (nearly every time I watch it). Each eukaryotic cell resembles a fine symphony orchestra, where every instrument has its own role. Mitosis can take up to one hour in most metazoans while in other systems, such as in insects, embryonic syncytial divisions can be as fast as few minutes. Regardless of this variability in timing amongst different organisms, all of them have in common significant changes in cell organization occurring at mitotic entry.

Mitosis is impressively robust, but it is not fail-safe. When errors in the choreography of this process occur, this can lead to aneuploidy – gain or loss of chromosomes – or instability of the genome. Consequently, aneuploidy can be either eliminated by cell death, or in the worst-case scenario, promote disease.

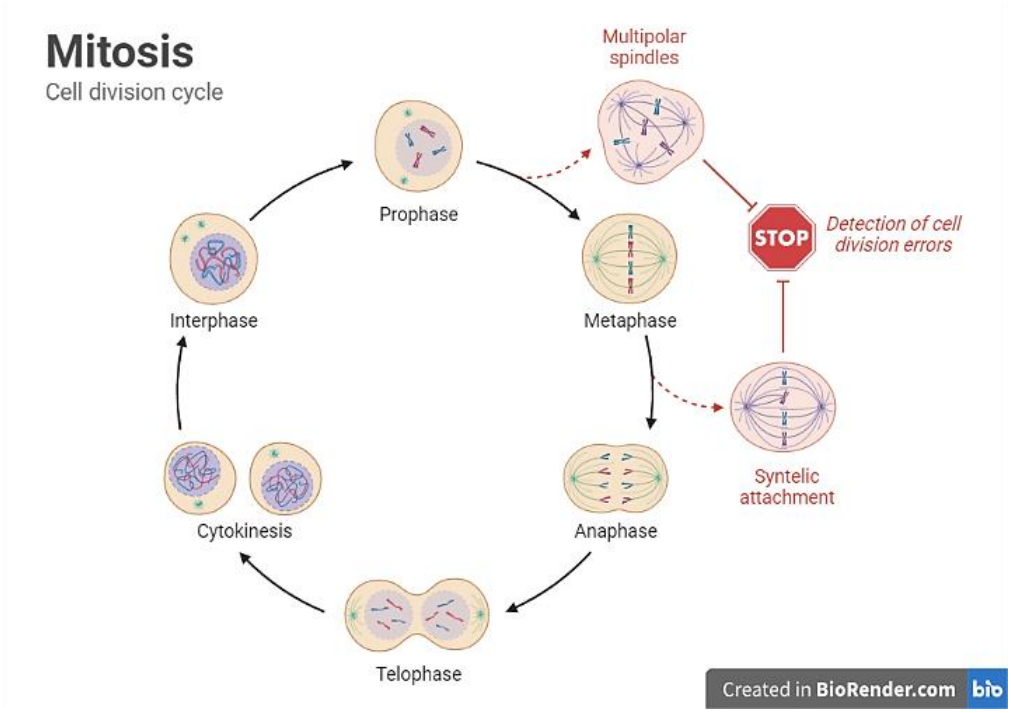

Figure 1.1. The cell division cycle. *Scheme depicting the main stages of mitosis. Retrieved from BioRender.com.*

Mitosis consists of different phases, which can be monitored by readily visible changes in chromatin and cytoskeletal morphology (Fig. 1.1.). Surveillance mechanisms, or checkpoints, control the entry into mitosis and its proper termination. Checkpoints will halt the progression of the cell cycle when spindle defects or DNA damage are detected (Nigg 2001). During prophase, the nuclear membrane enclosing the DNA falls apart – an event called nuclear envelope breakdown (NEBD) – and the entangled DNA is compacted and resolved into individual chromosomes. Even though chromatin architecture and condensation are still not completely understood, the main players involved have been quite well characterized: cohesin and condensin. While cohesin holds the two identical DNA molecules together after replication (Nasmyth and Haering 2009; Peters and Nishiyama 2012; Mirkovic et al. 2015), condensin mediates the structural reorganization of the DNA into resolved chromosomal units (Oliveira, Coelho, and Sunkel 2005; Hirano 2006; Piskadlo and Oliveira 2016). During metaphase, the duplicated centrosomes nucleate

microtubules (MTs) to form the bipolar spindle (see section 1.4.), emerging into the nuclear space to capture chromosomes. This facilitates chromosome congression into the cell equator, where they become aligned and form the so-called metaphase plate (reviewed in Maiato et al. 2017). At the end of metaphase, the cell encounters another quality control: only when all chromosomes are bi-oriented (attached to microtubules from both spindle poles) and are under tension (Musacchio and Desai 2017) chromosomes are symmetrically separated and the spindle disassembles. This depends on the Spindle Assembly Checkpoint (SAC), a safeguard mechanism which arrests metaphase preventing chromosome segregation defects (Khodjakov and Pines 2010). Once the cell establishes correct MT attachments, the mechanical basis for pulling force on each sister chromatid, the metaphase-to-anaphase transition takes place. At anaphase, cohesin is cleaved, and sister chromatids are separated towards the poles by the spindle (Uhlmann et al. 2000; Hauf, Waizenegger, and Peters 2001). Cyclin B-Cdk1 activity decreases, and during telophase the nuclear envelope reforms as to enclose the two identical daughter nuclei. Lastly, cytokinesis takes place, where the characteristic abscission of the newly formed daughter cells is triggered (Mierzwa and Gerlich 2014).

1.3. The microtubule cytoskeleton

Eukaryotic cells depend on the cytoskeleton not only to control their shape and motility but also for cell division. The microtubule (MT) cytoskeleton plays numerous roles and is essential for normal cell function. MTs are dynamic polymers formed by α- and β-tubulin and can grow up to the entire length of the cell (Desai and Mitchison 1997; Brouhard and Rice 2018). Due to their length and dynamic nature, MTs work as “tracks” inside cells enabling directed intra-cellular transport (Desai and Mitchison 1997), contacts with many organelles, and interaction with other cytoskeletal elements (Gudimchuk and McIntosh 2021). It is not surprising

that when we look at cells stained for tubulin under the microscope, we see an intricate network. The organization of MTs from head to tail makes them polar, which means that their two ends are distinct. This feature is crucial for many MT functions because it confers directionality, for example to the movement of motor-driven transport of vesicles and organelles. Structural polarity is also the basis for different kinetics of tubulin addition and loss at the two MT ends.

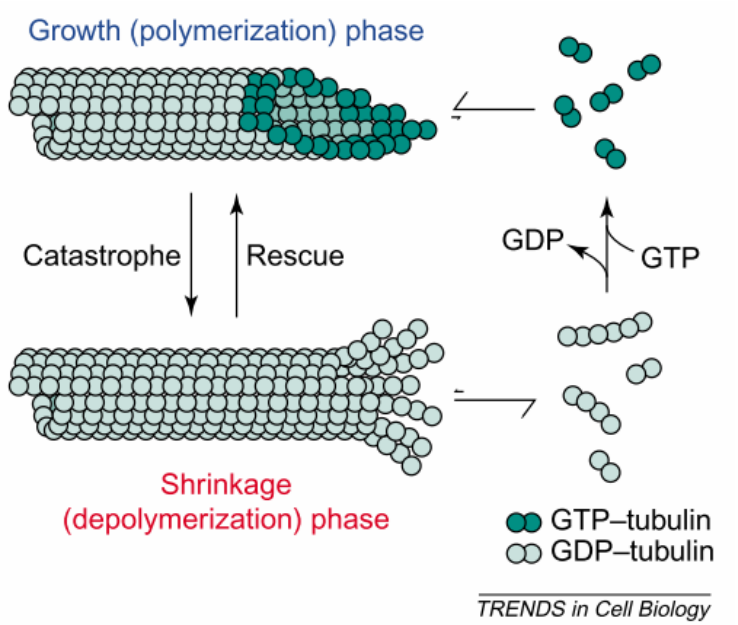

Figure 1.2. Dynamic instability of MTs. *The MT polymer undergoes cycles of growth (polymerization) by addition of GTP-tubulin dimers and shortening (depolymerization/catastrophe). Adapted from (Kinoshita, Habermann, and Hyman 2002).*

We know that MTs grow faster from their “plus-end” by the addition of GTP-tubulin dimers and forming a stabilizing cap (Figure 1.2., top) (Kinoshita, Habermann, and Hyman 2002). Tubulin dimers are in the GDP-bound state behind this cap due to the GTPase activity of tubulin (Carlier and Pantaloni 1981). End-binding (EB) proteins recognize the cap – more precisely the nucleotide state of tubulin (Maurer et al. 2012). MT “minus-ends” are anchored at the centrosome or MT organizing center

(MTOC) (Kinoshita, Habermann, and Hyman 2002). This results in the stochasticity of growing and shrinkage of MTs, a concept known as dynamic instability (Desai and Mitchison 1997). A plethora of other MT-associated proteins (MAPs) bind to the MT minus-end, namely kinesins, MT polymerases, and MT depolymerases favoring either growth or shrinkage. This can be used by cells to exert forces e.g., on chromosomes and promote their segregation.

1.4. The bipolar spindle: a highly complex molecular machine

Throughout the tree of life, nature has evolved similar cellular machines that operate robustly to segregate chromosomes accurately into two identical daughter cells. For higher eukaryotes, this machine is a bipolar assembly of microtubules, called spindle. The detailed structure of the spindle has been demonstrated in a seminal study by Shinya Inoué in living cells (Inoué 1953). Extraordinarily, Inoué designed an improved polarization microscope with increased sensitivity and resolution, describing metaphase and anaphase spindles in the oocyte of a marine annelid, and in the pollen mother cell of lily (Inoué 1953).

If spindle function was unfaithful, i.e., rather random, this would have tremendous consequences for transmission of the genetic material and would lead to considerable genetic aberrations. Conceivably, organelle partitioning and distribution, which depend on mitotic spindle function, would also be abrogated. Organelle dysfunction and abnormal cell physiology could be considered as possible outcomes in this scenario. Additionally, during cytokinesis, the central spindle forms a transient structure known as the spindle midbody (C. Hu et al. 2011). The spindle midbody is crucial for cytokinesis and defines the location of cell cleavage furrowing and abscission (Sharp and Ross 2012). Thus, the mitotic spindle is essential for the life of a cell.

The mitotic spindle is a rather large organelle and a molecular machine built up by the assembly of MTs and around 200 different MAPs (Petry 2016). The bipolar spindle is characterized by two distinct focus points, called poles, where typically, but not always, a centrosome organizes the microtubules. The spindle is composed of three different MT populations, all of them with important roles (Figure 1.3.). Kinetochore MTs or k-fibers, link the kinetochores to spindle poles and, therefore, are responsible for chromosome movement. Then, interpolar MTs, as the name puts forward,

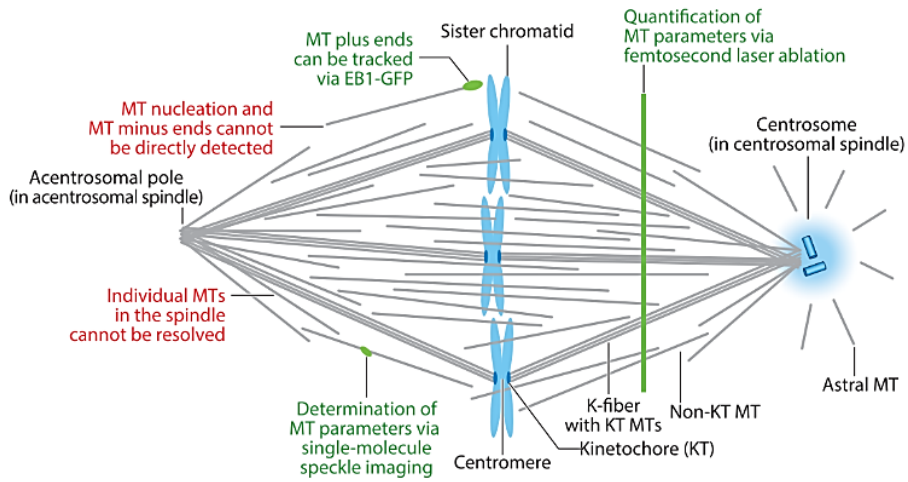

act together with MTs from the opposite pole but do not interact directly with kinetochores. Lastly, MTs emanating from each of the spindle poles, termed astral MTs, extend to the cell cortex (Inoué and Sato 2008). Astral MTs contribute to spindle positioning and orientation within the cell (Pietro et al. 2016). This is achieved by forces generated through interactions between the astral MTs and protein complexes bound to the cell cortex (Merdes et al. 1996).

Figure 1.3. Structure of the metaphase spindle depicting the major classes of MTs in a cell. *Kinetochore MTs or k-fibers, interpolar MTs (non-kinetochore MTs) and astral MTs are shown. Adapted from (Petry 2016).*

Recently, a specialized class of interpolar MTs has been described, named bridging fibers (Vukušić et al. 2017; Tolić, Novak, and Pavin 2019). Bridging fibers cross-link two k-fibers and, thereby, contribute to chromosome alignment (Vukušić et al. 2017).

Although much has been discovered about the components necessary to form such an apparatus like the spindle, we are still far from understanding how spindle assembly arises and how it accomplishes chromosome segregation so efficiently. Presumably, this is because the molecular players involved have multiple interactions or act in redundant pathways – different functions in different regions. Recent advances in biochemical perturbations, microscopy (Redemann et al. 2019; Ivec et al. 2021; Kletter et al. 2021), and computational models (Edelmaier et al. 2020) delivered new perspectives and visions to this problem.

The assembly of the spindle's fusiform structure (poles focused at centrosomes), which can have several micrometres in size (Kapoor 2017; Guilloux and Gibeaux 2020), comprises several events. Among those are the separation of centrosomes, NEBD, the organization of MTs to attain spindle bipolarity, and attachment of sister chromatids to MTs from both spindle poles. Surprisingly, all these events are accomplished in the minutes time scale. Mechanisms that repair DNA damage during cell division are suppressed. Thus, spindle assembly should be comparatively fast as otherwise it would compromise faithful chromosome segregation (Foley and Kapoor 2013).

The dynamics of polymerization/depolymerization of the building unit of MTs, tubulin, is central in spindle assembly kinetics. This became evident from experiments where tubulin displayed reversible and fast responses upon perturbation (Inoué 1967). Laser ablation experiments of MTs or centrosomes (MTOCs) has been extensively used to test the contribution of these spindle elements during chromosome segregation (Petry 2016; Cojoc et al. 2016). Using a method called single-molecule speckle

imaging, it was possible to assess tubulin turnover and MT length in the spindle (Yang et al. 2007). In addition, it was further shown that MTs are shorter near the poles and longer towards the center of the metaphase spindle from *Xenopus* egg extracts (Brugués et al. 2012). Insightful information emerged from experiments in the Shimamoto lab (Takagi et al. 2019). They reported that metaphase spindle structure maintains overall stability over minutes to hours despite the dynamic MT turnover and motility in *Xenopus* egg extract. In this case, they performed quantitative spindle micromanipulation assays using force-calibrated microneedles. Movements of the microneedle revealed force responses of individual MTs *in situ,* and allowed to map the physical nature (coupling, strength, fluidity) of MT-MT interaction at different locations of the spindle (Takagi et al. 2019). The authors concluded that the MT network around the spindle pole is solid-like whereas around the equator it is fluid-like. The MT arrays at the mid-half spindle (between the pole and the equator) are more mechanically compliant and can slide apart in response to a force that perturbs the overall spindle length. In this study, tracking of tubulin speckles showed that the spindle has looser MT overlaps between the equator and the pole, and that the equator and the spindle poles are strongly coupled with stiffer overlaps. Kinesin-5 and dynein were proven to be required to attain this mechanical heterogeneity of the spindle (Takagi et al. 2019). Thus, all these experiments were crucial to understand the fast turnover of MTs, and the robustness of the metaphase spindle.

1.5. MAPs and the regulation of MT dynamics

The mitotic spindle is still hard to grasp as it is one of the most dynamic cytoskeletal structures. Mitotic spindle assembly and disassembly takes one hour on average, with MTs that have a half-life of 60–90 seconds in *Xenopus* egg extracts (Sawin and Mitchison 1991; Inoué and Salmon

1995). In contrast, spindle assembly timing is very fast (100-150 seconds) during cleavage divisions in *C. elegans* embryos (Lacroix et al. 2018). The underlying cause for such different spindle assembly kinetics across different organisms may be due to differential usage of MAPS, which regulate the overall and local organization of MTs (Fig. 1.4.).

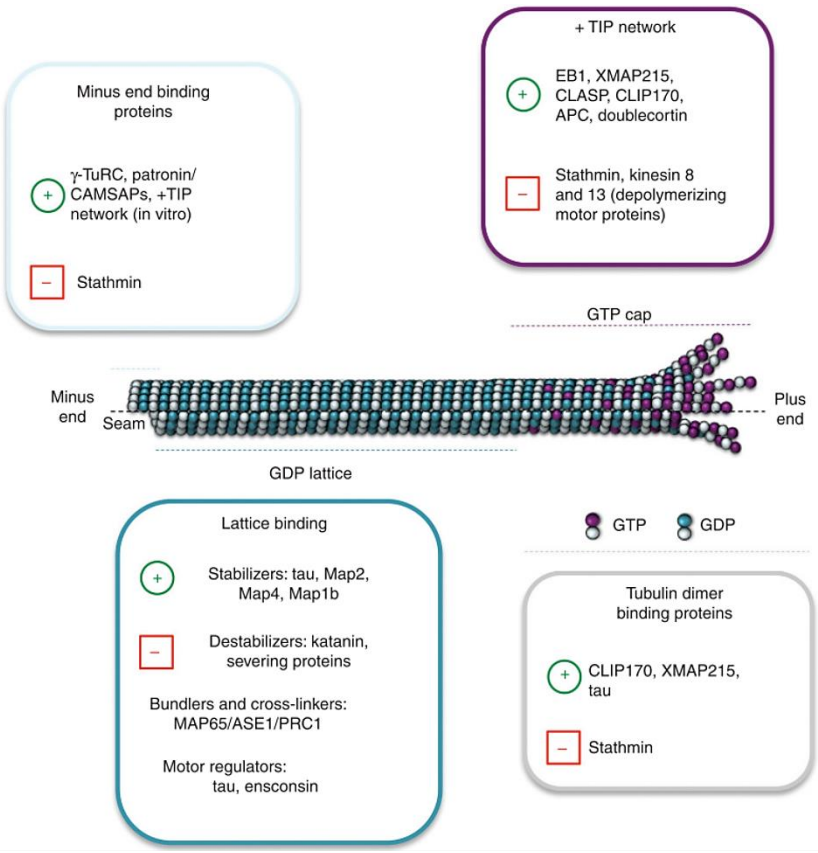

Figure 1.4. MT-binding proteins. *Main MT-binding proteins, their activities and localization on the MT. Green plus symbol (+) represents positive regulation and the red minus symbol (–) negative regulation. Adapted from (Goodson and Jonasson 2018).*

Besides regulating MT nucleation, MAPs also control MT dynamics, transport, and MT cross-linking in cells (Brouhard and Rice 2018). Particularly, the precise timing and location where MTs are formed is critical for the spindle. Importantly, the interaction of MAPs and MTs leads to the emergent property called self-organization (Nédélec, Surrey, and Karsenti 2003). Self-organization requires continuous consumption and dissipation of energy, to form what we know as a functional mitotic spindle (Gardner et al. 2011).

1.5.1. MT nucleation and polymerization

To generate new MTs, the cell relies on the process of nucleation. Primarily, MT nucleation factors generate MTs from MTOCs. Nucleation of MTs depends on γ-tubulin, which exists in the form of a γ-tubulin ring complex (γ-TuRC) in metazoans (Zheng et al. 1995; Oegema et al. 1999). The latest structural studies gave insight on how γ-tubulin and the γ-tubulin complex proteins (GCPs, GCP2 to GCP6) form the γ-TuRC (Thawani and Petry 2021). Single-molecule studies (cryo-EM) unraveled the high-resolution structure of the metazoan γ-TuRC, revealing that it arranges γ-tubulins into a helical geometry poised to nucleate MTs (Consolati et al. 2020; P. Liu et al. 2020; Wieczorek et al. 2020).

MT polymerases, also known as stabilizers, promote MT growth or rescue depolymerizing MTs (Petry 2016). Over the years, *Xenopus* egg extracts were widely used to study spindle assembly. The reason is because these extracts allow to impair the function of certain MAPs or spindle assembly factors by the addition of antibodies that inhibit target protein function. Using this system, XMAP215 was identified as a major MT stabilizer *in vivo*. Immunodepletion of XMAP215, which belongs to a conserved family of MT polymerases, led to smaller aster size and increased MT catastrophe frequency (Gard and Kirschner 1987). Recently, XMAP215a was identified as a second essential nucleation factor. This finding helped

to explain why the nucleation activity of γ-TuRC *in vitro* is relatively low (Thawani and Petry 2021).

MT dynamics are further regulated by MT plus-end tracking proteins (+TIPs) that recruit MT polymerases or depolymerases.

1.5.2. MT depolymerization and severing

MT depolymerases promote MT catastrophe and, thereby, MT disassembly. These include sequestering proteins, which bind to free tubulin subunits and prevent their incorporation into MTs (e.g. Stathmin, (Cassimeris 2002)). On the other hand, tip destabilizers directly attack the MT tip, such as the MT-depolymerizing kinesins (e.g., kinesin-13) that use ATP to remove subunits. These proteins can also depolymerize taxol- and GMPCPP-stabilized MTs (Walczak, Gayek, and Ohi 2013).

MT severing proteins can also lead to MT disassembly by using ATP to chop MTs into pieces. AAA ATPases such as Katanin, spastin, fidgetin, and related proteins sever MTs and can be found in different organisms (Roll-Mecak and McNally 2010). Katanin uses ATP hydrolysis to remove tubulin dimers from the lattice and destabilize the polymer. This creates new ends that lack GTP caps, which depolymerize rapidly (Sharp and Ross 2012).

1.5.3. MT sliding and cross-linkers

MTs are arranged by molecular motors and MT-bundling proteins. Cross-linking of MTs can occur at minus and plus ends or along the MT lattice. Kinesins, except kinesin 14, walk toward MT plus ends and exist as a large superfamily with varying motor properties and cargo-binding domains (Peterman and Scholey 2009). MT cross-linking is involved in the formation of the spindle midzone. Antiparallel MT overlaps in the spindle center and are important to establish bipolarity and to maintain stability of the spindle during mitosis (Bieling, Telley, and Surrey 2010). In

anaphase, the antiparallel MT array becomes bundled to form the midzone, which is essential for late mitotic events. PRC1 (Protein regulator of cytokinesis 1), is a key MT cross-linker. PRC1 was shown to cross-link bridging MTs and is responsible for the recruitment of kinesins to the bridging fiber. This facilitates chromosome alignment by overlap length-dependent forces transmitted to the associated k-fibers in human cells (Jagrić et al. 2021). Fascetto (Feo), the PRC1 homologue in *Drosophila*, is an antiparallel MT cross-linker and plays a central role in defining a minimal internuclear distance in the syncytial *Drosophila* preblastoderm embryo (Deshpande et al. 2021).

The astral MT network is also formed by MT cross-linking (Subramanian and Kapoor 2012). Immunodepletion of the protein NuMA in *Xenopus* extracts revealed that it has a dual role in organizing mitotic spindle poles and controlling spindle orientation in mitosis (Merdes et al. 2000; Hueschen et al. 2017).

Hence, MAPs are essential components of the spindle. MAPs are also involved in attachment of chromosomes to MTs, to generate the proper tension, sense errors and ultimately segregate chromosomes. Taken together, MAPs control the arrangement, dynamics, and cross-linking of MT arrays in space and time and are critical for the assembly of a functional metaphase spindle.

1.6. Spindle mechanics

How are forces generated within the spindle? How can we measure these forces inside cells?

Spindle assembly itself can be viewed as a mechanical process and forces are essential for spindle function (Karsenti and Vernos 2001). Micromanipulation experiments using microneedles (Shimamoto et al.

2011; Suresh, Long, and Dumont 2020) and magnetic tweezers allowed to probe and measure the forces generated by the spindle (Ferraro-Gideon et al. 2013; Garzon-Coral, Fantana, and Howard 2016). Amid those, pushing forces by growing MTs act on kinetochores during prometaphase for their alignment at the middle plane of the cell (Maiato et al. 2017; Jagrić et al. 2021). Once all chromosomes are aligned and bioriented (correctly attached to MTs from each pole) (Nicklas and Koch 1969), pulling forces by shortening MTs (Nicklas 1983) execute the main task of the spindle – chromosome segregation. Forces in the spindle on the order of tens of piconewtons per chromosome were measured by Nicklas (Nicklas 1983). A total internal force of ~1 nN was proposed to be developed in the spindle. Similar forces in *D. melanogaster* spindles were theoretically estimated (Roy Wollman et al. 2008). In a more recent study from the Maresca lab, two force sensors were used estimating 1–2 piconewtons of kinetochore forces at metaphase in *Drosophila* (Ye, Cane, and Maresca 2016). In this study, kinetochore fibers were proposed to employ hundreds of pNs of poleward-directed force on bioriented chromosomes (Ye, Cane, and Maresca 2016).

Within the spindle, both active force generation (molecular motors) and passive forces (elasticity and friction) are present (Elting, Suresh, and Dumont 2018). For the generation of active forces, chemical energy (ATP or GTP) is transduced into mechanical work, whereas passive forces store or dissipate energy (Elting, Suresh, and Dumont 2018). Elasticity and friction are important physical properties, conferring structural robustness to the spindle. Motors walk on MTs, and thereby generate forces. While most kinesins walk towards MT plus ends, dynein walks towards minus ends. These motors can generate 1-10 pN of force, with nanometer-size steps (Elting, Suresh, and Dumont 2018).

MT dynamics can under certain circumstances lead to force generation. In fact, MT polymerization and depolymerization are both thermodynamically favorable in the cell and can perform mechanical work. Growing MTs *in vitro* can generate pushing forces (Dogterom and Yurke 1997) whereas depolymerization of a single MT can generate pulling forces of up to ~30 pN (Grishchuk et al. 2005; Volkov et al. 2013). Removing all minus-end-directed motors in yeast did not prevent the spindle to move chromosomes towards the poles, suggesting that MT depolymerization plays a major role in poleward movement of chromosomes *in vivo* (Grishchuk and McIntosh 2006). Nevertheless, the yeast spindle is a very special case, which is formed by a single bundle of MTs that elongate during anaphase.

The spindle is embedded in a crowded, visco-elastic cytoplasm, which can conceivably limit or at least impose some resistance to MT polymerization or the length of growing MTs (Nazockdast and Redemann 2020). The environment surrounding the spindle has become an emerging topic in cell biology over the last years. Recently, stunning experiments based on micromanipulation of spindles in sea urchin embryos showed that the cytoplasm can impart visco-elastic reactive forces (Xie et al. 2022). These forces can move spindles, or objects with similar size, back to their original positions and are independent of cytoskeletal force generators. Remarkably, the cytoplasm visco-elastic forces reach hundreds of pN and seemed to scale with cytoplasm crowding (Xie et al. 2022). Therefore, it is possible that the density of the cytoplasm and even other non-cytoskeletal structures (e.g., organelles) that occupy the cytoplasmic space may play a role in spindle architecture and positioning.

Obstacles such as chromosomes, organelles/membranes, vesicles, etc are reasonable intracellular boundaries to consider. In fact, the flexibility

of the obstacle against which the MTs are polymerizing can affect the generated forces and polymerization velocities (Elbaum, Kuchnir Fygenson, and Libchaber 1996; Fygenson, Marko, and Libchaber 1997). To this date, we still have limited groundwork examining the role of intracellular membranes for forces during mitosis. The “search and capture model”, where MTs emanating from the centrosome come across a kinetochore and drive chromosome movement, is the classical model to explain chromosome capture and attachment to MTs. But this model alone is not sufficient and it has been calculated to take longer than the duration of mitosis (R. Wollman et al. 2005). Presumably, including a physical barrier in this model, therefore constraining MT growth and the position of chromosomes, might increase the probability of contact between MTs and kinetochores. The expected outcome would be the prompt incorporation of all chromosomes into the mitotic apparatus. In this context, the mechanical properties of chromosomes are of interest.

Chromosome compaction and even kinetochore structure or size may change the movement, or the force generated by polymerization and depolymerization. For example, it is unclear whether increased kinetochore size leads to binding of more MTs. Also, can stable kinetochore-MT attachments be established if chromosomes are less compacted? This question has been addressed due to reported missegregation of chromosomes upon reduction in their compaction in fission yeast (Saka et al. 1994). It was shown that when chromosomes are not rigid enough due to expression of mutant condensin proteins, their poleward movement becomes impaired (Saka et al. 1994).

Different chromosomes have variable sizes and structure; while some are very small (e.g., chromosome 21 in humans), others are big (human chromosome 1) (Nazockdast and Redemann 2020). The location of kinetochores also varies – can be in the center of the chromosome or at

the end of the chromosome (telocentric). Thus, it is reasonable to think that the structure and size of chromosomes influence the transmission of forces generated by MTs. In agreement with this, recent studies have reported that kinetochore size biases the segregation fidelity of certain chromosomes (Drpic et al. 2018; Worrall et al. 2018). It was demonstrated that MT binding capacity scales with kinetochore size and that chromosomes with bigger kinetochores established biorientation more efficiently (Drpic et al. 2018). These chromosomes showed a 2-fold bias to congress to the equator in a motor-independent manner. So, one can hypothesize that this bias could be due to changes in force generation induced by structural differences of specific chromosomes.

1.7. Scaling of the metaphase spindle

Why is spindle size regulated? What mechanisms govern spindle size?

Maintenance of spindle size may be important for force generation across the spindle. Studying force-generating mechanisms may shed light on how cells regulate the size of their internal structures. Supporting this idea, it was shown that metaphase spindle length is maintained constant in different cells (Dumont and Mitchison 2009; Goshima and Scholey 2010; Mogilner and Craig 2010).

For various experimental model systems, a theoretical force-balance model was proposed to explain how metaphase spindle length is regulated: antagonistic spindle motors – Kinesin 5 and Kinesin 14 – generate outward and inward forces on spindle poles to maintain the prometaphase spindle (Goshima et al. 2005; Syrovatkina, Fu, and Tran 2013; Guilloux and Gibeaux 2020). Spindles in *Drosophila* S2 cells showed a sensitive response to changes in MT dynamics: spindle length decreased with the depletion of MT stabilizers (EB1, Msps/chTOG, Mast/CLASP) or increased upon depletion of MT depolymerizers (Kinesin-13 Klp10A, Kinesin-8 Klp67A) (Goshima et al. 2005; Goshima

and Scholey 2010). Opposite effects were seen when these factors were overexpressed (Goshima et al. 2005). Mitotic spindles in the *Drosophila* embryo encompass only one Kinesin-5, called Klp61f (Heck et al. 1993). Klp61f is not required for initial spindle assembly, whereas it is necessary to prevent prometaphase spindle collapse driven by a Kinesin 14, Ncd (Brust-Mascher et al. 2009). Later, it was demonstrated that these two motors – Klp61f and Ncd – act together with a slowly disassembling lamin B nuclear envelope to maintain the appropriate spindle length during prometaphase in *Drosophila* syncytial embryos (Civelekoglu-Scholey et al. 2010).

Looking at closely related species also gave additional insight on how spindle size is regulated. Spindles in *Xenopus tropicalis* are smaller than in their counterparts *X. laevis* (Brown et al. 2007). Spindle size and architectural changes between *X. tropicalis* spindles *X. laevis* can be explained by differences in the activity of katanin and TPX2 (targeting factor for *Xenopus* kinesin-like protein 2) (Loughlin et al. 2011; Helmke and Heald 2014). *X. tropicalis* lacks an inhibitory phosphorylation site in the katanin catalytic subunit, which leads to increased katanin-driven MT severing (Loughlin et al. 2011). Moreover, TPX2 was found to be threefold more abundant in *X. tropicalis* extracts (Helmke and Heald 2014). When the levels of TPX2 were increased in *X. laevis* extracts, a reduction in spindle length was observed. TPX2 was shown to regulate spindle size and MT distribution through interaction with Eg5 (Kinesin-5). Higher levels of TPX2 promoted higher density of MTs at spindle poles due to recruitment of Eg5 (Helmke and Heald 2014). In human cells, it was also demonstrated that metaphase spindle length is regulated through the interaction between TPX2 and Aurora A (Bird and Hyman 2008).

Spindle length had previously been shown to scale with the number of chromosomes (ploidy). In 1980s, extraction of chromosomes from

Melanoplus differentialis spermatocytes demonstrated that the number of chromosomes defines spindle length (Nicklas and Gordon 1985). Using electron microscopy, the authors of this study found that kinetochore and non-kinetochore MT length was shortened upon removal of chromosomes (Nicklas and Gordon 1985). Spindle morphology was also shown to adjust to the quantity of DNA using haploid and polyploid *C. elegans* embryos (Hara and Kimura 2013). In this study, an increase in ploidy led to an increase in spindle width instead of the length (Hara and Kimura 2013).

Particularly during embryonic development, cell divisions are rapid and lead to smaller cells at each round. Thus, it is conceivable that intracellular structures can adapt to different sizes during embryonic divisions. This was beautifully shown in a system where cytoplasm of *Xenopus* eggs and embryos was encapsulated in cell-like compartments of specific sizes (Good et al. 2013). In this study, the amount of cytoplasmic material was demonstrated to determine the size and shape of the spindle during development rather than cell shape (Good et al. 2013). This finding was also documented later for nuclear size scaling (Jevtić and Levy 2015). Nuclear growth is fueled by the amount of perinuclear endoplasmic reticulum (ER) (Mukherjee et al. 2020). Thus, perinuclear ER membranes limit nuclear growth and size during development and partitioning of this membrane pool leads to smaller nuclei at each cell division.

1.8. Spindle architecture

The architecture of the spindle varies in different organisms and, remarkably, even between different cell types within the same organism. A few questions may arise from this observation: Why is spindle architecture and/or shape different between different cells? What regulates spindle architecture? Is spindle architecture important for its function?

The typical spindle configuration consists of a fusiform shape with two

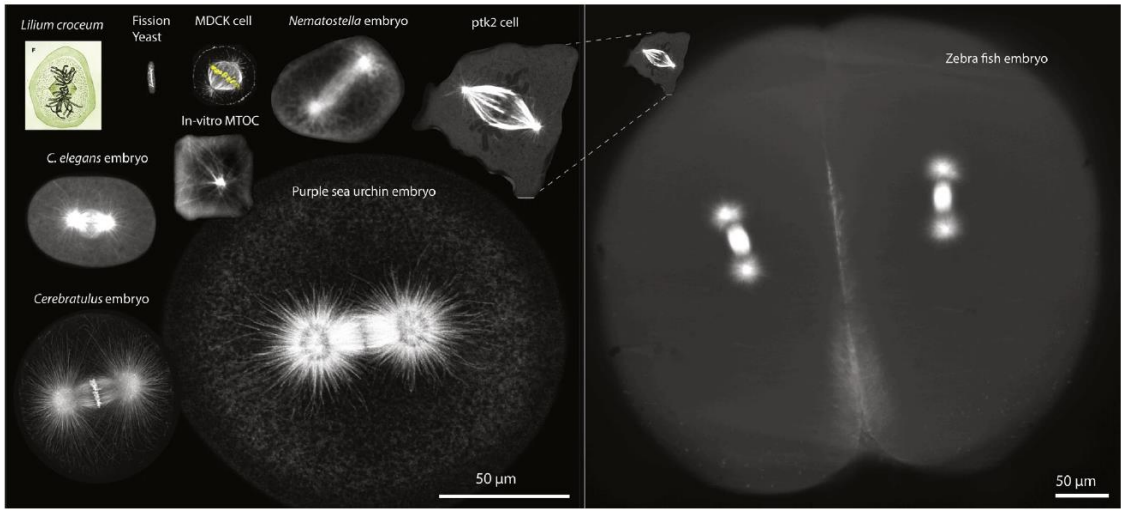

poles, structural focus points that are associated to a centrosome/MTOC. In other cases, the spindle adopts a barrel shape where centrosomes are absent, but poles are still focused. So, comparative analysis of different spindle configurations allowed to understand that centrosomes/MTOCs are not the only spindle elements responsible for MT nucleation and/or polymerization.

Figure 1.5. Mitotic spindles during metaphase in various eukaryotic cells and in vitro systems. *Retrieved from (Howard and Garzon-Coral 2017).*

In line with this observation, many species (fungi, plants, and protists) do not have centrosomes at all. In these instances, the specific genes related to centrosome assembly/formation were lost (Carvalho-Santos et al. 2011; Bettencourt-Dias 2013). Moreover, meiotic spindles in mammalian oocytes are acentrosomal and have unstable spindle poles (So et al. 2019). This instability was recently is caused by the lack of a spindle-stabilizing protein called KIFC1; elegant experiments in which KIFC1 was ectopically added to human oocytes rescued these unstable meiotic

spindles and the risk of aneuploidy (So et al. 2022). However, centrosomes seem to be important for certain cell divisions. For instance, meiotic divisions in *Drosophila* adult males with no centrosomes are highly abnormal (Rodrigues-Martins et al. 2008). Furthermore, without centrosomes, asymmetric cell divisions in neuroblasts (larval neural stem cells) can be aberrant (Debec, Sullivan, and Bettencourt-Dias 2010). Likewise, the centrosome and the spindle pole body are indispensable for spindle assembly and cytokinesis in *Caenorhabditis elegans* embryo and fission yeast, respectively (Debec, Sullivan, and Bettencourt-Dias 2010). Despite divergent spindle architectures, some similarities can still be found. For example, helical twist can be observed in the mammalian mitotic spindle (Tolić, Novak, and Pavin 2019). If we follow the spindle in the same plane/section starting from one pole to the other, a torque is revealed. This helical torsion of the spindle can also be found in other organisms such as the amoebae *Naegleria* (Velle et al. 2022).

1.9. Cell division: not only chromosomes and the MT-based spindle are at play

In the previous sections I have described the mechanisms of spindle assembly and size control in the light of the molecular factors which have an impact on MT dynamics, transport, and nucleation. Conceivably, other intracellular structures or factors may participate in the regulation of spindle size. One should consider especially those that interact directly or indirectly with MTs and/or that are localized in the vicinity of the spindle during mitosis. The structural and morphological changes of chromatin in the nuclear compartment may be the eye-catching event. But at mitotic entry, drastic remodelling and reorganization of other cellular components occur in parallel (Champion, Linder, and Kutay 2017; Taubenberger, Baum, and Matthews 2020; Carlton, Jones, and Eggert 2020).

1.9.1. Cytoskeleton remodeling

The cytoskeleton is profoundly reorganized during mitosis to accommodate for cell morphological changes. Cortical actin organization is key for the morphology of mitotic cells (Taubenberger, Baum, and Matthews 2020). Particularly, cortical actin dynamics is essential for eukaryotic cell shape, as cells round up to undergo division (Champion, Linder, and Kutay 2017; Ramkumar et al. 2021). Importantly, failure in mitotic cell rounding hinders bipolar spindle formation, chromosome segregation, and mitotic progression (Lancaster et al. 2013). Polarization of the cell cortex leads to contained cortical localization of dynein generating precise pulling forces on astral MTs (Fink et al. 2011; Clouds et al. 2015).

The actin network plays a role not only in mitosis, but also during meiosis: the actin filament network that surrounds meiotic chromosomes was shown to be important for chromosome capture in starfish oocytes (Lénárt et al. 2005). Indeed, in big cells such as oocytes, chromosome segregation cannot rely exclusively on spindle MTs simply because chromosomes are not within their length range. This was the first evidence demonstrating the existence of a non-MT element involved in chromosome capture.

During syncytial nuclear divisions in the *Drosophila* embryo, metaphase furrows are formed from actin caps (cortical actin domains of individual nuclei) (Lv et al. 2021). Metaphase furrows were previously compared to cytokinetic furrows of mononuclear cells. Just like mitotic cell rounding in mononuclear cells (Champion, Linder, and Kutay 2017), these furrows are formed from prophase to metaphase (Foe and Alberts 1983). Importantly, they are essential for cortical anchoring and lateral separation of mitotic spindles (Foe and Alberts 1983), But are actin furrows the only players involved? How are all these multiple spindles sharing the same cytoplasmic space compartmentalized? Since the typical plasma

membrane is absent during syncytial nuclear divisions, it is fair to speculate that intracellular membranes surrounding spindles possibly contribute to their separation.

1.9.2. Organelle remodelling

Although the mitotic spindle has unarguably been the focus of seminal studies to understand chromosome missegregation, less attention has been given to other elements of mitotic cells like intracellular membranes. Older studies showed that membranes are part of the spindle (Inoué 1953; Hepler and Wolniak 1984). Intracellular membranes are important features of mitotic cells, which also experience drastic reorganization to face division (Champion, Linder, and Kutay 2017). Carlton et al. (2020) reviewed all the severe cellular alterations associated with the onset of mitosis (Fig. 1.6.). The principles that govern organelle partitioning are intertwined with their remodelling processes. For this reason, when organelle remodelling is perturbed, it can compromise mitotic fidelity. Stochastic inheritance of organelles into the two daughter cells is promoted by their fragmentation, while association with the mitotic spindle will ensure organelle segregation during cell division. Organelles such as the NE, endoplasmic reticulum (ER) and Golgi apparatus experience disassembly or remodeling, being actively distributed or reformed (Fig. 1.6.). The NE and Golgi can become fragmented, and their fragments are then segregated by the cytoskeleton before they reform at the end of cell division.

Conversely, mitochondria are present abundantly in the cell but cannot disassemble. Instead, these small organelles take on morphological changes and are allocated into daughter cells stochastically. Mitochondria move on cytoskeletal tracks and experience fusion and fission continuously driven by GTPases from the dynamin superfamily (Labb, Murley, and Nunnari 2014). An impressive new study brought novel

insight into the mechanism underlying random segregation of mitochondria during mitosis (Moore et al. 2021).

Over the last years, various studies demonstrated that different organelles within the cell interact with each other (Rowland et al. 2014; Friedman et al. 2015; Guo et al. 2018). Organelle contacts have been proven to be important not only for organelle function but also for their distribution and segregation during mitosis (Carlton, Jones, and Eggert 2020). For instance, the ER forms various membrane contact sites (MCS) during interphase namely with the plasma membrane, endosomes, Golgi, mitochondria and cytoskeleton (Rowland et al. 2014; Phillips and Voeltz 2016). Particularly, MCSs are key not only for lipid transfer but also for communication between organelles. Besides the exchange of materials, MCSs contribute to organelle division (Cohen, Valm, and Lippincott-Schwartz 2018).

Division of both mitochondria and endosomes occur at sites of close contact with ER. Organelles like autophagosomes and peroxisomes obtain membrane from other organelles such as the ER and mitochondria. In addition, the control of Ca^{2+} signalling is one of the main functions of MCSs.

Figure 1.6. Organelle dynamics during mitosis. *Intracellular membranes and organelles surrounding the MT-based spindle. Adapted*

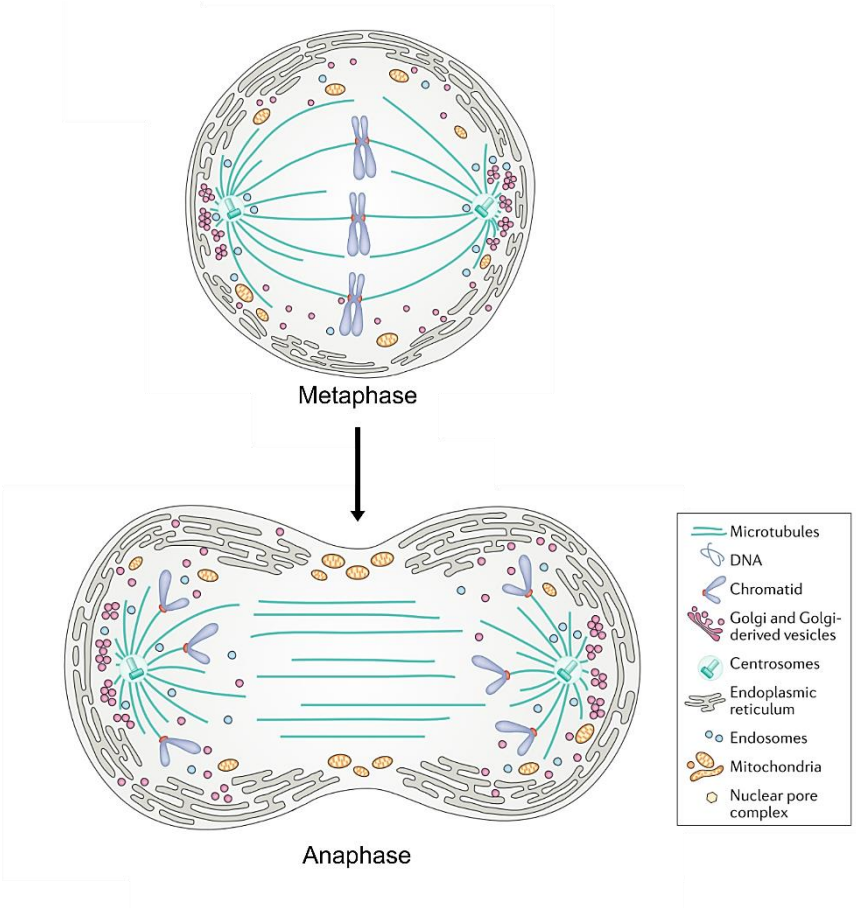

from (Carlton, Jones, and Eggert 2020).

1.10. The Nuclear Envelope (NE) and the Endoplasmic Reticulum (ER)

At mitotic entry, phosphorylation of inner nuclear membrane-chromatin and inner nuclear membrane-lamina tethers by CDK1 allows the NE to detach from chromatin and NE proteins are then reallocated into the mitotic ER (Champion, Linder, and Kutay 2017). *de novo* ER membrane formation is limited by inactivation of lipin, the phosphatidic acid phosphatase, which controls the phospholipid metabolism spatially leading to NE disassembly (Bahmanyar et al. 2014). Following NEBD, the NE and ER individual identities are gone, and NE proteins are segregated into daughter cells together with components of the ER. For example, Reticulons assist NE disassembly in *C. elegans,* proposing that the NE morphological transition into tubules could contribute to demembranation (Audhya, Desai, and Oegema 2007). Topologically, the ER forms a continuous membrane with the NE, all around the nucleus. The ER is the biggest membrane compartment within eukaryotic cells. This extensive organelle controls various canonical biological functions: folding, processing and transport of secretory and transmembrane proteins. It is the hub of lipid biosynthesis and acts as a store for intracellular calcium (Ca^{2+}).

1.11. ER-shaping proteins regulate the formation and maintenance of the ER network

During interphase, the ER exhibits diverse cisternal and tubulo-reticular domains. However, the precise morphology of the ER during mitosis is controversial. Depending on the methodology used to visualize the ER within cells, different aspects of ER morphology and structure have been revealed. For example, long curved membranes were observed by live cell imaging in mitotic cells (Lu et al., 2009; Lu et al., 2011) suggesting

cisternal organization of ER membranes. In turn, volume electron microscopy (Puhka et al. 2007; 2012) revealed that ER sheets have perforations (fenestrations) and tubulo-reticular structure, being the ER-shaping proteins REEP3 and REEP4 important for tubular morphology during division (Kumar et al. 2019). Prevalence of each morphological nature might be dependent on the cell type (Puhka et al. 2012).

Various ER-shaping proteins contribute for this highly dynamic network and its morphological changes during mitosis. Various proteins are involved in ER network formation: Reticulons (Rtns) are curvature-stabilizing proteins, Atlastins (ATLs) that are membrane-fusing GTPases, and the Lunapark protein (Lnp) (Orso et al. 2009a; J. Hu et al. 2009; S. Wang et al. 2018). Cooperation between these different proteins is critical and has been established as follows: maintenance requires a balance between ATL and reticulons, as too little ATL activity or too high Rtn concentrations cause ER fragmentation. Lnp only affects the abundance of three-way junctions and tubules. In mammalian cells, it was reported that the ER experiences a transition from sheet-to-tubule-like morphology (Puhka et al. 2007; 2012).

Depletion of ATLs leads to long non-branched ER tubules in tissue culture cells (J. Hu et al. 2009) and ER fragmentation in *Drosophila* (Orso et al. 2009a). In another study, *Xenopus* egg extracts were used to show that ATL is essential for the formation and maintenance of the ER network (S. Wang et al. 2013). The authors used the purified cytoplasmic fragment of *X. laevis* ATL (cytATL) as a dominant-negative reagent. Addition of purified *X. laevis* cytATL to interphase extracts completely blocked ER network formation. Moreover, inhibition of ATL function by cytATL also blocked ER network formation in mitotic extracts. This fragment contains the GTPase domain and the three-helix bundle but lacks the transmembrane segments and cytosolic tail of ATL (Bian et al. 2011; Byrnes and Sondermann 2011). The equivalent fragment of *Drosophila*

ATL inhibits the fusion of proteoliposomes (Orso et al. 2009a; Bian et al. 2011; T. Y. Liu et al. 2012), and the expression of the cytoplasmic domain of human ATL1 in tissue culture cells generates long, non-branched tubules (J. Hu et al. 2009). Hence, the fusion of ER membranes into a network appears to depend on ATL. Other studies also reported that depletion of ATL or expression of dominant-negative GTPase-defective mutants of ATL causes the conversion of the ER into small vesicles (S. Wang et al. 2016; Pawar et al. 2017; Montagna et al. 2020). Similarly, overexpression of Reticulon proteins was shown to cause ER fragmentation and discontinuity of ER membranes (S. Wang et al. 2016; Espadas et al. 2019). Thus, formation and maintenance of proper architecture is key for ER function. Abnormal ER morphology has been associated to a family of inherited neurological disorders called Hereditary spastic paraplegias (HSPs) (J. Hu et al. 2009; Lee et al. 2009; Goyal and Blackstone 2013; Montagna et al. 2020). As the name suggests, these disorders are characterized by spasticity and weakness of the lower body due to damaged distal ends of axons. The majority of these disorders is caused by autosomal dominant mutations in Atlastin-1, REEP1 or Spastin proteins (Park et al. 2010).

Previous studies have shown that disruption of MTs by depolymerizing drugs leads to a collapse of the ER network(Smyth et al. 2015; Bergman et al. 2015; Diaz et al. 2019). These studies focused on the structural changes of the ER and on the role of the MT cytoskeleton in the segregation of this organelle. It was also show before that the ER uses the MT cytoskeleton as tracks for movement during interphase and mitosis (Waterman-Storer and Salmon 1998; Nourbakhsh et al. 2021).
Even though human cells undergo what is considered “open” mitosis – complete disassembly of the nuclear envelope – the spindle is continuously enclosed by membranes. This “open” versus “closed” definition may be inaccurate in light of this observation. In mitotic cells,

the metaphase spindle is in an organelle-exclusion region (Schweizer et al. 2015). This was proposed to act as an organelle exclusion envelope and to promote molecular confinement of proteins required for mitotic spindle assembly (Schweizer et al. 2015). The ER is densely packed externally to this region and mitochondria were dispersed within the folds of ER in human cells (Nixon et al. 2017). After NEBD, the spindle becomes encased by a network of ER membranes associated with mitochondria, preventing their diffusion into the spindle zone. Serial block face scanning electron microscopy (SBF-SEM) confirmed that the spindle is clearly surrounded by membranes in human cells (Nixon et al. 2017). The same has been reported in *Drosophila* syncytial embryos, at the ultrastructural level and using time-lapse confocal microscopy to characterize the rapid ER reorganization during mitosis (Bobinnec et al. 2003). This was the first study describing a retraction/expansion cycle of the ER concurrently with the mitotic cycle. Indeed, further ultrastructural analysis of metaphase cells by transmission electron microscopy (TEM) has revealed that a quadruple nuclear membrane is formed in early prometaphase and that it disassembles during late prometaphase in *Drosophila* S2 cells (Strunov et al. 2018). In *Drosophila*, the ER remains closely linked to MTs during mitosis, not only in S2 cells, but also in meiotic spermatocytes (Smyth et al., 2015) and during embryonic nuclear divisions (Bergman et al., 2015; Smyth et al., 2015). In meiotic spermatocytes, the ER associates with astral MTs, while in embryonic nuclear divisions the ER is organized by centrosomes and forms a membranous envelope surrounding the spindle (Bergman et al. 2015; Diaz et al. 2019; Araújo et al. 2022).

In HeLa cells, although the ER is almost entirely dissociated from MTs during mitosis, especially in the inner spindle region, the ER displays obvious radial extensions organized around the spindle poles (Schlaitz et al. 2013; Smyth et al. 2015; Kumar et al. 2019). A role for astral MTs in this radial ER distribution was demonstrated by treatment with a MT

depolymerizing drug (colchicine), leading to loss of the radial-like organization of ER at the spindle poles (Smyth et al. 2015). When chromosomes fall beyond this “exclusion zone” they become entrapped within ER membranes leading to chromosome missegregation events and ultimately to the formation of micronuclei (Ferrandiz et al. 2022). By chemically inducing the relocalization of ER membranes to the plasma membrane in live cells by addition of rapamycin, the previously trapped chromosomes are transported back to the metaphase plate, and this rescues mitotic fidelity.

Regulation of membrane biogenesis is important for correct chromosome segregation (Bahmanyar et al. 2014). When the lipid biosynthesis pathway is manipulated, the ER membrane density in the cytoplasm of mitotic cells is increased (Merta et al. 2021). Excessive ER membranes increased the viscosity of the mitotic cytoplasm and, as a result, chromosome movements were physically constrained precluding the correction of errors. Consequently, this leads to the formation of micronuclei. The protein phosphatase CTDNEP1 (C-terminal domain nuclear envelope phosphatase 1) control of lipin 1 (a key enzyme for lipid synthesis) limits the synthesis of fatty acids for ER membrane biogenesis in interphase, which prevents chromosome missegregation in mitosis (Merta et al. 2021). ER membrane synthesis is uncoupled from ER reorganization during mitosis. In conclusion, the regulation of ER reorganization is important for mitotic fidelity.

1.12. Microtubule-ER interactions

Some ER-shaping proteins are phosphorylated during mitosis, introducing another layer of complexity in the regulation of ER morphology. ER morphology can be influenced by suppression of Lunapark multimerization (S. Wang et al. 2016; 2018), CLIMP63–MT

interactions (Vedrenne, Klopfenstein, and Hauri 2005) and the dissociation STIM1 from the MT-binding protein EB1 (Smyth et al. 2012). However, Climp-63 is not present in *Drosophila* and dSTIM1 (*Drosophila* STIM1) does not have an EB1-binding domain/sequence as described for mammalian STIM1 (Grigoriev et al. 2008; Smyth et al. 2012). Mainly, phosphoregulation of these ER proteins inhibits the interaction of the ER with MTs ensuring that the ER does not obstruct the assembly of the spindle (Smyth et al. 2012).

Human REEPs (REEP1-4) interact directly with MTs through a positively charged cytoplasmic domain (Schlaitz et al. 2013). The focus of the ER at spindle poles has been shown to require REEP3 and REEP4, precluding the untimely association of the spindle with chromatin and a consequent failed division (Schlaitz et al. 2013). Even though ER segregation is directed by spindle poles and astral microtubules (Smyth et al. 2015), how the spindle coordinates this task without affecting chromosome segregation is still unclear. When ER membranes are artificially tethered to metaphase chromatin this results in severe mitotic defects (Champion et al. 2019).

As alluded to before, the spatial proximity of other organelles/intracellular membranes to the spindle in different organisms indicates that the spindle is not an isolated entity in the cytoplasm. Moreover, several lines of evidence suggest that the environment surrounding the spindle (and MTs) imparts on their mechanical and structural features. Up to this date, many studies have shown that the MT-based spindle is the major force generator inside cells. Yet, less attention was given to other organelles and intracellular structures which could also impart compressive forces or at least confer visco-elastic properties to the spindle surrounding environment. Mainly, owing to the essential role of the mitotic apparatus, it has been difficult to assess the contribution of additional intracellular structures without compromising mitotic progression and fidelity.

1.13. Main aims

Mitotic spindle assembly and maintenance rely on interconnected networks of MTs, motors, chromosomes, and other regulatory factors. But whether interactions between other intracellular structures and the mitotic spindle help to maintain proper its size and contribute to its function remains less clear. Spindles assemble rapidly, with a high level of accuracy at every round of division. This led us to question how such robust molecular machines assemble so efficiently. Particularly in *Drosophila* syncytial embryos, how can multiple nuclei be compartmentalized and divide in such a rapid manner so efficiently? Could other intracellular structures contribute to the accuracy and efficiency of syncytial nuclear divisions in this system?

In this thesis I, aimed to provide answers to these questions. Uncovering additional forces and/or intracellular structures involved in spindle function will give insight and contribute to a more integrated view of cell division.

Aim 1. Uncover additional forces acting on chromosomes besides the ones generated by the MT-based spindle.

Aim 2. Probe for the role of ER membranes in mitotic spindle function.

Chapter 2

Exploring additional forces acting during mitosis

Author contribution:

Preliminary experiments that motivated the work developed in this chapter were performed by a former PhD student – Ewa Piskadlo. All the experiments presented in this chapter were performed and analyzed by Margarida Araújo. The experiments were designed by Margarida Araújo, Ivo A. Telley and Raquel A. Oliveira. Alexandra Tavares prepared and purified proteins used in some of the experiments.

2.1. Introduction

Cell division is essential for life. This fundamental process allows for the duplication of the genome and its equal distribution into two identical daughter cells. For this, a MT-based spindle apparatus must be assembled to generate the necessary forces that will align resolved chromosomes at the equator and only then pull them apart into opposite poles of the cell. Thus, cell division can be seen as a mechanical process, where forces generated by the spindle are essential to faithfully segregate the genetic material at each round of division. Simultaneously, other cellular components, namely cytoskeletal elements, and membrane organelles in the vicinity of the spindle, undergo drastic remodeling for their partitioning at the end of cell division. Moreover, the intracellular environment is very crowded and viscous. It is full of molecules, proteins, cytoskeletal filaments and organelles (Guigas, Kalla, and Weiss 2007; Collins et al. 2019). Thus, the forces generated by the spindle must overcome the resistance imposed by the crowded cytoplasm and ensure the separation of large objects like chromosomes. It is reasonable to assume that intracellular components besides the spindle contribute to the efficiency and synchrony of chromosome segregation in animal cells. Classical brightfield movies of dividing animal cells nicely portray the argument that neither the spindle nor chromosomes should be viewed as isolated entities inside cells (Cande, McDonald, and Meeusen 1981; O'Connell and Khodjakov 2007). So, having a more integrative view instead of looking at individual intracellular compartments may contribute to understanding the fundamental mechanisms governing cell division.

The description of the so-called spindle matrix and its involvement in spindle morphogenesis challenged the idea that the spindle is an isolated unit (Lince-Faria et al. 2009; Yao et al. 2012). It was also demonstrated that when organelles, such as the NE and ER, fail to be cleared from

chromatin this results in chromosome missegregation (Schlaitz et al. 2013; Champion et al. 2019). As mentioned in Chapter 1, an organelle-exclusion envelope assists mitosis and compartmentalizes molecules in the spindle region (Schweizer et al. 2015). This membranous system facilitates molecular confinement and, thereby, accumulation of important mitotic regulators in the spindle region like Mad2 and Megator/Tpr, and even soluble tubulin (Schweizer et al. 2015). Molecular crowding in the spindle area seems to be an important event for spindle assembly and signaling events within the spindle apparatus. However, whether this membranous envelope or other cytoplasmic structures also participate in spindle function or in the progression of the cell cycle has remained unclear. Presumably, different intracellular structures could contribute to the overall ability to generate force and robustness of the spindle. To explore additional factors involved in the efficiency of chromosome segregation, we aimed to establish a system that reveals other force generators acting on chromosomes upon removal of MTs, which are masked in the presence of spindle MTs.

Drosophila syncytial embryos are the perfect system to explore this question since we can follow live the dynamics of chromosome movements in multiple and synchronized nuclei. Using this model system, we can experimentally test what happens to artificially separated sister chromatids when MTs are removed, with an unprecedented timely controlled manner. Since we can induce a metaphase-arrest condition combined with acute removal of MTs by microinjection, this approach allows to test and analyze chromosome movement during metaphase in the absence of MT attachment.

2.2. Results

2.2.1. TEV-mediated cleavage system of cohesin as a tool to monitor the behavior of isolated sister chromatids

Efficient mitosis relies on the movement of large subcellular structures – the chromosomes – across the crowded cytoplasm. Hence, the behavior of these "cargos" can be used as an indirect read-out of the forces that act on them. To study chromosomal movement and the underlying forces (beyond the spindle), we established an assay that monitors the movement of isolated chromatids upon removal of the major force generator for chromosome movement: the mitotic spindle. For this purpose, we made use of a system, previously developed in the lab (Pauli et al. 2008; Oliveira et al. 2010), where sister chromatids could be artificially separated, and their movement tracked in real time. This system relies on the use of embryos solely expressing a genetically engineered cohesin complex containing Tobacco Etch Virus (TEV) protease recognition sites in the α kleisin subunit (Rad21 in *Drosophila*) (Pauli et al. 2008; Oliveira et al. 2010). TEV sites are inserted at position 550 in the Rad21 subunit of the cohesin complex and its cleavage, triggered by TEV protease, can mimic the separase-mediated cleavage during anaphase (Fig. 2.1., B).

In order to prevent the canonical cohesin cleavage step, we prevented anaphase onset by ectopic addition of a dominant-negative form of the E2 ubiquitin ligase, UbcH10^{C114S}. Injection of high doses of this modified protein is sufficient to induce a metaphase-arrest in syncytial embryos, characterized by the alignment of chromosomes at the equatorial plane of each nucleus (Oliveira et al. 2010).

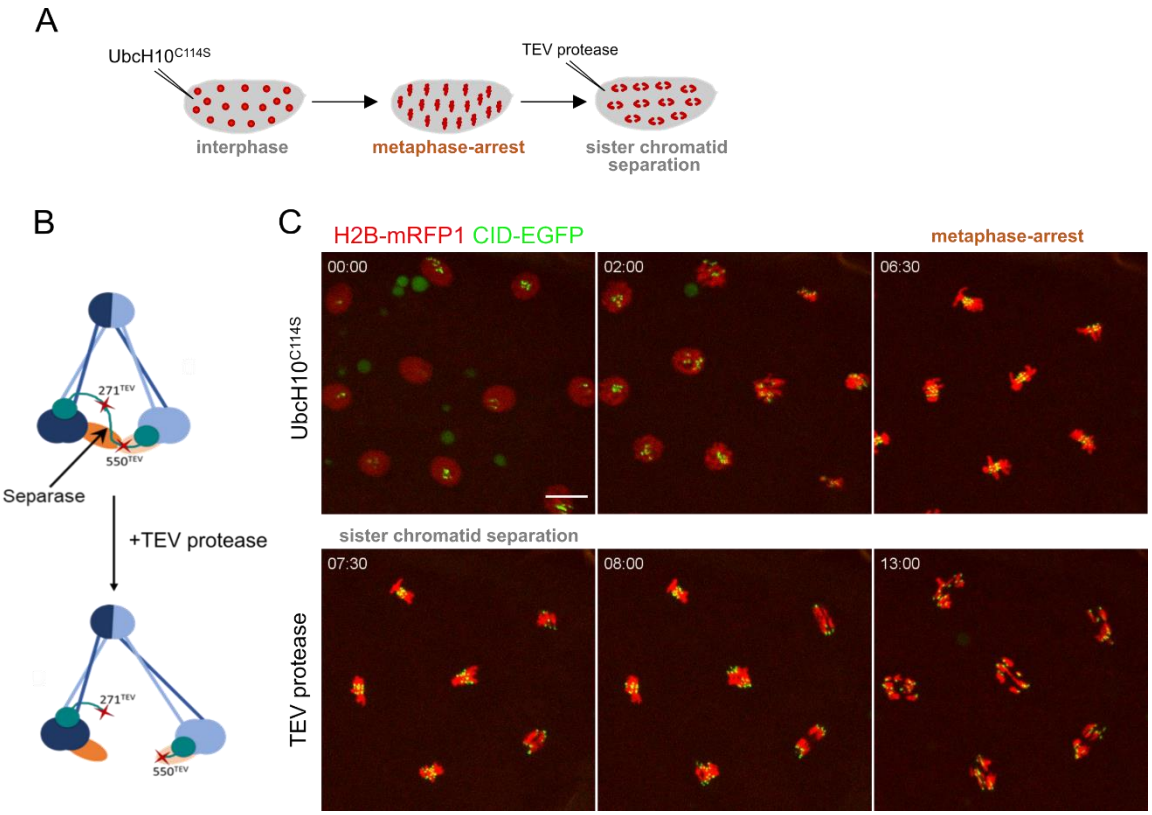

Figure 2.1. Experimental layout to separate sister chromatids in metaphase-arrested embryos. *(A) Scheme of the experimental layout. First, a microinjection with a dominant-negative version of the E2 ubiquitin-ligase UbcH10 (UbcH10^{C114S}) was performed to induce a metaphase-arrest, followed by microinjection of TEV protease to artificially separate sister chromatids. (B) Schematic representation of TEV-cleavable Rad21 (Rad21^{TEV}), adapted from (Carmo, Araújo, and Oliveira 2019). TEV site (550^{TEV}) in the Rad21 subunit at position 550 (Pauli et al. 2008). Rad21/Scc1 (brown), SMC3 (dark blue), SMC1 (light blue), and Scc3/SA (yellow). (C) Embryos solely expressing Rad21^{TEV} recombined with the Drosophila CENP-A protein (CID) tagged with EGFP, and histone H2Av-mRFP1 were used to visualize chromosomes. UbcH10^{C114S}-mediated arrest (30-40 µg/µl) leads to the formation of a metaphase plate (upper pannel, t=06:30; centromeres aligned, green). A*

second microinjection with TEV (10-12 µg/µl) is performed causing separation of sister chromatids (bottom pannel, t=07:30). Time (min:sec) is relative to microinjection of UbcH10^{C114S}. Scale bar is 5 µm.

Using this inducible metaphase-arrest approach, spindle assembly is unperturbed, and the formation of a proper bipolar spindle is achieved in this condition. Microinjection with TEV protease in these metaphase-arrested nuclei leads to the poleward movement of sister chromatids (Fig. 2.1. C, t=07:30-13:00). After a few minutes, sister chromatids initiate an oscillatory behavior along the spindle axis (Fig. 2.1.B, t=08:00-13:00; Movie 2.1.). This oscillatory motion of sister chromatids can be explained by the loss of cohesin leading to unstable kinetochore-MT attachments (Oliveira et al. 2010; Mirkovic et al. 2015).

Interestingly, the movement of separated sister chromatids upon cohesin cleavage is restricted to the spindle region and only rarely we see isolated sisters travelling beyond spindle poles. This observation means that either MTs are very quick at chromatid recapture or, alternatively, something is limiting their diffusion of isolated sisters. To check for the frequency of chromatid attachment, we probed for the checkpoint protein Mad2 (Fig. 2.2.). For this, microinjection with a mixture of UbcH10^{C114S} and TEV protease was performed. We observed that Mad2 localizes at the NE before NEBD (Fig. 2.2., t=00:00). After NEBD, some Mad2-EGFP foci were detected as chromosomes start to congress into the equator (Fig. 2.2., t=02:00). TEV-mediated cleavage of cohesin revealed that most isolated chromatids have significant levels of Mad2 at their kinetochores, supporting their unattachment state most of the time, at least for 10 min of live imaging (Fig. 2.2., t=05:30-10:00). If so, the restricted chromatid movement is more likely to be attributed to their large size or an external compartment limiting their movement.

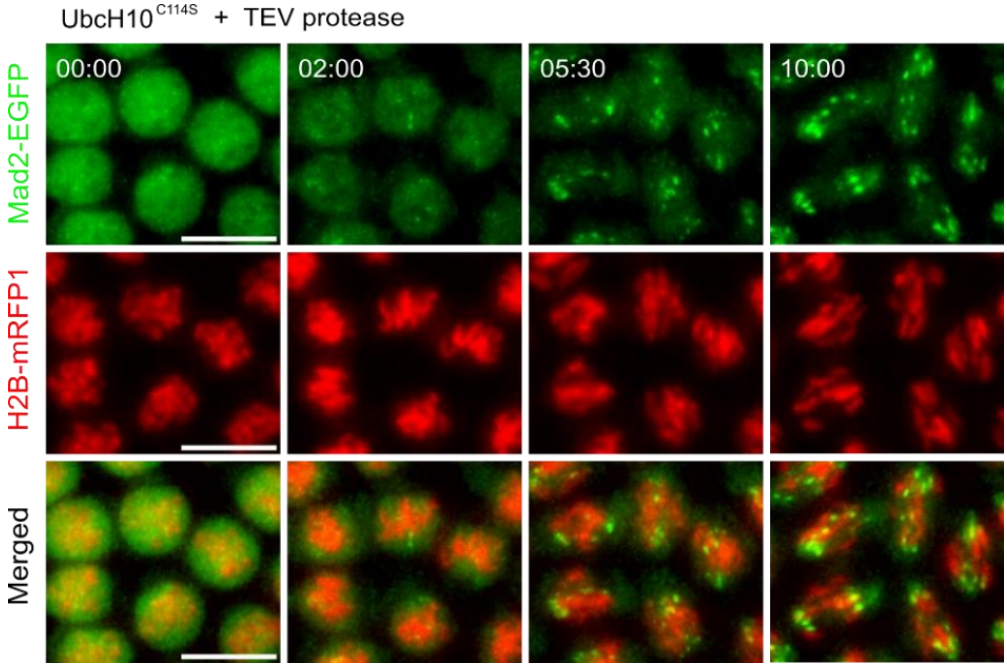

Figure 2.2. Artificially separated sister chromatids are frequently unattached. *Representative time-lapse images of embryos solely expressing Rad21^{TEV} recombined with H2B-mRFP1 (red), and Mad2-EGFP (green foci). Microinjection with a mix of UbcH10^{C114S} and TEV was performed causing separation of sister chromatids (t=00:00-02:00) and a metaphase-arrest. Mad2-EGFP foci can be seen in most sister chromatids (t=05:30-10:00) over 10 min of live imaging. Time (min:sec) is relative to microinjection. Scale bar is 10 µm.*

Having established a system to disperse isolated chromatids, we next sought out to investigate what force may define their movement and mobility. We predicted that removal of the spindle should detach chromatids from their main driving machine and hence allow the analysis of other forces that may act on chromosomes. To test this notion, we performed microinjection with a MT depolymerizing drug (colchicine), aiming to analyze how isolated chromatids move in the cytoplasm upon

spindle disassembly. Colchicine is a MT depolymerizing drug that binds to free tubulin and thereby blocks MT polymerization (Salmon, McKeel, and Hays 1984). We observed that colchicine injection in embryos with dispersed sister chromatids led to their clustering into the center of the nuclear space (Fig. 2.3.B, t=14:00-25:30; Movie 2.1.). The observed behavior was very intriguing, since the canonical movement of chromosomes, either alignment or segregation, are known to depend on MTs.

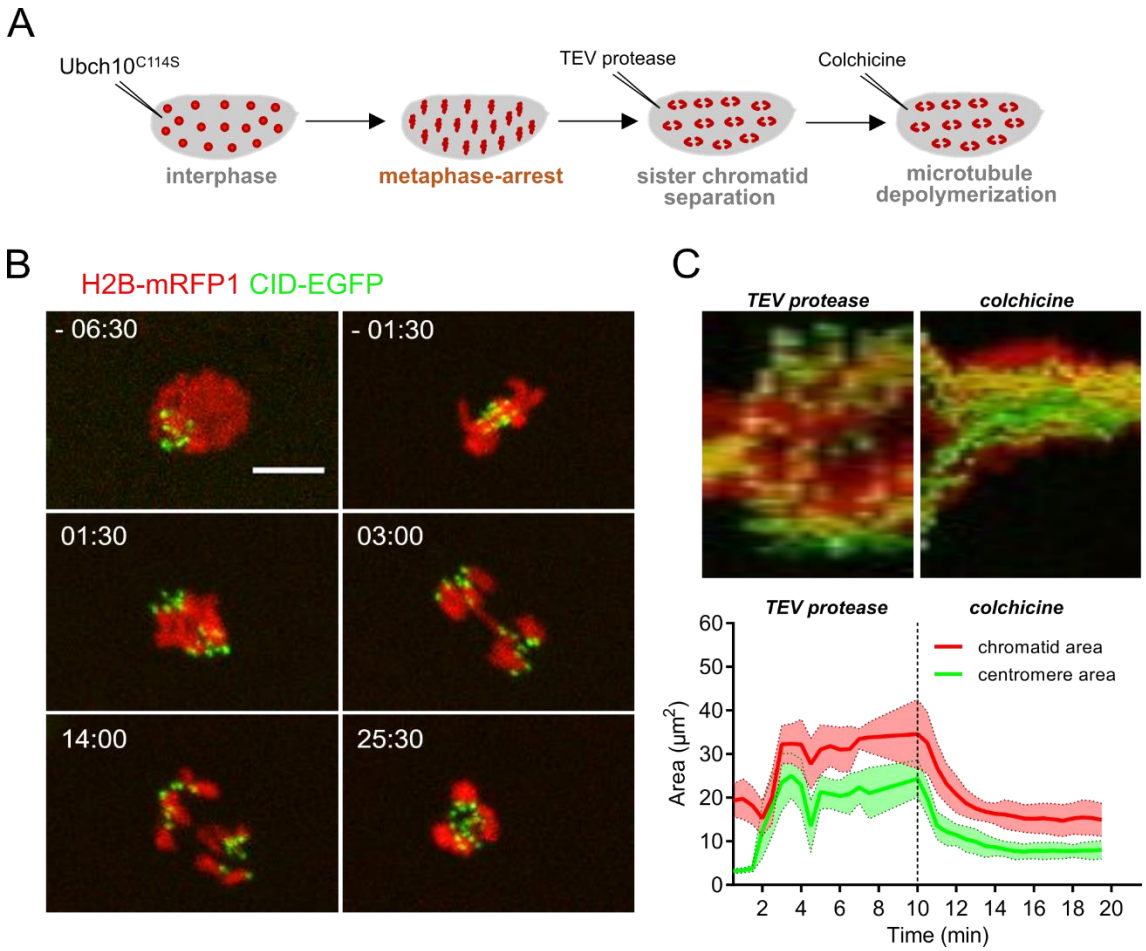

Figure 2.3. Separated sister chromatids move to the center of the nuclear space upon MT depolymerization. *(A) Experimental layout to separate sister chromatids in metaphase-arrested embryos. First, a microinjection with a dominant-negative version of the E2 ubiquitin-ligase*

UbcH10 (UbcH10^{C114S}) was performed to induce a metaphase-arrest, followed by microinjection of TEV protease to artificially separate sister chromatids. A third microinjection with colchicine was used to acutely depolymerize MTs. (B) Schematic representation of TEV-cleavable Rad21 (Rad21^{TEV}), adapted from (Carmo, Araújo, and Oliveira 2019). TEV site (550^{TEV}) in the Rad21 subunit at position 550 (Pauli et al. 2008). Rad21/Scc1 (brown), SMC3 (dark blue), SMC1 (light blue), and Scc3/SA (yellow). Embryos solely expressing Rad21^{TEV} recombined with the Drosophila CENP-A protein (CID) tagged with EGFP, and histone H2Av-mRFP1 were used to visualize chromosomes. UbcH10^{C114S}-mediated arrest (30-40 µg/µl) leads to the formation of a metaphase plate (t=-01:30; centromeres aligned, green). A second microinjection with TEV (10-12 µg/µl) is performed causing separation of sister chromatids (t=01:30). A third microinjection of colchicine (1 mM) was performed 10 minutes after sister chromatid separation (t=14:00), leading to clustering of sister chromatids at the center (t=25:30). Time (min:sec) is relative to microinjection of TEV. Scale bar is 5 µm. (C) Kymograph projection of sister chromatid (red) and centromere (green) positions in space and time. Graph shows the area occupied by sister chromatids (red) and centromeres (green) after injection of TEV protease (0-10 min) and of colchicine (10-20 min).

This finding revealed that MT depolymerization does not lead to free scattering of chromosomes, as predicted, but instead results in concentric movement towards the center of the nuclear space (Fig. 2.3. C, kymograph; reduced chromatid and centromere areas upon colchicine injection). Interestingly, this movement is observed in all isolated chromatids, and none was found to diffuse away from the equator region.

2.2.2. Probing for potential mechanism(s) underlying clustering of sister chromatids upon MT depolymerization

Given the observed clustering of isolated chromatids, we next aimed to understand what forces drive such movement. We hypothesized this movement could be either driven by the kinetics of MT depolymerization, by other non-MT forces, or a combination of both. To evaluate these possibilities, we estimated the kinetics of MT depolymerization upon addition of colchicine, using a transgenic line expressing fluorescently tagged Tubulin (β-Tubulin-RFP) to monitor microtubules and Cid-EGFP to access chromatid movement. Our goal was to understand how MT depolymerization (disassembly of MTs) was temporally correlated with the clustering of sister chromatids to the center.

Upon addition of colchicine, we observed progressive MT depolymerization, that accompanies the clustering movement of centromeres (Fig. 2.4.B, t=20:30). Moreover, we found that interpolar MTs were disassembled first, while k-fibers (MTs that attach to kinetochores) took longer to disappear (Fig. 2.4., t=11:30). We estimated the kinetics of spindle disassembly based on area of spindle, using the β-Tubulin-RFP channel, defined by automatic threshold. Centromere displacement was measured by the area of the dispersed centromeres over time, using the CID-EGFP channel. We found that the rate of spindle disassembly (decay in spindle area) was greater than the velocity of centromere/chromatid movement (Fig. 2.4. D, spindle area (red) and centromere area (green) curves). Moreover, the onset of MT depolymerization is observed earlier than centromere clustering, supporting that chromatid movement is initiated after spindle disassembly.

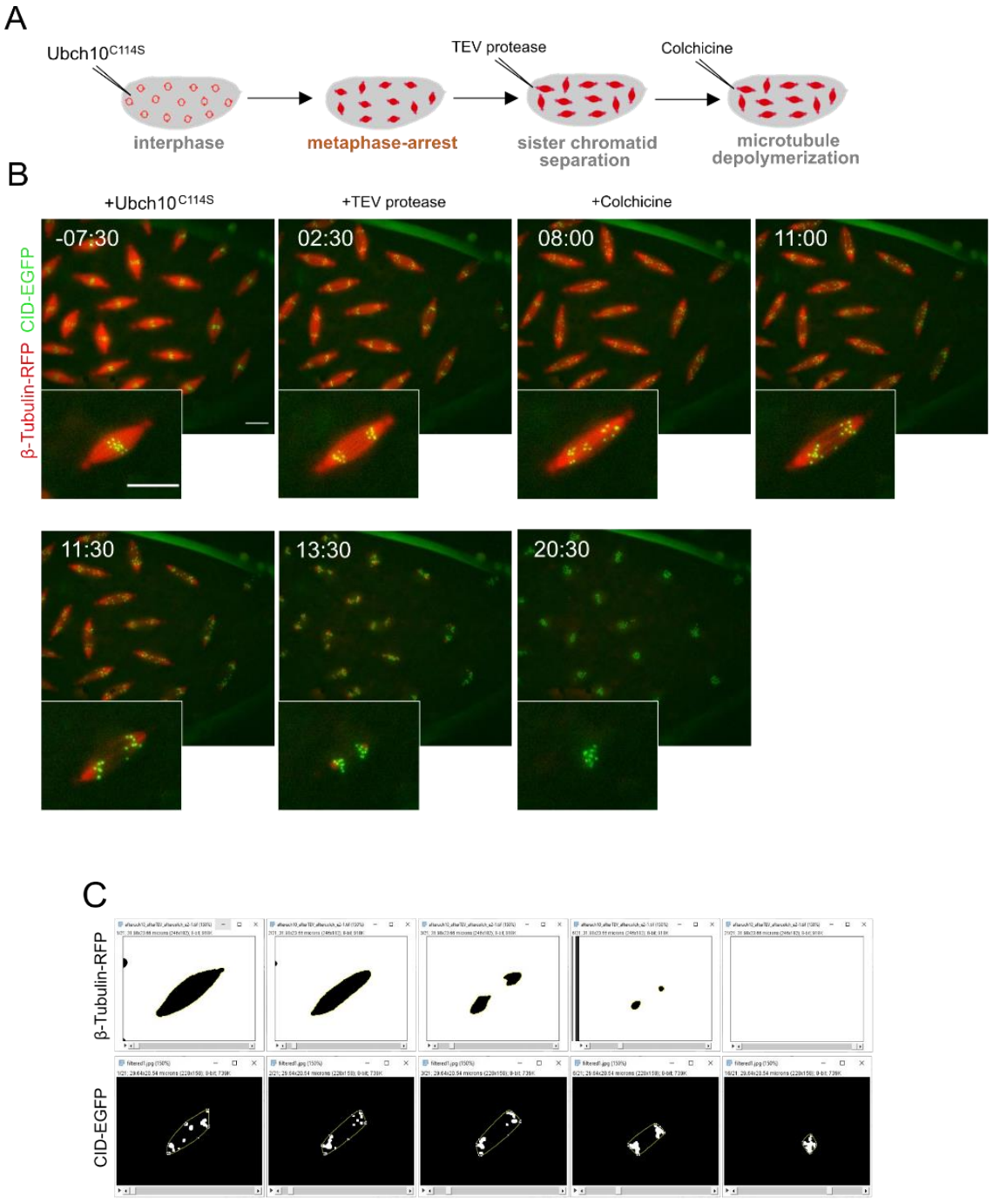
A
Ubch10C114S
TEV protease
Colchicine
interphase
metaphase-arrest
sister chromatid separation
microtubule depolymerization
B
+Ubch10C114S
+TEV protease
+Colchicine
β-Tubulin-RFP CID-EGFP
-07:30
02:30
08:00
11:00
11:30
13:30
20:30
C
β-Tubulin-RFP
CID-EGFP

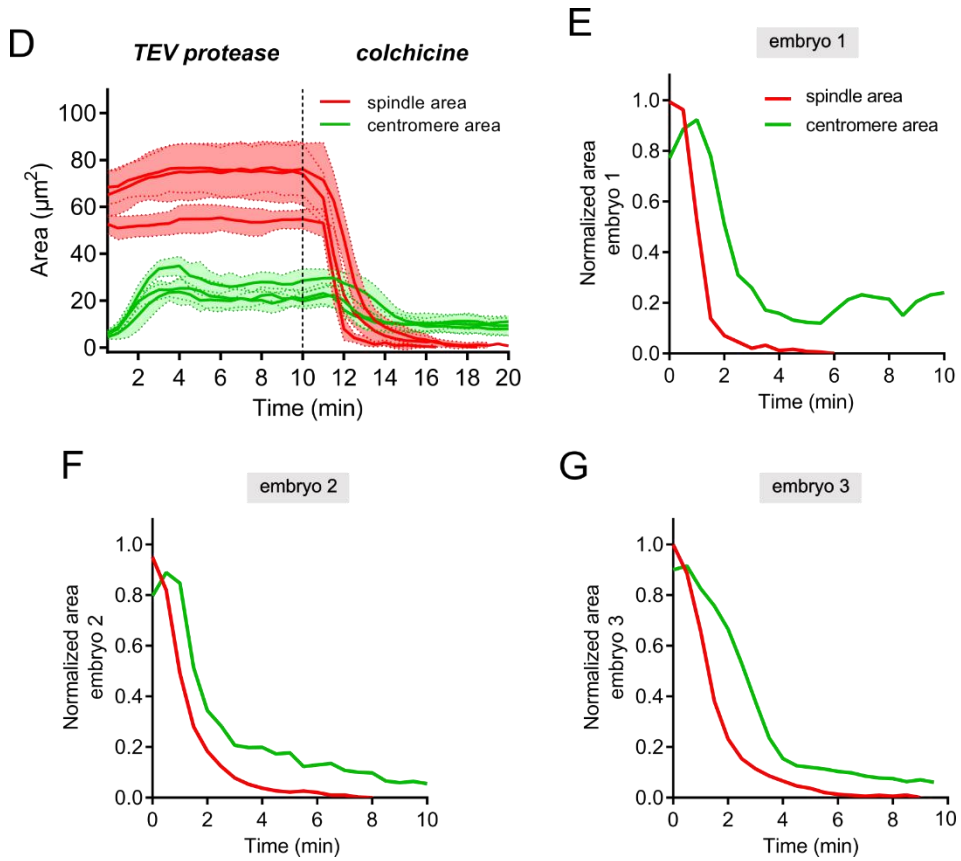

Figure 2.4. Microtubule depolymerization kinetics is faster than sister chromatid movement to the center of the nuclear space. *Embryos expressing solely a TEV-cleavable cohesin complex recombined with CID-EGFP (green), and β-Tubulin-RFP (red) were used to follow MT depolymerization and chromatid movement. (A) Experimental layout to disperse sister chromatids and subsequent MT depolymerization. (B) Microinjection with colchicine (1 mM) leads to depolymerization of spindle MTs (t=11:00 to t=20:30), accompanied by clustering of sister chromatids (centromeres) into the center. Time in min:sec, is relative to microinjection with TEV protease (t=02:30). Scale bar is 10 µm. (C) Threshold applied to the β-Tubulin-RFP chanel to measure spindle area over time. Area occupied by centromeres (CID-EGFP channel) was measured over time. (D) Graph depicts spindle (red)*

and centromere area (green) (absolute values, mean±SD). (E-G) Graphs depict spindle area (red) and centromere area (green) in 3 independent embryos (E – embryo 1, F – 2 and G – 3; normalized to maximum and minimum values after colchicine, mean). Image processing performed using Fiji. Data from 3 independent embryos, measuring 10 nuclei from each embryo, was plotted using GraphPad Prism software.

Remarkably, we find that clustering of centromeres occurs in a progressive manner (more and more reduced centromere area at each time point), with significant movement occurring even after full spindle disassembly. Thus, from these results we concluded that (i) chromatid movement starts at a delay compared to spindle disassembly and that (ii) there is chromatid movement when spindle MTs are not detected (below significant signal).

Given the temporal proximity between the events (with some differences, mentioned above), it was difficult to assess whether the observed clustering of sister chromatids into the center of the nuclear space could be promoted by MT depolymerization itself. To further test this possibility, we assessed the position of centrosomes relative to clustered sister chromatids. We repeated the same experiment using embryos containing GFP-tagged Spd2 (Spd2-GFP), a PCM and centriolar component (Dix and Raff 2007) (Fig. 2.5.).

We observed that the distance between centrosomes – length between the two centrosomes using Spd2-GFP as a centrosome marker – was progressively reduced (Fig. 2.5. B) We found that inter-centrosomal distance was drastically reduced a few time points after colchicine addition, supporting the collapse of the spindle (Fig. 2.5. C, distance at 0 min = 11.9 ± 0.67 µm versus distance at 10 min = 7.0 ± 1.8 µm, mean ±

SD). Shortening of inter-centrosomal distance occurs with a similar kinetics than spindle disassembly (Fig. 2.5.).

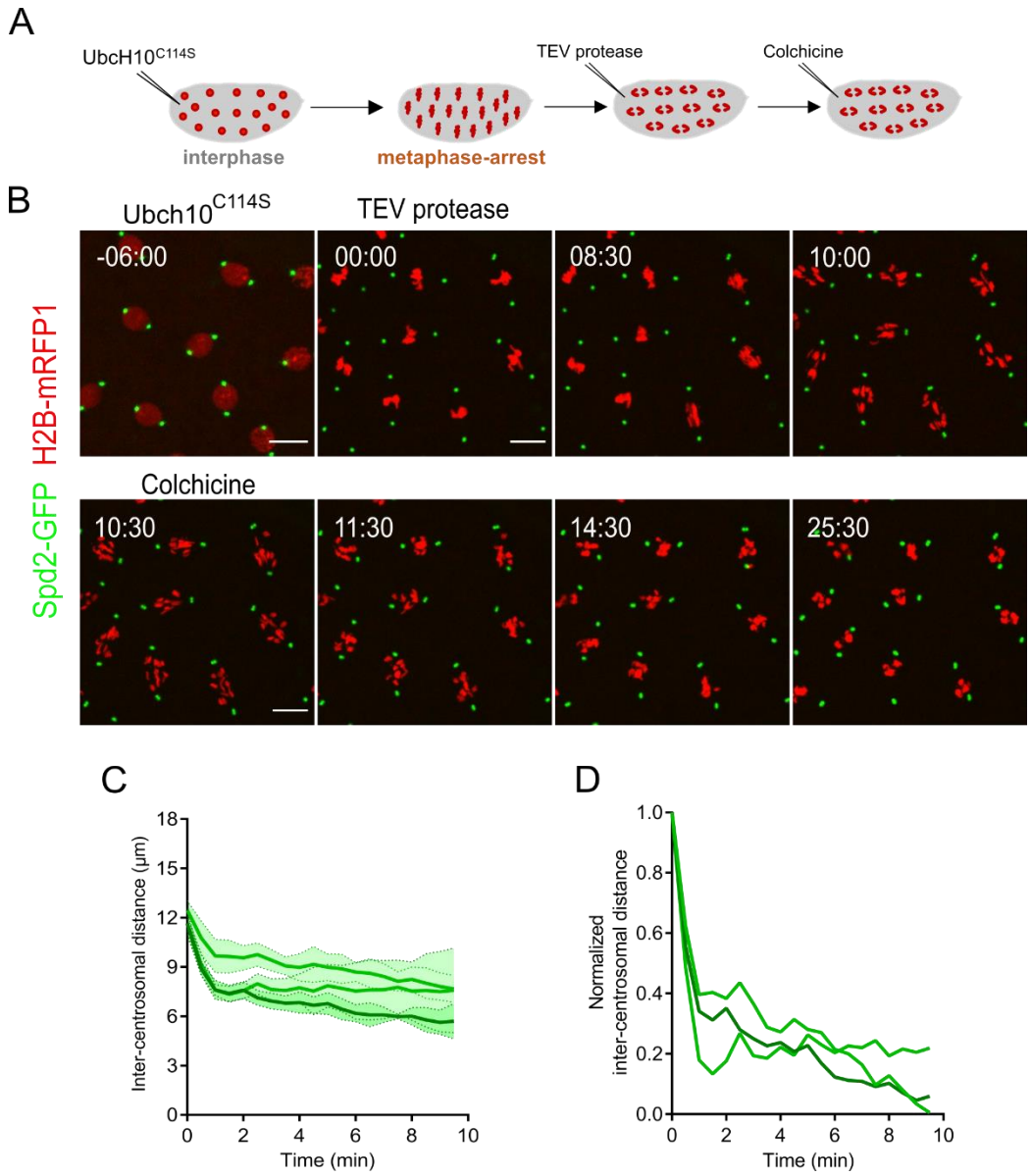

Figure 2.5. MT depolymerization leads to decreased distance between centrosomes. *(A) Scheme depicting the experimental layout to separate sister chromatids and remove spindle MTs in metaphase-*

arrested embryos. (B) Embryos expressing solely a TEV-cleavable cohesin complex recombined with H2B-mRFP1 (red), and the centrosome marker Spd2-GFP (green) were used to visualize chromosomes and centrosomes upon MT depolymerization. Microinjection with colchicine (1 mM) was performed 10 min after sister chromatid separation. Time in min:sec, is relative to microinjection with TEV protease. Scale bars are 10 µm. (C) Graph depicts inter-centrosomal distance (µm) over time after colchicine using the Spd2-GFP channel (absolute values, mean±SD). (D) Graph shows inter-centrosomal distance normalized to the maximum and minimum values (mean). Sample size is 3 independent embryos, where 4 nuclei were measured per embryo.

These findings could imply that shortening of the spindle is driving the clustering movement, at least at the initial stages. Indeed, we saw that k-fibers seem to be the last ones to depolymerize upon microinjection with colchicine (Fig. 2.4.B, t=11:30), which is in line with the notion that these k-fibers are more stable than the other MT populations of the spindle (Salmon, McKeel, and Hays 1984). These stable k-fibers could impose the clustering of isolated chromatids still attached to the disassembling spindle. If so, k-fiber mediated movement would be expected to be dependent on the presence of a centromere.

To test whether centromeres were required for the clustering, we attempted to generate acentric (lacking the centromere) chromosome fragments by laser ablation of chromosome arms protruding from the metaphase plate upon inducible metaphase-arrest. Then we performed laser ablation, followed by microinjection with TEV protease and a third microinjection with colchicine (Fig. 2.6.). Because this experiment required a high level of precision to ablate only the tip of chromosome arms (see Materials and Methods), our sample size was reduced to only a few embryos.

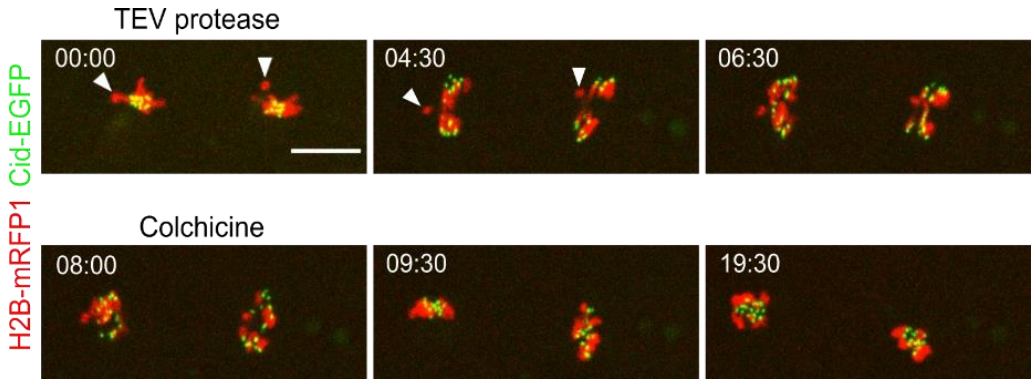

Figure 2.6. Centromeres are not required for the clustering of sister chromatids. *Acentric chromosome fragments were generated by laser ablation and their movements were tracked over time. Embryos expressing solely a TEV-cleavable cohesin complex recombined with H2Av-mRFP1 (red), and the centromere marker Cid-GFP (green) were used to visualize chromosomes and centromeres upon MT depolymerization. Microinjection with colchicine (1 mM) was performed 6.5 min after sister chromatid separation (t=08:00). Time in min:sec, is relative to microinjection with TEV protease. Scale bar is 10 µm. Sample size is 2 independent embryos, no statistical analysis was performed.*

We observed that with intact spindle, acentric fragments moved less compared to sister chromatids, but still did not move away from the spindle region (Movie 2.6.). Upon addition of Colchicine, acentric fragments did not lag behind and move collectively with sister chromatids into the center instead (Fig. 2.6., t=08:00-19:30). We therefore concluded that acentric movement is independent of attachment to the disassembling spindle. This notion is consistent with the finding that significant movement of centromeres is still observed even after full spindle disassembly (Fig. 2.4.).

Altogether, these findings suggest that additional forces besides the ones generated by spindle MTs may be contributing to the movement of isolated chromatids towards the center of the nuclear space. Thus, we next sought out to explore additional forces acting on the mitotic apparatus. An organelle exclusion zone has been previously reported as having an important role in tubulin confinement and concentration of spindle assembly factors (Schweizer et al. 2015). Importantly, this spindle envelope compartment plays an essential role in spindle assembly indicated by spindle defects once this membranous envelope is ruptured (Schweizer et al. 2015). So, we decided to investigate whether membranous organelles that are proximal to the spindle could be involved in clustering of sister chromatids upon MT depolymerization.

2.2.3. The partially disassembled NE in *Drosophila* syncytial embryos as a putative external force compartment

In contrast with canonical cell divisions in metazoan, which undergo "open" mitosis (when the NE disassembles completely) *Drosophila* embryos are an intermediate case, where the NE is only partially disassembled (De Souza and Osmani 2007; Katsani et al. 2008; Strunov et al. 2018). Hence, the partial NE that remains in these divisions could be a potential candidate for the extrinsic forces that restrict and direct chromosome movements in mitosis. Therefore, we decided to examine the dynamics and localization of the NE during embryonic syncytial divisions and upon UbcH10^{C114S}-mediated arrest, used in our experimental layout. For this, we expressed (UAS-)lamin B-GFP in syncytial embryos using a V32-Gal4 maternal driver. We observed that lamin B localizes to the NE prior to mitotic entry (Fig. 2.7., t=12:00-13:00). However, at NEBD, lamin B fluorescence intensity decreases as the NE partially disassembles (Fig. 2.7.A, t=14:00) and the protein seems to relocate into the neighbouring membranous structures at metaphase (Fig.

2.7.A, t=14:30) and anaphase (Fig. 2.7.A, t=15:30). In addition, we also imaged embryos arrested at metaphase using UbcH10^{C114S} microinjections (Fig. 2.7. B), allowing us to prolong the time spent at this stage of the cell cycle. This analysis revealed a residual lamin-GFP labelling as tubular-like structures, but not an intact NE structure.

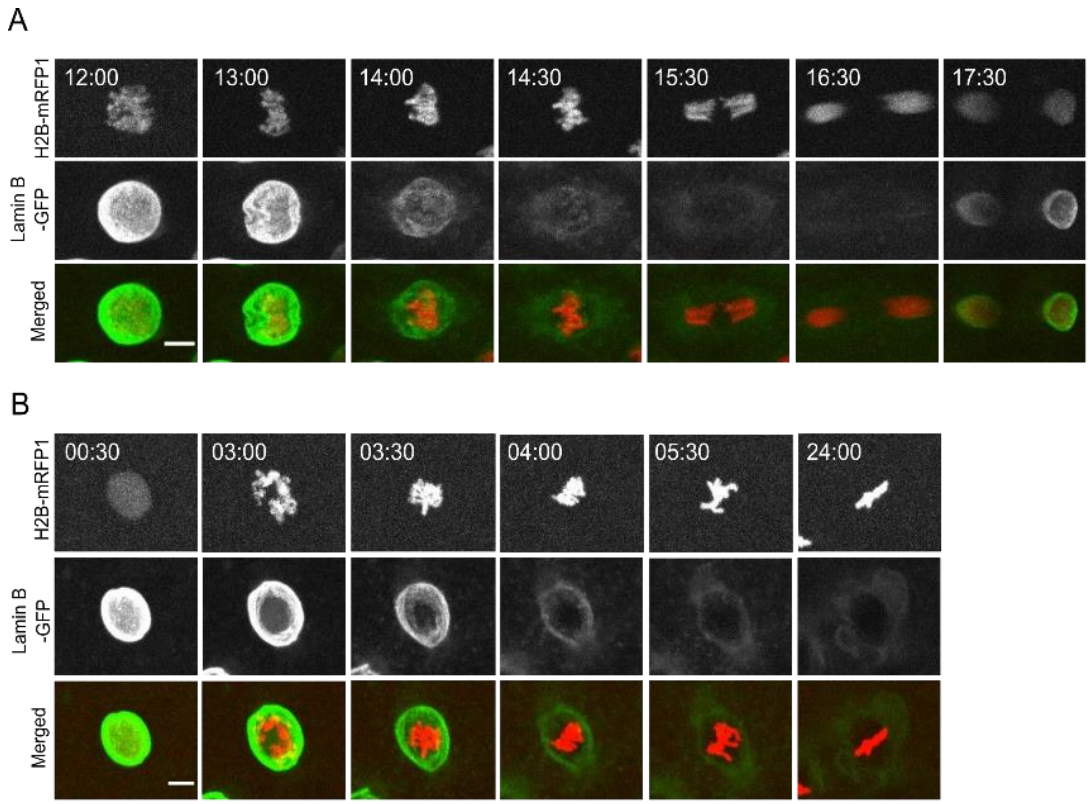

Figure 2.7. Disassembly of the nuclear lamina in cycling and metaphase-arrested Drosophila syncytial embryos. *Embryos expressing the maternal driver V32-Gal4, H2B-mRFP1 (red) and UAS-lamin B-GFP (green). (A) Partial disassembly of the nuclear lamina is seen in cycling embryos, indicated by the decrease in lamin B-GFP fluorescence intensity (t=13:00 versus 14:00). Lamin B-GFP fluorescence intensity is very weak but can still be detected at metaphase (t=14:30) and anaphase (t=15:30). Time in min:sec. (B) Appearance of the nuclear*

lamina upon artificial arrest at metaphase (UbcH10^{C114S}, 30 µg/µl). Disassembly at poles can be observed (t=03:30-04:00). Lamin B-GFP seems to localize to the ER at metaphase (t=05:30). Time is relative to microinjection with UbcH10^{C114S}. Scale bars are 5 µm.

These findings suggest that in the prolonged metaphase-arrest, most of the NE is disassembled resembling more a canonical open mitosis situation. Hence, we consider that the residual NE is unlikely to play a significant role as extrinsic force in our experimental set-up.

2.2.4. The Endoplasmic Reticulum (ER) forms a membranous envelope surrounding the mitotic spindle in *Drosophila* syncytial embryos

Next, we explored the potential role of the ER tubular network, which forms a continuum with the NE (Goyal and Blackstone 2013). When the NE breaks down in mitosis, allowing spindle MTs to interact with the chromosomes, the ER reorganizes in the vicinity of the spindle (Bobinnec et al. 2003). Thus, we imaged embryos where both the NE and the ER could be visualized, using lamin B-GFP and RFP-KDEL, respectively (Fig. 2.8.). KDEL is a small peptide sequence that targets proteins to the ER lumen (Raykhel et al. 2007). Once again, we found that lamin B-GFP signal decreased at mitotic entry (Fig. 2.8., t=01:00-03:00, green) and increased at telophase upon NE reformation (Fig. 2.7. A t=17:30, Fig. 2.8. t=05:00) compared to metaphase and anaphase.

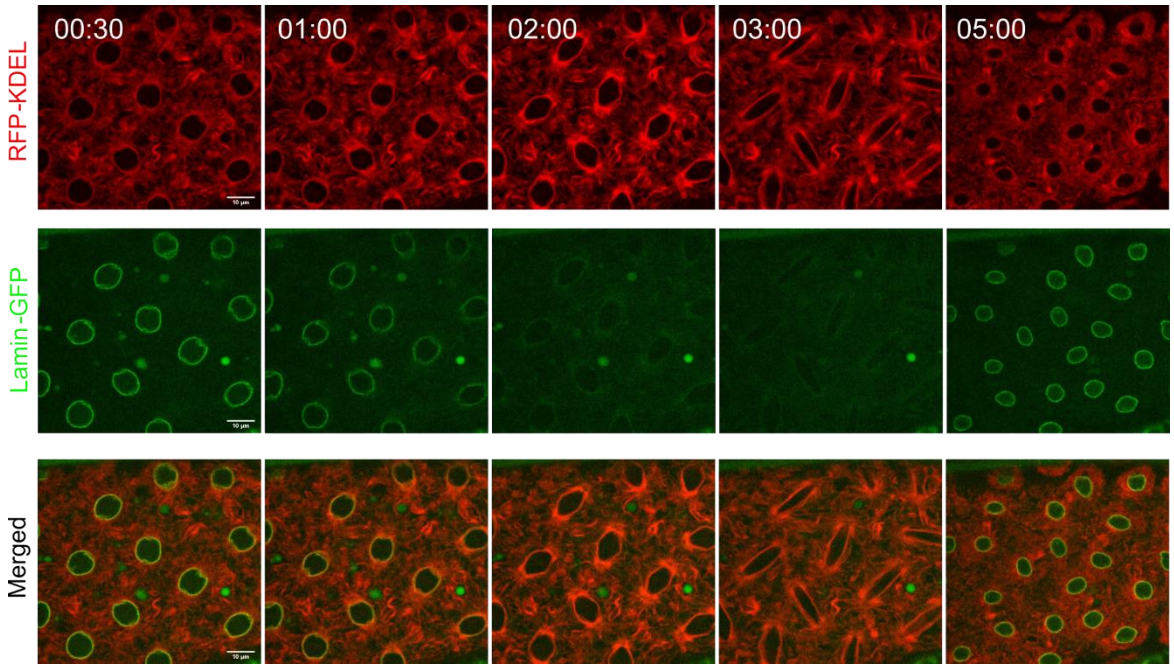

Figure 2.8. NE and ER localization during nuclear divisions in Drosophila syncytial embryos. *Nuclear divisions in embryos expressing lamin B-GFP (green) and RFP-KDEL (red) under the maternal driver G302-Gal4. Time min:sec. Scale bar is 10 µm.*

Conversely, ER membranes are present throughout the cell cycle, despite their drastic morphological changes (Fig. 2.8., RFP-KDEL channel). These results suggest that the ER is the major membrane compartment closer to the mitotic apparatus in *Drosophila* embryos.

To visualize the ER and spindle simultaneously during *Drosophila* syncytial embryonic divisions, we performed live imaging and followed ER localization throughout the cell cycle. We generated flies expressing the chromatin marker H2B–mRFP1, and either the ER marker EYFP–KDEL or the ER membrane-shaping protein Reticulon-like protein 1 (Rtnl1) fused to GFP (GFP–Rtnl1). We also marked microtubules by injecting

Alexa647-labelled tubulin (Fig. 2.9., Movie 2.9.). EYFP fused to the KDEL sequence reports all ER, while Rtnl1 specifically reports locations of membrane reshaping. Consistent with this notion, we observed an extended KDEL-labelled ER network in the entire cortex of the syncytial embryo and throughout mitosis (Fig. 2.9. A). However, at mitotic entry upon nuclear envelope breakdown, the concentration of ER in the vicinity of the spindle rose (Fig. 2.9. A, Metaphase). The signal of GFP–Rtnl1 also increased, exclusively around the spindle, and most prominently at the spindle poles (Fig. 2.9. B). This is consistent with prior reports showing an increase in ER proteins at spindle poles upon mitotic entry (Bobinnec et al. 2003; Diaz et al. 2019). However, it remains unclear how these changes in ER organization impart on ER morphology across different stages of spindle assembly.

Of note, both ER reporters shown are excluded from the spindle and resemble an envelope (Fig. 2.9. A-B, insets). At NEBD, we measured a reduction in the ER exclusion area (Fig. 2.9. C) supporting a transient contraction of the ER at this stage. This reduction is not accompanied by a decrease in the perimeter of the ER envelope (Fig. 2.9. E), due to an indentation of the ER envelope at spindle poles (Fig. 2.9. A, inset). During metaphase and anaphase, the area and perimeter of the ER exclusion gradually increase, matching closely that of the spindle main body, disregarding the spindle poles (Fig. 2.9. D). This comparative measurement emphasizes the shape similarity of the ER envelope and the spindle body. At telophase, the ER undergoes shape changes that accompanied nuclear envelope reformation (Fig. 2.9. A-B, Telophase). We also observed that both ER reporter proteins localized at the spindle midbody as previously reported (Bobinnec et al. 2003), suggesting that a considerable membrane reorganization occurs at this site (Fig. 2.9. A-B, Telophase, arrowhead).

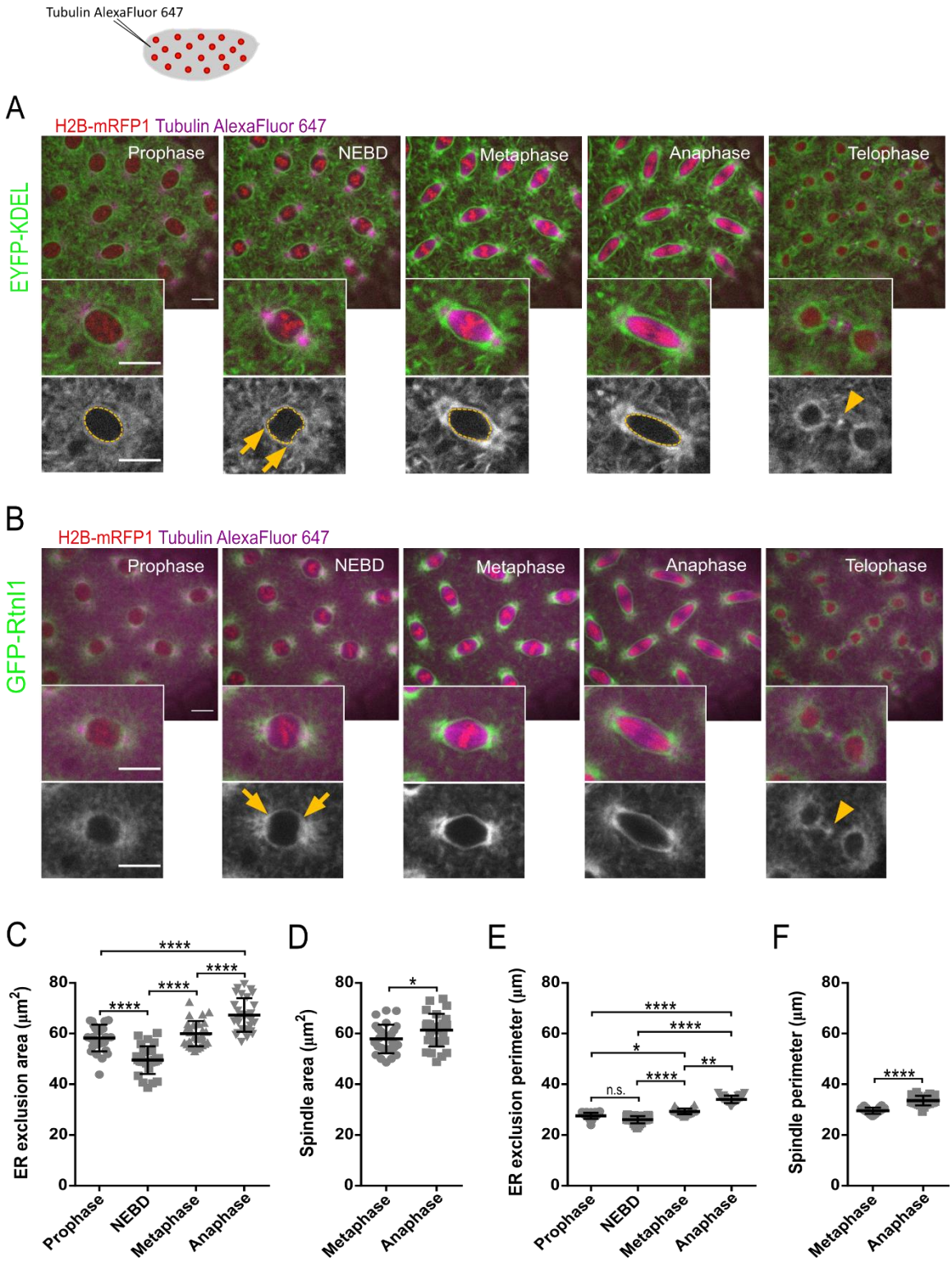
Tubulin AlexaFluor 647
A
H2B-mRFP1 Tubulin AlexaFluor 647
EYFP-KDEL
Prophase
NEBD
Metaphase
Anaphase
Telophase
B
H2B-mRFP1 Tubulin AlexaFluor 647
GFP-Rtnl1
Prophase
NEBD
Metaphase
Anaphase
Telophase
C
ER exclusion area (µm²)
D
Spindle area (µm²)
E
ER exclusion perimeter (µm)
F
Spindle perimeter (µm)
Prophase
NEBD
Metaphase
Anaphase
n.s.

Figure 2.9. The ER forms an envelope surrounding the mitotic spindle in syncytial embryos. *(A-B) Stills of embryonic divisions monitoring ER dynamics at different mitotic stages. ER was visualized with either EYFP-tagged ER retention sequence (EYFP–KDEL, green, A) or the ER-shaping protein Reticulon-like protein 1 (GFP–Rtnl1, green, B). Chromatin is labelled with Histone H2B–mRFP1 (red) and spindle microtubules with microinjected porcine Tubulin labeled with Alexa Fluor 647 (magenta). Grey panels depict ER labelling alone. Scale bar is 10 µm. Arrowheads show events of ER abscission at telophase. (C, D, E, F) Quantifications of the ER exclusion area (C), spindle area (D), ER exclusion perimeter (E), and spindle perimeter (F), measured at the middle plane of the nuclei using the ERsp-EYFP–KDEL strain; sample size: N = 7 embryos per condition, n = 5 nuclei per embryo; statistical analysis was performed using one-way ANOVA, multiple comparisons, P value adjusted to multiple comparisons (Tukey) (C), Kruskal–Wallis (Dunn's multiple comparisons test) (E), or two-sided paired t test (D, F); *P < 0.05, **P < 0.01, ****P < 0.0001, n.s., nonsignificant, P > 0.05.*

2.2.5. ER dynamics in interphase- and metaphase-arrested nuclei

Next, we wanted to understand if the observed ER shape changes, which closely follow those of the spindle body, arise from dynamic changes of ER membranes themselves. To this end, we performed Fluorescence Recovery after Photobleaching (FRAP) experiments using the GFP-tagged transmembrane protein Rtnl1, which labels membranes that are being re-shaped and tubular ER that is being formed (Espadas et al. 2019). To circumvent the inherent changes in intensity and morphology during the rapid cell cycle, which would impede proper FRAP analysis, we have performed all the experiments in artificially arrested embryos.

We first monitored the ER dynamics in interphase, by preventing mitotic entry with ectopic addition of the Cdk inhibitor p27 (Oliveira et al. 2010). Upon p27 injection, we observed that the ER maintained an interphase-like localization (Fig. 2.10.). For FRAP studies, we bleached two different arrested nuclei in distinct regions of interest (ROIs) and imaged their fluorescence recovery over time (Fig. 2.10., red circles, Movie 2.10.). We observed a high turnover of ER membranes, with half-times of recovery in the order of seconds. ER membranes localized proximal to the spindle poles are more dynamic compared to those localized at the equator (Fig. 2.10., $t_{1/2}$ poles: 11.4 ± 6.2 s; $t_{1/2}$ equator: 21.0 ± 8.6 s). However, the GFP–Rtnl1 mobile fraction at the poles is lower compared to the virtually complete recovery at the equator in interphase-arrested embryos (poles: 0.81 ± 0.06; equator: 0.9 ± 0.08). Our observations are in contrast to previous studies in yeast and mammalian cells, which detected a significant immobile fraction for Rtn1/Rtn4a (Shibata et al. 2008). These findings suggest a high level of reshaping of ER membranes in *Drosophila* embryos.

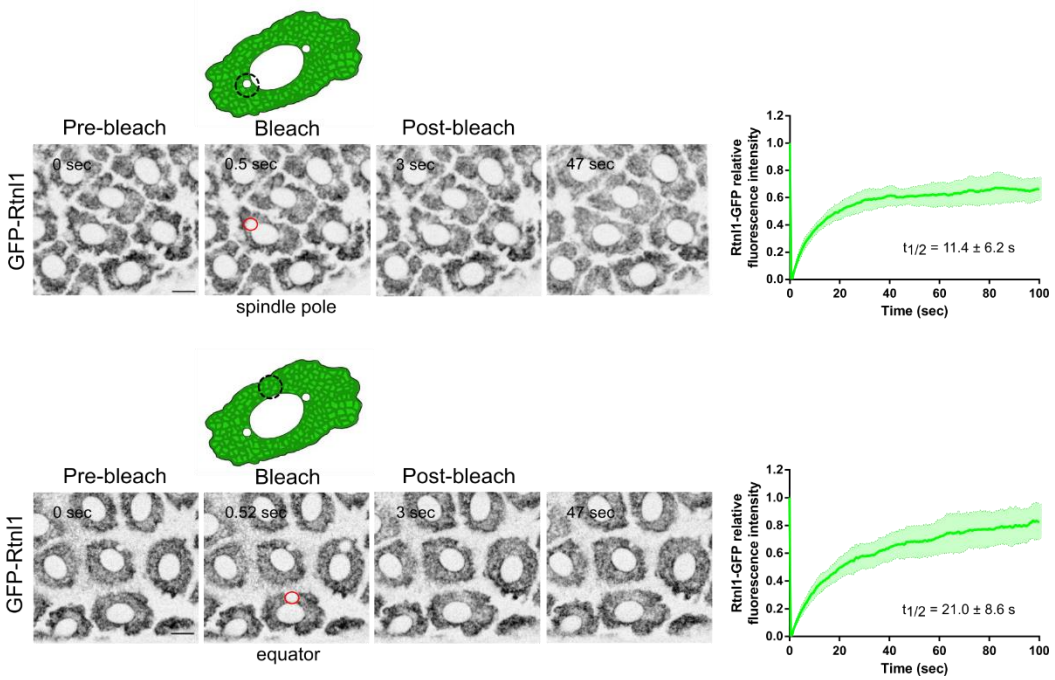

Figure 2.10. ER dynamics in interphase-arrested nuclei. *Fluorescence recovery after photobleaching (FRAP) of the membrane ER marker GFP–Rtnl1, upon microinjection of the Cdk inhibitor p27 to induce an interphase-arrest. Recovery of Rtnl1–GFP fluorescence intensity was quantified upon bleaching of the ER at the spindle pole region (upper panel; N=6 embryos, n=12 nuclei) or at the equator (lower panel; N=5 embryos, n=9 nuclei). In all experiments, average half-times of recovery are depicted, presented as mean ± SD. Scale bars are 10 µm.*

Changes in ER morphology are coupled to the cell cycle and are dependent on Cyclin A activity during *Drosophila* embryonic nuclear divisions (Diaz et al. 2019). To address if this morphological re-organization is accompanied by a change in the dynamic behavior of ER membranes, we repeated the same analysis in embryos arrested in metaphase. For this, embryos were microinjected with UbcH10^{C114S} (Oliveira et al. 2010). We bleached two different nuclei in distinct ROIs and imaged their fluorescence recovery over time (Fig. 2.11., red circles). Signal recovery of the ER shaping protein Rtnl1 was in the same order of magnitude as in interphase (Fig. 2.11., Movie 2.11.). Upon metaphase-arrest, we detected a slightly slower recovery of Rtnl1–GFP intensity at spindle poles compared to the equatorial region (poles: 14.4 ± 3.2 s; equator: 11.8 ± 2.1 s).

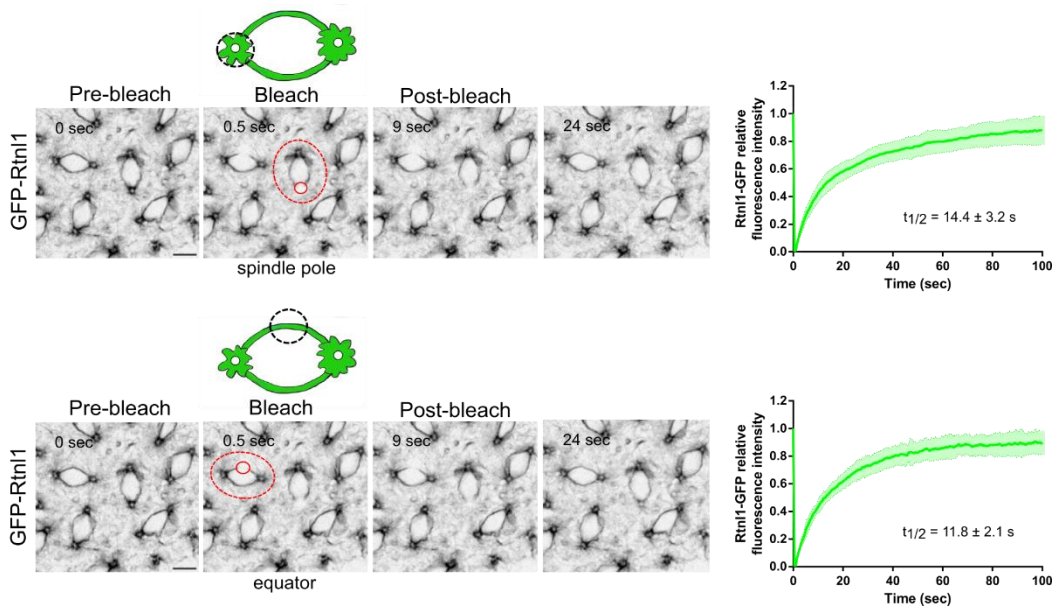

Figure 2.11. ER dynamics in metaphase-arrested nuclei. *FRAP analysis of GFP–Rtnl1 in embryos upon microinjection with the dominant-negative version of the E2 ubiquitin-ligase UbcH10 (UbcH10^{C114S}) to induce a metaphase-arrest. Graphs depict recovery of Rtnl1–GFP intensity upon bleaching at the spindle pole region (upper panel, N=9 embryos, n=17 nuclei) or at the equator (bottom panel, N=9 embryos, n=15 nuclei); red circles depict the area bleached in each experimental condition. In all experiments, average half-times of recovery are depicted, presented as mean ± SD. Scale bars are 10 µm.*

Interestingly, we observed virtually complete recovery of intensity in both cases (mobile fractions at pole: 0.92 ± 0.06; equator: 0.95 ± 0.04). This signal dynamics observed is slightly lower, but within the same magnitude of the turnover observed for the luminal ER reporter Lys–GFP–KDEL (Fig. 2.12., $t_{1/2}$: 3.81 ± 0.46 s, Movie 2.12.), which reflects ER shape changes occurring in the time scale of free diffusion events inside the ER. This is in agreement with previous studies, where rapid recovery of intensity was reported for both *Drosophila* oocyte fusome and syncytial embryos

expressing Lys–GFP–KDEL (Snapp et al. 2004; Frescas et al. 2006). These findings suggest that the ER in mitosis is undergoing significant reorganization.

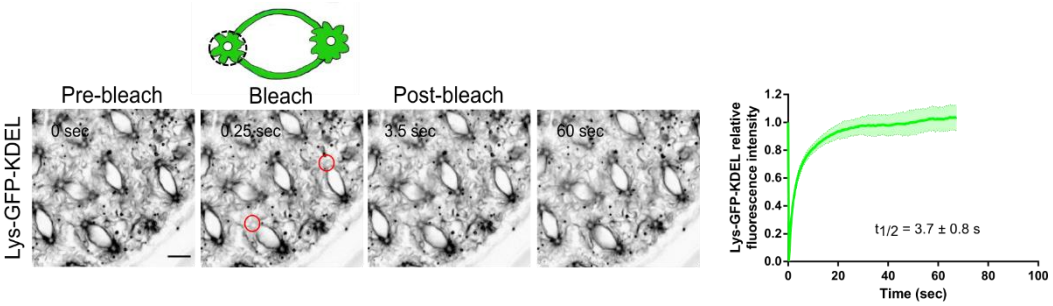

Figure 2.12. ER dynamics in metaphase-arrested nuclei measured using a luminal ER marker. *FRAP analysis of Lys–GFP–KDEL in metaphase-arrested embryos (UbcH10^{C114S}). Graph depicts recovery of Lys–GFP–KDEL after photobleaching at spindle poles (N=5 embryos, n=2 nuclei per embryo). In all experiments, average half-times of recovery are depicted, presented as mean ± SD. Scale bars are 10 µm.*

2.2.6. Microtubule depolymerization leads to fast ER membrane deformation

Given the spatial proximity of the ER to the mitotic apparatus and its dynamic remodeling during metaphase, we next investigated how this structure changes upon MT depolymerization.

The ER compartment is known to depend on the MT cytoskeleton to maintain its morphology. The association between the MT cytoskeleton and ER network has been well established (Terasaki, Chen, and Fujiwara 1986; Waterman-Storer and Salmon 1998; Frescas et al. 2006). Previous studies demonstrated that the ER is organized by MTs, in particular by astral MTs and centrosomes in the *Drosophila* syncytial embryo (Smyth et al. 2015).

We thus monitored the kinetics of ER deformation in embryos with isolated sister chromatids, in the presence/absence of an intact spindle. We used the same experimental layout described before to ensure that both mitotic spindle and ER assembly were unperturbed, allowing us to compare this with the previous experiments described in Figures 2.1. and 2.3.

This revealed that upon induced separation of sister chromatids the ER maintains an external compartment (envelope) surrounding the spindle region (Fig. 2.13., t=10:00). However, once MTs were depolymerized upon microinjection of colchicine, we observed deformation of ER membranes concomitant with the clustering of sister chromatids (Fig. 2.13., bottom panel, t=10:30-29:00). Of note, the kinetics of ER deformation is very fast, with most reduction of area occurring within the first 2 minutes after colchicine addition (Fig. 2.13., graph on the right, after colchicine). Moreover, ER deformation does not invade chromosomal-proximal regions and direct ER-chromatid contacts are rarely observed (Fig. 2.13., t=29:00).

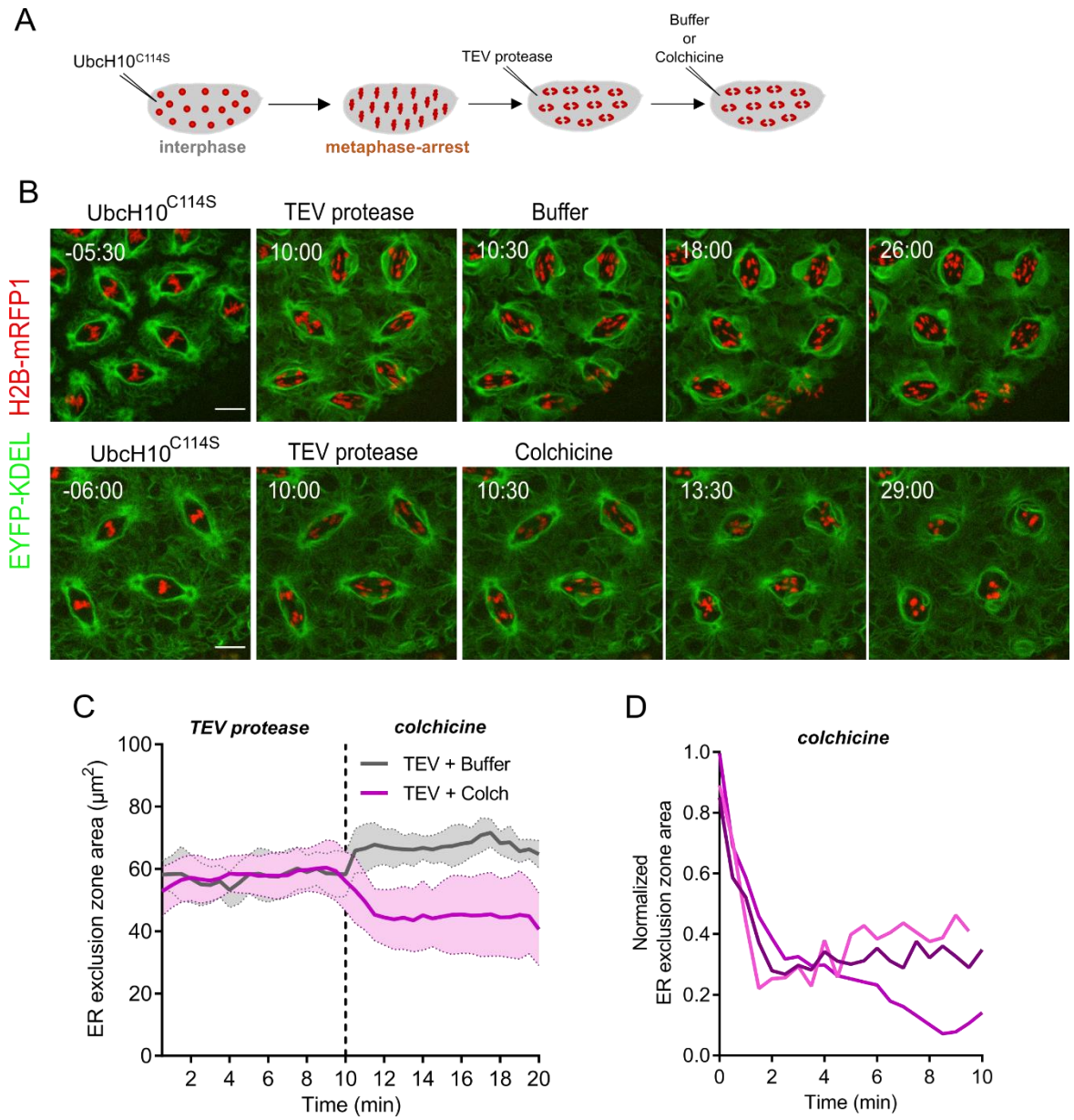

Figure 2.13. MT depolymerization after separation of sister chromatids leads to ER membrane deformation. *(A) Scheme shows the experimental layout to separate sister chromatids as described before. (B) Embryos expressing solely a TEV-cleavable cohesin complex recombined with H2B-mRFP1 (red), and the ER reporter EYFP-KDEL (green) were used to follow chromatin and ER morphology upon buffer*

(TEV+Buffer) or colchicine (TEV+Colch). Image processing was performed using Fiji software. Scale bar is 10 µm. Time is in min:sec and is relative to microinjection with TEV protease. (C) Graph shows ER exclusion area over time measured after microinjection with TEV and subsequent microinjection with either buffer (TEV+Buffer, grey) or colchicine (TEV+Colch, purple) (mean±SD; dotted line depicts the time point of microinjection of colchicine. (D) Graph shows ER exclusion area normalized to the maximum and minimum values after microinjection with colchicine, for 3 independent embryos (mean). Graphs were generated in GraphPad Prism.

Hence, ER deformation may contribute to the initial stages of centromere clustering. Nevertheless, given its kinetics of disassembly, it is unlikely to be the major structure generating the force driving centromere movement beyond the initial time points (after spindle disassembly). It thus remains unclear which cellular processes drive centromere/chromatid clustering in the absence of MTs. Nevertheless, my results highlighted a tight association between a highly dynamic ER network and the MT spindle during mitosis that has been underexplored at the functional level. Therefore, we next sought out to investigate a potential contribution of ER membranes in mitosis, as described in chapters 3 and 4.

Discussion

Our experiments showed that spatially separated sister chromatids move towards the center of the nuclear region upon MT depolymerization. In the first time points after colchicine addition, we found a drastic decay of both spindle area and sister chromatid area; we also found a second phase of chromatid movement once MTs could no longer be detected. These results suggest that MT depolymerization by addition of colchicine could itself contribute to the clustering of sister chromatids, at least at the initial time points. Moreover, we observed progressive MT depolymerization where interpolar MTs disassembled first, and more stable k-fibers (kinetochore MTs) later. This suggested that MT sliding is no longer present although sister chromatids were still attached to spindle MTs.

One possible interpretation of these results is that MT depolymerization induced by colchicine could, on its own, initiate sister chromatid movement into the center. Nonetheless, sister chromatids did not stop their movement even when spindle MTs could not be detected (second phase movement). Therefore, the effect of MT depolymerization is not sufficient to explain the further clustering of sister chromatids we observed. We think that the second phase of chromatid movement must be caused by alternative forces, which are not generated by spindle MTs. By generating acentric fragments through laser ablation, we tested the role of centromeres in the clustering of sister chromatids. We found that acentric fragments still clustered together with intact sister chromatids at the center upon MT depolymerization. Thus, this indicates that attachment to spindle MTs is not the factor contributing to sister chromatid movement upon MT depolymerization. These results support the idea that an external compartment surrounding the spindle apparatus may promote the movement of sister chromatids to the center even when spindle MTs are absent.

We predicted that additional factors could also contribute or could be involved, at least to some extent, in clustering of sister chromatids upon MT depolymerization. Namely, because a similar collapse event was reported for the visco-elastic matrix known to embed the spindle upon colchicine treatment (Lince-Faria et al. 2009; Yao et al. 2012). Colchicine treatment in *Drosophila* S2 cells led to retraction of Megator (a protein that is part of the spindle matrix) and loss of its fusiform shape (Lince-Faria et al. 2009). Moreover, a later study focusing on this proteinaceous spindle matrix showed that depolymerization of MTs with colchicine prior to metaphase resulted in contraction and coalescence of the spindle matrix around the chromosomes in *Drosophila* syncytial embryos (Yao et al. 2012). Even though we did not test the role of spindle matrix, it would be interesting to test whether clustering of sister chromatids occurs upon disruption of this matrix.

Additionally, it was shown that the NE does not confer a diffusion barrier, since different molecular mass labelled dextrans (70, 500 and 2000 kDa) entered the nuclear space after NEBD (Yao et al. 2012). In this study, the authors observed a 60% reduction in the length of the spindle matrix upon MT depolymerization (Yao et al. 2012). In agreement with this, we observed a reduction in the distance between centrosomes in a similar range (58.3%). Since contraction and coalescence of the spindle matrix by removal of spindle MTs were documented, this could explain to some extent the clustering effect on sister chromatids (if this visco-elastic matrix contracts it could in turn induce the clustering effect on semi-flexible objects such as sister chromatids).

Although spindle collapse could explain a reduction in the distance between centrosomes, why it would promote a reduction in the distance between separated sister chromatids was still not understood. So, by

following the behavior of external elements surrounding the spindle upon MT depolymerization, we found that the ER is the major external membrane compartment localized immediately after the spindle. This was supported by the observation that the lamin B-nuclear envelope has very low intensity both at metaphase in normal mitotic divisions and under the metaphase-arrest condition (UbcH10^{C114S}).

In addition, we observed that ER forms a membranous envelope surrounding the spindle and that the area of the ER exclusion zone closely follows the one of the spindle both in metaphase and anaphase. Since the organization of the ER is associated to the mobility of proteins in ER membranes or within the ER lumen (Snapp et al. 2004), we assessed transmembrane and luminal ER protein dynamics. In interphase-arrested embryos (p27), we observed a high turnover of the ER transmembrane protein Rtnl1 at spindle poles, although a lower mobile fraction was found in this region of the ER.

Since changes in ER morphology are coupled to the cell cycle during *Drosophila* embryonic nuclear divisions (Diaz et al. 2019), we repeated the same analysis in embryos arrested in metaphase (UbcH10^{C114S}). We found a slightly slower recovery at spindle poles compared to the equatorial region. These findings suggest that Rtnl1 has high mobility in the ER membrane in mitosis.

However, our results are not in agreement with what has been reported previously in other studies. For example, Rtn1p and Yop1p are immobile proteins in the ER membrane in *S. cerevisiae* and Rtn4a in mammalian cells (Shibata et al. 2008). In addition, we also found that GFP-Rtnl1 mobility in the ER membrane is similar to other ER resident proteins (Snapp et al. 2004). To further clarify this, we could perform FRAP assays using other endogenously tagged ER-shaping proteins (e.g., Atlastin-

GFP, generated in our study) or ER resident proteins such as Sec61α-GFP and compare their mobility with the results for GFP-Rtnl1 within the syncytial embryo.

On the other hand, Lys-GFP-KDEL is a luminal ER marker and seems to freely diffuse in the ER lumen in our experimental conditions. This result is in agreement with a previous study where FRAP assays revealed that Lys-GFP-KDEL fluorescence intensity recovers rapidly within the fusome (a cellular structure formed in *Drosophila* ovarian cysts) (Snapp et al. 2004).
However, with the two different ER reporters used in our FRAP assays (endogenously tagged GFP-Rtnl1 and Lys-GFP-KDEL), we were not able to infer if the recovery of intensity can be interpreted as ER remodeling events or simply reflects protein mobility on the ER. The detection of ER-shaping/remodeling events *in vivo* in *Drosophila* embryos would probably have to be done using electron microscopy or even by correlative light and electron microscopy (CLEM). CLEM would be advantageous because it allows to target the EM analysis to specific subcellular timepoints using the signal from fluorescent proteins (ER proteins).

In any case, the fact that ER membranes are associated to MTs and their obvious envelope-like shape around the spindle encouraged us to test their behavior upon MT depolymerization. We saw that ER membranes become deformed upon MT depolymerization, and that the kinetics of deformation correlates with spindle disassembly. Because of this, we believe that the resulting membrane configuration is unlikely to cause the movement or clustering of sister chromatids to the center. Nevertheless, we speculated that continuous remodeling of ER membranes might be important to maintain the membranous compartment surrounding the spindle in the context of syncytial divisions. Thus, we decided to explore the role of ER membranes during syncytial nuclear divisions. To do this,

we tested different strategies to disrupt this large organelle in an acute and timely controlled manner, as presented in the following chapter.

Materials and methods

Fly stocks

Fly expressing His2B-mRFP (Schuh, Lehner, and Heidmann 2007), EYFP-KDEL (LaJeunesse et al. 2004) and for induction of sister chromatid separation (Rad21^{ex15}, polyubiq-H2B-RFP, tubpr-Rad21$^{(550\text{-}3TEV)}$-myc10 (4c)) (Pauli et al. 2008; Oliveira et al. 2010) have been previously described. UAS-Lamin B-GFP and UASp-RFP-KDEL lines were crossed with V32-Gal4 and G302-Gal4 maternal drivers, respectively, to induce the expression of these reporters in syncytial embryos. For this, flies were maintained at 25°C throughout the course of the experiment (from the moment when the cross was established to the selection of the F1 progeny). A detailed list of the stocks can be found in Table 2.

Table 2. Fly stocks used in this section

Genotype	Reference
Avic\GFP$^{EYFP.sqh.Tag:SS(hCALR).Tag:ER(KDEL)}$ (EYFP–KDEL)	BDSC #7195 (LaJeunesse et al. 2004)
w[*]; P{w[+mC]=His2Av-mRFP1}II.2 Expresses RFP-tagged His2Av in all cells under the control of His2Av, on the second chromosome)	BDSC #23651
w;; Rad21^{ex15}, polyubiq-H2B-RFP, tubpr-Rad21$^{(550\text{-}3TEV)}$-myc10 (4c)*	Described in (Oliveira et al. 2010), named here #629
w; EYFP-ER; Rad21^{ex15}, polyubiq-H2B-RFP, tubpr-Rad21$^{(550\text{-}3TEV)}$-myc10 (4c)*	Derived from BDSC #7195 and #629 (see above)
y[1] w[*]; P{w[+mC]=UAS-Lam.GFP}3-3 Expresses GFP-tagged Lamin under UAS control. (UAS-Lamin–GFP)	BDSC #7376

w; P{UASp-RFP.KDEL}10/TM3, Sb1 (RFP-KDEL)*	BDSC #30909
y[1] w[*]; P{w[+mC]=UAS-Lam.GFP}3-3; P{UASp-RFP.KDEL}10/TM3, Sb1	Derived from BDSC #7376 and #30909
w[*]; P{w[+mC]=matalpha4-GAL-VP16}V2H (called V32-Gal4 here)	BDSC #7062
w[*]; P{w[+mC]=matalpha4-GAL-VP16}V2H; 629 (called V32-Gal4 here)	Derived from BDSC #7062 and #629
w;; G302-Gal4/MKRS *Maternal germline-specific driver*	Gift from M. Bettencourt-Dias, originally from Daniel St. Johnston; Gurdon Institute, UK.

BDSC – Bloomington *Drosophila* stock center

Protein purification

UbcH10^{C114S} and TEV protease were purified as previously described (Oliveira et al. 2010; Piskadlo, Tavares, and Oliveira 2017).

Microinjections

Microinjections were performed as previously described in (Carmo, Araújo, and Oliveira 2019), using an Eppendorf FemtoJet Microinjector controller and commercially available needles (Eppendorf™ Femtotips™ Diameter (Metric) Inner: 0.5 µm, 11883991). Briefly, dechorionated (7% Sodium hypochlorite, VWR) 1–1.5 h old embryos were aligned and glued onto a #1.5 coverslip (24x40 mm), dried at room temperature for 13 min, and subsequently covered in halocarbon oil. Buffer/protein/chemicals were microinjected at the following concentrations: buffer (10 mM HEPES, 100 mM KCl, 1 mM $MgCl_2$, 10% glycerol), UbcH10^{C114S} (20-30 mg/ml), TEV protease (12-18 mg/ml), Colchicine (1 mM, in buffer).

Microscopy

Time-lapse movies of live embryos were obtained using Confocal Z-series stacks with a Yokogawa CSU-X Spinning Disk confocal, mounted on a Leica DMi8 microscope, with a 63x 1.3NA Glycerine immersion objective, using the 488, 561 and 637 nm laser lines and an Andor iXon Ultra EMCCD 1024x1024 camera. The system was controlled with Metamorph software (Molecular Devices). For the sequential microinjection experiments, we used 30 sec time points and a total of 10 min for each time-lapse acquisition, with 0.4-0.5 µm z-step size and 15 slices.

Quantitative imaging analysis

Measurement of the area occupied by separated sister chromatids

Post-acquisition image analysis was performed with Fiji-ImageJ software. A macro script was designed with the help of the IGC Imaging facility (Nuno Pimpão Martins) to estimate the area of sister chromatid dispersion, either using the H2B-mRFP1 channel (labeling sister chromatids) or the Cid-GFP (labelling centromeres). This macro defines the outermost chromatids/centromeres occupancy using either the H2B-mRFP1 or Cid-EGFP chanel, respectively, and it measures the area occupied by sister chromatids at each time point. The position of sister chromatids over time was projected for a representative nucleus using the kymograph generator plugin in Fiji. For data visualization and generation of graphs Prism (RRID:SCR_002798, GraphPad, La Jolla, CA) was used.

Kinetics of spindle disassembly

Using the β-Tubulin-RFP chanel, a gaussian blur filter (2 pixels) was applied followed by thresholding (default) to measure spindle area at each time point (using the wand tool) with Fiji software. Absolute values of spindle area were then analyzed using Prism by fitting a non linear regression, exponential one phase decay, to estimate the kinetics of

spindle disassembly and of the chromatid (centromere) movement. The rate constant (K) was calculated in min^{-1}.

Generation of acentric chromosome fragments by laser ablation

A Micropoint UV-laser ablation module (Andor) optimized for a 63x objective and coupled to the spinning disk microscope was used. The Micropoint coordinate system was calibrated prior to the experiment for precise laser ablation. Embryos were microinjected with $UbcH10^{C114S}$ to induce a metaphase-arrest. After 5-6 min, a chromosome arm protruding from 1-2 metaphase plates was ablated using a small circle ROI (3x3 µm), with 10-15% attenuation plate (Micropoint-laser power) and 3 pulses.

ER shape measurements

To quantify the perimeter and aspect ratio of the ER exclusion zone upon MT depolymerization, max intensity projections of 3 slices for the ER channel corresponding to the middle plane of each nucleus were used. All the measurements were performed after gaussian blur filtering (2 pixels) with the *otsu* algorithm and applying a threshold on the ER channel in Fiji. The wand tool was used to estimate ER shape measurements.

Area and perimeter of ER exclusion zone and spindle

To quantify the area and perimeter of the ER exclusion zone and of the spindle, a single z slice corresponding to the middle plane of each nucleus was used. All the measurements were performed using the segmented line tool in Fiji (yellow shapes in Fig. 2.8.A, insets in gray LUT), for each channel (ER, spindle) separately.

ER dynamics – FRAP assays

FRAP experiments were performed using Andor's Mosaic system with a 470 nm laser, using 0.25 sec (Lys–GFP–KDEL expressing embryos) or

0.5 sec time points (Rtnl1-GFP expressing embryos) and a single z plane was acquired. Collective movement of spindles in the embryo was corrected using the *stackreg* plugin in Fiji (Thévenaz et al. 1998). The first time point was used as a prebleach reference of fluorescence intensity and bleaching was set to the second time point. Raw fluorescence intensity values were extracted from the time-lapse movies with the plot z-axis profile option in Fiji. FRAP recovery curves were analyzed using the easyFRAPweb tool. Briefly, three different regions of interest (ROIs) were measured over time: the bleached region (circle with 42 pixels diameter), the entire ER compartment of a single nucleus (variable size), and the background (region outside the embryo, circle with 95 pixels diameter). ROI positioning was kept constant throughout the time series (this led to occasional inflow of Lys–GFP–KDEL-labeled vesicles, which may slightly overestimate the mobile pool in this strain).

Chapter 3

Development of tools to acutely disrupt the ER

Author contribution:

All the experiments presented in this chapter were performed and analyzed by Margarida Araújo. The experiments were designed by Margarida Araújo, Ivo A. Telley and Raquel A. Oliveira. Alexandra Tavares and Diana Vieira prepared and purified some of the proteins used in this study.

3.1. Introduction

To explore the role of ER membranes during syncytial nuclear divisions in *Drosophila* embryos, we sought to find a strategy to specifically disrupt the ER in this system. Since syncytial nuclear divisions are quite fast, we conceived that the ER-disruptive effect would have to be induced in an acute and timely controlled manner. We reasoned that perturbing ER re-shaping could be a targeted way of inducing an ER membrane-specific disruptive effect without compromising other organelles.

The ER forms a network of membrane sheets and tubules. Within specialized regions of the ER, various important functions take place namely folding, processing and transport of secretory and transmembrane proteins, store for intracellular calcium and lipid biosynthesis (Bahmanyar et al. 2014; Carlton, Jones, and Eggert 2020). At mitotic entry, the ER undergoes drastic reorganization becoming enriched around spindle poles (Bergman et al. 2015; Diaz et al. 2019). At the end of anaphase, the ER is targeted to chromosomes providing the necessary material for nuclear envelope reformation (Schlaitz et al. 2013; Barton et al. 2014; Roubinet, White, and Baum 2021).

The formation and maintenance of ER network morphology are regulated by ER-shaping proteins. Amongst them, REEP (Receptor Expression Enhancing proteins) proteins have been shown to play a role in clearance of ER membranes from chromatin during mitosis (Schlaitz et al. 2013; Kumar et al. 2019). Knockdown of REEP3/4 in human cells leads to defects in NE structure, displaying several membrane structures inside the nucleus (Schlaitz et al. 2013). More importantly, it was shown that these NE defects arise during mitosis due to impaired clearance of ER membranes from the spindle and chromatin regions. The authors from this study showed that REEP3 and REEP4 have a MT binding domain and can bind directly with MTs (Schlaitz et al. 2013; Kumar et al. 2019).

Preventing REEP4-MT association leads to ER accumulation on metaphase chromatin, elegantly showing that the MT binding domain of REEP4 is important for the ER clearance function (Schlaitz et al. 2013). *Drosophila* has two REEP proteins – ReepA and ReepB – which are widely expressed and localize to the ER (Fig. 3.1.C-D) (Yalçın et al. 2017). Sequence alignments between *Drosophila* and mammalian REEP protein sequences indicated that ReepA is the single ortholog of the mammalian REEP1-REEP4 in *Drosophila*. *Drosophila* has two orthologs of the mammalian REEP5 and REEP6, ReepB and CG4960 (Fig. 3.1. A).

Another family of evolutionarily conserved transmembrane proteins called Reticulons (Rtns), are responsible for membrane fission and thereby are involved in the formation of the ER tubular network. In *Drosophila*, Reticulon-like protein 1 (Rtnl1), localizes strongly in axons. Knockdown of Rtnl1 leads to expansion of ER sheets and increases the ER stress response (O'Sullivan et al. 2012).

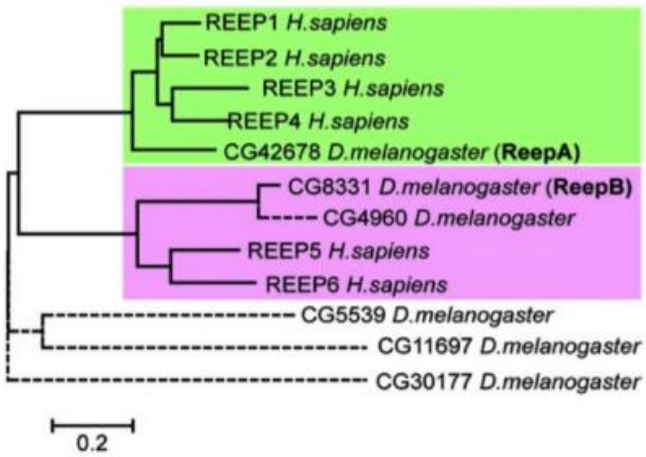

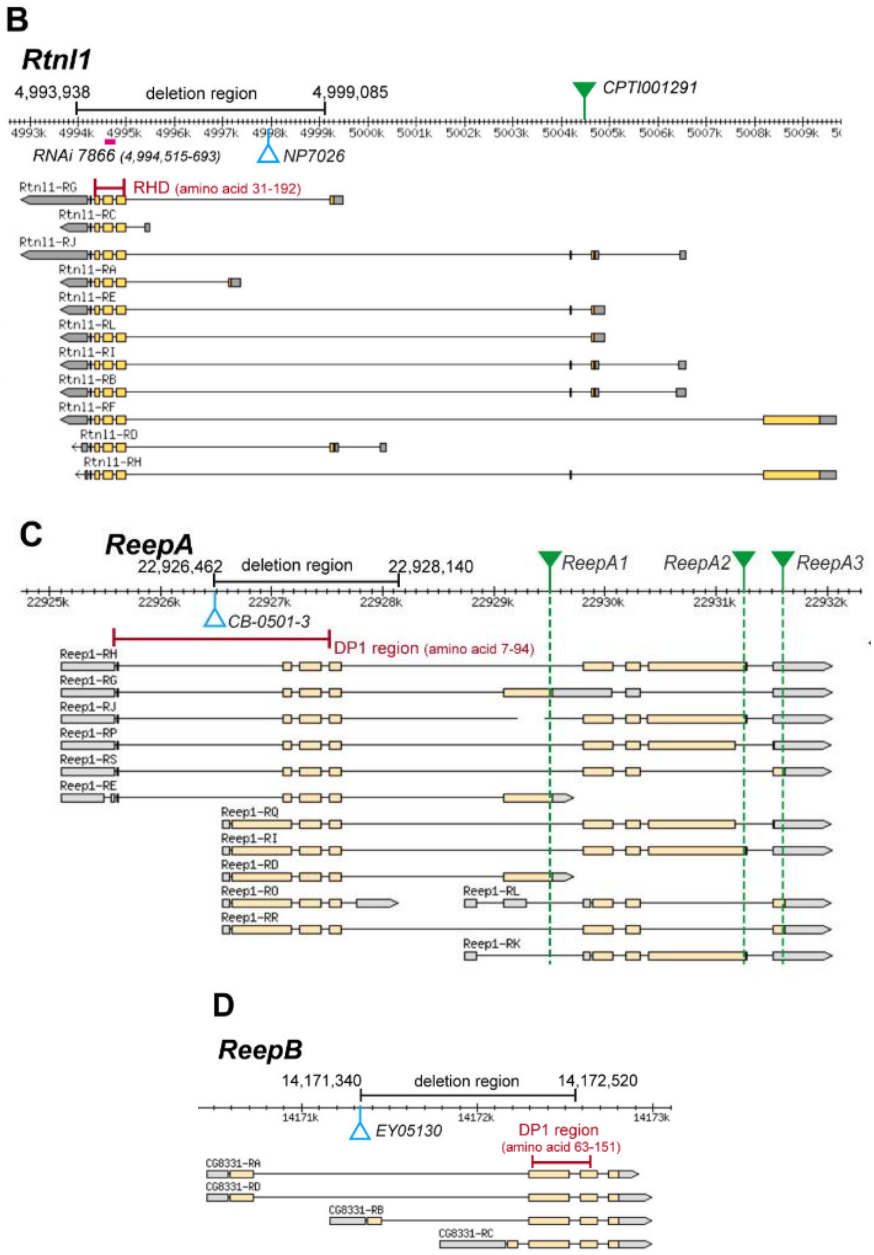

Figure 3.1. Drosophila Rtnl1 and REEP genes. *(A) Dendrogram based on sequence alignment of Drosophila and human REEP proteins. (B) Rtnl1 genomic and transcript map. (C) ReepA genomic and transcript map. (D) ReepB genomic and transcript map. Adapted from (Yalçın et al. 2017).*

Overexpression of Rtns has been previously shown to induce ER fragmentation in tissue culture cells (S. Wang et al. 2016; Espadas et al. 2019). Rtns and REEPs stabilize high membrane curvature by their transmembrane segments and are responsible for the formation of ER tubules (Fig. 3.3. A) (Voeltz et al. 2006; J. Hu et al. 2008). Modulating the levels of these proteins promotes the transition between the different ER structures: overexpression of Rtns and REEPs in *S. cerevisiae* and mammalian cells favors the formation of tubules over sheets (Voeltz et al. 2006; Shibata et al. 2010). In contrast, tubules become less abundant when phospholipid synthesis is increased or in the absence of these proteins (Voeltz et al. 2006; Shibata et al. 2010). Knockout of *C. elegans* Rtn RET-1 and its associated protein YOP-1 results in ER morphology defects during mitosis (Audhya, Desai, and Oegema 2007). Moreover, inhibition of *Xenopus* RTN4A by anti-RTN4A antibodies impairs NE assembly (Kiseleva et al. 2007). On the other hand, overexpression of Rtns was also shown to cause ER fragmentation both in human cells and *Drosophila* larval neurons (Wang et al. 2016; Espadas et al. 2019).

Membrane fusion is a key event to form an interconnected network of ER membranes. ER membrane fusion is mediated by membrane-anchored GTPases called Atlastins (ATLs) in metazoans and Sey1 and related proteins in yeast and plants (J. Hu et al. 2009; Orso et al. 2009b). Three closely related ATLs can be found in mammals: ATL1 is highly expressed in neurons, while ATL2 and ATL3 are expressed in different cell types (Zhu et al. 2003). *Drosophila* ATL is highly similar to and can functionally replace human ATLs (Wu et al. 2015). *Drosophila* has three different ATL isoforms – atl-PA, -PB and PC. During early oogenesis, ATL is expressed in the posterior compartment of the egg chamber and in the membrane and cytoplasm of nurse cells (Fig 3.2. A) (Lee et al. 2009). At oogenesis stage 9 it is found in the anterior cytoplasm of the oocyte. ATL protein is strongly expressed at stage 10 in follicle cells. During embryogenesis,

ATL is also highly expressed (Fig. 3.2. C). In the fly adult brain, it is ubiquitous, being strongly expressed in a subset of dopaminergic neurons (Fig. 3.2. A) (Lee et al. 2009).

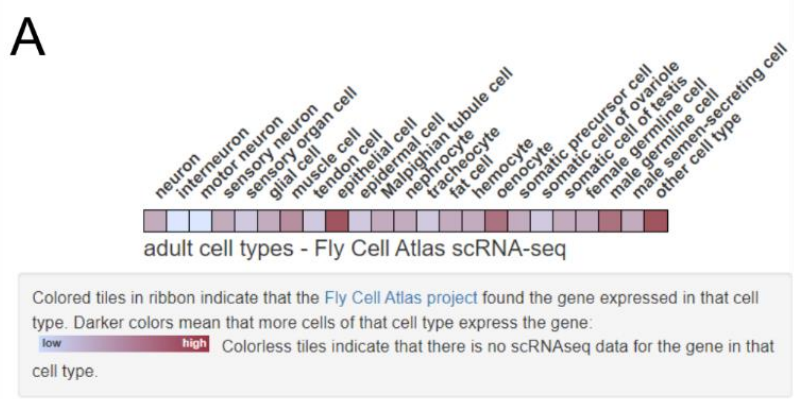

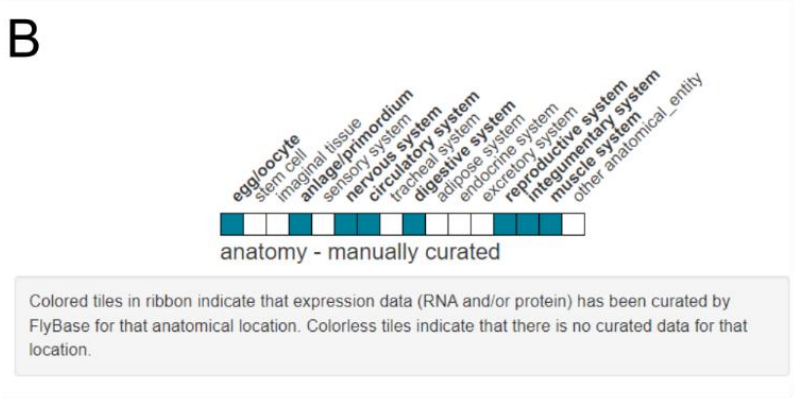

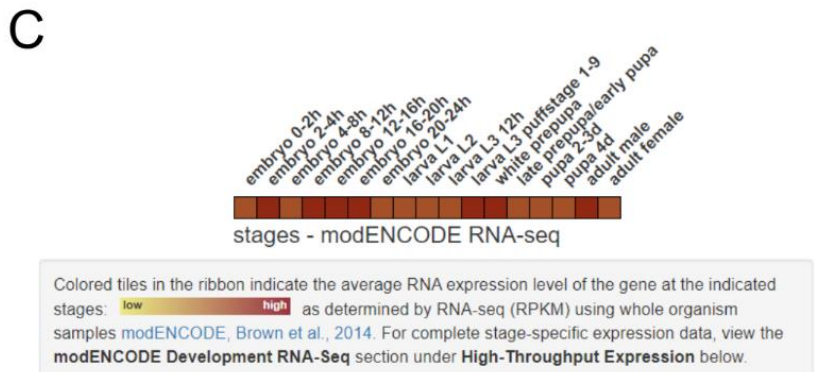

D

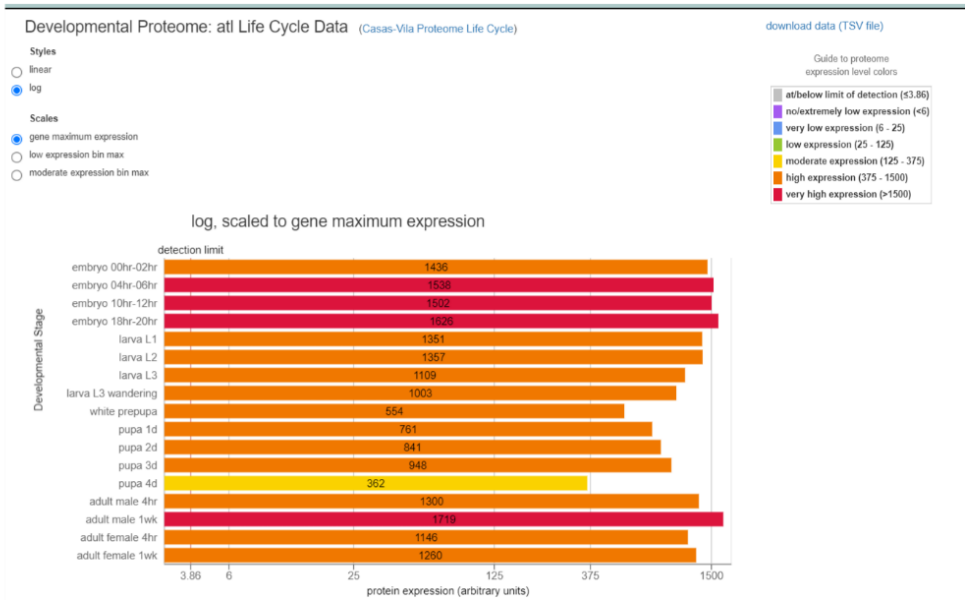

Figure 3.2. Expression data for Drosophila Atlastin. *Atl expression in different adult cell types (A), different anatomical regions (B) and in different developmental stages (C). (D) Atl is highly expressed during embryogenesis. Retrieved from flybase.org.*

ATLs contain a cytoplasmic GTPase domain, followed by a helical bundle, a membrane-inserted region, and an amphipathic helix (Fig. 3.3. B). Biochemical studies and the generation of crystal structures indicated that ATL molecules localized in different membranes dimerize through their GTPase domains undergoing a conformational change. This pulls the two membranes together and fuses them (reviewed in (J. Hu and Rapoport 2016). Fusion of membrane tubules forms three-way junctions (Goyal and Blackstone 2013; S. Wang et al. 2016), whichare thought to be stabilized by the lunapark protein (Lnp) (S. Wang et al. 2016; N. Wang and Rapoport 2019), another conserved membrane protein with two transmembrane segments (Fig. 3.3. C).

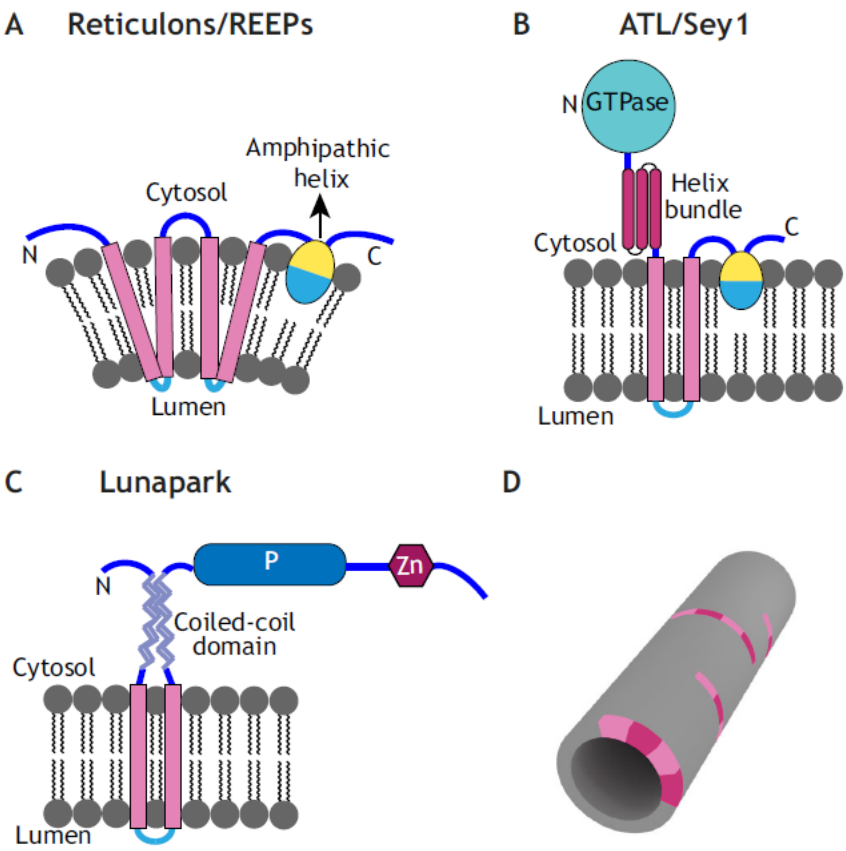

Figure 3.3. Structure of ER-shaping proteins. *These transmembrane proteins are inserted in the ER membrane. Adapted from (Wang and Rapoport 2019).*

Because the ER executes various important intracellular functions, it is difficult to understand the effect of perturbations in such an important organelle. For this reason, it was challenging to disrupt such a major organelle inside cells up to this date. In previous studies, depletion (either by knockout or knockdown) or overexpression of ER-shaping proteins were used to disrupt the ER network in human cells. ATL depletion, for example, was previously demonstrated to delay the targeting of inner nuclear membrane proteins that are synthesized in the peripheral ER (Pawar et al. 2017). ATL deleted cells showed reduced protein mobility in

the ER, revealing an unprecedented role of ER shaping in the early secretory pathway and export from the ER (Niu et al. 2019).

Recently, strategies to either disrupt or relocalize this large organelle inside cells were used. Approaches relying on relocalization of ER membranes have brought insight on the importance of ER clearance during mitosis. This strategy revealed that membranes need to be excluded from chromatin to allow for proper chromosome compaction and organization (Champion et al. 2019), and, more recently, also to avoid erroneous kinetochore-MT attachments due to entrapment of chromosomes by membranes (Ferrandiz et al. 2022). Many of these approaches took advantage of the ER-shaping proteins to modulate ER morphology.

Here we describe several attempts to establish a reliable system to induce acute perturbation of the ER, making use of critical proteins for ER biogenesis (e.g., Rtnl1 and Atlastin).

3.2. Strategies to induce acute disruption of ER membranes

3.2.1. Ectopic addition of His_6-tagged and GFP-tagged *Drosophila* Rtnl1 protein

Our first approach built on prior studies that demonstrated that overexpression of Rtns induces ER fragmentation in tissue culture cells (Wang et al. 2016; Espadas et al. 2019) . To adapt this strategy for an acute effect, we attempted to induce ER fragmentation by microinjection of purified *Drosophila* Reticulon-like protein 1.

Step 1 – Expression and Purification of His6-tagged Rtnl1

We followed the conditions from a previously established protocol for purification of Reticulon-like protein 1 (Rtnl1) (Espadas et al. 2019), the most widely expressed Reticulon in *D. melanogaster*. Purification of membrane proteins is known to be particularly challenging due to their

high hydrophobic nature. Hence, solubilization of full-length membrane proteins is commonly achieved by the addition of detergent during lysis and purification. This protocol relies on high concentration of TritonX-100 during lysis (4%) to enhance solubilization (Fig. 3.4. A-D).

We expressed His6-Rtnl1, isoform B from a previously cloned construct (pET28a-His6-Rtnl1B plasmid kindly provided by Andrea Daga, University of Padova, Italy). This construct has a hexa-histidine tag on the N-terminal region of *Drosophila* Rtnl1B protein sequence (molecular weight = ~29 kDa). The His6-Rtnl1B protein was expressed in bacteria using a standard protocol and was purified in HEPES-based buffer supplemented with Triton X-100 and 10% glycerol to maintain protein stability (for detailed protocol see Materials and Methods).

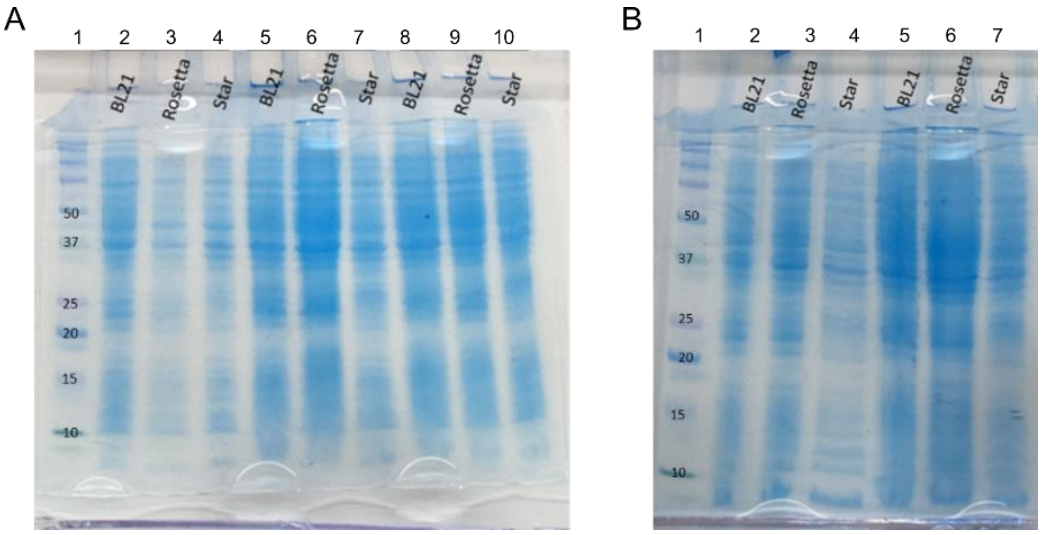

Figure 3.4. Expression of D. melanogaster histidine tagged Rtnl1 isoform B protein (Rtnl1B). *(A) 1 – Protein marker Kaleidoscope (Biorad), 2-4 – non-induced cultures of E. coli BL21, Rosetta and Star strains, respectively. 5-7 – induced cultures of E. coli BL21, Rosetta and Star strains, respectively with 0.5 mM IPTG for 3h at 37°C. 8-10 – induced cultures of E. coli BL21, Rosetta and Star strains, respectively with 0.5 mM IPTG for 3h at 18°C. (B) 1 – Protein marker Kaleidoscope (Biorad),*

2-4 – induced cultures of E. coli BL21, Rosetta and Star strains, respectively, with 0.5 mM IPTG overnight (10h) at 18°C. 5-7 - induced cultures of E. coli BL21, Rosetta and Star strains, respectively, with 0.5 mM IPTG overnight (>12h) at 18°C.

To optimize protein in expression, we tested several *E. coli* strains. Although we could not see a clear increase in the expression of His6-Rtnl1B (Fig. 3.4.) we observed that *E. coli* BL21 and Rosetta strains showed an expression pattern higher than the Star strain at 37°C compared to the expression at 18°C. Because the *E. coli* Rosetta strain showed a slightly higher expression pattern, we expressed His6-Rtnl1B using this strain at 37°C and proceed with the purification.

Briefly, the bacterial cells were harvested and lysed in 4% Triton X-100. The lysate was cleared by centrifugation and loaded on a column containing a resin with Ni^{2+}. The His6-tag present in the protein sequence has affinity to and, thus, binds to the resin in the column. The protein was primarily purified using an Äkta purifier (an automated flow pressure system) by affinity chromatography. Then, the His6-tag protein can be further purified and eluted from the resin by the addition of a buffer containing imidazole, which will compete with the Ni^{2+} and will release the His6-tagged protein. We performed a gradient to gradually decrease the concentration of Triton X-100 (from 4% to 0.1%). After that, we performed a gradient to gradually increase the concentration of imidazole in the elution step (from 20 mM to 500 mM imidazole, during 30 minutes at a constant flowrate of 1 ml/min). This approach allowed us to separate the protein extract in different fractions, ideally to remove contaminants and have higher purity.

In some subsequent purifications, we used a different method where the lysate was incubated with Ni^{2+} Sepharose beads (2-3 ml of beads, for details see Materials and Methods) instead of a column, which also relies on the same principles described above. We also gradually decreased the concentration of detergent in the washing step, by performing sequential washes of the beads with decreasing concentration of Triton X-100 in the wash buffer. With the conditions optimized in the previous purification using Äkta purifier, we established the imidazole gradient step by step for the purification method using Sepharose beads. The major difference between these two methods is that buffers are in contact with the protein extract inside the column through flow pressure in the Äkta purifier system, whereas in the method involving the use of Sepharose beads all the purification steps are performed manually by adding each specific buffer step by step.

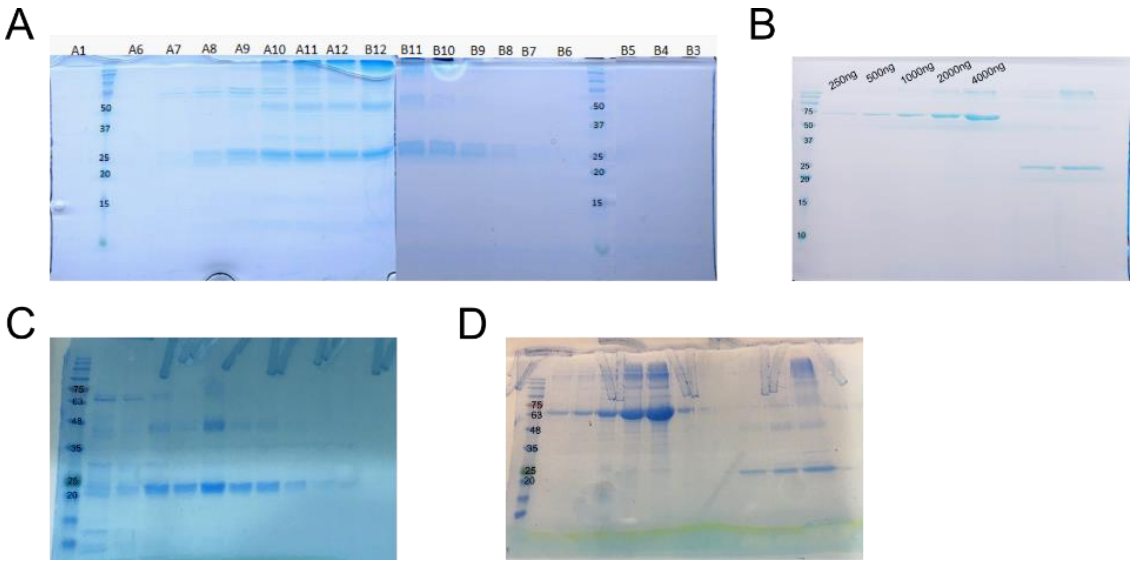

Figure 3.5. Purification of D. melanogaster Rtnl1 protein (Rtnl1B). *(A) Affinity chromatography from the His_6-Rtn1B eluted using an Imidazole gradient (0 to 500 mM) using an Äkta purifier (GE Healthcare). The molecular weight of His_6-Rtnl1B is ~29 kDa. (B) Different BSA standard*

concentration samples (250, 500, 1000, 2000 and 4000 ng, reconstituted in the same buffer as Rtnl1B) were used as references of protein amount (loaded 2 µl in each lane). Then 2 and 4 µl of the purified and concentrated protein sample were loaded to estimate His_6-Rtnl1B protein concentration after size exclusion chromatography and concentration. (C) Purification of His_6-Rtnl1B (29 kDa) using Nickel Sepharose beads (GE Healthcare) through affinity chromatography in a gravity column. (D) Serial dilutions of BSA (0.5, 1, 2, 5 and 10 µg/µl) reconstituted in the same buffer, were loaded as standard concentrations (2 µl of each) to estimate His_6-Rtnl1B protein concentration (2, 4 and 20 µl sample) after and concentration.

After the elution step, the fractions containing lower proportion of contaminants were dialyzed (overnight at 4°C) to exchange the elution buffer (containing high concentration of imidazole) into the protein storage buffer (10 mM HEPES pH 7.8, 100 mM KCl, 1 mM $MgCl_2$, 10% glycerol). Using these two methods, we were able to collect a protein of the expected Rtnl1B size (Fig. 3.5. A and C, ~29 kDa). The protein contaminant profile was similar in the two methods and, although we could detect their presence in the final sample, protein contaminants were in lower proportion compared to the protein of interest (Fig. 3.5. A and C).

Step 2 – Protein concentration

Since our goal was to disrupt ER membranes acutely, we reasoned that we would have to add ectopically a high concentration of Rtnl1, to achieve an acute ER disruptive effect during mitosis. After purification, protein yield for full length transmembrane proteins is usually low, due to their hydrophobic nature and lower solubility. Because of this we concentrated the protein fractions containing lower proportion of contaminants using a centricon column (10 kDa molecular weight cuttoff). The centricon column concentrates the protein sample by decreasing the sample volume at each cycle of centrifugation. From the purification method using the Äkta

purifier we pooled three fractions of 1 ml and concentrated to a final volume of 500 µl (Fig. 3.5. A-B). While using the method dependent on Sepharose beads we concentrated fractions of 5-10 ml to a final volume of 500 µl (Fig. 3.5. C-D), using the same centricon concentration column as described above. Therefore, we concentrated the sample 10-15 times using Sepharose beads as protein purification method.

Step 3 – Estimation of protein concentration

We subsequently used various approaches to estimate protein concentration. We used the BCA protein assay kit to determine protein concentration and estimated the concentration of Rtnl1B to be ~2 mg/ml (Appendix, Methods to estimate protein concentration) (Fig. 3.5. B). We attempted to use the canonical Bradford dye-binding assay, measuring absorbance at 595 nm after incubation with the dye. Protein concentration estimated using the Bradford assay was 3.5 mg/ml, compared to a rougher estimation method in which we loaded 2 µl of different BSA standard concentrations to use as references for protein amount in a 12% SDS gel (Fig. 3.5. B, increasing concentration of BSA). Even though BSA is not a membrane protein, this would allow us to compare defined protein concentrations with our purified protein sample. Then, we analyzed the intensity of the bands in the SDS gel, comparing the two lanes of purified Rtnl1B (2 and 4 µl) with the known BSA standard concentrations leading to an estimation between 6.67 and 10 mg/ml. Given the slight inconsistencies among the different methods, it was difficult to estimate the exact concentration. Nevertheless, we concluded that our concentrated sample should have between 2-10 mg/ml of purified protein.

Step 4 – Functional tests

Microinjection with His_6-Rtnl1 during interphase caused a very strong ER disruption phenotype. We observed a clear change in ER topology, indicated by a diffuse appearance of the ER (Fig. 3.6., Rtnl1B, t=12:30). We also observed an arrest of the cell cycle in most embryos, while in control embryos (microinjection with the storage buffer subjected to the same exchange and concentration procedure) no effect was observed (Fig. 3.6., Buffer versus cytATL).

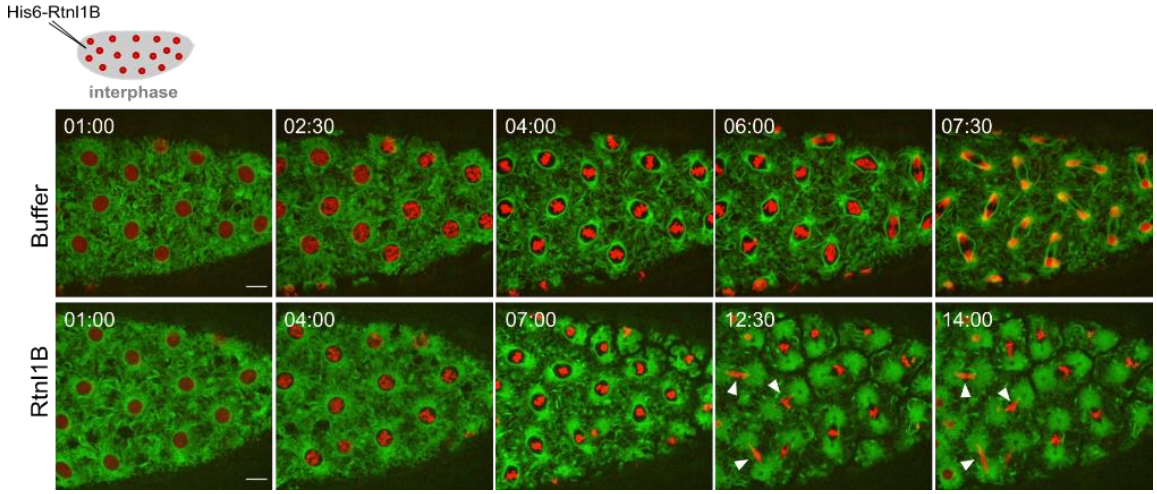

Figure 3.6. Representative images of a time-lapse upon microinjection with Rtnl1B or buffer as control. *Microinjection was performed during interphase in embryos expressing EYFP-KDEL (green) and H2B-mRFP1 (red). A noticeable effect on the ER can be seen after 7 minutes (Rtnl1B, t=07:00-14:00, white arrowheads). Scale bars are 10 µm. Time is in min:sec and is relative to microinjection with buffer/Rtnl1B.*

This was very interesting to us, because nuclei still entered in mitosis and chromosomes were able to congress and align at the equator but became arrested at metaphase.

Mitotic duration and the progression from metaphase to anaphase depend on the SAC (Foley and Kapoor 2013), which delays chromosome

segregation in response to unattached kinetochores. To understand if the arrest at metaphase we observed was dependent on SAC activation, we used a line expressing the checkpoint protein Mad2-EGFP and examined its localization under our experimental conditions. We observed transient Mad2-EGFP foci at kinetochores in control embryos (Fig. 3.7., Buffer, t=05:00, green foci over chromatin). This Mad2-EGFP signal eventually disappeared (Fig. 3.7., Buffer, t=06:00), with nuclei progressing into anaphase and exiting mitosis normally (Fig. 3.7. A, Buffer, t=06:30-08:30). Upon microinjection with Rtnl1, we found an increase in Mad2-EGFP signal, which initially appeared at kinetochores and later became accumulated at spindle poles compared to the control condition (Fig. 3.7. A, Rtnl1B, t=09:30-22:00; B, Rtnl1B – magenta). These nuclei displaying accumulation of Mad2-EGFP became arrested at metaphase as observed in our first experiments. Interestingly, our time-lapse images suggest that Mad2-EGFP signal is being transported from the kinetochores towards the poles. So, although poleward transport of Mad2-EGFP is not affected, its disassembly at spindle poles into the cytoplasm seems to be impaired. However, how Rtnl1-driven disruption of ER membranes leads to checkpoint activation and accumulation of Mad2-EGFP remain undetermined.

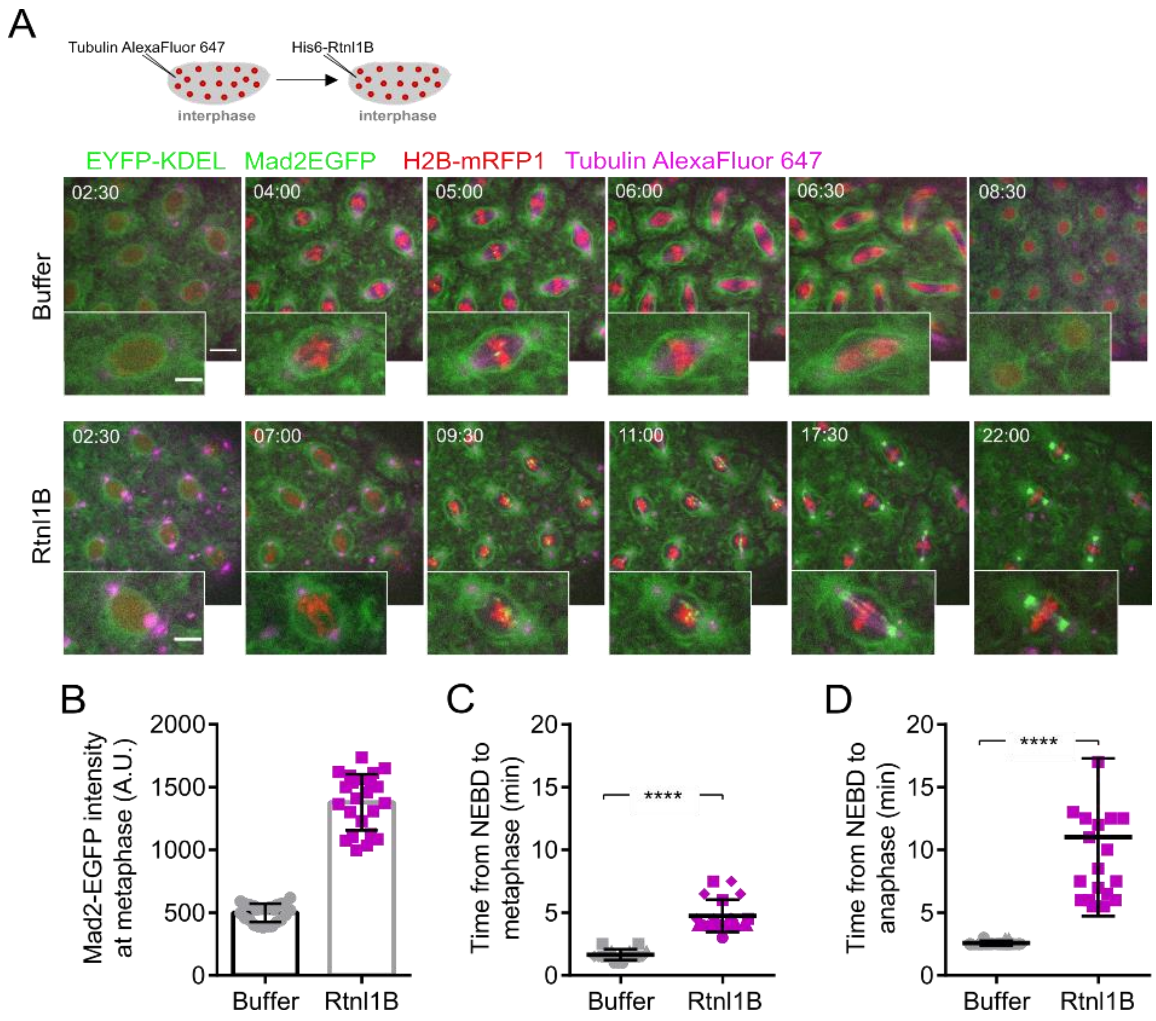

Figure 3.7. The checkpoint protein Mad2-EGFP accumulates at spindle poles upon microinjection with Rtnl1B. *(A) Microinjection with Tubulin AlexaFluor 647 (magenta) was immediately followed by a second microinjection with Buffer/Rtnl1B during interphase. Embryos expressing EYFP-KDEL (green), Mad2-EGFP (green) and H2B-mRFP1 (red) were used. Scale bars are 5 µm. Time is in min:sec and is relative to microinjection with buffer/Rtnl1B. (B) Mad2-EGFP fluorescence intensity measured at metaphase. Time from NEBD to metaphase (C) and to anaphase (D). NEBD time point was measured using the entry of labled tubulin into the nucleus. Sample size was 5 different embryos, measuring 5 nuclei per embryo. ****p<0.0001, unpaired t-test, two-tailed. Graphs and statistical analysis were performed in GraphPad.*

Strong accumulation of Mad2 suggested that checkpoint inactivation was affected upon microinjection with Rtnl1. These experiments, and all the controls performed at the time made us believe that we had in hands a good tool to acutely induce ER fragmentation in living embryos.
However, subsequent purifications of the Rtln1 protein led to significant inconsistencies between the various purification protocols used and the obtained phenotype when injected into embryos. In particular, we observed that the extension of ER disruption did not correlate with protein amount estimated to be in the prep. This inconsistency made us question whether the disruption effect was driven by additional confounding variables other than Rtln1 insertion.

To better monitor the amount of protein being inserted in the ER in each experiment, we cloned and purified a fusion version with a fluorescent GFP-tag (His_6-GFP-Rtnl1). This construct has a predicted molecular weight of ~50 kDa. Briefly, since we expected that this fusion protein would have higher solubility than the His6-tagged one, we used 1% Triton X-100 during lysis for His6-GFP-Rtnl1. The purification was done using the Äkta purifier, with a similar protocol (described in detail in Materials and Methods) but with an additional step using size exclusion chromatography to increase purity (Fig. 3.8. A-B). Since all fractions contained a similar ratio of co-purified contaminants and the protein of interest (Fig. 3.8. A, lanes 18-28), we pooled all fractions, and we performed similar buffer exchange (into storage buffer) and injected in a size exclusion chromatography column. After this step, fractions with lower proportion of contaminants were pooled and concentrated using a centricon (Fig. 3.8. B, lanes 17 and 24).

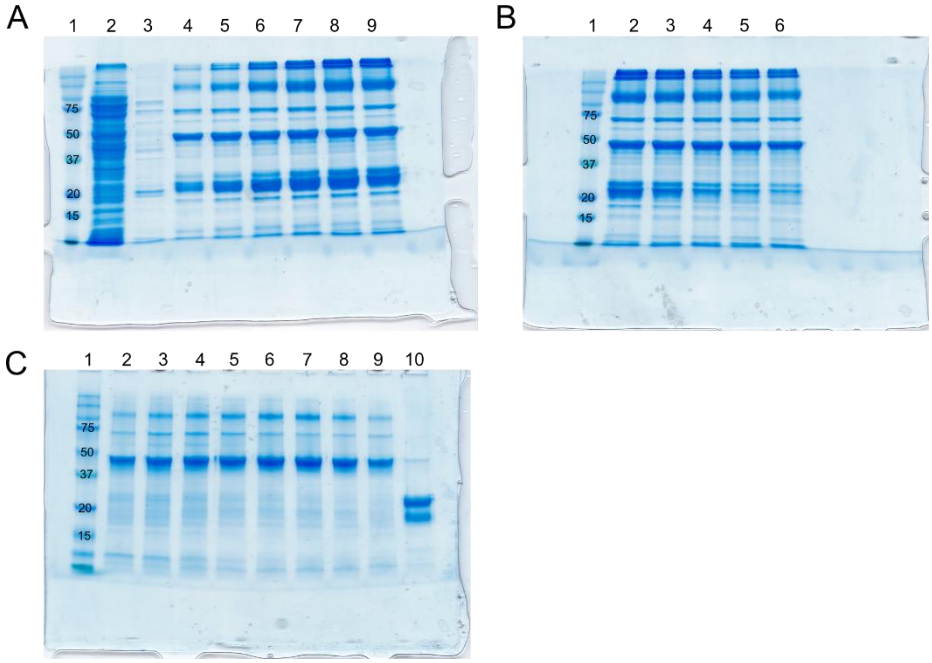

Figure 3.8. Purification of His6-GFP-Rtnl1. *(A) Affinity chromatography (Ni^{2+} resin column) followed by a gradient of imidazole (50 mM to 500 mM). 1 – Precision Plus Protein™ Kaleidoscope protein marker. 2 – flow through and washes from the column. 3 – wash. 4-9 – Fractions eluted with the imidazole gradient. (B) Fractions eluted with higher imidazole concentration. Fractions 4-9 (A) and 2-6 (B) were pooled together and the buffer exchanged into storage buffer. (C) Size exclusion chromatography of His6-GFP-Rtnl1. Fractions 2-9 were pooled together and further concentrated using a centricon column. Final concentration of the sample was 8 mg/ml. 10 – GFP tag.*

Microinjection into syncytial embryos revealed that His_6-GFP-Rtnl1 co-localized with the ER marker RFP-KDEL, which supports that injected protein is being actively integrated into the ER. Even after several rounds of nuclear divisions, the His_6-GFP-Rtnl1 maintained a very similar ER

localization (Fig. 3.9., green) comparable with the endogenously GFP-tagged Rtnl1 Trap line (Fig. 2.9.).

However, despite obvious integration, GFP-Rtln1injection did not show any ER disruption phenotype (Fig. 3.9., yellow color in the merged image).

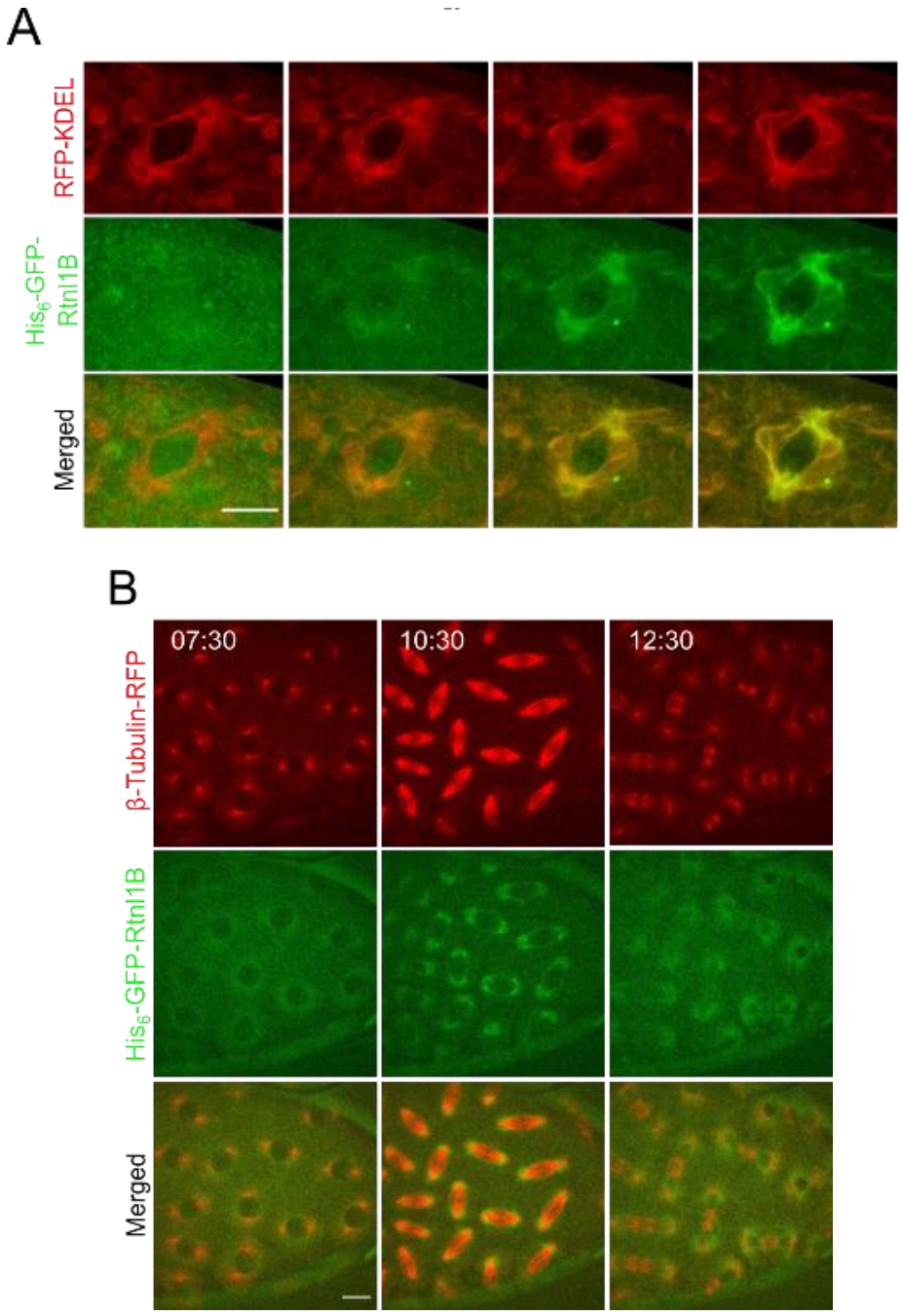

Figure 3.9. Purified His6-GFP-Rtnl1 localizes to the ER in syncytial embryos. *(A) Embryos expressing RFP-KDEL using the maternal driver G302-Gal4 were arrested at metaphase using UbcH10^{C114S} (30 µg/µl) and after 5 minutes, injected with His6-GFP-Rtnl1 (1 µg/µl). (B) A few minutes after microinjection, the GFP-tagged Rtnl1 starts to co-localize with the ER marker RFP-KDEL (t=05:00, yellow color in the merged channel). (C) Embryos expressing β-Tubulin-RFP were injected with His6-GFP-Rtnl1 (1 µg/µl) during interphase and imaged throughout several cycles. Scale bars are 10 µm. Time is in min:sec and is relative to microinjection with buffer/Rtnl1B.*

Although we cannot exclude that GFP-tagged Rtnl1 could be less effective at tubule constriction/fragmentation, as demonstrated previously in COS 7 cells after ectopic expression (Espadas et al. 2019), it further supported that high doses of Rtnl1 were insufficient to cause ER disruption.

Given these inconsistencies, we tested what could be the confounding variable that was giving different results depending on sample preparation for both GFP-Rtln1 and his-Rtln1 samples. After several tests, we concluded that the concentrated samples were retaining a high percentage of detergent, despite their transition into a low triton injection buffer. This was evidenced by analysis of the protein concentration on a nanodrop, that consistently gave us an overestimation of protein concentration when compared to other protein estimation methods (e.g., 57 mg/ml on a Nanodrop vs 2-10 mg/ml across various other methods, see above). Subsequent tests revealed that Triton X-100 absorbs at 280 nm (Fig. 3.10.), possibly due to the presence of a phenyl group in its structure. Hence, abnormal retention of detergent could be the source for higher absorbance obtained on Nanodrop. We attributed this to a

significant assembly of micelles surrounding the protein (highly hydrophobic), that remain attached to it to stabilize the transmembrane domains even after buffer exchange.

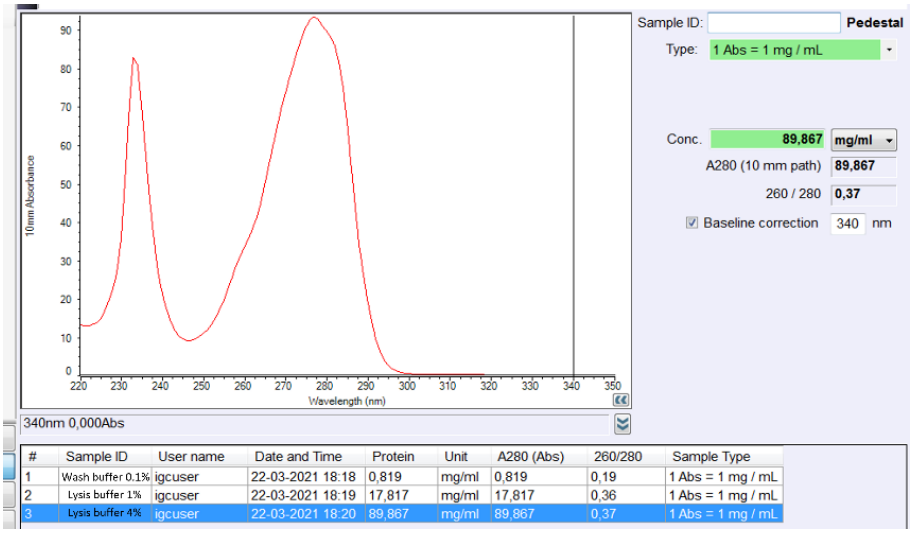

Figure 3.10. Buffers containing increasing Triton X-100 concentrations show absorbance at 280 nm in Nanodrop. *We analyzed the Nanodrop profile for each Triton X-100 concentration using wash buffer without Triton X-100 as blank. According to this estimation method, Wash buffer with 0.1% Triton X-100 = 0.82 mg/ml and Lysis buffer with 1% = 17.8 mg/ml. Higher concentration of Triton X-100 leads to higher absorbance at 280 nm (Lysis buffer 4%).*

Given the suspicion for high detergent concentration in our samples, we assumed that the previously observed phenotype could be caused by this detergent used during the purification protocol in addition to (or rather than) from Rtnl1 itself.

Therefore, we tested three different concentrations of Triton X-100 in storage buffer (10 mM HEPES, 100 mM KCl, 1 mM $MgCl_2$, 10% glycerol): 0.1, 4 and 10%. The storage buffer with 0.1% Triton X-100 was our

expected theoretical concentration (since the elution buffer contained 0.1% Triton X-100). While the storage buffer with 0.1% Triton X-100 did not have a detectable effect on the ER and in cell cycle progression (Fig. 3.9. B), microinjection with storage buffer containing 4% Triton did show some delay in mitosis but did not alter ER morphology significantly (Fig. 3.11. C). Microinjection with storage buffer containing 10% Triton into embryos resulted in the same strong ER disruption phenotype as we had seen before with the “concentrated” Rtln1 protein sample upon microinjection (Fig. 3.11. D).

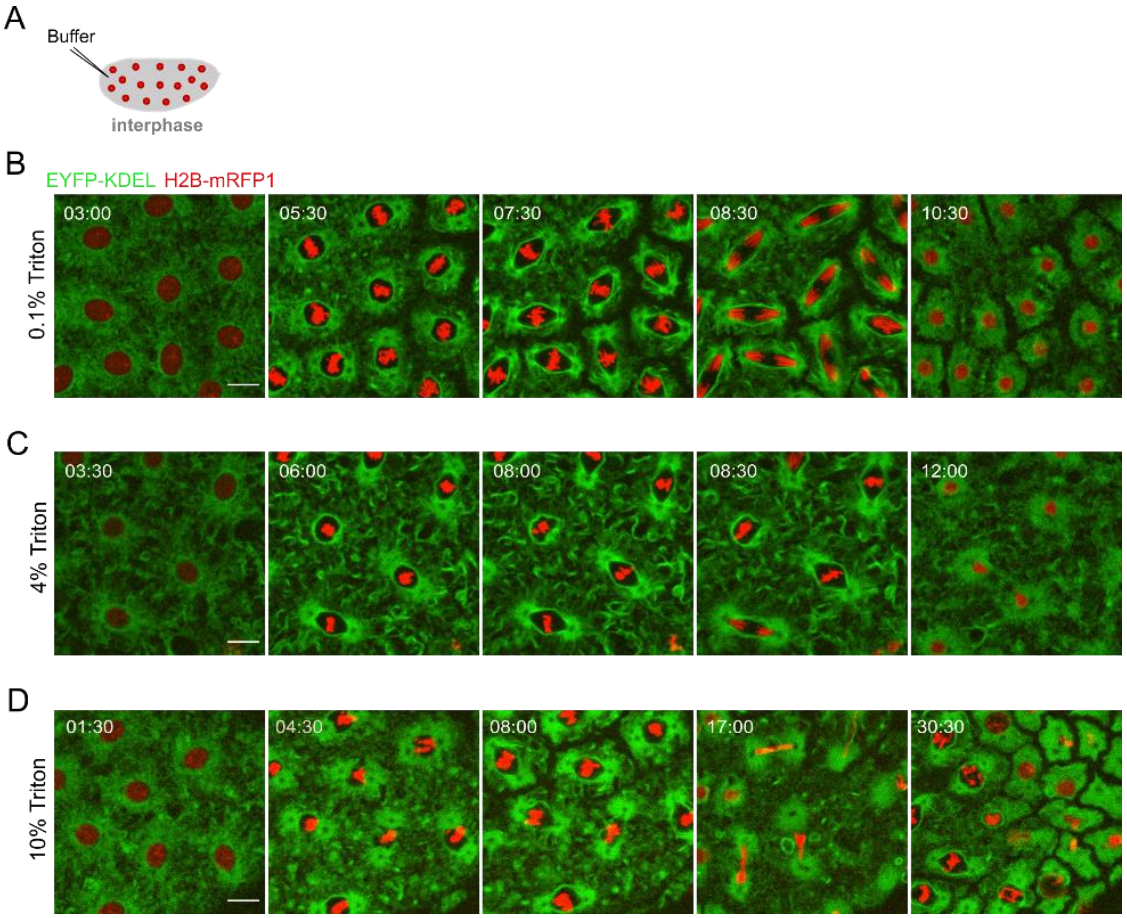

Figure 3.11. Microinjection with storage buffer containing increasing Triton X-100 concentration in syncytial embryos.

Embryos expressing EYFP-KDEL (green) and H2B-mRFP1 (red) were used. (A) Microinjection of storage buffer containing different concentrations of Triton X-100 (0.1, 4 and 10% Triton) was performed during interphase. (B) Microinjection with 0.1% Triton X-100 did not lead to any detectable effect on the ER. (C) Microinjection with 4% Triton X-100 has a mild effect on the ER and leads to a slight delay in mitosis. (D) Microinjection with 10% Triton X-100 shows a similar phenotype on the ER as seen before with "Rtnl1 concentrated sample", accompanied by a considerable arrest at metaphase (t=08:00) and chromosome segregation errors (t=17:00). Sample size for each Triton X-100 concentration tested was 2 independent embryos per condition. Scale bars are 10 µm.

Given the similarities of the phenotypes observed with high Triton doses and our Rtnl1 microinjections, and the likelihood for high detergent accumulation in the Rtnl1 sample, we concluded that the ER disruption phenotype could be caused (at least partially) by the detergent in the sample.

We attempted to circumvent these technical issues using another detergent (Brij-35) and performed the same purification protocol with Ni^{2+} beads. The Brij-35 is also a non-ionic detergent like Triton X-100, but that has a Critical Micelle Concentration (CMC) lower (0.09 mM, or 0.011%, w/v) than Triton X-100 (0.24 mM, or 0.155%, w/v). In contrast to Triton X-100, Brij-35 does not absorb at 280 nm but at 225 nm instead. Therefore, we would be able to monitor protein and detergent concentration independently and in an accurate manner. In this purification, we used 4% Brij-35 during lysis and we performed sequential washes with decreasing concentration of Brij-35 (4%, 2%, 1%, 0.1%, 0.01% Brij-35 and without Brij-35). The final washing step was performed without Brij-35. For elution of the protein, we used 100, 200, 300 and 500 mM imidazole and collected each fraction. A first fraction was eluted in 10 ml, followed by a second

fraction eluted in 5 ml. A sample from each fraction was collected to run a 12% SDS gel and identify the ones containing the purified protein. After this assessment, the fractions eluted with 100 mM imidazole containing the purified protein were dialyzed into storage buffer (100 mM HEPES pH 7.8, 10 mM KCl, 1 mM $MgCl_2$, 10% glycerol) and concentrated using a centricon (10 kDa cutoff). This purified protein sample was concentrated to 2.5 µg/µl (nanodrop estimation method using absorbance at 280 nm as described before). However, the resulting protein samples contained several contaminants and did not induce any ER disruption phenotype upon microinjection into syncytial embryos (not shown).

Lastly, we attempted to follow the initial lysis protocol with the 4% Triton X-100 with the goal to remove the detergent during the elution step: the elution buffer did not contain Triton X-100 and we followed Triton concentration in the Nanodrop after several washes until no Triton was being detected at 280 nm. This way, we were able to elute the His_6-Rtnl1 protein with virtually no detectable detergent. Nonetheless, after exchanging the elution buffer into the storage buffer the protein precipitated. Thus, we concluded that this protein needs a high amount of detergent to maintain its solubility and stability, being the most stable at high detergent concentration. Hence, its use in the absence of the confounding variable of the detergent effect was not achievable.

3.2.2. Ectopic expression of mRNA encoding His_6-tagged and GFP-tagged *Drosophila* Rtnl1

Given the failures to use purified Rtnl1, I decided to test an alternative method that bypasses the need for Rtnl1 protein purification. Previously, it was shown that ectopic expression of the human Rtn4b protein leads to perinuclear ER disruption in sea urchin embryos (Mukherjee et al. 2020). The authors also used microinjections as a technique to deliver the mRNA encoding the human GFP-Rtn4b (Mukherjee et al. 2020). Therefore, I decided to clone *Drosophila* His_6-Rtnl1 and His_6-GFP-Rtnl1 sequences into a pRNA plasmid for mRNA preparation *in vitro*. We used microinjections with RNase-free water (used to elute mRNA) as controls for microinjections with the mRNA.

A few experiments using high concentration of mRNA (1-4 µg/µl) revealed that ectopic expression of mRNA encoding the His_6-Rtnl1 has a very strong disruptive effect in some embryos (Fig. 3.12.). In some nuclei, chromosome segregation defects were observed and nuclear spacing was visibly compromised leading to some nuclear fusion events (Fig. 3.12. B-D). Because of this, we titrated down the concentration of mRNA to 700 and 350 ng/µl. However, some embryos became arrested after one or two rounds of nuclear division (Fig. 3.12. C-D). In other cases, we did not see any detectable effect on the ER using lower concentrations of mRNA (Fig. 3.12. B), suggesting that ectopic expression of Rtnl1 in *Drosophila* syncytial embryos might have an all or nothing effect. Microinjection with mRNA encoding His_6-GFP-Rtnl1 merely showed the localization of GFP-Rtnl1 on the ER, like what we observed for the GFP-tagged Rtnl1 purified protein. Therefore, we concluded that mRNA injection was not able to provide a reproducible disruption of ER membranes in Drosophila early embryos.

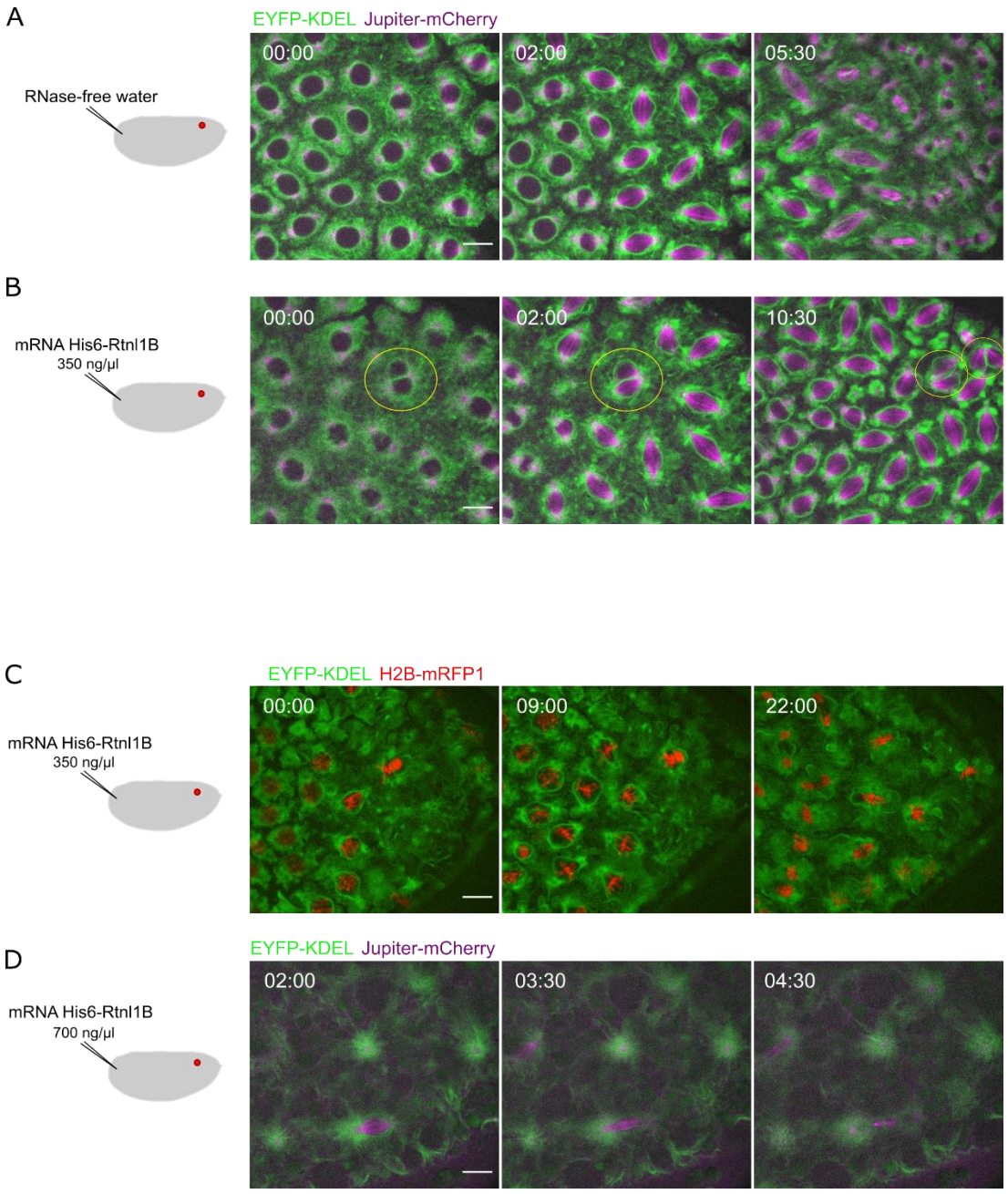
A
EYFP-KDEL Jupiter-mCherry
RNase-free water
00:00
02:00
05:30
B
mRNA His6-Rtnl1B
350 ng/µl
00:00
02:00
10:30
C
EYFP-KDEL H2B-mRFP1
mRNA His6-Rtnl1B
350 ng/µl
00:00
09:00
22:00
D
EYFP-KDEL Jupiter-mCherry
mRNA His6-Rtnl1B
700 ng/µl
02:00
03:30
04:30

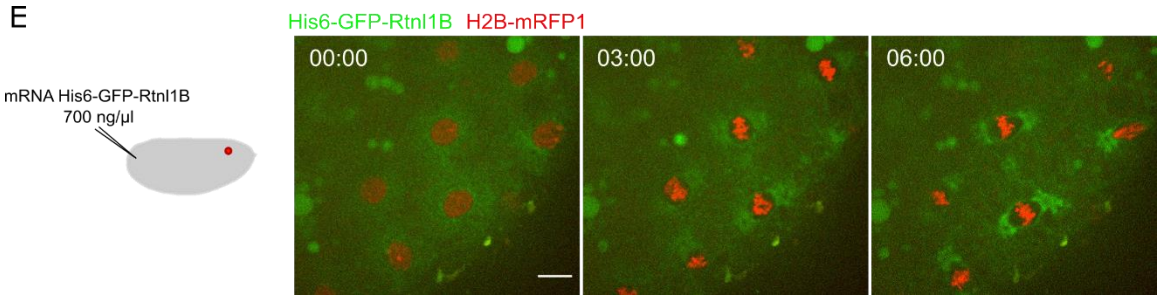

Figure 3.12. Microinjection with mRNA encoding His_6-tagged and His_6-GFP-tagged Drosophila Rtnl1 leads to variable phenotypes in syncytial embryos. *(A,B) Embryos expressing EYFP-KDEL (green) and Jupiter-mCherry (magenta) to visualize the ER together with MTs were used. Microinjection with RNase-free water (control) or mRNA encoding His_6-Rtnl1B at 350 ng/µl was followed by incubation at 22°C for 1.5-2h to allow for mRNA translation. (B) At this mRNA concentration, we observed some events of failed "cytokinesis", characterized by non-separated daughter nuclei, which progressed and led to more failed separation defects (t=00:00 to 10:30, yellow circle). (C) In other cases, microinjection with mRNA at 350 ng/µl led to delayed mitotic divisions, and eventually to an arrest. (D) Increasing the concentration of mRNA encoding His_6-Rtnl1B to 700 ng/µl led to more drastic phenotypes in syncytial embryos, where sometimes only one round of division was observed with some nuclei completely arrest (t=02:00, visible spindle at the bottom of the image; the other nuclei did not divide). (E) Embryos expressing H2B-mRFP1 (red) were used to test the mRNA encoding His_6-GFP-Rtnl1B at 700 ng/µl. The still images show the characteristic localization of His_6-Rtnl1B (green) on the ER, but without any detectable disruption phenotype (t=00:00-06:00). Decreasing the concentration to 350 ng/µl also did not induce any visible disruption effect on the ER (data not shown). Time-lapses started 1.5-2h after microinjection with RNase-free water/mRNA. Scale bar is 10 µm. N=3 independent embryos.*

3.2.4. Ectopic addition of the *Drosophila* cytosolic domain of Atlastin (cytATL)

Given the solubility issues encountered with Rtnl1 purification, and the absence of acute and time-controlled perturbation upon mRNA injections, we sought to test an alternative approach that enabled fast ER disruption only upon microinjection. We focused on alternative strategies that did not encompass transmembrane domains to allow purification protocols in the absence of detergent. The cytosolic domain of Atlastin (cytATL) has been used before as a dominant-negative factor in *Xenopus* egg extracts to impair the membrane fusion activity of Atlastin on the ER (S. Wang et al. 2013). Moreover, later studies reported that overexpression of cytATL in human cells leads to ER fragmentation (S. Wang et al. 2016; Pawar et al. 2017), and that the dominant-negative effect depends on the dimerization activity of cytATL with the endogenous atlastin protein (Pawar et al. 2017). Thus, we purified cytATL from *D. melanogaster* to induce an acute disruption of ER membranes upon microinjection.

Expression was achieved in bacteria and purification was optimized using Ni^{2+} Sepharose beads, as described in detail in Materials and Methods. This protocol was successful at recovering high doses of protein at the expected size (~49 kDa) with few contaminants co-purified (Fig. 3.13.). Samples were further concentrated using a centricon to reach a final concentration of ~60 mg/ml (measured by both Bradford and nanodrop).

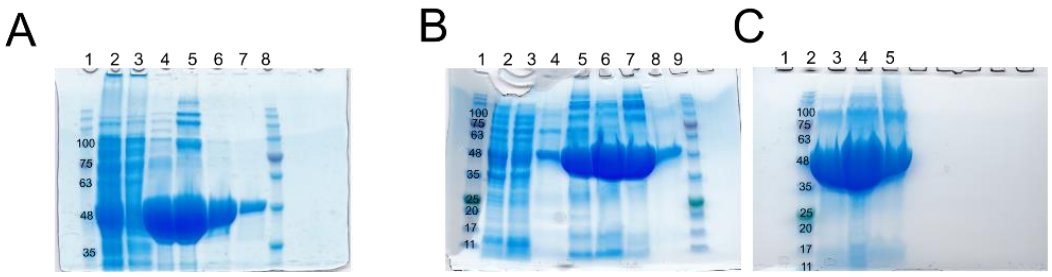

Figure 3.13. Expression and purification of D. melanogaster cytoplasmic domain of Atlastin (His6-cytATL). *(A) First His6-cytATL protein purification using Ni sepharose beads (see Materials and Methods for detailed protocol). 1 – Marker (NZY tech protein marker III). 2 – Supernatant after lysis. 3 – Supernatant after incubation with beads. 4, 5, 6 and 7 are fraction eluted with 80, 150, 300 and 400 mM imidazole respectively. Pooled fractions (6 and 7) were dialyzed overnight into storage buffer, concentrated to 60 mg/ml, flash frozen in liquid nitrogen and stored at -80°C. His6-cytATL protein size is 49 kDa. (B) Second purification using the same protocol as in (A), but increased volume of beads to 3 ml. 1 – Marker, 2 – supernatant after lysis, 3 – supernatant after incubation with beads. 4, 5, 6, 7, 8 – fraction eluted with 40, 80, 150, 300 and 400 mM imidazole. 9 – Marker. (C) Fractions 6 (lane 2 and 3, 5 and 10 µl purified protein loaded on the gel) and 8 (lane 5, 5 µl purified protein) were separately dialyzed overnight into storage buffer, concentrated to 60 mg/ml, aliquoted, flash frozen and stored (-80°C).*

Microinjection with cytATL during late telophase/early interphase led to a mild ER phenotype compared to control embryos (Fig. 3.14. A-B). In this condition, we detected the presence of some vesicles in the ER channel (Fig. 3.14. B, white and yellow arrowheads in merged and inverted LUT images, respectively). However, the overall morphology of the ER seemed to be unaffected, and nuclei progressed normally through the cell cycle like the control condition. This suggests that at mitotic entry, the ER is not sensitive to the dominant-negative effect of cytATL.

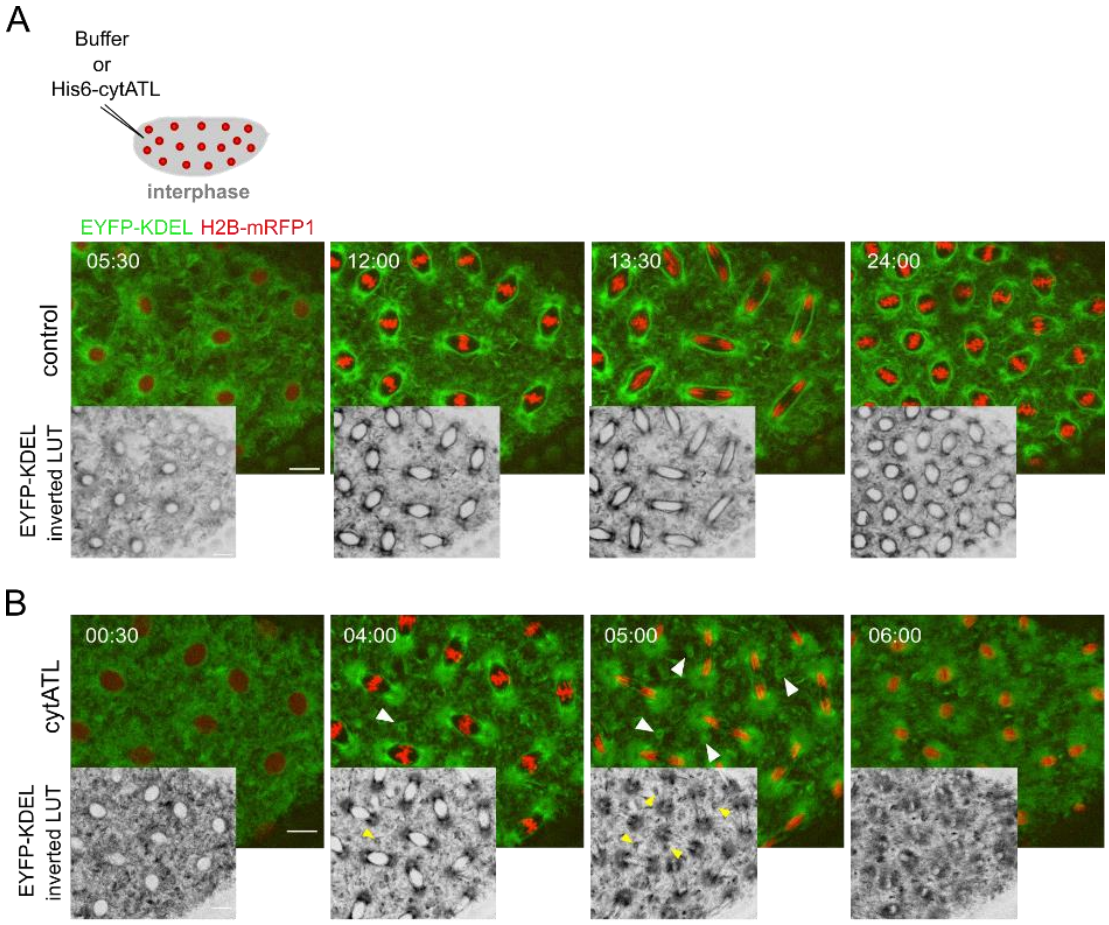

Figure 3.14. Microinjection with cytATL during interphase has a very mild effect on ER morphology. *Embryos expressing EYFP-KDEL (green) and H2B-mRFP1 (red) were used to visualize the ER and chromatin. Still images from time-lapses representative of microinjection with the storage buffer of cytATL (A, control) or cytATL (B). A slightly grainy appearance of the ER was found during metaphase-telophase stages upon microinjection with cytATL, but embryos divide normally (B, t=04:00-05:00). EYFP-KDEL labeled vesicles appeared upon microinjection with cytATL (t=04:00-05:00, white arrowheads in the merged image, yellow arrowheads in the inverted LUT image). Scale bar is 10 µm. The sample size was 3 independent embryos. A representative embryo is shown for qualitative analysis.*

Strong disruption of the ER could only be observed after a consecutive round of microinjection with cytATL (Fig 3.15.). Specifically, we found the presence of vesicle-like structures being formed in the cytoplasm, which can be observed in the green channel (Fig. 3.15. B and C, t=05:00 and t=08:30, respectively, arrowheads). We hypothesize that these vesicles might be formed by unbalanced fission since Atlastin-fusion activity is compromised upon addition of cytATL. Moreover, under this condition, we observed higher frequency of defects after a second round of nuclear division (50% of nuclei show nuclear fusion events and 17% show enlarged metaphase chromosomes; data not shown).

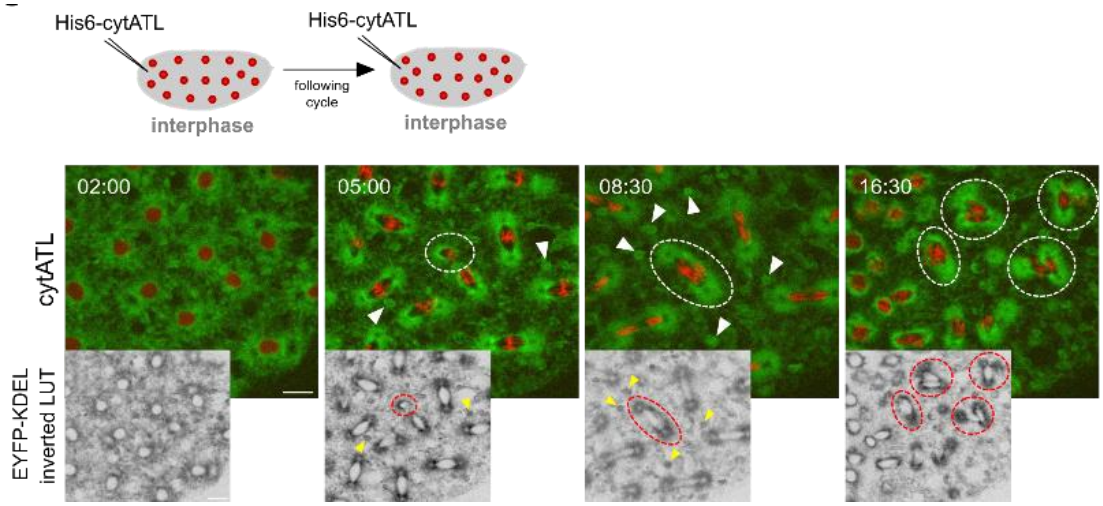

Figure 3.15. Consecutive microinjections with cytATL during interphase lead to a stronger disruptive effect on the ER. *Embryos expressing EYFP-KDEL (green) and H2B-mRFP1 (red) were used to visualize the ER and chromatin. Still images from time-lapses representative of microinjection with cytATL. Nuclear fusion events started to become evident (t=16:30, dashed white circles). Scale bar is 10 µm. The sample size was 3 independent embryos. A representative embryo is shown for qualitative analysis.*

To visualize cytATL localization upon microinjection, we decided to clone the cytATL protein sequence with a mCherry tag (see Materials and Methods). Because we knew that the cytATL fragment contains the GTPase domain at the N-terminus (J. Hu et al. 2009), we decided to clone the mCherry tag at the C-terminal region of the sequence to avoid compromising GTPase function.

We transformed *E. coli* Rosetta cells with His6-cytATL-mCherry plasmid and proceeded with protein expression and purification (Fig. 3.16.). Our purification using Ni^{2+} Sepharose beads resulted in a mixed sample containing the fusion protein His6-cytATL-mCherry (~75 kDa), and two contaminants – one with a molecular weight of ~49 kDa and another with ~25 kDa (Fig. 3.16 A-B). Even after passing the sample through a 30 kDa cuttoff centricon column, we were not able to separate the contaminants from the His6-cytATL-mCherry fusion protein. Nevertheless, we decided to test this batch and probe for cytATL localization on the ER.

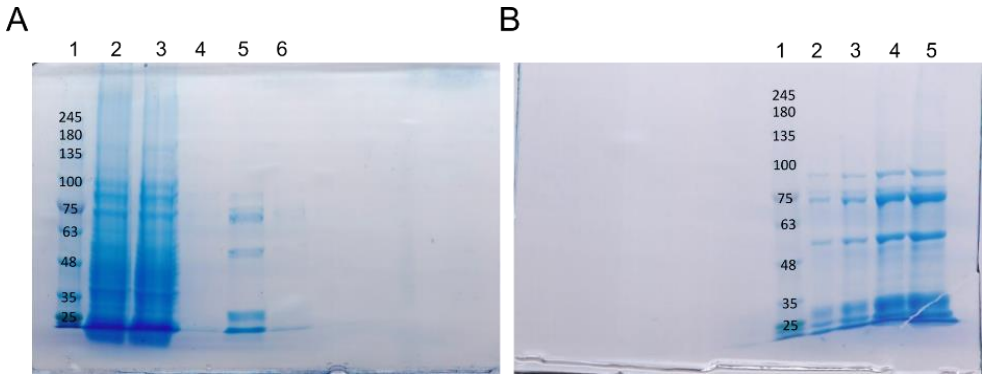

Figure 3.16. Expression and purification of His6-cytATL-mCherry. *(A) SDS gel showing His6-cytATL-mCherry purification using Ni beads (GE Healthcare) and same buffers and protocol as for His6-cytATL. 1 – NZY tech protein marker, 2 – supernatant after lysis, supernatant after beads, 3 – wash buffer 10 mM imidazole, 4 – elution buffer 80 mM imidazole, 5 – elution buffer 150 mM imidazole, 6 – elution buffer 300 mM*

imidazole. The fusion protein His6-cytATL-mCherry expected molecular weight is ~75 kDa. The expected molecular weight of His6-cytATL without the mCherry tag is ~49 kDa. the molecular weight of the mCherry tag is ~25 kDa. (B) Elution of His6-cytATL-mCherry, each fraction was eluted in 5 ml volume. 1 – NZY tech protein marker. Protein was concentrated using a vivaspin column (Ambion) to 30 mg/ml. The concentrated protein sample was diluted 5 times to run on a SDS gel: 2 – 1 µl, 3 – 1.5 µl, 4 – 2 µl, 5 – 2.5 µl.

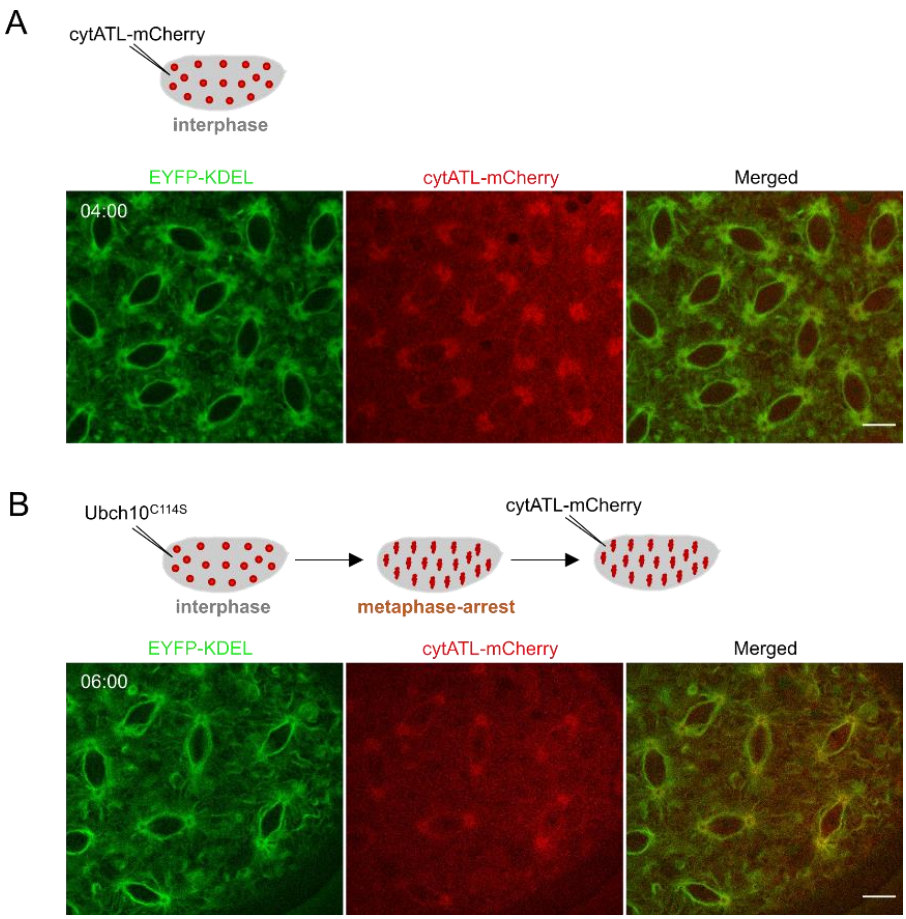

Figure 3.17. Microinjection with His6-cytATL-mCherry confirms cytATL localization on the ER. *Embryos expressing EYFP-KDEL (green) were used to visualize the ER. Still images from time-lapses are*

shown. (A) cytATL-mCherry co-localizes with EYFP-KDEL on ER (cytATL-mCherry, yellow color in the Merged image). (B) Microinjection with cytATL-mCherry was then performed after the inducible arrest at metaphase (UbcH10^{C114S}). Evident colocalization was found in this experimental layout as well (cytATL-mCherry, yellow color in the Merged image). Scale bar is 10 µm. The sample size was 3 independent embryos. A representative embryo is shown for qualitative analysis.

Microinjection of low doses of His6-cytATL-mCherry (~3 mg/ml, total protein concentration) led to localization of cytATL on the ER, indicated by partial colocalization with the EYFP-KDEL ER marker used in our experiments (Fig. 3.17. A-B). This co-localization was observed both upon microinjection during interphase and microinjection into metaphase-arrested embryos (Fig. 3.17. B, merged image). Curiously, we saw stronger localization of cytATL-mCherry around spindle poles, compared to ER localized at the equator.

Microinjection with undiluted sample (~30 mg/ml total protein) led to a strong ER disruptive effect like what we have seen before with cytATL alone (not shown). Since we cannot exclude if one of the contaminants is untagged His6-cytATL, it is difficult to claim whether the ER disruptive effect is caused by its presence or the fusion protein. In either case, the ER localization supports the specific targeting to the ER.

These results suggested that microinjection with cytATL into syncytial embryos was the most promising strategy to successfully achieve an ER disruptive effect. We observed nuclear separation defects after microinjection with cytATL specifically at telophase, indicating that Atlastin might be involved in the abscission of ER membranes at the end of mitosis in this system.

Next, we thought to use the cytATL protein as a dominant-negative reagent specifically during metaphase. This approach allowed us to assess the contribution of mitotic ER membranes surrounding the spindle in a precise and controlled manner.

3.2.5. Ectopic addition of cytATL changes mitotic ER topology around spindle poles in metaphase-arrest nuclei

To induce ER membrane disruption in an acute and controlled manner, we decided make use of the inducible metaphase-arrest described before. Because of the fast nuclear divisions in *Drosophila* syncytial embryos, the arrest at metaphase would allow us to increase the time of exposure to the dominant-negative effect of cytATL (since the time from interphase to metaphase is quite short, roughly 5 minutes). This would allow us to induce the disruption of ER membranes upon unperturbed spindle assembly and ER network formation around the spindle. Consequently, due to this experimental layout, we were able to address the impact of intact ER membranes on the mitotic spindle.

To monitor the ER specifically during metaphase, embryos were previously arrested with UbcH10^{C114S}, as above (Fig. 3.18. A). We observed that subsequent microinjection of cytATL in metaphase-arrested embryos alters mitotic ER topology compared to controls (Fig. 3.18.B-C, Movie 3.18.). Over time, EYFP–KDEL labelled ER membranes lose their linear arrangement, typical of a tubular structure, and a acquire diffuse and homogeneous appearance (Fig. 3.18. B-C, t=10:00 min). Quantitative analysis reveals that there is no change in the mean intensity of the ER reporter at spindle poles, with or without cytATL injection (Fig. 3.18. D). However, the spatial distribution of the signal was altered, as evidenced by the significantly decreasing variance upon cytATL injection (Fig. 3.18. E). This suggests that ER distribution or configuration changes. In contrast, centrosome-distal regions do not change significantly both in

mean and distribution of the signal (Fig. 3.18. D-E). These findings reveal that the disruptive effect of cytATL is exclusively observed at ER membranes surrounding spindle poles. In addition to the change in spatial ER concentration, ectopic addition of cytATL caused a significant reduction in the ER exclusion zone (Fig. 3.18. F). We therefore concluded that ER membranes at the spindle poles are more sensitive to the disruptive effect of cytATL, whose addition leads to acute changes in morphology at this sub-region of the ER network.

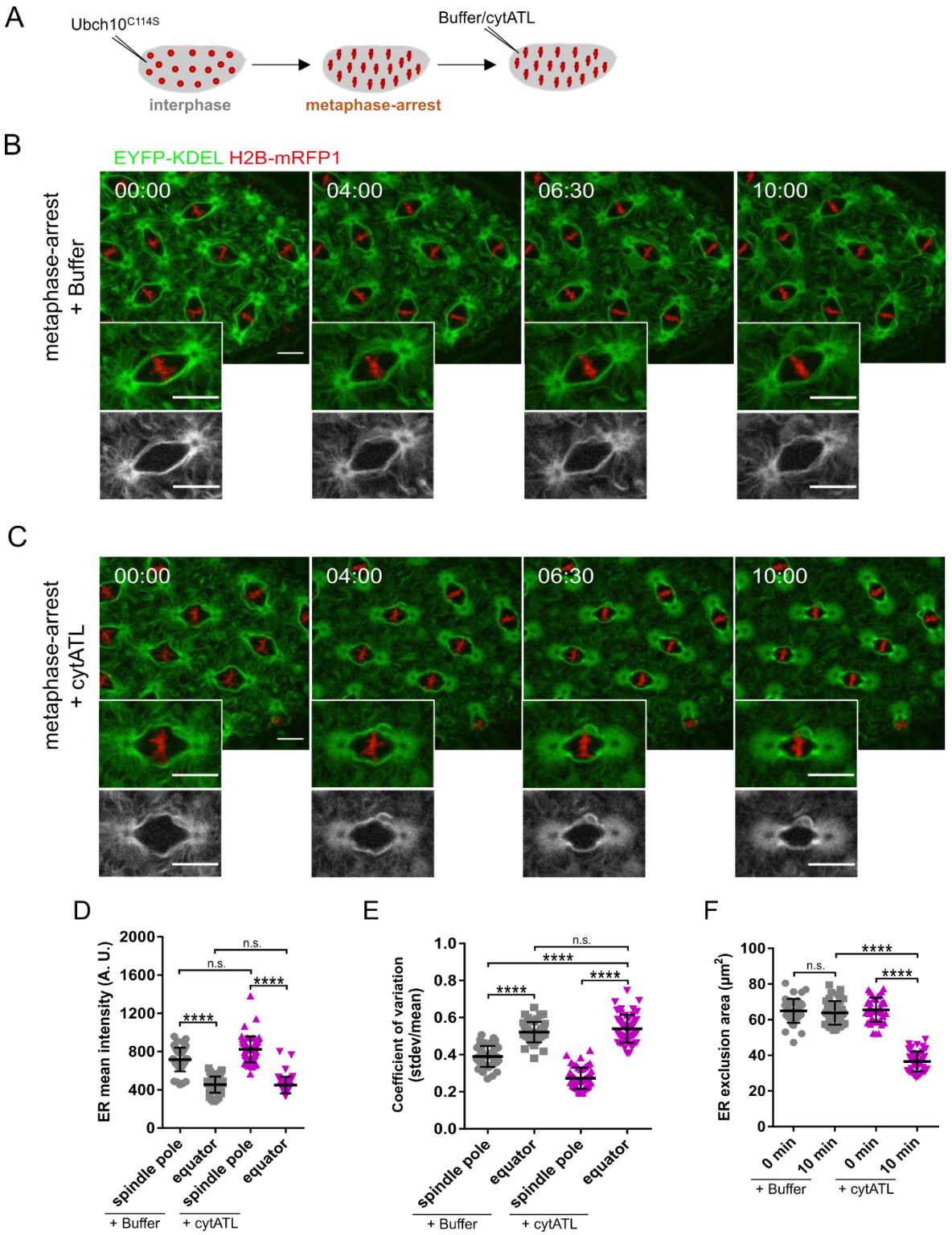
A
Ubch10C114S
Buffer/cytATL
interphase
metaphase-arrest
B
EYFP-KDEL H2B-mRFP1
metaphase-arrest + Buffer
00:00
04:00
06:30
10:00
C
metaphase-arrest + cytATL
00:00
04:00
06:30
10:00
D
ER mean intensity (A. U.)
2000
1600
1200
800
400
0
n.s.
n.s.
****
****
spindle pole
equator
spindle pole
equator
+ Buffer
+ cytATL
E
Coefficient of variation (stdev/mean)
1.0
0.8
0.6
0.4
0.2
0.0
n.s.
****
****
****
spindle pole
equator
spindle pole
equator
+ Buffer
+ cytATL
F
ER exclusion area (µm²)
100
80
60
40
20
0
n.s.
****
****
0 min
10 min
0 min
10 min
+ Buffer
+ cytATL

Figure 3.18. Microinjection with cytATL in metaphase-arrested nuclei leads to strong disruption of the ER at spindle poles. *(A) Experimental layout: inducible metaphase-arrest by microinjection with UbcH10^{C114S}. After arrest (~5 min) embryos were subjected to a second microinjection. ER dynamics was monitored by EYFP–KDEL (green) and chromatin by H2B–mRFP1 (red). (B-C) Stills depicting changes in ER morphology (EYFP–KDEL, green) after microinjection of buffer (B) or cytATL protein (C) in metaphase-arrested embryos; time (min:s) is relative to the second microinjection (buffer/cytATL). Grey panels depict ER channel alone. Scale bar is 10 µm. (D) Quantitative analysis of mean fluorescence intensity of EYFP–KDEL in spindle poles or equatorial regions 10 min after buffer/cytATL injection. (E) Coefficient of variation, calculated by the ratio of the standard deviation over the mean (stdev/mean), 10 min after buffer/cytATL injection. (F) ER exclusion area in control (buffer-injected, grey) and cytATL (magenta) conditions at the first (t=0 min) and last (t=10 min) time point of the time-lapse. Statistical analysis using N=10 embryos, n=5 nuclei per embryo. (D, E, F) Asterisks represent statistical significance derived from Kruskal–Wallis (Dunn's multiple comparisons test) (D) or one-way ANOVA (E, F), multiple comparisons, P value adjusted to multiple comparisons (Tukey). ****P < 0.0001, n.s., nonsignificant, P > 0.05.*

The observed expansion of ER signal at spindle poles was very puzzling to us. We questioned why cytATL dominant-negative effect was stronger or caused stronger ER membrane disruption at these specific areas. So, we anticipated that having a *Drosophila* strain with endogenously tagged Atlastin (full length) could be useful to assess its localization on the ER. Using the fly transgenics service at the IGC, a *Drosophila* strain with a GFP sequence inserted in the C-terminal region of the Atlastin locus was generated (CRISPR/Cas9 knock in; detailed protocol in APPENDIX).

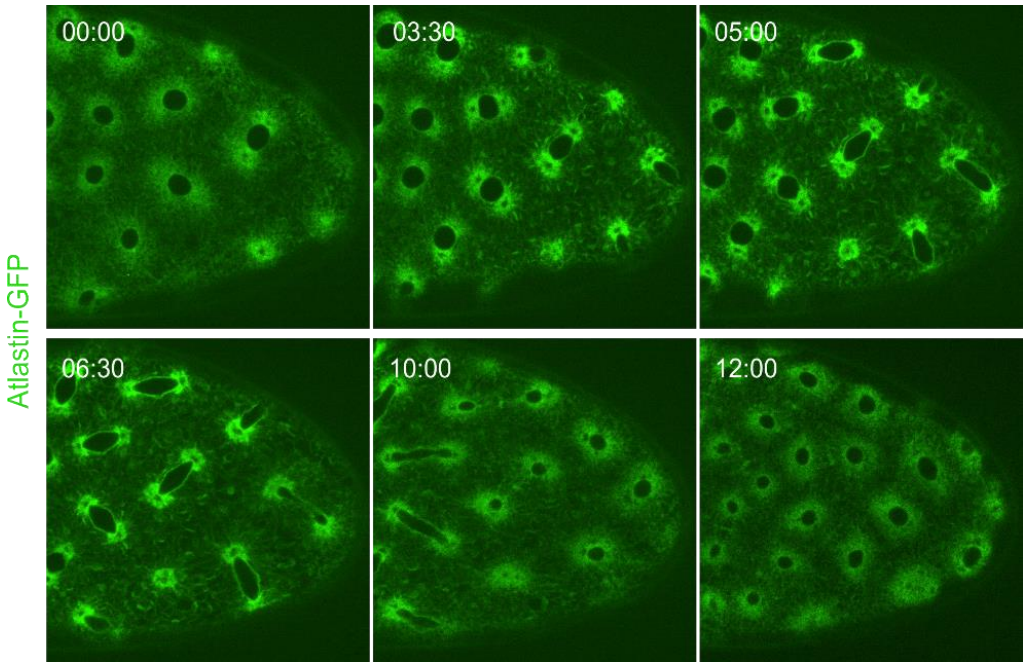

Figure 3.19. Localization of endogenously tagged Atlastin-GFP in Drosophila syncytial embryos. *Time-lapse images of a representative embryo expressing Atlastin-GFP. A clear accumulation of ER signal around spindle poles can be observed at metaphase (t=05:30). Sample size is 3 independent embryos. Scale bar is 10 µm.*

Live imaging of embryos expressing endogenously tagged Atlastin-GFP revealed that Atlastin localizes throughout the ER, resembling the EYFP-KDEL pattern of localization (Fig. 3.19.). However, we observed that Atlastin-GFP becomes strikingly concentrated around spindle poles from prometaphase to anaphase (Fig. 3.19., t=03:30-06:30). We also observed that Atlastin-GFP localizes at the spindle midbody as previously shown for the other ER reporters we used (EYFP-KDEL and Rtnl1-GFP) (Fig. 3.19. t=10:00-12:00). Atlastin-GFP localization may help to explain the expansion of ER signal at spindle poles. One possibility is that more ER sheets are recruited around spindle poles, providing a larger ER surface for cytATL dominant-negative effect. It is also possible that ER

membranes around centrosomes are more sensitive to cytATL effect than other regions of the ER envelope. In a previous study, it was shown that there is clustering of extended ER cisternae at the spindle poles during metaphase in *Drosophila* syncytial embryos (Bergman et al. 2015). ER cisternae may be, for some reason, more susceptible to cytATL.

Discussion

Owing to the importance of the ER in cells, to this date, it was challenging to disrupt this large organelle in a specific and acute manner.

This chapter describes the development and testing of various tools to acutely perturb the ER, using ER-shaping proteins as modulators of ER morphology *in vivo*. Because Reticulons and Atlastins had been described as the key regulators of ER morphology (Orso et al. 2009a; Espadas et al. 2019; S. Wang et al. 2013), we focused on these two candidates.

Here, we tested different strategies including ectopic addition of either mRNA encoding for or bacterial expressed and purified ER-shaping proteins. Microinjection with purified proteins is usually the favorite strategy we use in the lab. This is because we can monitor immediately the effect during mitosis by prompt delivery into embryos (microinjection). Usually, mitotic duration and presence of mitotic defects (chromosome segregation errors, spindle defects) are the parameters analyzed to assess the effect of the protein of interest.

Purification of full-length Rtnl1 – an ER transmembrane protein – was the first strategy we tested to induce ER membrane disruption. Purification of full-length transmembrane proteins relies on the use of detergent to facilitate their solubilization. We successfully purified Rtnl1 protein using an established protocol reported previously (Espadas et al. 2019) adapted to His-tagged Rtnl1.

Upon microinjection with Rtnl1 into embryos, we observed a strong effect not only on the ER, but also in cell cycle progression. This was unexpected because chromosomes were still able to congress and form a metaphase plate but did not progress into anaphase at the site of microinjection. When we looked at the localization of the SAC protein Mad2(-EGFP), we found that it became strikingly accumulated upon microinjection with Rtnl1. This was a surprising finding as SAC proteins

usually localize to kinetochores upon checkpoint activation and disappear once it is satisfied (Howell et al. 2000). This intriguing phenotype really surprised us at the time because it suggested that disruption of membranes activated the checkpoint in our experiments. Moreover, Mad2-EGFP accumulation at poles suggested that the checkpoint cannot be inactivated. Although we observed that Mad2 is transported along MTs towards the spindle poles, it seemed that Mad2 cannot disassemble from the poles in this condition.

However, we found later that our purified Rtnl1 sample retained high concentration of detergent due to our purification protocol. We think that because of Rtnl1 high hydrophobicity, and the CMC of Triton X-100 used in our lysis buffer, this led to the formation of micelle-protein complexes. These detergent micelle-protein complexes likely contributed to protein solubility and stability, but also to overestimation of protein concentration in our samples. Bellow, several observations that led to this conclusion are discussed.

Because we found that microinjection with buffer containing high doses (10%) of Triton X-100 induces a similar phenotype, this led us to suspect that the ER disruption phenotype we observed before was possibly being caused by a combination of the detergent with the Rtnl1 protein. Because of this confounding factor – protein + detergent – we considered that this was not a suitable strategy to induce specific ER membrane disruption. Microinjection with detergent causes a very strong and broad perturbation on membranes, and it can even have a denaturation effect on other proteins.
So, we tried an alternative strategy using mRNA encoding Rtnl1 protein – in which protein translation occurs *in embryo*. This strategy had also been documented before in sea urchin embryos using a human reticulon protein (Parry, McDougall, and Whitaker 2005; Mukherjee et al. 2020).

In contrast with a previous study where mRNA encoding for the human Rtn4b protein was microinjected into sea urchin embryos (Mukherjee et al. 2020), in our experiments using microinjection with mRNA encoding *Drosophila* Rtnl1 (isoform B) we found variable results. In some cases, no disruptive effect could be seen on the ER, while in others there was a very drastic disruption of the ER and arrested nuclei were observed. We attempted to titrate down the concentration of microinjected mRNA encoding Rtnl1, but even so we could not get an intermediate phenotype. This could be explained by a fine threshold in the expression levels of Rtnl1, or even by the insertion of the protein on the ER. If the insertion of Rtnl1 is the limiting step, perhaps we would have to co-microinject purified chaperone proteins responsible for the insertion of transmembrane proteins in the ER membrane. Another possible explanation is that very high amounts of mRNAs and proteins are deposited in the embryo, so finding the precise threshold to induce an “overexpression” is difficult to achieve.

We also cloned the GFP-Rtnl1 construct to visualize the fusion protein within the syncytial embryos, but we found that although GFP-Rtnl1 localizes to the ER, the morphology of ER membranes was apparently unaffected. A possible reason for this is that the size of the GFP tag might compromise protein function in this case as described before (Espadas et al. 2019). In any case, microinjection of mRNA has the caveat of not being an acute strategy, because it relies on the limiting step that is the translation process *in embryo,* taking at least one hour after microinjection in very early embryos. This means that the efficiency of protein synthesis depends on the translation capacity within the syncytial embryo, which cannot be enhanced in our experimental conditions. Therefore, this strategy should be viewed more as an ectopic expression experiment, rather than as an overexpression one.

The next strategy we tested was based on the previous knowledge that cytATL could be used as a dominant-negative reagent to induce ER fragmentation in different systems (S. Wang et al. 2013; 2016; Pawar et al. 2017). Therefore, we used cytATL to acutely disrupt the ER in *Drosophila* syncytial embryos by microinjection.

This strategy, when coupled to microinjection has the advantage of controlling the time of addition of the dominant-negative reagent, cytATL, instead of doing chronic overexpression of this fragment. When we performed microinjection with cytATL during interphase, neither ER morphology nor chromosome segregation were affected significantly. However, we only performed live imaging of these embryos using confocal light microscopy. Even though we detected a slightly diffuse appearance in ER morphology compared to control embryos, normal nuclear divisions were still observed. Yet, we cannot exclude that ER morphology becomes altered at the ultrastructural level, since we did not assess that. To see ER structure at this level, we could use electron microscopy and compare control versus cytATL microinjected embryos.

Another possibility is that due to major ER reorganization events occurring at mitotic entry, this leads to increased sensitivity to cytATL's dominant negative effect. Also, the activity and/or mobility of endogenous full-length Atlastin may potentially be very rapid, promoting fusion of ER membranes efficiently.

An alternative explanation leading to lower sensitivity to cytATL is based on the time interval between interphase and mitosis in this system: the short duration of interphase in the syncytial stage might limit the time for cytATL effect. The phenotype described in human cells upon cytATL overexpression seems to clearly alter ER morphology (S. Wang et al. 2016), even the mitotic ER network. In opposition, ER fragmentation was not observed in *S. cerevisiae* cells lacking the Atlastin orthologue Sey1p (J. Hu et al. 2009). This may be explained by the fact that *S. cerevisiae*

also has ER SNAREs that could provide an alternative mechanism of ER fusion (Anwar et al. 2012).

Indeed, microinjection with cytATL in two consecutive rounds of nuclear divisions induced a stronger ER disruptive effect compared to the single microinjection experiment (e.g., appearance of vesicles in the ER channel, more diffuse appearance of the ER, some mitotic defects like nuclear fusion were detected). Yet, this experimental layout was still not ideal because it could likely be affecting calcium storage, protein synthesis and other ER canonical functions during mitosis upon consecutive nuclear divisions. Therefore, we performed microinjection with cytATL under the metaphase-arrest condition, to induce a more controlled perturbation on the ER.

We found that microinjection with cytATL in metaphase-arrested nuclei led to marked disruption of ER membranes proximal to spindle poles. Specifically, we observed an expansion of ER fluorescence intensity at spindle poles, but not in other regions of the ER envelope. This localized effect of cytATL was also associated to significantly reduced area of the ER exclusion zone compared to the control condition. The ER network proximal to spindle poles might be organized into sheets or cisternae during metaphase. If this is confirmed, it could help to explain why the dominant-negative effect of cytATL is stronger at spindle poles.

Generating a fluorescently tagged cytATL(-mCherry) construct confirmed that the protein is targeted to the ER, indicated by colocalization with the ER markers used in this study. Moreover, live imaging of syncytial embryos expressing endogenously tagged Atlastin protein (Atlastin-GFP, generated by CRISPR/Cas9 knock-in) confirmed that Atlastin is enriched in the ER network proximal to the spindle poles. Whether this preferential localization of Atlastin is important for spindle pole/centrosome integrity or function remains an open question.

Interestingly, a very recent preprint showed that a specialized network of ER membranes around centrosomes can also be found in *C. elegans* embryos (Maheshwari et al. 2022). In this study, the authors analysed the ER around the centrosome at the ultrastructural level by volume electron microscopy (vEM), revealing a reticular nature of these specific centrosome associated membranes (Maheshwari et al. 2022). Finally, they proposed that this specialized ER membranes may be important for tethering the centrosome to the NE during mitosis.

In summary, we were able to find a tool that specifically disrupts ER membranes in a few minutes after microinjection. This tool allowed us to test the impact of ER membranes proximal to the spindle poles and address the consequences of a localized ER disruption effect. Since the ER-envelope encloses the spindle during mitosis, especially during metaphase, we examined the spindle under this localized disruption of the ER. In the following chapter, we utilize cytATL as a tool to assess the role of ER membranes on mitotic spindle morphology and function.

Materials and Methods

Fly stocks

Fly strains expressing EYFP-ER (LaJeunesse et al. 2004) , Rtnl1–GFP (Morin et al. 2001) fluorescent markers, and for induction of artificial sister chromatid separation (Pauli et al. 2008; Oliveira et al. 2010) have been previously described. UASp-RFP-KDEL line was crossed with the G302-Gal4 maternal driver to induce the expression of this reporter in syncytial embryos. For this, flies were maintained at 25°C throughout the course of the experiment (from the moment when the cross was established to the selection of the F1 progeny). Briefly, newly ecloded flies were screened to select the correct genotype in the progeny (see Appendix). To maximize egg laying, cages were prepared with flies 5 days after eclosion. A detailed list of the stocks can be found in Table 3.

Table 3. List of *Drosophila* stocks used in this chapter

Genotype	**Reference**
Avic\GFP$^{EYFP.sqh.Tag:SS(hCALR).Tag:ER(KDEL)}$ (EYFP–KDEL)	BDSC #7195 (LaJeunesse et al. 2004)
GFP-tagged Rtnl1 protein expressed from its endogenous locus (GFP–Rtln1)	Kyoto stock center #110579. (Morin et al. 2001)
w[*];P{w[+mC]=UASp-Ggal\LYZ.GFP.KDEL}401/CyO Expresses GFP-tagged chicken lysozyme with an ER retention sequence under UAS control. (UASp-Lys-GFP-KDEL)	BDSC #31423

w[*]; P{w[+m]=betaTub56D-EGFP.I}17-1, H2Av-mRFP1; MKRS/TM6B*	Described in (de-Carvalho et al. 2022). Originally described in (Y. H. Inoue et al. 2004); Kyoto Stock Center #109603
w;; Rad21^{ex15}, polyubiq-H2B-RFP, tubpr-Rad21$^{(550\text{-}3TEV)}$-myc10 (4c)*	Described in (Oliveira et al. 2010), named here #629
w; EYFP-ER; Rad21^{ex15}, polyubiq-H2B-RFP, tubpr-Rad21$^{(550\text{-}3TEV)}$-myc10 (4c)*	Derived from BDSC #7195 and #629 (see above)
w;Rtnl1-GFP; Rad21^{ex15}, polyubiq-H2B-RFP, tubpr-Rad21$^{(550\text{-}3TEV)}$-myc10 (4c)*	Derived from BDSC #110579 and #629 (see above)
w;; Atlastin-GFP/TM6B *Insertion of a GFP sequence at the C-terminal region of the endogenous locus of Atlastin*	Knock in generated by CRISPR/Cas9 by the Fly transgenics facility at IGC (Leonardo Guilgur)

BDSC – Bloomington *Drosophila* stock center

Cloning of fluorescently tagged ER proteins

The plasmid containing the sequence of *Drosophila* Rtnl1B (Reticulon-like protein 1, isoform B), pET28a-His$_6$-Rtnl1B, was a gift from Andrea Daga (University of Padova, Italy). His$_6$-Rtnl1B sequence was cloned into a N-terminal GFP-tagged pET28a (pET28a-GFP-Scc4, Oliveira lab) with EcoRI and XhoI sites. To amplify Rtnl1B sequence we used the primers forward – 5' GCAGAATTCATGTCCGCATTTGGTGAA 3' and reverse – 5' GCACTCGAGTTACTTGTCCTTCTCAGA 3'. Phusion HF polymerase (NEB, reference M0530S) protocol was used, preparing PCR reactions with the following components: 5X Phusion HF buffer, 10 mM dNTPs, forward primer at 10 µM, reverse primer at 10 µM, template DNA at 100 ng/µl, 0.5 µl Phusion HF and nuclease-free water. The following PCR cycle was used: initial denaturation at 98˚C for 2 min, then denaturation

at 95˚C for 30 sec, annealing at 59˚C for 30 sec, extension at 72˚C for 30 sec for 30 cycles, final extension at 72˚C for 5 min and hold at 12˚C. The PCR product amplified (723 bp) was precipitated using the DNA precipitation protocol for PCR fragments described below.

Plasmid digestion and PCR fragment was performed using EcoRI and XhoI restriction enzymes (NEB, reference R3101T and R0146S, respectively; 2h at 37˚C in a water bath). Both digestion reactions were further run in 1% agarose gel and the DNA purified using Zymoclean Gel DNA Recovery Kit. The plasmid DNA and PCR fragment were then ligated with T4 Ligase (Thermo Scientific, EP0061). The ligated plasmid was transformed into chemically competent *E.coli* DH5α cells cultured with the appropriate selective conditions (Kanamycin resistance LB agar plates), and plates were screened for colonies. To confirm the correct insertion (GFP sequence upstream of the His6-Rtnl1B sequence), the primers forward – 5' GGAAGGAAGCTTatggtgagcaagggcgaggag 3' and reverse – 5' GCACTCGAGTTACTTGTCCTTCTCAGA 3' were used for colony PCR. The condition for the DreamTaq PCR were: 95˚C for 3 min, annealing at 55˚C for 30 sec, extension at 72˚C for 30 sec for 24 cycles, final extension at 72˚C for 5 min and hold at 12˚C. Positive clones were further sent for Sanger sequencing (Sequencing barcodes eurofins).

For mRNA expression, both His_6-Rtnl1B and His_6-GFP-Rtnl1B sequences were cloned into pRNA plasmids using the primers forward – 5' GCAGAATTCATGGGCAGCAGCCATCATCA 3' and reverse – 5' GCAGCGGCCGCTTACTTGTCCTTCTCAGACTCGGCAG 3', forward – 5' GCACAATTGATGGGCAGCAGCCATCATCA 3' and reverse 5' GCAGCGGCCGCTTACTTGTCCTTCTCAGACTCGGCAG 3', respectively.

The plasmid containing the sequence of human GFP-Rtn4b, pCS107 plasmid (pDL34), was a gift from Daniel Levy (University of Wyoming, USA) (Jevtić and Levy 2015).

mCherry-tagged His6-cytATL

To clone His_6-cytATL with a C-terminal mCherry tag we used NdeI restriction sites and inserted His_6-cytATL into a pET28a already containing a mCherry tag (generated by Diana Vieira, Telley lab). pET28a-His_6-cytATL was a gift from Jiunjie Hu (Nankai University, China). was used as template with the primers forward – 5' GGGAATTCCATATGatgggcggtagtgcagtg 3' and reverse – 5' GGGAATTCCATATGgctttcgttgtgcgcctg – 3'. Phusion HF DNA polymerase protocol was used with a total volume of 50 µl per reaction: 5X Phusion HF buffer, 10 mM dNTPs, forward primer at 10 µM, reverse primer at 10 µM, template DNA to a final concentration of 100 ng/µl, 0.5 µl Phusion HF and nuclease-free water up to 50 µl. The PCR protocol used for this fragment was the following: 98˚C for 2 min, then denaturation at 98˚C for 30 sec, annealing at 59˚C for 30 sec, extension at 72˚C for 30 min for 30 cycles, final extension at 72˚C for 5 min and hold at 12˚C. The PCR product amplified (1245 bp) was precipitated using the DNA precipitation protocol for PCR fragments described below. Restriction reaction with NdeI was left overnight at 37˚C for the cytATL fragment (5x CutSmart Buffer NEB, 1 µl of NdeI NEB, 5 µg of DNA, milliQ water up to a final volume of 50 µl) and for 2h for the pET28a-mCherry plasmid (5x CutSmart Buffer NEB, 1 µl of NdeI NEB, 2 µg of DNA, milliQ water up to a final volume of 50 µl). To prevent recircularization of the plasmid caused by a single cut, we included an extra step of incubation with Antarctic phosphatase (NEB) for 1h at 37˚C, adding the required components directly into the restriction reaction with pET28a-mCherry: 6 µl of 10x Antarctic Phosphatase buffer, 2 µl of Antarctic Phosphatase, and 2 µl of sterile milliQ water. Antarctic Phosphatase was inactivated for 10 min at 65˚C. The entire volume of these restriction reactions was separately run with an agarose gel electrophoresis. The bands corresponding the plasmid (~6000 bp) and fragment (1245 bp) were cut using a scalpel and purified with a Zymoclean Gel DNA Recovery Kit according to

manufacturer instructions. The plasmid DNA and PCR fragment were then ligated with T4 Ligase (Thermo Scientific, EP0061). The ligated plasmid was transformed into chemically competent *E.coli* DH5α cells cultured with the appropriate selective conditions (Kanamycin resistance LB agar plates), and plates were screened for colonies. With this cloning strategy, His_6-cytATL can be inserted in both orientations.

To screen for colonies having the correct orientation, we used two primer sets: forward and reverse described above and a separate reaction to confirm correct orientation of the sequence was prepared with the primers forward – T7 promoter 5' TAATACGACTCACTATAGGG 3' and reverse – 5' ctggctatcaaatgcaccc 3'. Colony PCR was done using DreamTaq polymerase protocol: 10x GreenDreamTaq buffer, 10 mM dNTPs, forward primer at 10 µM, reverse primer at 10 µM, 2 µl of each pricked colony (diluted in 20 µl sterile milliQ water), 0.1 µl DreamTaq polymerase and nuclease-free water up to 20 µl. The PCR protocol used was 95˚C for 5 min, then denaturation at 95˚C for 30 sec, annealing at 55˚C for 30 sec, extension at 72˚C for 30 sec for 25 cycles, final extension at 72˚C for 5 min and hold at 12˚C. Colonies were considered positive (correct orientation) when both reactions showed the expected PCR product size (1267 and 518 bp, respectively). For Sanger sequencing (eurofins barcodes), the primers described above together with a primer specific for the mCherry tag (5' GCACTCGAGTAACTTGTACAGCTCGTCCATG 3') were used.

DNA precipitation protocol for PCR fragments

PCR reactions with a total volume of 50 µl were prepared in duplicates for each fragment. Sodium acetate was added at 0.1 vol/vol directly onto the PCR product, followed by the addition of (ice cold) absolute ethanol at 2.5 vol/vol. The reaction was mixed and left for 1h on dry ice (or -80°C) to

precipitate DNA. Using a microcentrifuge at room temperature, DNA was spun down by centrifugation at 15 000 g for 15 min, discarding the supernatant. DNA pellets were washed with 750 ul 70% molecular grade ethanol, followed by centrifugation at 15 000 g for 15 min, and the supernatant was discarded. The tubes containing DNA pellets were left open to evaporate residual ethanol from the tubes for 10-15 min at room temperature. DNA was reconstituted with sterile MilliQ water and concentration was estimated using a Nanodrop.

mRNA preparation

mRNA was synthesized by *in vitro* transcription with the mMessage mMachine T3 kit (Ambion, Austin, TX), followed by precipitation of mRNA with LiCl according to manufacturer instructions with some modifications and reconstitution in RNase-free water. mRNA encoding the human GFP-Rtn4b was synthesized by *in vitro* transcription with the mMessage mMachine SP6 kit (Ambion, Austin, TX; kindly lent by Dr Elias Barriga, IGC), *In vitro* transcription reactions were prepared in triplicate and left for 4h at 37˚C to increase the yield of mRNA. Embryos were incubated at 22˚C for 1.5–2h to allow for protein translation after microinjection with mRNA.

Microinjections

Microinjections were performed as previously described in (Carmo, Araújo, and Oliveira 2019) and in the Materials and Methods section of Chapter 2 (page X). Buffer/protein/chemicals were microinjected at the following concentrations: Buffer (10 mM HEPES, 100 mM KCl, 1 mM $MgCl_2$, 10% glycerol), $UbcH10^{C114S}$ (30-40 mg/ml), p27 (4 mg/ml), TEV protease (18 mg/ml), cytATL (60 mg/ml), cytATL-mCherry (3 mg/ml), UbcH10 wild-type (60 mg/ml). Porcine Tubulin labelled with AlexaFluor 647 (Tubulin HILyte Fluor™ 647 labelled, cat. # 1L670M, 20 µg;

Cytoskeleton) was reconstituted in freshly prepared and filtered 1X BRB80 buffer (80 mM PIPES, 1 mM $MgCl_2$, 1 mM EGTA, pH 7.8) to a final concentration of 2.5 mg/ml, immediately frozen in liquid nitrogen and stored at -80°C. To visualize spindle microtubules upon metaphase-arrest, labelled Tubulin was mixed with $UbcH10^{C114S}$ protein at 1:1 ratio (at a final concentration of 1.25 mg/ml). To visualize spindle microtubules during nuclear division cycles, Tubulin was used at 2.5 mg/ml.

Protein purification

$UbcH10^{C114S}$, p27, TEV protease were purified as previously described (Oliveira et al. 2010; Piskadlo, Tavares, and Oliveira 2017).

His_6-Rtnl1B was expressed and purified from *E. coli* Rosetta cells. A single colony was used to prepare a starting culture with 10 ml LB medium, grown overnight at 37°C. Using the starting culture, 10 ml were used to inoculate 1L of LB and expression was induced with 500 µl IPTG (0.5 mM) at O.D. 0.6-0.7, and incubated at 37°C for 3h. Lysis was performed in a French Press system (Emulsiflex C5 High Pressure Homogeneizer) with 4% Triton in the lysis buffer (50 mM HEPES, 400 mM NaCl, 10% glycerol, 1 mM PMSF, 1 mM β-mercaptoethanol, one tablet protease inhibitors, Roche, DNase at 10 units/µl). Affinity chromatography of His6-Rtn1B was performed using a 1 ml Nickel column (GE Healthcare). Elution of the protein was induced using an Imidazole gradient (0 to 500 mM) in Äkta purifier (GE Healthcare). Purified His6-Rtn1B buffer exchanged into storage buffer (10 mM HEPES, 100 mM KCl, 1 mM $MgCl_2$, 10% glycerol) using a PD-10 column. Serial dilutions of BSA, reconstituted in the same buffer, were loaded as standard concentrations to estimate His6-Rtnl1B protein concentration after size exclusion chromatography and concentration. Further purifications of His6-Rtnl1B were done using Nickel Sepharose beads (GE Healthcare) through affinity chromatography in a gravity column. To estimate protein concentration,

we first used Bradford and BCA methods, which did not seem to be accurate considering our analysis comparing His6-Rtnl1B and BSA standard concentrations in SDS gels. Later, we used nanodrop absorbance at 280 nm, with the estimated extinction coefficient for His6-Rtnl1B (30940 M^{-1} cm^{-1}, when reduced). We realized that our estimations of protein concentration were always compromised due to the high concentrations of Triton in our samples as described in the results section.

Purification of His6-Rtnl1B using Brij-35 detergent

To decrease the Critical Micelle Concentration (CMC) and, thus, to avoid high concentration of detergent during our purification protocol, we attempted to use Brij-35 (BRIJ® 35 Detergent, Protein Grade®, 10% Solution, Sterile-Filtered - CAS 9002-92-0 – Calbiochem) instead of Triton X-100. To do this, we prepared the lysis buffer as described above with 4% Brij-35. Wash buffers (50 mM HEPES, 400 mM NaCl, 10% glycerol, 1 mM β-mercaptoethanol, 20 mM imidazole) with decreasing concentration of Brij-35 were prepared to remove Brij-35 in a gradual manner (4%, 2%, 1%, 0.1%, 0.01% Brij-35 and without Brij-35). The final washing step was performed without Brij-35. For elution of the protein, we eluted and collected each fraction (first fraction eluted in 10 ml, followed by a second fraction eluted in 5 ml) with 100, 200, 300 and 500 mM imidazole. A sample from each fraction was collected to run a 12% SDS gel and identify the fractions containing the purified protein. After, the fractions eluted with 100 mM imidazole containing the purified protein were dialyzed overnight at 4°C into storage buffer (100 mM HEPES pH 7.8, 10 mM KCl, 1 mM $MgCl_2$, 10% glycerol) and concentrated using a centricon (10 kDa cutoff). This purified protein sample was concentrated to 2.5 µg/µl (nanodrop estimation method using absorbance at 280 nm as described before).

His_6-GFP-Rtnl1B was expressed and purified from *E.coli* Rosetta cells. Briefly, 1 L of auto-induction medium (NZY tech) was inoculated with 10 ml of a starting culture grown overnight at 37°C. Induction and expression

were done overnight at 25°C. Cells were harvested by centrifugation at 4200 rpm for 45 min. Lysis was performed in a French Press system (Emulsiflex C5 High Pressure Homogeneizer) with 1% Triton in the lysis buffer (50 mM HEPES, 400 mM NaCl, 10% glycerol, 1 mM PMSF, 1 mM β-mercaptoethanol, one tablet protease inhibitors, Roche, DNase at 10 units/µl). Wash buffer used was prepared as 50 mM HEPES, 400 mM NaCl, 10% glycerol, 0.1% Triton, 20 mM imidazole. A 5 ml Nickel column was loaded with the extract in the Äkta purifier (GE Healthcare). His_6-GFP-Rtnl1B fractions were collected after the affinity chromatography upon an Imidazole gradient (0 to 500 mM). His_6-GFP-Rtnl1B was buffer exchanged into storage buffer (10 mM HEPES, 100 mM KCl, 1 mM $MgCl_2$, 10% glycerol) and concentrated to 500 µl and injected into a size exclusion chromatography column (HiLoad Superdex 200 pg GE Healthcare). Further purifications of His_6-GFP-Rtnl1B were performed using the same expression and lysis protocols but using Nickel beads (GE Healthcare). Elution from the beads was performed into separated fractions with gradually increasing concentration of imidazole (50 mM HEPES, 400 mM NaCl, 10% glycerol, 0.1% Triton with imidazole – 100, 200, 300, 400 and 500 mM). A sample of each fraction (20 µl) was loaded in a 12% SDS gel to evaluate purity of each fraction. In this case, buffer exchange was performed using a centricon column with 30 kDa cuttoff (Ambion) previously equilibrated with storage buffer (10 mM HEPES, 100 mM KCl, 1 mM $MgCl_2$, 10% glycerol). Estimation of protein concentration was done in Nanodrop with the extinction coefficient for His_6-GFP-Rtnl1B (53080 M^{-1} cm^{-1}, when reduced).

For cytATL, the bacterial expression plasmid containing *D. melanogaster* cytATL sequence (pET28a-His_6-cytATL; kindly provided by Junjie Hu, Nankai University, China) was used to transform *E. coli* BL21 cells. Bacterial cells from an overnight-grown starting culture were grown in 1L LB medium, supplemented with Kanamycin (50 µg/ml), and incubated at

37°C. Protein expression was induced by adding 0.2 mM IPTG once the $O.D._{600}$ was at 0.8. The culture was grown at 18°C overnight and bacteria were harvested by centrifugation at 4200 rpm for 45 min, at 4°C. For protein purification, the following buffers were prepared freshly and filtered: 0.1 M KPi at pH 7.2; wash buffer (50 mM KPi pH 7.2, 400 mM NaCl, 1 mM ß-Mercaptoethanol, 7 mM imidazole), lysis buffer (50 mM KPi pH 7.2, 400 mM NaCl, 1 mM ß-Mercaptoethanol, 7 mM imidazole, 0.1% Triton X-100 supplemented with 1 tablet of protease inhibitors (Pierce™ Protease Inhibitor Mini Tablets, EDTA-free, reference A32955, Thermo Scientific) and DNAseI), elution buffer 1 (50 mM KPi pH7.2, 400 mM NaCl, 1 mM ß-Mercaptoethanol, 400 mM imidazole), elution buffer 2 (50 mM KPi pH7.2, 400 mM NaCl, 1 mM ß-Mercaptoethanol, without imidazole). Bacterial pellets were re-suspended in 10 ml lysis buffer, adding DNase and a protease inhibitor tablet onto the pellet directly. The lysate was then passed through a French press system (Emulsiflex C5 High Pressure Homogeneizer). Protein extract was spun at 16000 rpm for 45 min at 4°C, and the pellet was discarded. Ni sepharose beads (2-3 ml; GE Healthcare, 17-5318-01) were added into a 50 ml falcon tube. Beads were previously equilibrated in wash buffer. Protein extract was incubated with beads for 1h at 4°C with gentle agitation. Beads were washed 3 times with wash buffer (each round at 700 g for 5 min) and packed into a column PD-10 empty (GE Healthcare). The protein was eluted in distinct fractions with increasing concentrations of imidazole (80, 150, 300, 400 mM). The two fractions eluted with 300 and 400 mM imidazole were pooled together and dialyzed overnight at 4°C using a cassette (Slide-A-Lyzer Dialysis Cassettes 7 KDa MWCO, 12 ml, Life Technologies) into a 1 L volume of cytATL storage buffer (10 mM HEPES pH 7.8, 100 mM KCl, 1 mM $MgCl_2$, 10% glycerol). To concentrate the purified cytATL protein we used Amicon ultra centrifugal filter 15 mL with a 30 kDa cut-off (Millipore) and protein concentration was quantified in a Nanodrop using the A280 and the extinction coefficient 44350 $M^{-1}\,cm^{-1}$, when reduced.

Measurement of Mad2-EGFP intensity upon microinjection with Buffer/cytATL

Mad2-EGFP fluorescence intensity (mean intensity) was measured at metaphase, using the segmented line tool in Fiji to define the area of Mad2 foci over the metaphase plate and spindle MTs (excluding the ER signal). Graphs were generated in GraphPad Prism software. The statistical test used was unpaired t-test (using 0.01 as a confidence level for the analysis), two-tailed, also performed in GraphPad.

ER fluorescence intensity

ER mean intensity of control- (+Buffer) and cytATL-injected embryos was measured for the last time point (t=10 min) of the time-lapse imaging. A circle ROI with the same area was used to measure the mean intensity at the spindle pole or at the equator regions in the ER channel. Relative signal dispersion was calculated by the ratio between the standard deviation (stdev) and the mean fluorescence intensity (mean).

Area and perimeter of ER exclusion zone and spindle

To quantify the area and perimeter of the ER exclusion zone and of the spindle, a single z slice corresponding to the middle plane of each nucleus was used. All the measurements were performed using the segmented line tool in Fiji (yellow shapes in Fig. 2.8.A, insets), for each channel (ER, spindle) separately.

Chapter 4

ER membranes are continuously required to maintain mitotic spindle size and forces

Author contribution:

All the experiments presented in this chapter were performed and analyzed by Margarida Araújo. The experiments were designed by Margarida Araújo, Ivo A. Telley and Raquel A. Oliveira. Alexandra Tavares prepared, and purified proteins used in some of the experiments.

4.1. Introduction

ER membranes have recently been proposed to hinder efficient chromosome segregation. When ER membrane biogenesis is increased by enhanced fatty acid synthesis, this leads to higher viscosity of the cytoplasm and ultimately to chromosome mis-segregation (Merta et al. 2021). Moreover, chromosomes that become unsheathed by the ER are more prone to segregation errors (Ferrandiz et al. 2022). Hence, ER reorganization may be a passive event, required for faithful mitosis and even distribution of this organelle to daughter cells (Smyth et al. 2015). Reciprocally, it has also been proposed that ER reorganization plays a functional role during mitosis.

On one hand, the ER enclosing the spindle could act as a molecular exclusion barrier sorting or concentrating for cell cycle and spindle relevant proteins (Schweizer et al. 2015). On the other hand, it is conceivable that the ER plays a mechanical role and balances spindle forces, thus adjusting e.g. the spindle length (Dumont and Mitchison 2009). This is mostly supported by the observation that functional disruption, at mitotic entry, of another membranous structure – the nuclear envelope – perturbs spindle assembly (Tsai et al. 2006; Z. Liu and Zheng 2009; L. Ma et al. 2009; Civelekoglu-Scholey et al. 2010). At the molecular level, REEP proteins were shown to be involved in the exclusion of ER membranes from the spindle region during mitosis (Schlaitz et al. 2013). Furthermore, the ER targeting kinase TAOK2 is important for tethering of ER membranes to the MT cytoskeleton and for ER mobility along MTs during mitosis (Nourbakhsh, Ferrecccio, and Yadav 2021). Altogether, these studies exposed the role of membranes during mitosis and demonstrated that the association between the ER and MTs is important for spindle assembly. Whether this association is required continuously, even after unperturbed spindle assembly, is currently unknown.

Deciphering an actively contributing versus passively hindering role of the ER during mitosis is critical. However, investigating these potential roles is technically challenging due to the inability to perturb such a critical structure for cell physiology in a fast and temporally controlled manner. Here, we used microinjection approaches to disrupt acutely ER membranes in a metaphase-arrested state and examine mitotic spindle morphology and function upon loss of ER integrity. We uncovered that ER membranes surrounding the spindle pole are important for the maintenance of mitotic spindle architecture and forces.

4.2. Results

4.2.2. Acute disruption of spindle pole-proximal ER membranes decreases mitotic spindle size

Having established a method that acutely disrupts ER integrity in mitosis (Chapter 3), particularly at centrosome-proximal regions, we next sought out to evaluate the effect this disruption has on mitotic spindle architecture. For this, we co-injected UbcH10^{C114S} with porcine Tubulin labelled with AlexaFluor 647 to visualize spindle microtubules during the metaphase arrest (Movie 4.2.). Upon cytATL-induced ER disruption, we found that the morphology of the spindle is significantly altered (Fig. 4.2. B-C, t=10:00 min). Changes in spindle architecture are evidenced by a reduction in spindle length and width, whereas no significant changes were observed in control embryos (Fig. 4.2. D-E). Thus, we conclude that ER morphological changes mediated by the dominant-negative effect of cytATL lead to smaller mitotic spindle size. In addition to this effect, we also observed, at considerable frequency, the detachment of the spindle pole microtubule-organizing center (MTOC) upon ectopic addition of cytATL.

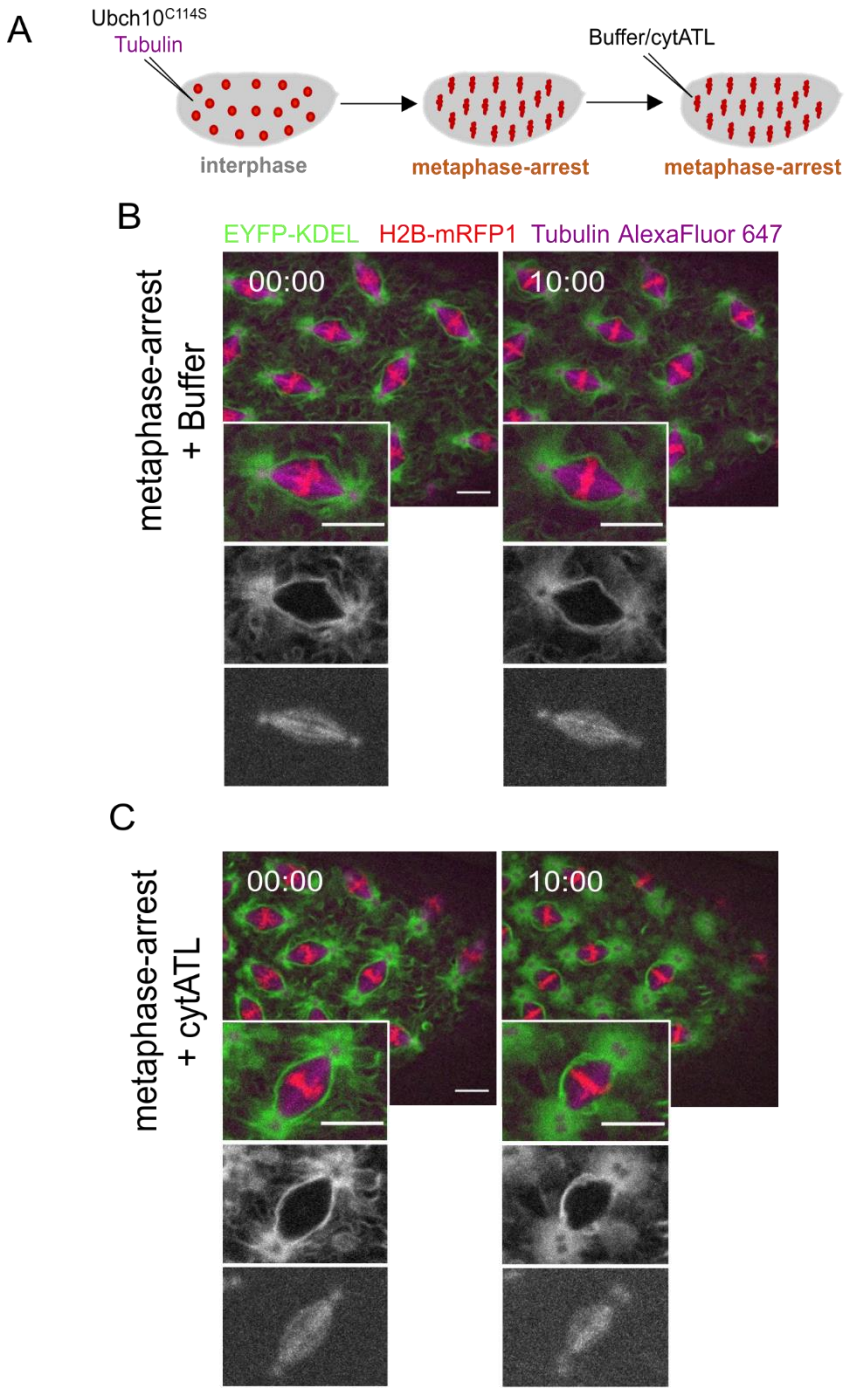
A
Ubch10C114S
Tubulin
Buffer/cytATL
interphase
metaphase-arrest
metaphase-arrest
B
EYFP-KDEL H2B-mRFP1 Tubulin AlexaFluor 647
metaphase-arrest
+ Buffer
00:00
10:00
C
metaphase-arrest
+ cytATL
00:00
10:00

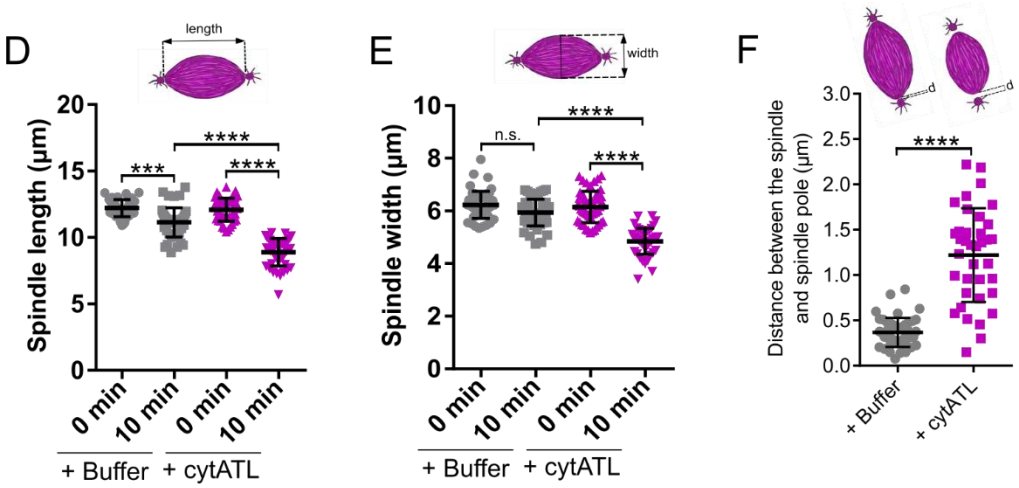

Figure 4.2. Spindle shape is affected upon cytATL-mediated ER disruption. *(A) Schematics of the experimental layout: embryos were microinjected with UbcH10^{C114S} and Alexa Fluor 647-labelled Tubulin (to visualize spindle microtubules), followed by subsequent microinjection with buffer/cytATL. (B-C) Representative control (B) and cytATL-injected embryos (C), showing the ER (EYFP–KDEL, green), chromosomes (H2B–mRFP, red) and the spindle (magenta) at the first (t=00:00 min) and last (t=10:00 min) time points after microinjection with buffer/cytATL. Grey panels depict ER (top) and spindle (bottom) alone. Scale bar is 10 µm. (D, E) Quantification of spindle length (D) and width (E) in control (+buffer, grey) and cytATL (+cytATL, magenta) embryos at the first (t = 0 min) and last (t = 10 min) time points of the time lapse. Asterisks depict the statistical significance derived from Kruskal–Wallis test (D, E), Dunn's multiple comparisons test ***P = 0.0001, ****P < 0.0001, n.s. P > 0.05 (N = 10 embryos, n = 5 nuclei). (F) Distance d between the focal point of the spindle and the spindle pole. Asterisks depict the statistical significance derived from the unpaired two-tailed Mann–Whitney (nonparametric) test, ****P < 0.0001 (N = 10 embryos, n = 5 nuclei).*

To quantify this, we measured the distance between the focal point of the spindle body and the MTOC; this distance was markedly higher upon ectopic addition of cytATL, on average 3 times the distance measured in control embryos (Fig. 4.2. F, 0.4 ± 0.2 µm versus 1.2 ± 0.5 µm). Overall, our spatially resolved perturbation of ER membranes reveals that the ER surrounding the spindle poles plays multiple roles in spindle architecture, including spindle size and spindle pole attachment.

Given the observed changes in spindle architecture upon impairment of spindle pole-proximal ER membranes, we next investigated whether spindle dynamics would also be affected. We used FRAP to bleach one half of the spindle in metaphase-arrested embryos and analyzed spindle microtubule turnover. We used embryos expressing β-tubulin–GFP and monitored the recovery of the fluorescence intensity after photobleaching (Fig. 4.3. G, Movie 4.3.). In control (buffer-injected) conditions, this analysis revealed that spindle microtubules recover very fast, with a half-time of recovery of 10.7 ± 2.2 s (Fig. 4.3. G, grey).

We next repeated the same analysis after cytATL-mediated ER disruption. In this condition, we found that MT turnover remained unaltered relative to controls (Fig. 4.3. G, magenta). These results imply that despite the marked difference in spindle size, the dynamic behavior of MTs remains unaltered.

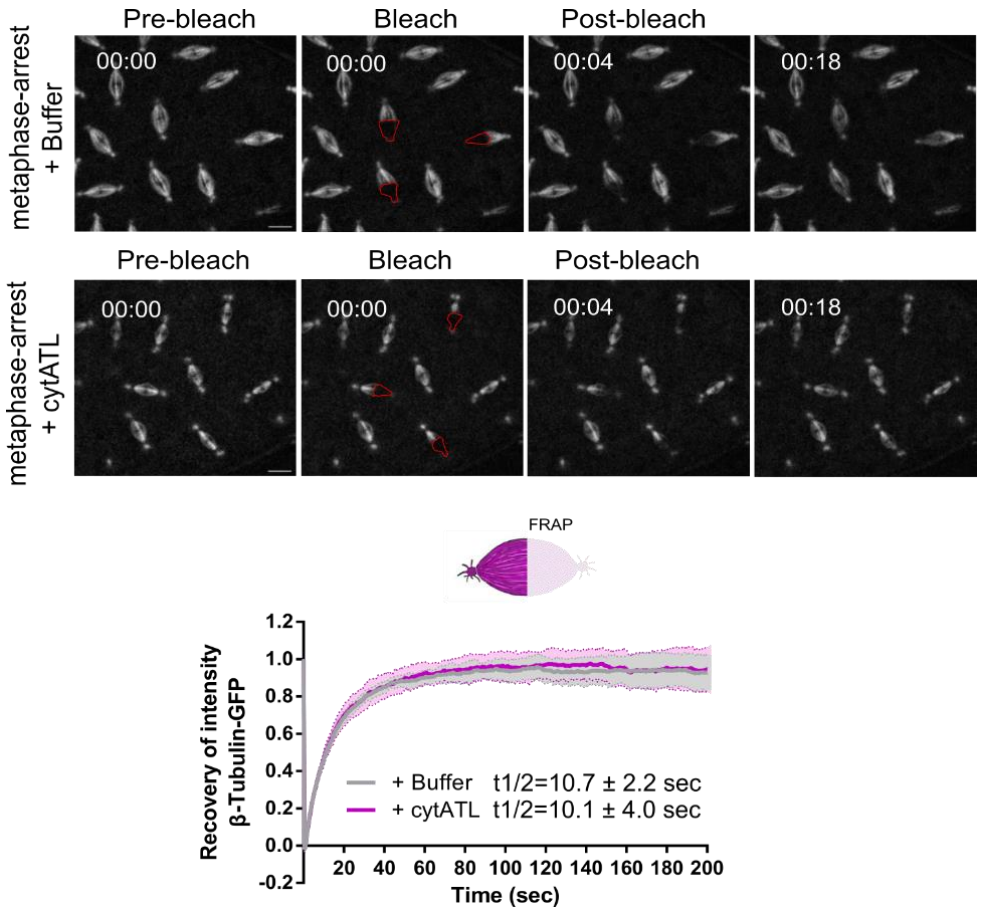

Figure 4.3. MT dynamics is unaffected upon cytATL-driven disruption of the ER. *FRAP assay of β-tubulin–GFP in UbcH10^{C114S}-arrested embryos (metaphase arrest) in control (Buffer injection) and ER disruption (+ cytATL) conditions. Right: graph depicts recovery of β-tubulin-GFP intensity after bleaching in both conditions and calculated half times of recovery (mean ± SD, N=5 embryos, n=3 nuclei). Scale bar is 10 µm.*

To confirm this notion, next we measured MT growth using the plus-end protein EB1 and time-lapse imaged embryos expressing a GFP-tagged EB1 protein (EB1–GFP) in control or cytATL injected embryos (Fig. 4.4. H, left, Movie 4.4.). Since EB1–GFP localizes to growing microtubule ends it displayed moving speckles within the spindle in time-lapse images. To

estimate MT growth speed, we generated space-time projections (kymographs) along the spindle axis, which transform the continuously moving speckles to linear signals (Fig. 4.4. H, middle). However, analysis of growth speed revealed no significant differences between control and cytATL injected embryos (Fig. 4.4., right). Thus, we conclude that the observed changes in spindle architecture upon ectopic addition of cytATL are not accompanied by changes of microtubule dynamics. From this insight, we hypothesized that the ER confers constraining mechanical force on the mitotic spindle, which could play a role in spindle function.

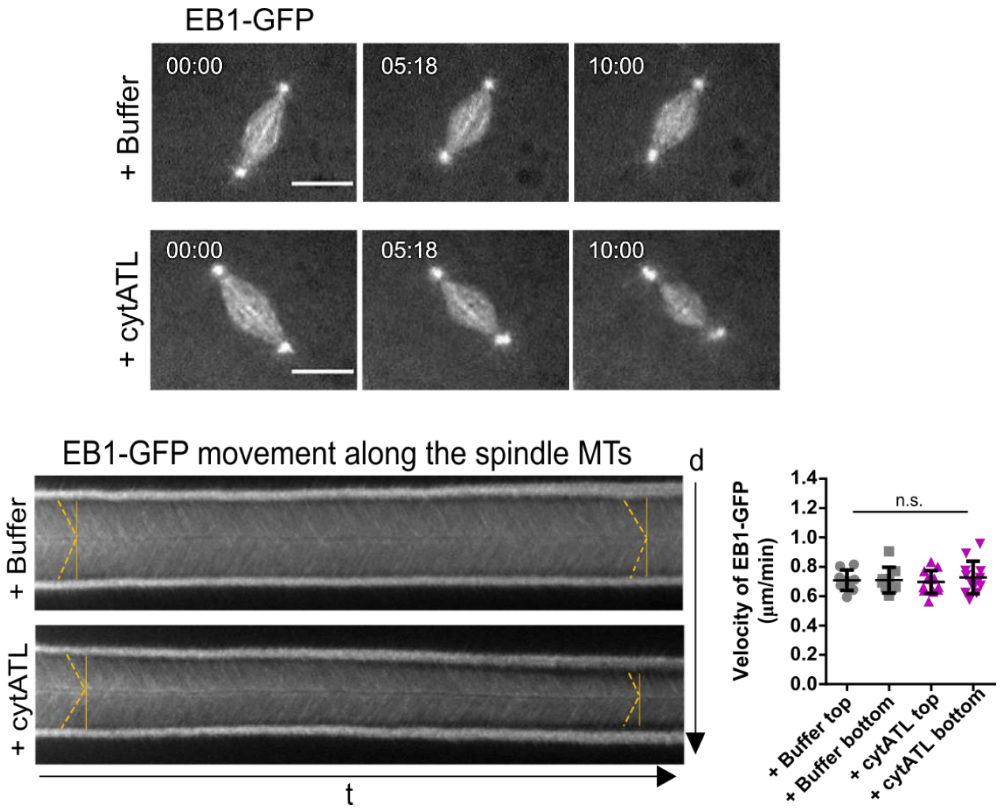

Figure 4.4. EB1 dynamics is unaffected upon cytATL-driven disruption of the ER. *Analysis of MT growth rate with and without ER disruption (buffer/cytATL injection) in metaphase arrested embryos. Microtubule plus-ends were monitored using a GFP-tagged EB1*

transgene. Time (min:s) is relative to microinjection with buffer/cytATL. Scale bar is 10 µm. Middle: Kymographs of EB1–GFP intensity were generated, and the angles of EB1 tracks (yellow lines) were used to estimate the velocities of MT growth, shown on the right. Statistical analysis was performed using one-way ANOVA. n.s., nonsignificant, P > 0.05 (N = 4 embryos, n = 3 nuclei).

4.2.3. cytATL-mediated disruption of the ER impairs mitotic spindle pulling forces

We next asked how the smaller spindles that result from acute and local perturbation of spindle pole-proximal ER membranes behave at the functional level. For this, we took advantage of a molecular tool that enables the artificial separation of sister chromatids. With this approach, fast Cohesin inactivation is achieved by the Tobacco Etch Virus (TEV) protease in embryos surviving on a modified version of Rad21 that contains TEV cleavage sites (Pauli et al. 2008). Upon microinjection of TEV protease, sister chromatid separation is observed within 1–2 minutes (Oliveira et al. 2010; Carmo, Araújo, and Oliveira 2019). This tool allowed us to investigate changes in pulling force on chromatids, as poleward movement of separated sister chromatids relies on how efficiently they are pulled apart by spindle microtubules. Embryos were first arrested in metaphase, followed by ectopic addition of cytATL or buffer. 10 minutes after cytATL/buffer injection, embryos were injected with TEV protease to trigger artificial sister chromatid separation (Fig. 4.5. A, Movie 4.5.).

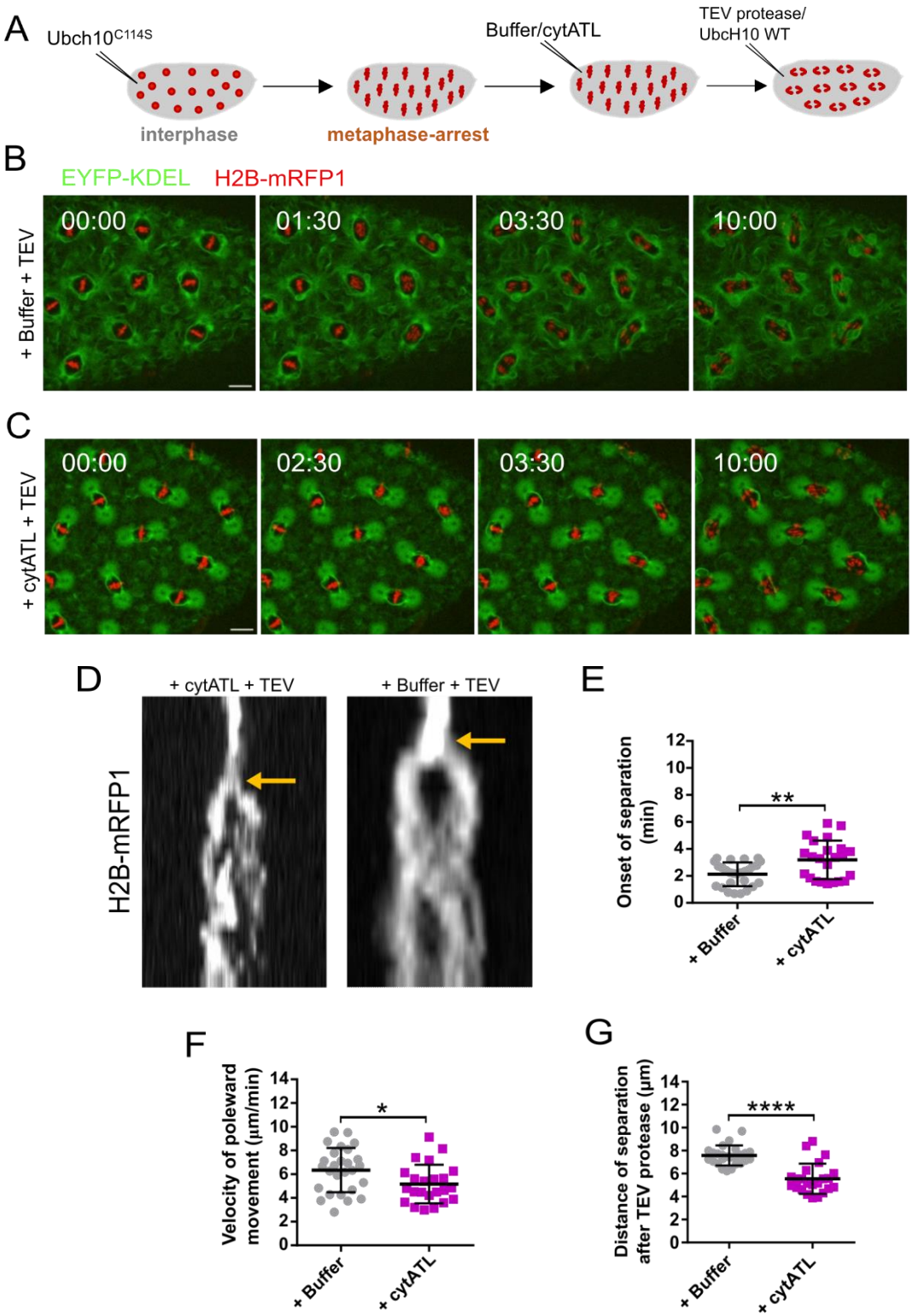
A
Ubch10C114S
interphase
metaphase-arrest
Buffer/cytATL
TEV protease/
UbcH10 WT
B
EYFP-KDEL
H2B-mRFP1
+ Buffer + TEV
00:00
01:30
03:30
10:00
C
+ cytATL + TEV
00:00
02:30
03:30
10:00
D
+ cytATL + TEV
+ Buffer + TEV
H2B-mRFP1
E
Onset of separation (min)
**
+ Buffer
+ cytATL
F
Velocity of poleward movement (µm/min)
*
+ Buffer
+ cytATL
G
Distance of separation after TEV protease (µm)
****
+ Buffer
+ cytATL

Figure 4.5. Lower efficiency of sister chromatid separation was revealed upon cytATL-driven disruption of the ER. *(A) Experimental layout: embryos were arrested in metaphase (UbcH10^{C114S} microinjection), followed by microinjection with buffer/cytATL. After 10 min, embryos were subjected to a third microinjection with TEV protease, to induce acute sister chromatid separation. Embryos surviving solely on a TEV-cleavable version of Rad21 (Cohesin) were used for these experiments. (B-C) Stills from embryos after microinjection with buffer/cytATL were subsequently microinjected with TEV protease to trigger cohesin cleavage (+Buffer+TEV, B; +cytATL+TEV, C); ER is labelled in green (EYFP–KDEL) and chromosomes in red (H2B–mRFP1); scale bar is 10 µm; time (min:sec) is relative to microinjection with TEV. (D) Kymographs depict chromosome positioning over time; arrows highlight the onset of chromatid separation. (E-G) Quantification of the onset of separation (E), velocity of poleward movement (F) and distance of chromatids separation (G) induced by cohesin cleavage (+TEV), in conditions with intact ER (+Buffer) or disrupted ER (+cytATL). Sample size: N=5 embryos, n=5 different nuclei for each experimental condition. (E, F, G) Asterisks refer to statistical significance, derived from unpaired t tests (two-sided) (E, F), nonparametric Mann–Whitney test (G) *P < 0.05, **P < 0.01, ***P < 0.001, ****P < 0.0001, n.s., nonsignificant, P > 0.05.*

Under both conditions sister chromatids separated (Fig. 4.5. B-C). Analysis of chromosome movement was performed based on kymographs that display chromosome position over time (Fig. 4.5. D). In control embryos, we found that sister chromatid separation, defined by the bifurcation in the kymograph (Fig. 4.5. D, arrow), is elicited within ~2 minutes upon microinjection with TEV protease while it is delayed upon ectopic addition of cytATL (Fig. 4.5. E). Moreover, the velocity of initial poleward-movement of sister chromatids along the spindle axis, as

estimated by the angle of signal bifurcation in the kymograph, is reduced upon cytATL-driven ER disruption compared to the control condition (Fig. 4.5. F). The range of chromatid separation along the spindle axis is also reduced upon cytATL addition (Fig. 4.5. G), which we attribute to lower separation velocity and overall shorter spindle size. After the initial separation, isolated sisters from both experimental conditions (buffer/cytATL) were equally able to engage into oscillatory movements driven by cycles of chromosome capture/detachment (Fig. 4.6. A). Nevertheless, the range of separation of sister chromatids is lower than in the control, depicted by a smaller area occupied by sister chromatids upon cytATL-driven disruption of the ER (Fig. 4.6. B, magenta). A clear shift in frequency distribution also corroborates this result: compared to the control, cytATL-microinjected embryos show lower frequency distribution of distances between sister chromatids (Fig. 4.6. C, magenta).

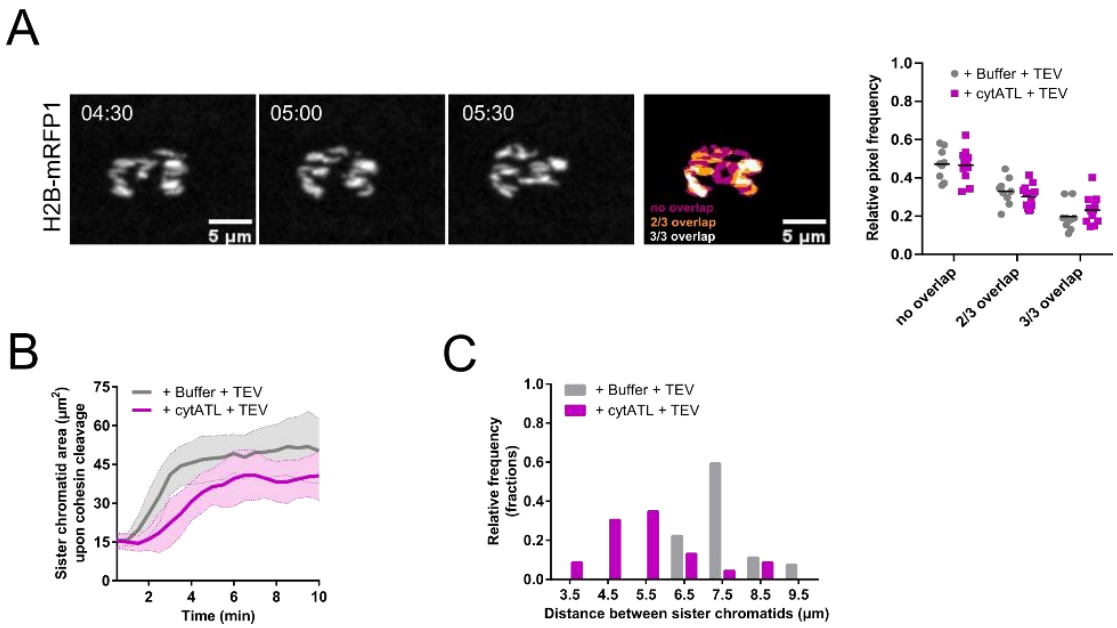

Figure 4.6. Quantification of oscillatory movements upon sister chromatid separation induced by TEV-mediated cleavage of

cohesin. *(A) Quantification of the oscillatory behavior of separated sister chromatids (relative to Fig. 4.5.). The movement of sister chromatids was estimated by measuring the overlap between them in three consecutive time frames (no overlap – magenta, 2 out of 3 frames overlap – orange, 3 out of 3 frames overlap – white). Relative pixel frequency for each category is quantified, displaying no significant difference between the two conditions (Buffer – grey, cytATL – magenta). Statistical analysis using N=5 embryos, n=5 nuclei per embryo, using unpaired t-test, two-sided. (B) Quantification of the area occupied by sister chromatid upon TEV-cleavage of Cohesin, depicting a delay in the onset of sister chromatid separation and a lower area occupied in space for cytATL (magenta) compared to control embryos (grey). (C) Frequency distribution of distance between sister chromatids indicating an increased frequency of measurements ≤ 5.5 µm for cytATL embryos (magenta).*

We conclude that the short spindles imposed by acute ER disruption are still able to pull and capture chromatids. However, poleward chromatid movement occurs at slower velocity, implying a decrease in pulling forces on chromatids.

4.2.4. cytATL-driven disruption of the ER affects nuclear spacing upon release from the metaphase arrest

Our previous work has revealed that the spindle pole MTOC plays a crucial role in daughter nuclei separation and nuclear spacing in the syncytial embryo (Telley et al. 2012; de-Carvalho et al. 2022). Having observed spindle pole detachment upon cyATL injection (Fig. 4.2.), we next aimed to probe nuclear separation after disruption of the ER in embryos undergoing the changes characteristic of a normal mitotic exit.

For this we took advantage of an inducible release of the metaphase-arrest reported previously (Piskadlo, Tavares, and Oliveira 2017) we

induced a metaphase-arrest in division cycle 10 using the dominant-negative UbcH10^{C114S} for 5 min, followed by injection of buffer/cytATL and waited for 10 min to allow for ER disruption. Embryos were subsequently injected with a wild-type version of UbcH10 protein, which induces anaphase onset and, thus, mitotic exit in 4–8 min (Fig. 4.7. A). Using this approach coupled to time-lapse imaging, we then generated kymographs of the chromatin signal and tracked chromosome segregation and daughter nuclei separation. This analysis revealed that sister chromatids are separated at a similar velocity during anaphase in both control and cytATL conditions (Fig. 4.7. E-F, Movie 4.7.). This contrasts with what we observed in embryos arrested in metaphase (+TEV cleavage of cohesin) suggesting that anaphase-specific changes may compensate for the reduced pulling forces observed upon ER disruption in metaphase. However, despite normal segregation speeds, daughter nuclei were not efficiently separated during telophase and early interphase upon ER disruption (Fig. 4.7. D-H). This process is driven by the centrosome-nucleated microtubule aster (Telley et al. 2012) and, therefore, the reduced separation upon ER disruption is likely caused by the defects observed on spindle pole attachment. Furthermore, the inefficient separation led to a lower nuclear ordering in the subsequent interphase. In our control experiments, UbcH10-arrest/release approach is able to reproduce the non-sibling internuclear distance recently reported for this division cycle (cycle 11) (de-Carvalho et al. 2022). In contrast, upon ER disruption, sibling nuclear distance was shorter and the distances between non-sibling nuclei were longer when compared to the control condition (Fig. 4.7. H).

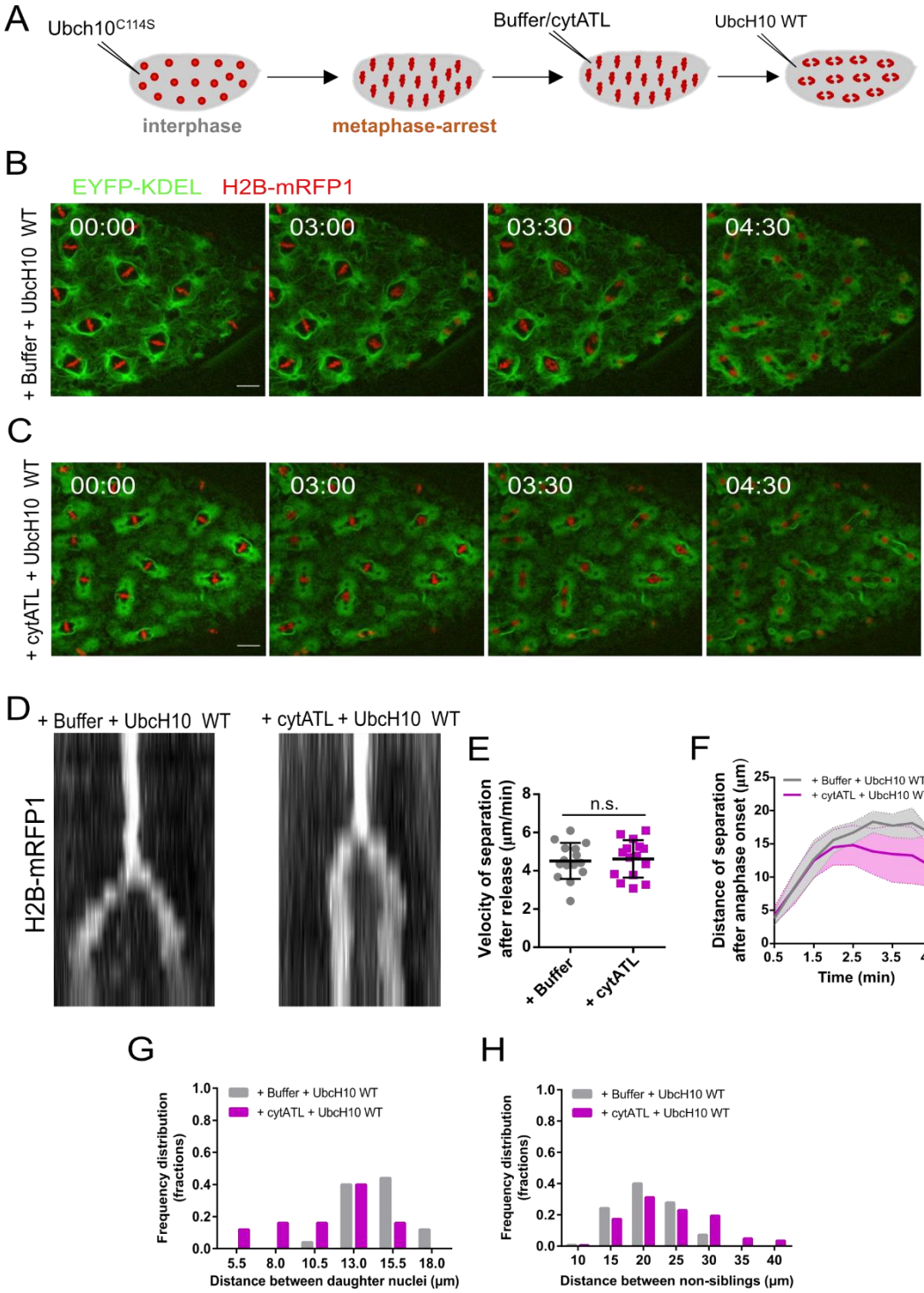
A
Ubch10C114S
Buffer/cytATL
UbcH10 WT
interphase
metaphase-arrest
B
EYFP-KDEL H2B-mRFP1
+ Buffer + UbcH10 WT
00:00
03:00
03:30
04:30
C
+ cytATL + UbcH10 WT
00:00
03:00
03:30
04:30
D
+ Buffer + UbcH10 WT
+ cytATL + UbcH10 WT
H2B-mRFP1
E
Velocity of separation after release (µm/min)
n.s.
+ Buffer
+ cytATL
F
Distance of separation after anaphase onset (µm)
+ Buffer + UbcH10 WT
+ cytATL + UbcH10 WT
Time (min)
G
Frequency distribution (fractions)
+ Buffer + UbcH10 WT
+ cytATL + UbcH10 WT
Distance between daughter nuclei (µm)
H
Frequency distribution (fractions)
+ Buffer + UbcH10 WT
+ cytATL + UbcH10 WT
Distance between non-siblings (µm)

Figure 4.7. Nuclear spacing is affected upon cytATL-mediated ER disruption. *(A) Experimental layout: embryos were arrested in metaphase (UbcH10^{C114S} microinjection), followed by microinjection with buffer/cytATL. After 10 min, embryos were subjected to a third microinjection with UbcH10 WT, to induce anaphase onset. Time lapse images of induced anaphase in unperturbed ER (B, +Buffer+UbcH10^{WT}) and perturbed ER (C, +cytATL+UbcH10^{WT}) conditions; ER is labelled in green (EYFP–KDEL) and chromosomes in red (H2B–mRFP1); scale bar is 10 µm; time (min:sec) is relative to microinjection with UbcH10^{WT}. (D) Kymographs depict chromosome positioning over time. (E-F) Quantification of the velocity of chromosome separation (E) and distance of chromosome separation (F) triggered upon artificial induction of anaphase (UbcH10^{WT}) in embryos previously injected with buffer or cytATL. Sample size: N=5 embryos, n=3 different nuclei for each experimental condition. (G-H) Frequency distributions of distance between daughter nuclei (G) and non-sibling nuclei (H) measured 3 minutes after anaphase onset; sample size: 3-4 measurements, N=5 embryos (H) and 6 measurements, N=5 embryos (G). Statistical significance, derived from unpaired t tests: n.s. = non-significant, p>0.05.*

Thus, these results suggest that disruption of the ER at centrosome-proximal regions decreases the efficiency of sister chromatid separation and affects nuclear spacing upon mitotic exit. We showed that the ER around centrosomes might be important to maintain proper spindle architecture and function in *Drosophila* syncytial embryos.

Discussion

This chapter focused on understanding the role of the ER in spindle architecture and function. Our main finding was that ER membranes located in the vicinity of the spindle poles are critical for maintenance of proper mitotic spindle shape. This novel role for ER membranes is required throughout metaphase, even after unperturbed spindle assembly. Specifically, we observed that under the effect of cytATL, spindles became smaller concurrently with detached spindle poles from the spindle body.

Towards understanding if the spindle architectural changes we observed were biologically relevant, we sought to probe spindle function. To do this, we took advantage of the TEV-cleavage system of cohesin, which enabled us to artificially separate sister chromatids. Using this tool, we found that the efficiency of sister chromatid separation was lower upon cytATL-mediated disruption of the ER. Briefly, we observed a slight delay and a reduced distance of sister chromatid separation under the effect of cytATL compared to the control condition. Nevertheless, the oscillatory behavior of sister chromatids did not change between the control and cytATL conditions.

The tool described above was used as an artificial way to induce the separation of sister chromatids during metaphase. However, this experimental set-up does not recapitulate the forces generated by the spindle under a normal anaphase. Thus, this motivated us to induce the release of metaphase-arrest to monitor sister chromatid separation under an anaphase-like spindle configuration. Using this approach, we found that although the efficiency of separation was similar to the control, a reduced distance between daughter nuclei was observed upon cytATL-driven ER disruption.

In our control experiments, the metaphase-arrest/release approach was able to reproduce the non-sibling internuclear distance recently reported for this division cycle (cycle 11) (de-Carvalho et al. 2022). In contrast, upon ER disruption, sibling nuclear distance was shorter and the distances between non-sibling nuclei were longer when compared to the control condition.
In summary, these results highlighted that the role of the ER in spindle architecture goes well beyond the phase of spindle assembly at early mitotic stages, as previously reported (Schweizer et al. 2015; Z. Liu and Zheng 2009).

ER shaping and MT dynamics were previously molecularly linked. Specifically, the human ortholog Atlastin-1 interacts with Spastin, a microtubule-severing ATPase, within tubular ER membranes in neurons (Park et al. 2010). Spastin is known to participate in important cellular processes such as cytokinesis, endosomal tubulation, and axon development (Goyal et al. 2014). Whether the interaction between Atlastin and Spastin is conserved during mitosis is not known. Nonetheless, our results indicate that MT dynamics is not affected upon cytATL-driven disruption of the ER.

Previous work suggested that membranous structures surrounding the spindle can affect molecular crowding and thereby impact on spindle assembly (Schweizer et al. 2015). Although we cannot exclude whether changes in the molecular composition are also imposed in our experiments, the finding that spindle dynamics remains largely unaltered suggests this is not the case. In agreement with our results, a recent study showed that Atlastin depletion by RNAi leads to altered distribution of MTs in human cells without compromising MT dynamics (Tikhomirova, Kadosh, and Saukko-paavola 2022). Importantly, this study revealed that ER dynamics impacts on the distribution of MTs in the cell. When atlastin

is depleted, the balanced junction dynamics becomes disrupted leading to instability of the ER–MT system and MT bundling (Tikhomirova, Kadosh, and Saukko-paavola 2022). In cells where MT distribution must be well regulated like in motile cells or in neuronal axons this mechanism may be relevant. But, whether the same mechanism acts on the mitotic spindle MTs remains elusive.

Despite these referred examples of a direct role of ATL or ATL-binding partners in MT dynamics, we believe that no MT bundling is taking place in our experiments. If this was the case, we would expect to find either longer spindles or stronger tubulin intensity upon impairment of Atlastin function by cytATL, Still, further investigation would be required to determine what is exactly causing spindle shortening. Alternatively, our results suggest that the ER is playing a role in the integrity of spindle poles. It remains to be determined how the centrosome-proximal ER membranes maintain spindle shape. A caveat of our live imaging is that we had the ER, chromatin, and the spindle MTs labeled and, thus, imaging of three different channels limited the depth of our z-stacks.
For live imaging experiments of living *Drosophila* embryos, one must compromise on the intensity, time resolution and the depth of the z stacks. The main reason for this is because we need to image in a shorter time scale than the usual live imaging of other mitotic cells/tissues. Syncytial nuclear divisions in these embryos are extremely rapid (~8 min), and so, time is not in our favor. We generated a 3D reconstruction of metaphase nuclei and found that the centrosomes/MTOCs are outside the exclusion zone of the spindle. Contrary to mammalian cells, for example, in which centrosomes are inside the ER exclusion zone (Ferrandiz et al. 2022). These membranes enclosing centrosomes/MTOCs can also be found during embryonic divisions in other organisms like sea urchin and *C. elegans* (Mukherjee et al. 2020; Maheshwari et al. 2022). It is conceivable that a specialized network of ER or that ER organization around the

centrosome is required for segregation of this organelle during fast embryonic divisions. Alternatively, it is also reasonable to think that this configuration of the ER network might have an active role during mitosis. Since the molecular aspect of the spindle seemed to be unchanged in our experiments, we favored that the ER could have role in mechanical force transmission and balancing of forces generated by the spindle. ER membranes in this gap region may be important in attachment of the spindle pole MTOC and the anchoring of the microtubule aster to the nuclear envelope. This is particularly relevant during syncytial divisions, as ordered nuclear positioning needs to be established in the absence of proximal cell (plasma) membrane.

In support of this idea, a new study recently showed that specialized ER membranes associated with the centrosome – denominated by the authors as “centriculum” (centrosome-associated membrane reticulum) – can regulate centrosome size and function in *C. elegans* divisions (Maheshwari et al. 2022). Using volume electron microscopy, they showed that increasing centriculum size leads to expansion of the PCM and increased MT nucleation. This is quite surprising, as the PCM is a membrane-less compartment. Depletion of different PCM proteins by RNAi led to the disappearance of the centriculum, showing that its formation requires the presence of the PCM. Increasing centriculum size by changing ER organization with mild depletion of Atlastin and an auxin-degron system for Atlastin, also increased centrosome size (Maheshwari et al. 2022).

A very interesting conclusion from the study mentioned above, is that it revealed a clear interdependency between the centrosome/PCM and this ER structure around the centrosome. This was elegantly shown by conditions that abrogated the formation of the centriculum, which also led to disrupted centrosome and/or MT assembly.

The authors of this study also proposed that these centrosome-associated membranes may limit the number of extended microtubules by restricting the size of the PCM – which limits MT nucleation – and blocking the extension of MTs beyond these membranes (Maheshwari et al. 2022).

Another exciting speculation put forward by this study was that these centrosome-associated ER membranes may be less able to resist to centrosome-associated forces upon downregulation of atlastin, promoting an increase in centrosome size (Maheshwari et al. 2022).
However, in this study, only the 1 cell stage *C. elegans* embryo was used to analyse the structure of the centriculum, which in my view is a very narrow and particular stage of embryonic development. In *C. elegans* 1 cell-embryos, there is a large pool of ER membranes in the cytoplasm and the two parental nuclei fuse before the first mitotic division. This process in itself is under considerable nuclear remodelling events, which as such might largely depend on the pool of ER membranes available in the cell. Because of this, it would be important to look at the subsequent cell divisions to understand whether this could be a general mechanism governing centrosome size in this system.
Even though we only used light microscopy in our work, we showed that changing ER topology at spindle poles affects not only spindle size but also spindle function both in an artificial and in a more like a normal mitotic exit.

One thing that we did not test in our study is whether the secretory pathway is affected under the effect of cytATL. However, Orso et al. (2009) found that downregulation of atlastin does not affect secretory traffic in *Drosophila* larval neurons (Orso et al. 2009a). Instead, loss of atlastin induced ER fragmentation but neither affected Golgi architecture, ER exit sites nor mCD8-GFP membrane transport. The results in this

study suggested that Atlastin is unlikely to play a role in secretory traffic (Orso et al. 2009a).

We also did not address whether the changes in ER morphology in our experiments are caused due to ER stress upon addition of cytATL. To test for this, we could use tunicamycin (inhibits glycosylation of ER proteins), thapsigargin (perturbs ER calcium homeostasis) or DTT (blocks disulfide bond formation necessary for the folding of many ER proteins) as ER-stress inducing drugs and add through microinjection into syncytial embryos. We would have to compare the effect on the ER upon microinjection of these drugs with the one we observed for cytATL. Alternatively, we could probe for the upregulation of the ER-stress reporter Xbp1 (O'Sullivan et al. 2012) upon microinjection of cytATL comparing to the control condition.

In the last years, the development of novel methods namely serial section electron tomography, volume electron microscopy and lattice light-sheet microscopy, allowed to examine the ultrastructure and morphology of microtubules, nuclear and ER membranes in detail (Redemann et al. 2019; Penfield et al. 2020; Moore et al. 2021; Maheshwari et al. 2022). The use of such technologies led to the emergence of several studies describing different aspects of the mitotic spindle and ER membranes.

It has become more and more evident that ER membranes are not just passive membranes that must be equally partitioned at the end of mitosis. They are rather implicated in spindle assembly (Schweizer et al. 2015), in the establishment of proper kinetochore-spindle attachments in human cells (Merta, Harris, and Needleman 2021; Ferrandiz et al. 2022), in maintaining proper spindle shape in *Drosophila* syncytial embryos (Araújo et al. 2022), and, intriguingly, in centrosome size and function in *C. elegans* fist mitotic divisions (Maheshwari et al. 2022).

Taken together, these different studies shed light on the contribution of the ER in cell division.

Materials and Methods

Fly stocks

Fly strains expressing EYFP-ER (LaJeunesse et al. 2004) and for induction of artificial sister chromatid separation (Pauli et al. 2008; Oliveira et al. 2010) have been previously described. Flies were maintained at 25°C throughout the course of the experiment (from the moment when the cross was established to the selection of the F1 progeny). To maximize egg laying, cages were prepared with flies 5 days after eclosion. A detailed list of the stocks can be found in Table 4.

Table 4. List of *Drosophila* stocks used in this study

Genotype	Reference
Avic\GFP$^{EYFP.sqh.Tag:SS(hCALR).Tag:ER(KDEL)}$ (EYFP–KDEL)	BDSC #7195 (LaJeunesse et al. 2004)
w[*]; P{w[+m]=betaTub56D-EGFP.I}17-1, H2Av-mRFP1; MKRS/TM6B*	Described in (de-Carvalho et al. 2022). Originally described in (Y. H. Inoue et al. 2004); Kyoto Stock Center #109603
w[1118]; P{w[+mC]=ncd-Eb1.GFP}M1F3 Expresses GFP-tagged Eb1 protein during oogenesis and early mbryogenesis under control of ncd regulatory sequences. (ncd>EB1–GFP)	BDSC #57327
w;; Rad21^{ex15}, polyubiq-H2B-RFP, tubpr-Rad21$^{(550-3TEV)}$-myc10 (4c)*	Described in (Oliveira et al. 2010), named here #629
w; EYFP-ER; Rad21^{ex15}, polyubiq-H2B-RFP, tubpr-Rad21$^{(550-3TEV)}$-myc10 (4c)*	Derived from BDSC #7195 and #629 (see above)

Microscopy

Time-lapse movies of live embryos were obtained using Confocal Z-series stacks with a Yokogawa CSU-X Spinning Disk confocal, mounted on a Leica DMi8 microscope, with a 63x 1.3NA glycerine immersion objective, using the 488 nm, 561 nm and 637 nm laser lines and a Andor iXon Ultra EMCCD 1024x1024 camera. The system was controlled with Metamorph software (Molecular Devices). For the sequential microinjection experiments, we used 30 sec time points and a total of 10 min for each time-lapse acquisition, with 0.4-0.5 µm z-step size and 15 slices.

Quantification of MT growth and sister chromatid movement

Analysis of EB1 dynamics and chromatid poleward movement was performed based on kymographs, created using the FIJI kymograph plug-in (written by J. Rietdorf and A. Seitz, EMBL, Heidelberg, Germany). The speed was estimated by measuring the angle of the linear signals (EB1–GFP for MT growth, histone H2B–mRFP1 for chromatid movement) in the kymographs. The area occupied by sister chromatids (Fig. 4.4.) was calculated using a macro script that filters (gaussian blur), creates a mask and subsequently fits a convex hull algorithm enclosing all the sister chromatids. Then, a spline connecting all the sister chromatids is created. The area of this fitted spline is measured at each time point, estimating the area occupied by sister chromatids at each time frame. Quantification of chromosome movement (Fig. 4.6.) was performed as previously described (Mirkovic et al. 2015). Briefly, H2B–mRFP1 was imaged at 30 sec intervals and images were segmented to select the chromosomal regions, based on an automatic threshold (set in the last frame, 10 min after TEV injection). For each binary-images movie, a walking average of 3 frames was produced (using kymograph plug-in, written by J. Rietdorf and A. Seitz, EMBL, Heidelberg, Germany) creating a merged image in which the intensity is proportional to the overlap between consecutive

frames. Intensity profiles were used to estimate the percentage of non-overlapping, 2-frame and 3-frame overlap pixels.

Distance between sibling and non-sibling nuclei

Measurements of distance between sibling (daughter) and non-sibling nuclei were done using the line tool in Fiji, 3 min after anaphase onset (counting from the time point of sister chromatid separation). On average, 5 pairs of daughter nuclei and 6 non-sibling (neighboring) nuclei were measured. Graphic representation was performed using Prism seven software.

Chapter 5

General Discussion

General Discussion

In this work, we aimed to provide a more integrated view of mitosis, focusing on a particular interaction between the mitotic spindle and ER membranes.

In the next paragraphs, I will describe several arguments that can help to further understand our findings in a broader context. Most of these arguments were not tested but are potentially interesting open questions to follow up in the future. To include a more critical part in this discussion, I also disclose some caveats that are implied in our work.

As described in Chapter 2, we started with a broader question – what forces could be acting on chromosomes during mitosis besides the ones generated by spindle microtubules. In my present-day perspective, this was a very difficult question to address mainly because we know that microtubules and the spindle machine are essential for the cell. Nonetheless, we had the perfect experimental set-up to test this in the lab, which convinced me to tackle this question using *Drosophila* syncytial embryos. When we removed the major force generator driving sister chromatid movement – spindle microtubules – we found an unexpected response: isolated chromatids moved towards the center. Further experiments confirmed that our initial question would be hard to grasp. Since we used colchicine to induce MT depolymerization, our phenotype was irreversible. It would be interesting to test a photoactivatable MT depolymerizing drug, which we could switch on and off to further understand the inward movement of isolated chromatids. This would allow MT “re”-polymerization and re-attachment of MTs to sister chromatids. However, whether it would be possible to reassemble a proper spindle in this reversible experiment is unknown.

These experiments directed our initial question to a new problem – a membranous structure enclosing the spindle during mitosis – the ER

envelope. Even though an ER envelope had been described before, we were puzzled by the morphology of this membranous structure, its proximity to the spindle and accumulation at spindle poles.

At this point, we sought to find a strategy to disrupt the ER specifically during mitosis, described in Chapter 3. During this effort, we encountered a few drawbacks. Developing a strategy to acutely disrupt the ER in our system – *Drosophila* syncytial embryos – seemed a somewhat ambitious task, but still feasible. Naively, I focused all my attention on trying to purify a full-length transmembrane protein (Rtnl1) but missed the intrinsic caveats of such approach. The goal was to add ectopically Rtnl1 into embryos, increasing acutely the protein levels to induce ER fragmentation. Later, we concluded that this was not the best strategy as we previously thought. After several controls and thorough analysis, we found that the ER disruption phenotype observed using this strategy was likely caused by a combination of the effect of detergent (like soap destroying phospholipidic membranes) and increased levels of Rtnl1 (which, in theory, would promote ER fragmentation). Using an alternative strategy to induce a similar type of perturbation at this stage would probably raise all the red flags and suspicions we encountered.

Eventually, after testing a previously described dominant-negative reagent (cytATL) we were able to successfully establish a strategy to acutely disrupt the ER. We subsequently used the dominant-negative effect driven by cytATL in a metaphase-arrest condition to test the immediate consequences, which is described in detail in Chapter 4. With this approach, we were able to test the contribution of the ER in the maintenance of mitotic spindle architecture. Our main finding when we employed this experimental layout was that ER membranes-proximal to the spindle poles seem to be important for spindle architecture and function. Yet, the significantly smaller spindles resulting from the ectopic addition of cytATL were still able to pull sister chromatids apart. This was

a surprising result and suggests that spindles are very robust, fine-tuned and can adapt to generate forces even when their shape is altered.

As this approach (cytATL) has an irreversible effect on the ER, we were not able to rescue normal ER topology in our experiments. Rescuing ER topology at spindle poles would be the ideal experiment to understand if spindle shape and function really depend on this specialized ER localization. If restoring normal ER topology at spindle poles would promote the rescue of spindle size and function to control levels, we could clearly demonstrate that ER organization at spindle poles is an essential factor.

Whether this phenotype can also be observed in the context of mononuclear divisions is unknown. Although syncytial nuclear divisions in *Drosophila* embryos are a very powerful system to study mitosis, there a few specificities that need to be considered. First, contrary to mammalian cells, the first nuclear divisions in the *Drosophila* embryo occur in the absence of a canonical plasma membrane. Therefore, it is possible that the phenotype we observed is specific to this mode of division, where ER membranes are the major membrane compartment. Due to this specificity, the ER can also have an essential role in the compartmentalization of each nucleus.

Nevertheless, the fact that by impairing Atlastin's function leads to nuclear fusion in the next division cycle is quite interesting and should be explored further. This would be interesting to test in an "embryonic development" context. Whether ER compartments are important to define the position of nuclei and play a role during cellularization is a very exciting question. Yet, this would be a challenging experiment to do because it involves three sequential microinjections, and it is possible that the embryos would not develop into the cellularization stage.

To test if the contribution of the ER in spindle architecture is conserved, a similar approach would have to be employed in other *Drosophila* dividing tissues or even in mammalian cells. A possible way to do this in a mononuclear division mode in *Drosophila*, would be to deplete Atlastin by RNAi in a specific dividing tissue (e.g., third instar larval brain, where neuroblast divisions are easily trackable by live imaging). In order to induce a semi-acute depletion by RNAi, we could use a heat-shock promoter and image larval brains immediately after heat-shock. A potential issue with this approach is that Atlastin depletion would not be as acute, and all neuroblast divisions would occur under this condition. Alternatively, in order to induce acute Atlastin depletion, we could also test the deGradFP system, which is a method to inactivate GFP-tagged proteins (Caussinus, Kanca, and Affolter 2012). Since we now have a fly line expressing endogenously tagged Atlastin-GFP, we could use the deGradFP system to induce acute degradation of Atlastin in other *Drosophila* tissues.

Moreover, we simply do not know what would happen upon Atlastin depletion in this asymmetric cell division context. If Atlastin depletion would disrupt ER morphology in neuroblasts, this could potentially lead to changes in the asymmetry of the two daughter cells. It would be very interesting to test this hypothesis. Another exciting aspect to look at would be whether Atlastin knockdown hinders spindle architecture in these cells as well. This would allow us to infer whether this phenotype is conserved in these cells.

Additionally, using the same type of approach in a human cell line would also be interesting to test. In this case, we would need to develop an inducible expression system to ectopically express human cytATL (keeping the acute impairment of Alastin function). Specifically, we could

generate an inducible expression plasmid for human cytATL (rapamycin or tetracycline promoters) for transfection and establishment of a stable cell line. However, three closely related Atlastins can be found in mammals (ATL1, 2 and 3) (Zhu et al. 2003), so we would probably have to target more than one ATL protein using this approach. Overexpression of cytATL2 in U2OS cells led to unbranched ER morphology and a reduction of ER dynamics (Pawar et al. 2017). But the morphology of the ER during mitosis in these cells was not documented in this study. So, it would be interesting to monitor ER morphology in a stable cell line where we could induce the overexpression of cytATLs in a controlled manner. Would this approach lead to altered mitotic ER topology? Would it have a similar effect on the spindle in human cells?
With this approach, we would have to monitor only mitotic cells or a single round of cell division under cytATL-driven dominant-negative effect. Since we would not be able to use MT depolymerizing drugs (would disassemble spindle MTs), we would have to test the proteasome inhibitor MG132, for example, to arrest cells in metaphase.

A recent study used an approach to relocalize ER membranes from the spindle region via tethering to the plasma membrane (Ferrandiz et al. 2022). Since the ER is the largest organelle and its membranes fill the entire cytoplasm, it would be interesting to see how cells divide in a condition where it is no longer enclosing the spindle. Would these cells divide at all? Is spindle architecture affected? Unfortunately, these very interesting questions remain unanswered.

Another consideration from our work is that we focused mainly on the role of ER membranes during metaphase. This was mainly because we had a strategy to arrest nuclei specifically at this stage of the cell cycle in a controlled manner. Even so, some of our experiments suggest that perturbing the ER at mitotic exit can also have consequences not only in

nuclear spacing but can lead to nuclear fusions in the subsequent divisions as well. Whether this is caused by direct impairment of Atlastin function, which was described to be involved in cytokinesis, remains unclear. Nevertheless, this was a very exciting result that we did not have time to follow up. Future experiments in this context could potentially reveal the importance of ER re-shaping during cytokinesis in this system.

Also, we do not know whether the perturbation we induced on the ER has a collateral effect in other organelles. Several lines of evidence indicate that membrane organelles do not function as isolated entities. Because we know that the ER interacts with many other organelles, we cannot exclude that some functions dependent on the ER (Ca^{2+} storage, protein synthesis, transport, amongst others) become impaired upon cytATL-driven disruption. Importantly, we do not know if the transfer of molecules like Ca^{2+} or lipids between the ER and other organelles is precluded upon microinjection with cytATL. Even if these ER functions are only impaired acutely in metaphase, it is plausible that this could have consequences in the function of other organelles.

Furthermore, disrupting a large membranous organelle might have an impact on the overall biophysical properties (e.g., density and viscosity) of the cytoplasm, which remains to be addressed. We discussed several times in the lab and in meetings whether ER disruption could alter the mechanical properties of the cytoplasm or even of the spindle. Recent work regarding this question revealed that the cytoplasm exerts forces on the spindle, which are essential for spindle positioning inside cells, and that the ER is one of the cellular structures involved (Xie et al. 2022). Perhaps, using the *Drosophila* embryo to further characterize how cytoplasm density/viscosity impact on spindle mechanics would provide valuable insights. The “cell-free” extract system in the Telley lab would be a suitable method to test this since it allows a more accessible way to manipulate and measure cytoplasmic physical properties.

Although the ER is the major organelle in the cytoplasm, other membrane organelles (Golgi complex, mitochondria, endosomes, etc) and cytoskeletal elements which are present in the cytoplasm presumably impart on spindle architecture and function. Exploring the role of other membrane-bound structures on spindle architecture could be interesting to pursue in the future.

Overall, this work shows that ER membranes are important structures for mitotic spindle function *in vivo*. This work also provides further evidence that ER membranes are not just passively recruited to the spindle and spindle poles. Together with other research groups, we have reported that the interplay between the ER and MTs is not unidirectional. Rather, the ER is also an active player when it comes to this interaction.

As a provocative ending sentence of this thesis, I propose that mitotic ER membranes must be considered as part of the spindle apparatus.

Finally, I leave this stunning image depicting the complexity of the cytoplasm inside a human cell.

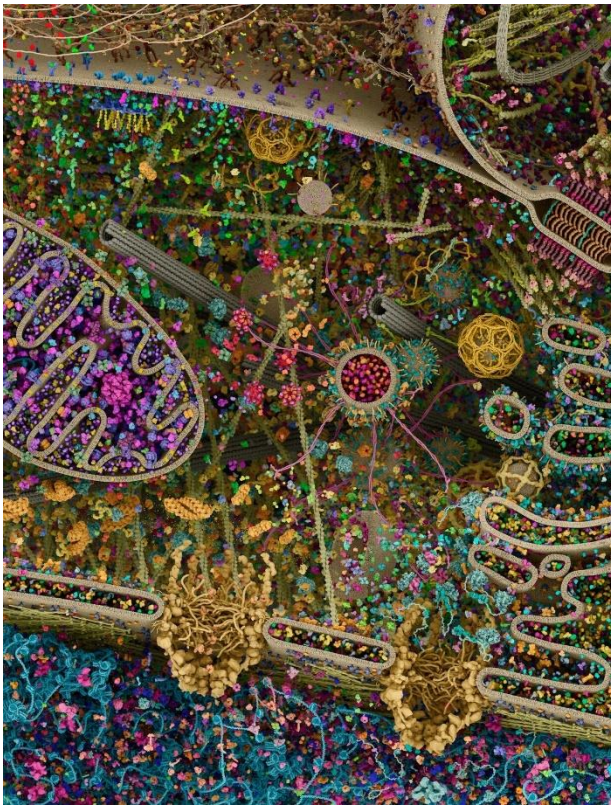

Cellular landscape cross-section through a eukaryotic cell. By Evan Ingersoll and Gael McGill.

https://t.co/YERCmdIJXH

References

Anwar, Kamran, Robin W. Klemm, Amanda Condon, Katharina N. Severin, Miao Zhang, Rodolfo Ghirlando, Junjie Hu, Tom A. Rapoport, and William A. Prinz. 2012. “The Dynamin-like GTPase Sey1p Mediates Homotypic ER Fusion in S. Cerevisiae.” *Journal of Cell Biology* 197 (2): 209–17. https://doi.org/10.1083/jcb.201111115.

Araújo, Margarida, Alexandra Tavares, Diana V Vieira, Ivo A Telley, and A Raquel. 2022. “Endoplasmic Reticulum Membranes Are Continuously Required to Maintain Mitotic Spindle Size and Forces.” *BioRxiv*. https://doi.org/10.1101/2022.05.14.491942.

Audhya, Anjon, Arshad Desai, and Karen Oegema. 2007. “A Role for Rab5 in Structuring the Endoplasmic Reticulum.” *Journal of Cell Biology* 178 (1): 43–56. https://doi.org/10.1083/jcb.200701139.

Bahmanyar, Shirin, Ronald Biggs, Amber L. Schuh, Arshad Desai, Thomas Müller-Reichert, Anjon Audhya, Jack E. Dixon, and Karen Oegema. 2014. “Spatial Control of Phospholipid Flux Restricts Endoplasmic Reticulum Sheet Formation to Allow Nuclear Envelope Breakdown.” *Genes and Development* 28 (2): 121–26. https://doi.org/10.1101/gad.230599.113.

Barton, Lacy J., Shameika R. Wilmington, Melinda J. Martin, Hannah M. Skopec, Kaylee E. Lovander, Belinda S. Pinto, and Pamela K. Geyer. 2014. “Unique and Shared Functions of Nuclear Lamina LEM Domain Proteins in Drosophila.” *Genetics* 197 (2): 653–65. https://doi.org/10.1534/genetics.114.162941.

Bergman, Zane J., Justin D. McLaurin, Anthony S. Eritano, Brittany M. Johnson, Amanda Q. Sims, and Blake Riggs. 2015. “Spatial Reorganization of the Endoplasmic Reticulum during Mitosis Relies on Mitotic Kinase Cyclin a in the Early Drosophila Embryo.” *PLoS ONE* 10 (2): 1–23. https://doi.org/10.1371/journal.pone.0117859.

Bettencourt-Dias, Mónica. 2013. “Q&A: Who Needs a Centrosome?” *BMC Biology* 11: 1–7. https://doi.org/10.1186/1741-7007-11-28.

Bian, X., R. W. Klemm, T. Y. Liu, M. Zhang, S. Sun, X. Sui, X. Liu, T. A. Rapoport, and J. Hu. 2011. “Structures of the Atlastin GTPase Provide Insight into Homotypic Fusion of Endoplasmic Reticulum Membranes.” *Proceedings of the National Academy of Sciences* 108 (10): 3976–81. https://doi.org/10.1073/pnas.1101643108.

Bieling, Peter, Ivo A. Telley, and Thomas Surrey. 2010. “A Minimal Midzone Protein Module Controls Formation and Length of

Antiparallel Microtubule Overlaps." *Cell* 142 (3): 420–32. https://doi.org/10.1016/j.cell.2010.06.033.

Bird, Alexander W., and Anthony A. Hyman. 2008. "Building a Spindle of the Correct Length in Human Cells Requires the Interaction between TPX2 and Aurora A." *Journal of Cell Biology* 182 (2): 289–300. https://doi.org/10.1083/jcb.200802005.

Bobinnec, Yves, Christiane Marcaillou, Xavier Morin, and Alain Debec. 2003. "Dynamics of the Endoplasmic Reticulum during Early Development of Drosophila Melanogaster." *Cell Motility and the Cytoskeleton* 54 (3): 217–25. https://doi.org/10.1002/cm.10094.

Brouhard, Gary J., and Luke M. Rice. 2018. "Microtubule Dynamics: An Interplay of Biochemistry and Mechanics." *Nature Reviews Molecular Cell Biology* 19 (7): 451–63. https://doi.org/10.1038/s41580-018-0009-y.

Brown, Katherine S., Michael D. Blower, Thomas J. Maresca, Timothy C. Grammer, Richard M. Harland, and Rebecca Heald. 2007. "Xenopus Tropicalis Egg Extracts Provide Insight into Scaling of the Mitotic Spindle." *Journal of Cell Biology* 176 (6): 765–70. https://doi.org/10.1083/jcb.200610043.

Brugués, Jan, Valeria Nuzzo, Eric Mazur, and Daniel J. Needleman. 2012. "Nucleation and Transport Organize Microtubules in Metaphase Spindles." *Cell* 149 (3): 554–64. https://doi.org/10.1016/j.cell.2012.03.027.

Brust-Mascher, Ingrid, Patrizia Sommi, Dhanya K. Cheerambathur, and Jonathan M. Scholey. 2009. "Kinesin-5–Dependent Poleward Flux and Spindle Length Control in Drosophila Embryo Mitosis." *Molecular Biology of the Cell* 20: 1749–62. https://doi.org/10.1091/mbc.E08-10-1033.

Byrnes, Laura J., and Holger Sondermann. 2011. "Structural Basis for the Nucleotide-Dependent Dimerization of the Large G Protein Atlastin-1/SPG3A." *Proceedings of the National Academy of Sciences of the United States of America* 108 (6): 2216–21. https://doi.org/10.1073/pnas.1012792108.

Cande, W. Z., K. McDonald, and R. L. Meeusen. 1981. "A Permeabilized Cell Model for Studing Cell Division: A Comparison of Anaphase Chromosome Movement and Cleavage Furrow Constriction in Lysed PtK1 Cells." *Journal of Cell Biology* 88 (3): 618–29. https://doi.org/10.1083/jcb.88.3.618.

Carlier, Marie France, and Dominique Pantaloni. 1981. "Kinetic Analysis of Guanosine 5'-Triphosphate Hydrolysis Associated with Tubulin

Polymerization." *Biochemistry* 20 (7): 1918–24. https://doi.org/10.1021/bi00510a030.

Carlton, Jeremy G., Hannah Jones, and Ulrike S. Eggert. 2020. "Membrane and Organelle Dynamics during Cell Division." *Nature Reviews Molecular Cell Biology*, 1–16. https://doi.org/10.1038/s41580-019-0208-1.

Carmo, Catarina, Margarida Araújo, and Raquel A. Oliveira. 2019. "Microinjection Techniques in Fly Embryos to Study the Function and Dynamics of SMC Complexes." *SMC Complexes. Part of the Methods in Molecular Biology Book Series (MIMB, Volume 2004)* 2004: 1–32. https://doi.org/10.1007/978-1- 4939-9520-2_19).

Carvalho-Santos, Zita, Juliette Azimzadeh, José B. Pereira-Leal, and Mónica Bettencourt-Dias. 2011. "Tracing the Origins of Centrioles, Cilia, and Flagella." *Journal of Cell Biology* 194 (2): 165–75. https://doi.org/10.1083/jcb.201011152.

Cassimeris, Lynne. 2002. "The Oncoprotein 18/Stathmin Family of Microtubule Destabilizers." *Current Opinion in Cell Biology* 14 (1): 18–24. https://doi.org/10.1016/S0955-0674(01)00289-7.

Caussinus, Emmanuel, Oguz Kanca, and Markus Affolter. 2012. "Fluorescent Fusion Protein Knockout Mediated by Anti-GFP Nanobody." *Nature Structural and Molecular Biology* 19 (1): 117–22. https://doi.org/10.1038/nsmb.2180.

Champion, Lysie, Monika I. Linder, and Ulrike Kutay. 2017. "Cellular Reorganization during Mitotic Entry." *Trends in Cell Biology* 27 (1): 26–41. https://doi.org/10.1016/j.tcb.2016.07.004.

Champion, Lysie, Sumit Pawar, Naemi Luithle, Rosemarie Ungricht, and Ulrike Kutay. 2019. "Dissociation of Membrane–Chromatin Contacts Is Required for Proper Chromosome Segregation in Mitosis." *Molecular Biology of the Cell* 30 (4): 427–40. https://doi.org/10.1091/mbc.e18-10-0609.

Civelekoglu-Scholey, Gul, Li Tao, Ingrid Brust-Mascher, Roy Wollman, and Jonathan M. Scholey. 2010. "Prometaphase Spindle Maintenance by an Antagonistic Motor-Dependent Force Balance Made Robust by a Disassembling Lamin-B Envelope." *Journal of Cell Biology* 188 (1): 49–68. https://doi.org/10.1083/jcb.200908150.

Clouds, Subcortical Actin, Mijung Kwon, Maria Bagonis, David Pellman, Mijung Kwon, Maria Bagonis, Gaudenz Danuser, and David Pellman. 2015. "Direct Microtubule-Binding by Myosin-10 Orients Centrosomes toward Retraction Fibers and Article Direct Microtubule-Binding by Myosin-10 Orients Centrosomes toward

Retraction Fibers and Subcortical Actin Clouds." *Developmental Cell* 34 (3): 323–37. https://doi.org/10.1016/j.devcel.2015.06.013.

Cohen, Sarah, Alex M. Valm, and Jennifer Lippincott-Schwartz. 2018. "Interacting Organelles." *Current Opinion in Cell Biology* 53: 84–91. https://doi.org/10.1016/j.ceb.2018.06.003.

Cojoc, Gheorghe, Emanuele Roscioli, Lijuan Zhang, Alfonso García-Ulloa, Jagesh V. Shah, Michael W. Berns, Nenad Pavin, Daniela Cimini, Iva M. Tolic, and Juraj Gregan. 2016. "Laser Microsurgery Reveals Conserved Viscoelastic Behavior of the Kinetochore." *Journal of Cell Biology* 212 (7): 767–76. https://doi.org/10.1083/jcb.201506011.

Collins, Matthew, Farzad Mohajerani, Subhadip Ghosh, Rajarshi Guha, Tae Hee Lee, Peter J. Butler, Ayusman Sen, and Darrell Velegol. 2019. "Nonuniform Crowding Enhances Transport." *ACS Nano* 13 (8): 8946–56. https://doi.org/10.1021/acsnano.9b02811.

Consolati, Tanja, Julia Locke, Johanna Roostalu, Zhuo Angel Chen, Julian Gannon, Jayant Asthana, Wei Ming Lim, et al. 2020. "Microtubule Nucleation Properties of Single Human ΓTuRCs Explained by Their Cryo-EM Structure." *Developmental Cell* 53 (5): 603-617.e8. https://doi.org/10.1016/j.devcel.2020.04.019.

de-Carvalho, Jorge, Sham Tlili, Lars Hufnagel, Timothy E. Saunders, and Ivo A. Telley. 2022. " Aster Repulsion Drives Short-Ranged Ordering in the Drosophila Syncytial Blastoderm ." *Development* 149 (2). https://doi.org/10.1242/dev.199997.

Debec, Alain, William Sullivan, and Monica Bettencourt-Dias. 2010. "Centrioles: Active Players or Passengers during Mitosis?" *Cellular and Molecular Life Sciences* 67 (13): 2173–94. https://doi.org/10.1007/s00018-010-0323-9.

Desai, Arshad, and Timothy J Mitchison. 1997. "Microtubule Polymerization Dynamics." *Annual Review of Cell and Developmental Biology*, no. 13: 83–117.

Deshpande, Ojas, Jorge De-Carvalho, Diana V. Vieira, and Ivo A. Telley. 2021. "Astral Microtubule Cross-Linking Safeguards Uniform Nuclear Distribution in the Drosophila Syncytium." *Journal of Cell Biology* 221 (1). https://doi.org/10.1083/JCB.202007209.

Diaz, Ulises, Zane J. Bergman, Brittany M. Johnson, Alia R. Edington, Matthew A. De Cruz, Wallace F. Marshall, and Blake Riggs. 2019. "Microtubules Are Necessary for Proper Reticulon Localization during Mitosis." *PLoS ONE* 14 (12): 1–25. https://doi.org/10.1371/journal.pone.0226327.

Dix, Carly I., and Jordan W. Raff. 2007. “Drosophila Spd-2 Recruits PCM to the Sperm Centriole, but Is Dispensable for Centriole Duplication.” *Current Biology* 17 (20): 1759–64. https://doi.org/10.1016/j.cub.2007.08.065.

Dogterom, Marileen, and Bernard Yurke. 1997. “Measurement of the Force-Velocity Relation for Growing Microtubules.” *Science* 278 (5339): 856–60. https://doi.org/10.1126/science.278.5339.856.

Drpic, Danica, Ana C. Almeida, Paulo Aguiar, Fioranna Renda, Joana Damas, Harris A. Lewin, Denis M. Larkin, Alexey Khodjakov, and Helder Maiato. 2018. “Chromosome Segregation Is Biased by Kinetochore Size.” *Current Biology* 28 (9): 1344-1356.e5. https://doi.org/10.1016/j.cub.2018.03.023.

Dumont, Sophie, and Timothy J. Mitchison. 2009. “Compression Regulates Mitotic Spindle Length by a Mechanochemical Switch at the Poles.” *Current Biology* 19 (13): 1086–95. https://doi.org/10.1016/j.cub.2009.05.056.

Edelmaier, Christopher J., Adam R. Lamson, Zachary R. Gergely, Saad Ansari, Robert Blackwell, J. Richard McIntosh, Matthew A. Glaser, and Meredith D. Betterton. 2020. “Mechanisms of Chromosome Biorientation and Bipolar Spindle Assembly Analyzed by Computational Modeling.” *ELife* 9: 1–48. https://doi.org/10.7554/eLife.48787.

Elbaum, Michael, Deborah Kuchnir Fygenson, and Albert Libchaber. 1996. “Buckling Microtubules in Vesicles.” *Physical Review Letters* 76 (21): 4078–81. https://doi.org/10.1103/PhysRevLett.76.4078.

Elting, Mary Williard, Pooja Suresh, and Sophie Dumont. 2018. “The Spindle: Integrating Architecture and Mechanics across Scales.” *Trends in Cell Biology* 28 (11): 896–910. https://doi.org/10.1016/j.tcb.2018.07.003.

Espadas, Javier, Diana Pendin, Rebeca Bocanegra, Artur Escalada, Giulia Misticoni, Tatiana Trevisan, Ariana Velasco del Olmo, et al. 2019. “Dynamic Constriction and Fission of Endoplasmic Reticulum Membranes by Reticulon.” *Nature Communications* 10 (1): 1–11. https://doi.org/10.1038/s41467-019-13327-7.

Ferrandiz, Nuria, Laura Downie, Georgina P Starling, and Stephen J Royle. 2022. “Endomembranes Promote Chromosome Missegregation by Ensheathing Misaligned Chromosomes.” *J. Cell Biol.* 221 (6): 2021.04.23.441091. https://doi.org/doi.org/10.1083/jcb.202203021.

Ferraro-Gideon, J., R. Sheykhani, Q. Zhu, M. L. Duquette, M. W. Berns,

and A. Forer. 2013. “Measurements of Forces Produced by the Mitotic Spindle Using Optical Tweezers.” *Molecular Biology of the Cell* 24 (9): 1375–86. https://doi.org/10.1091/mbc.e12-12-0901.

Fink, Jenny, Nicolas Carpi, Timo Betz, Angelique Bétard, Meriem Chebah, Ammar Azioune, Michel Bornens, et al. 2011. “External Forces Control Mitotic Spindle Positioning.” *Nature Publishing Group* 13 (7): 771–78. https://doi.org/10.1038/ncb2269.

Foe, V. E., and B. M. Alberts. 1983. “Studies of Nuclear and Cytoplasmic Behavior during the Five Mitotic Cycles That Precede Gastrulation in Drosophila Embryogenesis.” *Journal of Cell Science* Vol. 61: 31–70. https://doi.org/10.1242/jcs.61.1.31.

Foley, Emily A., and Tarun M. Kapoor. 2013. “Microtubule Attachment and Spindle Assembly Checkpoint Signalling at the Kinetochore.” *Nature Reviews Molecular Cell Biology* 14 (1): 25–37. https://doi.org/10.1038/nrm3494.

Frescas, David, Manos Mavrakis, Holger Lorenz, Robert DeLotto, and Jennifer Lippincott-Schwartz. 2006. “The Secretory Membrane System in the Drosophila Syncytial Blastoderm Embryo Exists as Functionally Compartmentalized Units around Individual Nuclei.” *Journal of Cell Biology* 173 (2): 219–30. https://doi.org/10.1083/jcb.200601156.

Friedman, Jonathan R, Arnaud Mourier, Justin Yamada, J Michael Mccaffery, and Jodi Nunnari. 2015. “MICOS Coordinates with Respiratory Complexes and Lipids to Establish Mitochondrial Inner Membrane Architecture.” *ELife*, 1–25. https://doi.org/10.7554/eLife.07739.

Fygenson, Deborah Kuchnir, John F. Marko, and Albert Libchaber. 1997. “Mechanics of Microtubule-Based Membrane Extension.” *Physical Review Letters* 79 (22): 4497–4500. https://doi.org/10.1103/PhysRevLett.79.4497.

Gard, D. L., and M. W. Kirschner. 1987. “A Microtubule-Associated Protein from Xenopus Eggs That Specifically Promotes Assembly at the plus-End.” *Journal of Cell Biology* 105 (5): 2203–15. https://doi.org/10.1083/jcb.105.5.2203.

Gardner, Melissa K., Blake D. Charlebois, Imre M. Jánosi, Jonathon Howard, Alan J. Hunt, and David J. Odde. 2011. “Rapid Microtubule Self-Assembly Kinetics.” *Cell* 146 (4): 582–92. https://doi.org/10.1016/j.cell.2011.06.053.

Garzon-Coral, Carlos, Horatiu A. Fantana, and Jonathon Howard. 2016. “A Force-Generating Machinery Maintains the Spindle at the Cell

Center during Mitosis." *Science* 352 (6289): 1124–27. https://doi.org/10.1126/science.aad9745.

Good, Matthew C., Michael D. Vahey, Arunan Skandarajah, Daniel A. Fletcher, and Rebecca Heald. 2013. "Cytoplasmic Volume Modulates Spindle Size during Embryogenesis." *Science* 342 (6160): 856–60. https://doi.org/10.1126/SCIENCE.1243147.

Goodson, Holly V, and Erin M Jonasson. 2018. "Microtubules and Microtubule-Associated Proteins." *Cold Spring Harbor Perspectives in Biology* 10. https://doi.org/10.1101/cshperspect.a022608.

Goshima, Gohta, and Jonathan M. Scholey. 2010. "Control of Mitotic Spindle Length." *Annual Review of Cell and Developmental Biology* 26: 21–57. https://doi.org/10.1146/annurev-cellbio-100109-104006.

Goshima, Gohta, Roy Wollman, Nico Stuurman, Jonathan M. Scholey, and Ronald D. Vale. 2005. "Length Control of the Metaphase Spindle." *Current Biology* 15 (22): 1979–88. https://doi.org/10.1016/j.cub.2005.09.054.

Goyal, Uma, and Craig Blackstone. 2013. "Untangling the Web: Mechanisms Underlying ER Network Formation." *Biochimica et Biophysica Acta - Molecular Cell Research* 1833 (11): 2492–98. https://doi.org/10.1016/j.bbamcr.2013.04.009.

Goyal, Uma, Benoît Renvoisé, Jaerak Chang, and Craig Blackstone. 2014. "Spastin-Interacting Protein NA14/SSNA1 Functions in Cytokinesis and Axon Development." *PLoS ONE* 9 (11). https://doi.org/10.1371/journal.pone.0112428.

Grigoriev, Ilya, Susana Montenegro Gouveia, Babet van der Vaart, Jeroen Demmers, Jeremy T. Smyth, Srinivas Honnappa, Daniël Splinter, et al. 2008. "STIM1 Is a MT-Plus-End-Tracking Protein Involved in Remodeling of the ER." *Current Biology* 18 (3): 177–82. https://doi.org/10.1016/j.cub.2007.12.050.

Grishchuk, Ekaterina L., and J. Richard McIntosh. 2006. "Microtubule Depolymerization Can Drive Poleward Chromosome Motion in Fission Yeast." *EMBO Journal* 25 (20): 4888–96. https://doi.org/10.1038/sj.emboj.7601353.

Grishchuk, Ekaterina L., Maxim I. Molodtsov, Fazly I. Ataullakhanov, and J. Richard McIntosh. 2005. "Force Production by Disassembling Microtubules." *Nature* 438 (7066): 384–88. https://doi.org/10.1038/nature04132.

Gudimchuk, Nikita B., and J. Richard McIntosh. 2021. "Regulation of Microtubule Dynamics, Mechanics and Function through the

Growing Tip." *Nature Reviews Molecular Cell Biology* 22 (12): 777–95. https://doi.org/10.1038/s41580-021-00399-x.

Guigas, Gernot, Claudia Kalla, and Matthias Weiss. 2007. "The Degree of Macromolecular Crowding in the Cytoplasm and Nucleoplasm of Mammalian Cells Is Conserved." *FEBS Letters* 581 (26): 5094–98. https://doi.org/10.1016/j.febslet.2007.09.054.

Guilloux, Gabriel, and Romain Gibeaux. 2020. "Mechanisms of Spindle Assembly and Size Control." *Biology of the Cell* 112 (12): 369–82. https://doi.org/10.1111/boc.202000065.

Guo, Yuting, Di Li, Siwei Zhang, Jennifer Lippincott-schwartz, Eric Betzig, Yuting Guo, Di Li, et al. 2018. "Visualizing Intracellular Organelle and Cytoskeletal Interactions at Nanoscale Resolution on Millisecond Resource Visualizing Intracellular Organelle and Cytoskeletal Interactions at Nanoscale Resolution on Millisecond Timescales." *Cell*, 1430–42. https://doi.org/10.1016/j.cell.2018.09.057.

Hara, Yuki, and Akatsuki Kimura. 2013. "An Allometric Relationship between Mitotic Spindle Width, Spindle Length, and Ploidy in Caenorhabditis Elegans Embryos." *Molecular Biology of the Cell* 24 (9): 1411–19. https://doi.org/10.1091/mbc.E12-07-0528.

Hauf, S., I. C. Waizenegger, and J. M. Peters. 2001. "Cohesin Cleavage by Separase Required for Anaphase and Cytokinesis in Human Cells." *Science* 293 (5533): 1320–23. https://doi.org/10.1126/science.1061376.

Heck, Margarete M. S., Andrea Pereira, Patty Pesavento, Yvonne Yannoni, Allan C. Spradling, and Lawrence S. B. Goldstein. 1993. "The Kinesin-like Protein KLP6IF Is Essential for Mitosis in Drosophila." *Journal of Cell Biology* 123 (3): 665–79. https://doi.org/10.1083/jcb.123.3.665.

Helmke, Kara J., and Rebecca Heald. 2014. "TPX2 Levels Modulate Meiotic Spindle Size and Architecture in Xenopus Egg Extracts." *Journal of Cell Biology* 206 (3): 385–93. https://doi.org/10.1083/jcb.201401014.

Hepler, P. K., and S. M. Wolniak. 1984. "Membranes in the Mitotic Apparatus: Their Structure and Function." *International Review of Cytology* VOL. 90: 169–238. https://doi.org/10.1016/s0074-7696(08)61490-4.

Hirano, Tatsuya. 2006. "At the Heart of the Chromosome: SMC Proteins in Action." *Nature Reviews Molecular Cell Biology* 7 (5): 311–22. https://doi.org/10.1038/nrm1909.

Howard, Jonathon, and Carlos Garzon-Coral. 2017. “Physical Limits on the Precision of Mitotic Spindle Positioning by Microtubule Pushing Forces: Mechanics of Mitotic Spindle Positioning.” *BioEssays* 39 (11). https://doi.org/10.1002/bies.201700122.

Howell, B. J., D. B. Hoffman, G. Fang, A. W. Murray, and E. D. Salmon. 2000. “Visualization of Mad2 Dynamics at Kinetochores, along Spindle Fibers, and at Spindle Poles in Living Cells.” *Journal of Cell Biology* 150 (6): 1233–49. https://doi.org/10.1083/jcb.150.6.1233.

Hu, Chi-kuo, Margaret Coughlin, Timothy J Mitchison, and Stephen Doxsey. 2011. “Midbody Assembly and Its Regulation during Cytokinesis.” *Molecular Biology of the Cell* 23: 1024–34. https://doi.org/10.1091/mbc.E11-08-0721.

Hu, Junjie, and Tom A. Rapoport. 2016. “Fusion of the Endoplasmic Reticulum by Membrane-Bound GTPases.” *Seminars in Cell and Developmental Biology* 60: 105–11. https://doi.org/10.1016/j.semcdb.2016.06.001.

Hu, Junjie, Yoko Shibata, Christiane Voss, Tom Shemesh, Zongli Li, Margaret Coughlin, Michael M. Kozlov, Tom A. Rapoport, and William A. Prinz. 2008. “Membrane Proteins of the Endoplasmic Reticulum Induce High-Curvature Tubules.” *Science* 319 (5867): 1247–50. https://doi.org/10.1126/science.1153634.

Hu, Junjie, Yoko Shibata, Peng Peng Zhu, Christiane Voss, Neggy Rismanchi, William A. Prinz, Tom A. Rapoport, and Craig Blackstone. 2009. “A Class of Dynamin-like GTPases Involved in the Generation of the Tubular ER Network.” *Cell* 138 (3): 549–61. https://doi.org/10.1016/j.cell.2009.05.025.

Hueschen, Christina L., Samuel J. Kenny, Ke Xu, and Sophie Dumont. 2017. “NuMA Recruits Dynein Activity to Microtubule Minus-Ends at Mitosis.” *ELife* 6: 1–26. https://doi.org/10.7554/eLife.29328.

Huguet, Florentin, Shane Flynn, and Paola Vagnarelli. 2019. “The Role of Phosphatases in Nuclear Envelope Disassembly and Reassembly and Their Relevance to Pathologies.” *Cells* 8 (7): 687. https://doi.org/10.3390/cells8070687.

Inoue, S. 1967. “Cell Motility by Labile Association of Molecules: The Nature of Mitotic Spindle Fibers and Their Role in Chromosome Movement.” *The Journal of General Physiology* 50 (6): 259–92. https://doi.org/10.1085/jgp.50.6.259.

Inoué, Shinya. 1953. “Polarization Optical Studies of the Mitotic Spindle. 1. The Demonstration of Spindle Fibers in Living Cells.” *Chromosoma* 5: 487–500.

Inoué, Shinya, and Edward D. Salmon. 1995. “Force Generation by Microtubule Assembly/Disassembly in Mitosis and Related Movements.” *Molecular Biology of the Cell* 6: 1619–40. https://doi.org/10.1007/BF01599753.

Inoué, Shinya, and Hidemi Sato. 2008. “Cell Motility by Labile Association of Molecules: The Nature of Mitotic Spindle Fibers and Their Role in Chromosome Movement.” *Collected Works of Shinya Inoue: Microscopes, Living Cells, and Dynamic Molecules*, 263–98. https://doi.org/10.1142/9789812790866_0025.

Inoue, Yoshihiro H., Matthew S. Savoian, Takao Suzuki, Endre Máthé, Masa Toshi Yamamoto, and David M. Glover. 2004. “Mutations in Orbit/Mast Reveal That the Central Spindle Is Comprised of Two Microtubule Populations, Those That Initiate Cleavage and Those That Propagate Furrow Ingression.” *Journal of Cell Biology* 166 (1): 49–60. https://doi.org/10.1083/jcb.200402052.

Ivec, Arian, Monika Trupinić, Iva M. Tolić, and Nenad Pavin. 2021. “Oblique Circle Method for Measuring the Curvature and Twist of Mitotic Spindle Microtubule Bundles.” *Biophysical Journal* 120 (17): 3641–48. https://doi.org/10.1016/j.bpj.2021.07.024.

Jagrić, Mihaela, Patrik Risteski, Jelena Martinčić, Ana Milas, and Iva M. Tolić. 2021. “Optogenetic Control of PRC1 Reveals Its Role in Chromosome Alignment on the Spindle by Overlap Length-Dependent Forces.” *ELife* 10: 1–79. https://doi.org/10.7554/eLife.61170.

Jevtić, Predrag, and Daniel L. Levy. 2015. “Nuclear Size Scaling during Xenopus Early Development Contributes to Midblastula Transition Timing.” *Current Biology* 25 (1): 45–52. https://doi.org/10.1016/j.cub.2014.10.051.

Kapoor, Tarun M. 2017. “Metaphase Spindle Assembly.” *Biology* 6 (1). https://doi.org/10.3390/biology6010008.

Karsenti, E, and I Vernos. 2001. “The Mitotic Spindle : A Self-Made Machine” 294 (October): 543–48.

Katsani, Katerina R. Institut Curie, France Karess, Roger E. Centre National de la Recerche Scinetifique, Centre de Génétique Moléculaire, Unité Propre de Recherche 2167, Gif-sur-Yvette, F-91198, Université Paris-Sud, F-91405 Orsay Cedex, France and Unité Pierre et Marie Currie, F75005, Paris, Nathalie Institut Curie Dostani, and Valérie Institut Curie Doye. 2008. “In Vivo Dynamics of Drosophila Nuclear Envelope Components.” *Molecular Biology of the Cell* 19 (September): 3652–66. https://doi.org/10.1091/mbc.E07.

Khodjakov, Alexey, and Jonathon Pines. 2010. “Centromere Tension: A Divisive Issue.” *Nature Cell Biology* 12 (10): 919–23. https://doi.org/10.1038/ncb1010-919.

Kinoshita, Kazuhisa, Bianca Habermann, and Anthony A. Hyman. 2002. “XMAP215: A Key Component of the Dynamic Microtubule Cytoskeleton.” *Trends in Cell Biology* 12 (6): 267–73. https://doi.org/10.1016/S0962-8924(02)02295-X.

Kiseleva, Elena, Ksenia N. Morozova, Gia K. Voeltz, Terrence D. Allen, and Martin W. Goldberg. 2007. “Reticulon 4a/NogoA Locates to Regions of High Membrane Curvature and May Have a Role in Nuclear Envelope Growth.” *Journal of Structural Biology* 160 (2): 224–35. https://doi.org/10.1016/j.jsb.2007.08.005.

Kletter, Tobias, Sebastian Reusch, Tommaso Cavazza, Nils Dempewolf, Christian Tischer, and Simone Reber. 2021. “Volumetric Morphometry Reveals Spindle Width as the Best Predictor of Mammalian Spindle Scaling.” *Journal of Cell Biology* 221 (1). https://doi.org/10.1083/jcb.202106170.

Kumar, Darshan, Banafsheh Golchoubian, Ilya Belevich, Eija Jokitalo, and Anne-Lore Schlaitz. 2019. “REEP3 and REEP4 Determine the Tubular Morphology of the Endoplasmic Reticulum during Mitosis.” *Molecular Biology of the Cell*, mbc.E18-11-0698. https://doi.org/10.1091/mbc.e18-11-0698.

Labb, Katherine, Andrew Murley, and Jodi Nunnari. 2014. “Determinants and Functions of Mitochondrial Behavior.” *Annual Review of Cell and Developmental Biology*, no. 30: 357–91. https://doi.org/10.1146/annurev-cellbio-101011-155756.

Lacroix, Benjamin, Gaëlle Letort, Laras Pitayu, Jérémy Sallé, Marine Stefanutti, Gilliane Maton, Anne-Marie Ladoucer, et al. 2018. “Microtubule Dynamics Scale with Cell Size to Set Spindle Length and Assembly Timing Article Microtubule Dynamics Scale with Cell Size to Set Spindle Length and Assembly Timing.” *Developmental Cell*, no. 45: 496–511. https://doi.org/10.1016/j.devcel.2018.04.022.

LaJeunesse, Dennis Richard, Stephanie M. Buckner, Jeffrey Lake, Charles Na, Amanda Pirt, and Kathryn Fromson. 2004. “Three New Drosophila Markers of Intracellular Membranes.” *BioTechniques* 36 (5): 784–90. https://doi.org/10.2144/04365st01.

Lancaster, Oscar M., Maël LeBerre, Andrea Dimitracopoulos, Daria Bonazzi, Ewa Zlotek-Zlotkiewicz, Remigio Picone, Thomas Duke, Matthieu Piel, and Buzz Baum. 2013. “Mitotic Rounding Alters Cell Geometry to Ensure Efficient Bipolar Spindle Formation.” *Developmental Cell* 25 (3): 270–83.

https://doi.org/10.1016/j.devcel.2013.03.014.

Lee, Mihye, Sang Kyoo Paik, Min Jung Lee, Yoon Jung Kim, Sungdae Kim, Minyeop Nahm, Soo Jin Oh, et al. 2009. “Drosophila Atlastin Regulates the Stability of Muscle Microtubules and Is Required for Synapse Development.” *Developmental Biology* 330 (2): 250–62. https://doi.org/10.1016/j.ydbio.2009.03.019.

Lénárt, Péter, Christian P Bacher, Nathalie Daigle, Arthur R Hand, Roland Eils, Mark Terasaki, and Jan Ellenberg. 2005. “A Contractile Nuclear Actin Network Drives Chromosome Congression in Oocytes.” *Nature* 436 (7052): 812–18. https://doi.org/10.1038/nature03810.

Lince-Faria, Mariana, Stefano Maffini, Bernard Orr, Yun Ding, Cláudia Florindo, Claudio E. Sunkel, Álvaro Tavares, Jørgen Johansen, Kristen M. Johansen, and Helder Maiato. 2009. “Spatiotemporal Control of Mitosis by the Conserved Spindle Matrix Protein Megator.” *Journal of Cell Biology* 184 (5): 647–57. https://doi.org/10.1083/jcb.200811012.

Liu, Peng, Erik Zupa, Annett Neuner, Anna Böhler, Justus Loerke, Dirk Flemming, Thomas Ruppert, et al. 2020. “Insights into the Assembly and Activation of the Microtubule Nucleator γ-TuRC.” *Nature* 578 (7795): 467–71. https://doi.org/10.1038/s41586-019-1896-6.

Liu, Tina Y., Xin Bian, Sha Sun, Xiaoyu Hu, Robin W. Klemm, William A. Prinz, Tom A. Rapoport, and Junjie Hu. 2012. “Lipid Interaction of the C Terminus and Association of the Transmembrane Segments Facilitate Atlastin-Mediated Homotypic Endoplasmic Reticulum Fusion.” *Proceedings of the National Academy of Sciences of the United States of America* 109 (32). https://doi.org/10.1073/pnas.1208385109.

Liu, Zhonghua, and Yixian Zheng. 2009. “A Requirement for Epsin in Mitotic Membrane and Spindle Organization.” *Journal of Cell Biology* 186 (4): 473–80. https://doi.org/10.1083/jcb.200902071.

Loughlin, Rose, Jeremy D. Wilbur, Francis J. McNally, Franois J. Nédélec, and Rebecca Heald. 2011. “Katanin Contributes to Interspecies Spindle Length Scaling in Xenopus.” *Cell* 147 (6): 1397–1407. https://doi.org/10.1016/j.cell.2011.11.014.

Lv, Zhiyi, Jorge de-Carvalho, Ivo A. Telley, and Jorg Großhans. 2021. “Cytoskeletal Mechanics and Dynamics in the Drosophila Syncytial Embryo.” *Journal of Cell Science* 134 (4). https://doi.org/10.1242/jcs.246496.

Ma, Hoi Tang, and Randy Y.C. Poon. 2011. “How Protein Kinases Co-Ordinate Mitosis in Animal Cells.” *Biochemical Journal* 435: 17–31. https://doi.org/10.1042/BJ20100284.

Ma, Li, Ming-Ying Tsai, Shusheng Wang, Bingwen Lu, Rong Chen, John R Yates Iii, Xueliang Zhu, and Yixian Zheng. 2009. “Requirement for Nudel and Dynein for Assembly of the Lamin B Spindle Matrix.” *Nature Cell Biology* 11 (3): 247–56. https://doi.org/10.1038/ncb1832.

Maheshwari, Richa, Mohammad M. Rahman, Seth Drey, Megan Onyundo, Gunar Fabig, Michael A. Q. Martinez, David Q. Matus, Thomas Müller-Reichert, and Orna Cohen-Fix. 2022. “The Caenorhabditis Elegans Centrosome Is Surrounded by a Membrane Reticulum, the Centriculum, That Affects Centrosome Size and Function.” *BioRxiv*. https://doi.org/https://doi.org/10.1101/2022.06.15.496339.

Maiato, Helder, Ana Gomes, Filipe Sousa, and Marin Barisic. 2017. “Mechanisms of Chromosome Congression during Mitosis.” *Biology* 6 (1): 13. https://doi.org/10.3390/biology6010013.

Malumbres, Marcos. 2014. “Cyclin-Dependent Kinases.” *Genome Biology* 15 (122): 1–10. https://doi.org/10.1186/gb4184.

Maurer, Sebastian P., Franck J. Fourniol, Gergodblac Bohner, Carolyn A. Moores, and Thomas Surrey. 2012. “EBs Recognize a Nucleotide-Dependent Structural Cap at Growing Microtubule Ends.” *Cell* 149 (2): 371–82. https://doi.org/10.1016/j.cell.2012.02.049.

Merdes, Andreas, Rebecca Heald, Kumiko Samejima, William C. Earnshaw, and Don W. Cleveland. 2000. “Formation of Spindle Poles by Dynein/Dynactin-Dependent Transport of NuMA.” *Journal of Cell Biology* 149 (4): 851–61. https://doi.org/10.1083/jcb.149.4.851.

Merdes, Andreas, Kasra Ramyar, Janet D. Vechio, and Don W. Cleveland. 1996. “A Complex of NuMA and Cytoplasmic Dynein Is Essential for Mitotic Spindle Assembly.” *Cell* 87 (3): 447–58. https://doi.org/10.1016/S0092-8674(00)81365-3.

Merta, Holly, Jake W. Carrasquillo Rodríguez, Maya I. Anjur-Dietrich, Tevis Vitale, Mitchell E. Granade, Thurl E. Harris, Daniel J. Needleman, and Shirin Bahmanyar. 2021. “Cell Cycle Regulation of ER Membrane Biogenesis Protects against Chromosome Missegregation.” *Developmental Cell*, 1–16. https://doi.org/10.1016/j.devcel.2021.11.009.

Merta, Holly, Thurl E Harris, and Daniel J Needleman. 2021. “Article Cell Cycle Regulation of ER Membrane Biogenesis Protects against Chromosome Missegregation Cell Cycle Regulation of ER Membrane Biogenesis Protects against Chromosome Missegregation,” 1–16. https://doi.org/10.1016/j.devcel.2021.11.009.

Mierzwa, Beata, and Daniel W. Gerlich. 2014. “Cytokinetic Abscission: Molecular Mechanisms and Temporal Control.” *Developmental Cell* 31 (5): 525–38. https://doi.org/10.1016/j.devcel.2014.11.006.

Mirkovic, Mihailo, Lukas H. Hutter, Béla Novák, and Raquel A. Oliveira. 2015. “Premature Sister Chromatid Separation Is Poorly Detected by the Spindle Assembly Checkpoint as a Result of System-Level Feedback.” *Cell Reports* 13 (3): 469–78. https://doi.org/10.1016/j.celrep.2015.09.020.

Mogilner, Alex, and Erin Craig. 2010. “Towards a Quantitative Understanding of Mitotic Spindle Assembly and Mechanics.” *Journal of Cell Science* 123 (20): 3435–45. https://doi.org/10.1242/jcs.062208.

Montagna, Aldo, Nicola Vajente, Diana Pendin, and Andrea Daga. 2020. “In Vivo Analysis of CRISPR/Cas9 Induced Atlastin Pathological Mutations in Drosophila.” *Frontiers in Neuroscience* 14 (October): 1–10. https://doi.org/10.3389/fnins.2020.547746.

Moore, Andrew S, Stephen M Coscia, Cory L Simpson, Fabian E Ortega, Eric C Wait, John M Heddleston, Jeffrey J Nirschl, et al. 2021. “Actin Cables and Comet Tails Organize Mitochondrial Networks in Mitosis.” *Nature* 591 (March). https://doi.org/10.1038/s41586-021-03309-5.

Morin, Xavier, Richard Daneman, Michael Zavortink, and William Chia. 2001. “A Protein Trap Strategy to Detect GFP-Tagged Proteins Expressed from Their Endogenous Loci in Drosophila.” *Proceedings of the National Academy of Sciences of the United States of America* 98 (26): 15050–55. https://doi.org/10.1073/pnas.261408198.

Mukherjee, Richik Nilay, Jérémy Sallé, Serge Dmitrieff, Katherine M. Nelson, John Oakey, Nicolas Minc, and Daniel L. Levy. 2020. “The Perinuclear ER Scales Nuclear Size Independently of Cell Size in Early Embryos Ll Ll Article The Perinuclear ER Scales Nuclear Size Independently of Cell Size in Early Embryos.” *Developmental Cell*, no. 54: 395–409. https://doi.org/10.1016/j.devcel.2020.05.003.

Musacchio, Andrea, and Arshad Desai. 2017. “A Molecular View of Kinetochore Assembly and Function.” *Biology* 6 (1).

https://doi.org/10.3390/biology6010005.

Nasa, Isha, Scott F. Rusin, Arminja N. Kettenbach, and Greg B. Moorhead. 2018. “Aurora B Opposes PP1 Function in Mitosis by Phosphorylating the Conserved PP1-Binding RVxF Motif in PP1 Regulatory Proteins.” *Science Signaling* 11 (530). https://doi.org/10.1126/scisignal.aai8669.

Nasmyth, Kim, and Christian H. Haering. 2009. “Cohesin: Its Roles and Mechanisms.” *Annual Review of Genetics* 43: 525–58. https://doi.org/10.1146/annurev-genet-102108-134233.

Nazockdast, Ehssan, and Stefanie Redemann. 2020. “Mechanics of the Spindle Apparatus.” *Seminars in Cell and Developmental Biology* 107 (June): 91–102. https://doi.org/10.1016/j.semcdb.2020.06.018.

Nédélec, François, Thomas Surrey, and Eric Karsenti. 2003. “Self-Organisation and Forces in the Microtubule Cytoskeleton.” *Current Opinion in Cell Biology* 15 (1): 118–24. https://doi.org/10.1016/S0955-0674(02)00014-5.

Nicklas, R. B. 1983. “Measurements of the Force Produced by the Mitotic Spindle in Anaphase.” *Journal of Cell Biology* 97 (2): 542–48. https://doi.org/10.1083/jcb.97.2.542.

Nicklas, R. B., and G. W. Gordon. 1985. “The Total Length of Spindle Microtubules Depends on the Number of Chromosomes Present.” *Journal of Cell Biology* 100 (1): 1–7. https://doi.org/10.1083/jcb.100.1.1.

Nicklas, R. B., and C. A. Koch. 1969. “Chromosome Micromanipulation. 3. Spindle Fiber Tension and the Reorientation of Mal-Oriented Chromosomes.” *The Journal of Cell Biology* 43 (1): 40–50. https://doi.org/10.1083/jcb.43.1.40.

Nigg, Erich A. 2001. “The Process of Nuclear Division. CYTOKINESIS.” *Nature Reviews Molecular Cell Biology* 2 (January): 21–32. www.nature.com/reviews/molcellbio.

Niu, Liling, Tianji Ma, Feng Yang, Bing Yan, Xiao Tang, Haidi Yin, Qian Wu, et al. 2019. “Atlastin-Mediated Membrane Tethering Is Critical for Cargo Mobility and Exit from the Endoplasmic Reticulum.” *Proceedings of the National Academy of Sciences of the United States of America* 116 (28): 14029–38. https://doi.org/10.1073/pnas.1908409116.

Nixon, Faye M., Thomas R. Honnor, Nicholas I. Clarke, Georgina P. Starling, Alison J. Beckett, Adam M. Johansen, Julia A. Brettschneider, Ian A. Prior, and Stephen J. Royle. 2017.

"Microtubule Organization within Mitotic Spindles Revealed by Serial Block Face Scanning Electron Microscopy and Image Analysis." *Journal of Cell Science* 130 (10): 1845–55. https://doi.org/10.1242/jcs.203877.

Nourbakhsh, Kimya, Amy Ferrecccio, and Smita Yadav. 2021. "TAOK2 Is an ER Kinase That Catalyzes the Dynamic Tethering of ER to Microtubules." *The FASEB Journal* 35 (S1): 1–13. https://doi.org/10.1096/fasebj.2021.35.s1.02216.

Nourbakhsh, Kimya, Amy A. Ferreccio, Matthew J. Bernard, and Smita Yadav. 2021. "TAOK2 Is an ER-Localized Kinase That Catalyzes the Dynamic Tethering of ER to Microtubules." *Developmental Cell*, 1–13. https://doi.org/10.1016/j.devcel.2021.11.015.

O'Connell, Christopher B., and Alexey L. Khodjakov. 2007. "Cooperative Mechanisms of Mitotic Spindle Formation." *Journal of Cell Science* 120 (10): 1717–22. https://doi.org/10.1242/jcs.03442.

O'Sullivan, Niamh C., Thomas R. Jahn, Evan Reid, and Cahir J. O'Kane. 2012. "Reticulon-like-1, the Drosophila Orthologue of the Hereditary Spastic Paraplegia Gene Reticulon 2, Is Required for Organization of Endoplasmic Reticulum and of Distal Motor Axons." *Human Molecular Genetics* 21 (15): 3356–65. https://doi.org/10.1093/hmg/dds167.

Oegema, Karen, Christiane Wiese, Ona C Martin, Ronald A Milligan, Akihiro Iwamatsu, Timothy J Mitchison, Yixian Zheng, B M Alberts, and K Oegema J Cell Biol. 1999. "Characterization of Two Related Drosophila γ-Tubulin Complexes That Differ in Their Ability to Nucleate Microtubules" 144 (4): 721–33.

Oliveira, Raquel A., Paula A. Coelho, and Claudio E. Sunkel. 2005. "The Condensin I Subunit Barren/CAP-H Is Essential for the Structural Integrity of Centromeric Heterochromatin during Mitosis." *Molecular and Cellular Biology* 25 (20): 8971–84. https://doi.org/10.1128/mcb.25.20.8971-8984.2005.

Oliveira, Raquel A., Russell S. Hamilton, Andrea Pauli, Ilan Davis, and Kim Nasmyth. 2010. "Cohesin Cleavage and Cdk Inhibition Trigger Formation of Daughter Nuclei." *Nature Cell Biology* 12 (2): 185–92. https://doi.org/10.1038/ncb2018.

Orso, Genny, Diana Pendin, Song Liu, Jessica Tosetto, Tyler J. Moss, Joseph E. Faust, Massimo Micaroni, et al. 2009a. "Homotypic Fusion of ER Membranes Requires the Dynamin-like GTPase Atlastin." *Nature* 460 (7258): 978–83. https://doi.org/10.1038/nature08280.

———. 2009b. “Homotypic Fusion of ER Membranes Requires the Dynamin-like GTPase Atlastin.” *Nature* 460 (7258): 978–83. https://doi.org/10.1038/nature08280.

Park, Seong H., Peng Peng Zhu, Rell L. Parker, and Craig Blackstone. 2010. “Hereditary Spastic Paraplegia Proteins REEP1, Spastin, and Atlastin-1 Coordinate Microtubule Interactions with the Tubular ER Network.” *Journal of Clinical Investigation* 120 (4): 1097–1110. https://doi.org/10.1172/JCI40979.

Parry, Huw, Alex McDougall, and Michael Whitaker. 2005. “Microdomains Bounded by Endoplasmic Reticulum Segregate Cell Cycle Calcium Transients in Syncytial Drosophila Embryos.” *Journal of Cell Biology* 171 (1): 47–59. https://doi.org/10.1083/jcb.200503139.

Pauli, Andrea, Friederike Althoff, Raquel A. Oliveira, Stefan Heidmann, Oren Schuldiner, Christian F. Lehner, Barry J. Dickson, and Kim Nasmyth. 2008. “Cell-Type-Specific TEV Protease Cleavage Reveals Cohesin Functions in Drosophila Neurons.” *Developmental Cell* 14 (2): 239–51. https://doi.org/10.1016/j.devcel.2007.12.009.

Pawar, Sumit, Rosemarie Ungricht, Peter Tiefenboeck, Jean Christophe Leroux, and Ulrike Kutay. 2017. “Efficient Protein Targeting to the Inner Nuclear Membrane Requires Atlastin-Dependent Maintenance of ER Topology.” *ELife* 6: 1–25. https://doi.org/10.7554/eLife.28202.

Penfield, Lauren, Raakhee Shankar, Erik Szentgyörgyi, Alyssa Laffitte, Michael Sean Mauro, Anjon Audhya, Thomas Müller-Reichert, and Shirin Bahmanyar. 2020. “Regulated Lipid Synthesis and LEM2/CHMP7 Jointly Control Nuclear Envelope Closure.” *Journal of Cell Biology* 219 (5). https://doi.org/10.1083/jcb.202002179.

Peterman, Erwin J.G., and Jonathan M. Scholey. 2009. “Mitotic Microtubule Crosslinkers: Insights from Mechanistic Studies.” *Current Biology* 19 (23): R1089–94. https://doi.org/10.1016/j.cub.2009.10.047.

Peters, Jan Michael, and Tomoko Nishiyama. 2012. “Sister Chromatid Cohesion.” *Cold Spring Harbor Perspectives in Biology* 4 (11). https://doi.org/10.1101/cshperspect.a011130.

Petry, Sabine. 2016. “Mechanisms of Mitotic Spindle Assembly.” *Annual Review of Biochemistry* 85 (1): 659–83. https://doi.org/10.1146/annurev-biochem-060815-014528.

Phillips, Melissa J., and Gia K. Voeltz. 2016. “Structure and Function of ER Membrane Contact Sites with Other Organelles.” *Nature*

Reviews Molecular Cell Biology 17 (2): 69–82. https://doi.org/10.1038/nrm.2015.8.

Pietro, Florencia, Arnaud Echard, and Xavier Morin. 2016. “Regulation of Mitotic Spindle Orientation: An Integrated View.” *EMBO Reports* 17 (8): 1106–30. https://doi.org/10.15252/embr.201642292.

Piskadlo, Ewa, and Raquel A. Oliveira. 2016. “Novel Insights into Mitotic Chromosome Condensation [Version 1; Referees: 2 Approved].” *F1000Research* 5: 1–11. https://doi.org/10.12688/F1000RESEARCH.8727.1.

Piskadlo, Ewa, Alexandra Tavares, and Raquel A. Oliveira. 2017. “Metaphase Chromosome Structure Is Dynamically Maintained by Condensin I-Directed DNA (de)Catenation.” *ELife* 6: 1–22. https://doi.org/10.7554/eLife.26120.

Puhka, Maija, Merja Joensuu, Helena Vihinen, Ilya Belevich, and Eija Jokitalo. 2012. “Progressive Sheet-to-Tubule Transformation Is a General Mechanism for Endoplasmic Reticulum Partitioning in Dividing Mammalian Cells.” *Molecular Biology of the Cell* 23 (13): 2424–32. https://doi.org/10.1091/mbc.E10-12-0950.

Puhka, Maija, Helena Vihinen, Merja Joensuu, and Eija Jokitalo. 2007. “Endoplasmic Reticulum Remains Continuous and Undergoes Sheet-to-Tubule Transformation during Cell Division in Mammalian Cells.” *Journal of Cell Biology* 179 (5): 895–909. https://doi.org/10.1083/jcb.200705112.

Ramkumar, Nitya, Jigna V Patel, Jannis Anstatt, and Buzz Baum. 2021. “Aurora B-dependent Polarization of the Cortical Actomyosin Network during Mitotic Exit.” *EMBO Reports* 22 (10): 1–13. https://doi.org/10.15252/embr.202152387.

Raykhel, Irina, Heli Alanen, Kirsi Salo, Jaana Jurvansuu, Dat Nguyen Van, Maria Latva-Ranta, and Lloyd Ruddock. 2007. “A Molecular Specificity Code for the Three Mammalian KDEL Receptors.” *Journal of Cell Biology* 179 (6): 1193–1204. https://doi.org/10.1083/jcb.200705180.

Redemann, Stefanie, Sebastian Fürthauer, Michael Shelley, and Thomas Müller-Reichert. 2019. “Current Approaches for the Analysis of Spindle Organization.” *Current Opinion in Structural Biology* 58 (Figure 1): 269–77. https://doi.org/10.1016/j.sbi.2019.05.023.

Rodrigues-Martins, Ana, Maria Riparbelli, Giuliano Callaini, David M. Glover, and Monica Bettencourt-Dias. 2008. “From Centriole Biogenesis to Cellular Function: Centrioles Are Essential for Cell

Division at Critical Developmental Stages." *Cell Cycle* 7 (1): 11–16. https://doi.org/10.4161/cc.7.1.5226.

Roll-Mecak, Antonina, and Francis J. McNally. 2010. "Microtubule-Severing Enzymes." *Current Opinion in Cell Biology* 22 (1): 96–103. https://doi.org/10.1016/j.ceb.2009.11.001.

Roubinet, Chantal, Ian J. White, and Buzz Baum. 2021. "Asymmetric Nuclear Division in Neural Stem Cells Generates Sibling Nuclei That Differ in Size, Envelope Composition, and Chromatin Organization." *Current Biology* 31 (18): 3973-3983.e4. https://doi.org/10.1016/j.cub.2021.06.063.

Rowland, Ashley A, Patrick J Chitwood, Melissa J Phillips, and Gia K Voeltz. 2014. "Article ER Contact Sites Define the Position and Timing of Endosome Fission." *Cell*, 1027–41. https://doi.org/10.1016/j.cell.2014.10.023.

Saka, Yasushi, Takashi Sutani, Yukiko Yamashita, Shigeaki Saitoh, Masahiro Takeuchi, Yukinobu Nakaseko, and Mitsuhiro Yanagida. 1994. "Fission Yeast Cut3 and Cut14, Members of a Ubiquitous Protein Family, Are Required for Chromosome Condensation and Segregation in Mitosis." *EMBO Journal* 13 (20): 4938–52. https://doi.org/10.1002/j.1460-2075.1994.tb06821.x.

Salmon, E. D., M. McKeel, and T. Hays. 1984. "Rapid Rate of Tubulin Dissociation from Microtubules in the Mitotic Spindle in Vivo Measured by Blocking Polymerization with Colchicine." *Journal of Cell Biology* 99 (3): 1066–75. https://doi.org/10.1083/jcb.99.3.1066.

Sawin, K. E., and T. J. Mitchison. 1991. "Poleward Microtubule Flux in Mitotic Spindles Assembled in Vitro." *Journal of Cell Biology* 112 (5): 941–54. https://doi.org/10.1083/jcb.112.5.941.

Schlaitz, Anne Lore, James Thompson, Catherine C.L. Wong, John R. Yates, and Rebecca Heald. 2013. "REEP3/4 Ensure Endoplasmic Reticulum Clearance from Metaphase Chromatin and Proper Nuclear Envelope Architecture." *Developmental Cell* 26 (3): 315–23. https://doi.org/10.1016/j.devcel.2013.06.016.

Schuh, Melina, Christian F. Lehner, and Stefan Heidmann. 2007. "Incorporation of Drosophila CID/CENP-A and CENP-C into Centromeres during Early Embryonic Anaphase." *Current Biology* 17 (3): 237–43. https://doi.org/10.1016/j.cub.2006.11.051.

Schweizer, Nina, Nisha Pawar, Matthias Weiss, and Helder Maiato. 2015. "An Organelle-Exclusion Envelope Assists Mitosis and Underlies Distinct Molecular Crowding in the Spindle Region." *Journal of Cell Biology* 210 (5): 695–704.

https://doi.org/10.1083/jcb.201506107.

Sharp, David J., and Jennifer L. Ross. 2012. “Microtubule-Severing Enzymes at the Cutting Edge.” *Journal of Cell Science* 125 (11): 2561–69. https://doi.org/10.1242/jcs.101139.

Shibata, Yoko, Tom Shemesh, William A. Prinz, Alexander F. Palazzo, Michael M. Kozlov, and Tom A. Rapoport. 2010. “Mechanisms Determining the Morphology of the Peripheral ER.” *Cell* 143 (5): 774–88. https://doi.org/10.1016/j.cell.2010.11.007.

Shibata, Yoko, Christiane Voss, Julia M. Rist, Junjie Hu, Tom A. Rapoport, William A. Prinz, and Gia K. Voeltz. 2008. “The Reticulon and Dp1/Yop1p Proteins Form Immobile Oligomers in the Tubular Endoplasmic Reticulum.” *Journal of Biological Chemistry* 283 (27): 18892–904. https://doi.org/10.1074/jbc.M800986200.

Shimamoto, Yuta, Yusuke T. Maeda, Shin’Ichi Ishiwata, Albert J. Libchaber, and Tarun M. Kapoor. 2011. “Insights into the Micromechanical Properties of the Metaphase Spindle.” *Cell* 145 (7): 1062–74. https://doi.org/10.1016/j.cell.2011.05.038.

Smyth, Jeremy T., Amber M. Beg, Shilan Wu, James W. Putney, and Nasser M. Rusan. 2012. “Phosphoregulation of STIM1 Leads to Exclusion of the Endoplasmic Reticulum from the Mitotic Spindle.” *Current Biology* 22 (16): 1487–93. https://doi.org/10.1016/j.cub.2012.05.057.

Smyth, Jeremy T., Todd A. Schoborg, Zane J. Bergman, Blake Riggs, and Nasser M. Rusan. 2015. “Proper Symmetric and Asymmetric Endoplasmic Reticulum Partitioning Requires Astral Microtubules.” *Open Biology* 5 (8). https://doi.org/10.1098/rsob.150067.

Snapp, Erik L, Takako Iida, David Frescas, Jennifer Lippincott-schwartz, Mary A Lilly, and Drosophila Stocks. 2004. “The Fusome Mediates Intercellular Endoplasmic Reticulum Connectivity in Drosophila Ovarian Cysts.” *Molecular Biology of the Cell* 15 (October): 4512–21. https://doi.org/10.1091/mbc.E04.

So, Chun, Katerina Menelaou, Julia Uraji, Katarina Harasimov, Anna M. Steyer, K. Bianka Seres, Jonas Bucevičius, et al. 2022. “Mechanism of Spindle Pole Organization and Instability in Human Oocytes.” *Science* 375 (6581). https://doi.org/10.1126/science.abj3944.

So, Chun, K. Bianka Seres, Anna M. Steyer, Eike Mönnich, Dean Clift, Anastasija Pejkovska, Wiebke Möbius, and Melina Schuh. 2019. “A Liquid-like Spindle Domain Promotes Acentrosomal Spindle Assembly in Mammalian Oocytes.” *Science* 364 (6447).

https://doi.org/10.1126/science.aat9557.

Souza, Colin P.C. De, and Stephen A. Osmani. 2007. “Mitosis, Not Just Open or Closed.” *Eukaryotic Cell* 6 (9): 1521–27. https://doi.org/10.1128/EC.00178-07.

Strunov, Anton, Lidiya V. Boldyreva, Evgeniya N. Andreyeva, Gera A. Pavlova, Julia V. Popova, Alena V. Razuvaeva, Alina F. Anders, et al. 2018. “Ultrastructural Analysis of Mitotic Drosophila S2 Cells Identifies Distinctive Microtubule and Intracellular Membrane Behaviors.” *BMC Biology* 16 (1). https://doi.org/10.1186/s12915-018-0528-1.

Subramanian, Radhika, and Tarun M. Kapoor. 2012. “Building Complexity: Insights into Self-Organized Assembly of Microtubule-Based Architectures.” *Developmental Cell* 23 (5): 874–85. https://doi.org/10.1016/j.devcel.2012.10.011.

Suresh, Pooja, Alexandra F. Long, and Sophie Dumont. 2020. “Microneedle Manipulation of the Mammalian Spindle Reveals Specialized, Short-Lived Reinforcement near Chromosomes.” *ELife* 9: 1–22. https://doi.org/10.7554/eLife.53807.

Suryadinata, Randy, Martin Sadowski, and Boris Sarcevic. 2010. “Control of Cell Cycle Progression by Phosphorylation of Cyclin-Dependent Kinase (CDK) Substrates.” *Bioscience Reports* 30 (4): 243–55. https://doi.org/10.1042/BSR20090171.

Syrovatkina, Viktoriya, Chuanhai Fu, and Phong T. Tran. 2013. “Antagonistic Spindle Motors and MAPs Regulate Metaphase Spindle Length and Chromosome Segregation.” *Current Biology* 23 (23): 2423–29. https://doi.org/10.1016/j.cub.2013.10.023.

Takagi, Jun, Ryota Sakamoto, Gen Shiratsuchi, Yusuke T. Maeda, and Yuta Shimamoto. 2019. “Mechanically Distinct Microtubule Arrays Determine the Length and Force Response of the Meiotic Spindle.” *Developmental Cell* 49 (2): 267-278.e5. https://doi.org/10.1016/j.devcel.2019.03.014.

Taubenberger, Anna V., Buzz Baum, and Helen K. Matthews. 2020. “The Mechanics of Mitotic Cell Rounding.” *Frontiers in Cell and Developmental Biology* 8 (August): 1–16. https://doi.org/10.3389/fcell.2020.00687.

Telley, Ivo A., Imre Gáspár, Anne Ephrussi, and Thomas Surrey. 2012. “Aster Migration Determines the Length Scale of Nuclear Separation in the Drosophila Syncytial Embryo.” *Journal of Cell Biology* 197 (7): 887–95. https://doi.org/10.1083/jcb.201204019.

Terasaki, M., L. B. Chen, and K. Fujiwara. 1986. “Microtubules and the Endoplasmic Reticulum Are Highly Interdependent Structures.” *Journal of Cell Biology* 103 (4): 1557–68. https://doi.org/10.1083/jcb.103.4.1557.

Thawani, Akanksha, and Sabine Petry. 2021. “Molecular Insight into How γ-TuRC Makes Microtubules.” *Journal of Cell Science* 134 (14). https://doi.org/10.1242/jcs.245464.

Thévenaz, Philippe, Urs E. Ruttimann, and Michael Unser. 1998. “A Pyramid Approach to Subpixel Registration Based on Intensity.” *IEEE Transactions on Image Processing* 7 (1): 27–41. https://doi.org/10.1109/83.650848.

Tikhomirova, Maria S, Avihay Kadosh, and Aksel J Saukko-paavola. 2022. “A Role for Endoplasmic Reticulum Dynamics in the Cellular Distribution of Microtubules.” *PNAS* 119 (15): 1–12. https://doi.org/10.1073/pnas.2104309119/-/DCSupplemental.Published.

Tolić, Iva M., Maja Novak, and Nenad Pavin. 2019. “Helical Twist and Rotational Forces in the Mitotic Spindle.” *Biomolecules* 9 (4). https://doi.org/10.3390/biom9040132.

Tsai, Ming Ying, Shusheng Wang, Jill M. Heidinger, Dale K. Shumaker, Stephen A. Adam, Robert D. Goldman, and Yixian Zheng. 2006. “A Mitotic Lamin B Matrix Induced by RanGTP Required for Spindle Assembly.” *Science* 311 (5769): 1887–93. https://doi.org/10.1126/science.1122771.

Uhlmann, Frank, Dominik Wernic, Eugene V Koonin, and Kim Nasmyth. 2000. “Uhlmann_Cell02” 103: 12. papers2://publication/uuid/88ADE173-EC89-4C2A-B826-E6F298269010.

Vedrenne, Cécile, Dieter R. Klopfenstein, and Hans-Peter Hauri. 2005. “Phosphorylation Controls CLIMP-63–Mediated Anchoring of the Endoplasmic Reticulum to Microtubules.” *Mol Biol Cell* 16 (April): 1928–37. https://doi.org/10.1091/mbc.E04-07-0554.

Velle, Katrina B., Andrew S. Kennard, Monika Trupinić, Arian Ivec, Andrew J.M. Swafford, Emily Nolton, Luke M. Rice, Iva M. Tolić, Lillian K. Fritz-Laylin, and Patricia Wadsworth. 2022. “Naegleria’s Mitotic Spindles Are Built from Unique Tubulins and Highlight Core Spindle Features.” *Current Biology* 32 (6): 1247-1261.e6. https://doi.org/10.1016/j.cub.2022.01.034.

Voeltz, Gia K., William A. Prinz, Yoko Shibata, Julia M. Rist, and Tom A. Rapoport. 2006. “A Class of Membrane Proteins Shaping the

Tubular Endoplasmic Reticulum." *Cell* 124 (3): 573–86. https://doi.org/10.1016/j.cell.2005.11.047.

Volkov, Vladimir A., Anatoly V. Zaytsev, Nikita Gudimchuk, Paula M. Grissom, Alexander L. Gintsburg, Fazly I. Ataullakhanov, J. Richard McIntosh, and Ekaterina L. Grishchuk. 2013. "Long Tethers Provide High-Force Coupling of the Dam1 Ring to Shortening Microtubules." *Proceedings of the National Academy of Sciences of the United States of America* 110 (19): 7708–13. https://doi.org/10.1073/pnas.1305821110.

Vukušić, Kruno, Renata Buđa, Agneza Bosilj, Ana Milas, Nenad Pavin, and Iva M. Tolić. 2017. "Microtubule Sliding within the Bridging Fiber Pushes Kinetochore Fibers Apart to Segregate Chromosomes." *Developmental Cell* 43 (1): 11-23.e6. https://doi.org/10.1016/j.devcel.2017.09.010.

Walczak, Claire E., Sophia Gayek, and Ryoma Ohi. 2013. "Microtubule-Depolymerizing Kinesins." *Annual Review of Cell and Developmental Biology* 29: 417–41. https://doi.org/10.1146/annurev-cellbio-101512-122345.

Wang, Ning, and Tom A. Rapoport. 2019. "Reconstituting the Reticular ER Network – Mechanistic Implications and Open Questions." *Journal of Cell Science* 132 (4): 1–7. https://doi.org/10.1242/jcs.227611.

Wang, Songyu, Robert E. Powers, Vicki A.M. Gold, and Tom A. Rapoport. 2018. "The ER Morphology-Regulating Lunapark Protein Induces the Formation of Stacked Bilayer Discs." *Life Science Alliance* 1 (1): 1–11. https://doi.org/10.26508/lsa.201700014.

Wang, Songyu, Fabian B. Romano, Christine M. Field, Tim J. Mitchison, and Tom A. Rapoport. 2013. "Multiple Mechanisms Determine ER Network Morphology during the Cell Cycle in Xenopus Egg Extracts." *Journal of Cell Biology* 203 (5): 801–14. https://doi.org/10.1083/jcb.201308001.

Wang, Songyu, Hanna Tukachinsky, Fabian B. Romano, and Tom A. Rapoport. 2016. "Cooperation of the ER-Shaping Proteins Atlastin, Lunapark, and Reticulons to Generate a Tubular Membrane Network." *ELife* 5 (September): 1–29. https://doi.org/10.7554/eLife.18605.

Waterman-Storer, Clare M., and E. D. Salmon. 1998. "Endoplasmic Reticulum Membrane Tubules Are Distributed by Microtubules in Living Cells Using Three Distinct Mechanisms." *Current Biology* 8 (14): 798–807. https://doi.org/10.1016/s0960-9822(98)70321-5.

Wieczorek, Michal, Linas Urnavicius, Shih Chieh Ti, Kelly R. Molloy, Brian T. Chait, and Tarun M. Kapoor. 2020. “Asymmetric Molecular Architecture of the Human γ-Tubulin Ring Complex.” *Cell* 180 (1): 165-175.e16. https://doi.org/10.1016/j.cell.2019.12.007.

Wollman, R., E. N. Cytrynbaum, J. T. Jones, T. Meyer, J. M. Scholey, and A. Mogilner. 2005. “Efficient Chromosome Capture Requires a Bias in the ‘search-and-Capture’ Process during Mitotic-Spindle Assembly.” *Current Biology* 15 (9): 828–32. https://doi.org/10.1016/j.cub.2005.03.019.

Wollman, Roy, Gul Civelekoglu-Scholey, Jonathan M. Scholey, and Alex Mogilner. 2008. “Reverse Engineering of Force Integration during Mitosis in the Drosophila Embryo.” *Molecular Systems Biology* 4 (195): 1–13. https://doi.org/10.1038/msb.2008.23.

Worrall, Joseph Thomas, Naoka Tamura, Alice Mazzagatti, Nadeem Shaikh, Tineke van Lingen, Bjorn Bakker, Diana Carolina Johanna Spierings, Elina Vladimirou, Floris Foijer, and Sarah Elizabeth McClelland. 2018. “Non-Random Mis-Segregation of Human Chromosomes.” *Cell Reports* 23 (11): 3366–80. https://doi.org/10.1016/j.celrep.2018.05.047.

Wu, Fuyun, Xiaoyu Hu, Xin Bian, Xinqi Liu, and Junjie Hu. 2015. “Comparison of Human and Drosophila Atlastin GTPases.” *Protein and Cell* 6 (2): 139–46. https://doi.org/10.1007/s13238-014-0118-0.

Xie, Jing, Javad Najafi, Rémi Le Borgne, Jean Marc Verbavatz, Catherine Durieu, Jeremy Sallé, and Nicolas Minc. 2022. “Contribution of Cytoplasm Viscoelastic Properties to Mitotic Spindle Positioning.” *Proceedings of the National Academy of Sciences of the United States of America* 119 (8). https://doi.org/10.1073/pnas.2115593119.

Yalçın, Belgin, Lu Zhao, Martin Stofanko, Niamh C. O’Sullivan, Zi Han Kang, Annika Roost, Matthew R. Thomas, et al. 2017. “Modeling of Axonal Endoplasmic Reticulum Network by Spastic Paraplegia Proteins.” *ELife* 6: 1–27. https://doi.org/10.7554/eLife.23882.

Yang, Ge, Benjamin R. Houghtaling, Jedidiah Gaetz, Jenny Z. Liu, Gaudenz Danuser, and Tarun M. Kapoor. 2007. “Architectural Dynamics of the Meiotic Spindle Revealed by Single-Fluorophore Imaging.” *Nature Cell Biology* 9 (11): 1233–42. https://doi.org/10.1038/ncb1643.

Yao, C., U. Rath, H. Maiato, D. Sharp, J. Girton, K. M. Johansen, and J. Johansen. 2012. “A Nuclear-Derived Proteinaceous Matrix Embeds the Microtubule Spindle Apparatus during Mitosis.” *Molecular Biology of the Cell* 23: 3532–41. https://doi.org/10.1091/mbc.E12-

06-0429.

Ye, Anna A., Stuart Cane, and Thomas J. Maresca. 2016. “Chromosome Biorientation Produces Hundreds of Piconewtons at a Metazoan Kinetochore.” *Nature Communications* 7: 1–9. https://doi.org/10.1038/ncomms13221.

Zheng, Yixian, Mei Lie Wong, Bruce Alberts, and Tim Mitchison. 1995. “Nucleation of Microtubule Assembly by a γ-Tubulin-Containing Ring Complex.” *Nature* 378 (7): 603–5.

Zhu, Peng Peng, Andrew Patterson, Brigitte Lavoie, Julia Stadler, Marwa Shoeb, Rakesh Patel, and Craig Blackstone. 2003. “Cellular Localization, Oligomerization, and Membrane Association of the Hereditary Spastic Paraplegia 3A (SPG3A) Protein Atlastin.” *The Journal of Biological Chemistry* 278 (49): 49063–71. https://doi.org/10.1074/jbc.M306702200.

APPENDIX

Scheme of the genetic crosses used in this study

All fly stocks were double balanced (see the following scheme as an example) to generate lines with the desired insertions/tagged proteins.

♀ $\frac{If}{CyO}$; $\frac{MKRS}{TM6B}$ X ♂ $\frac{UAS-Lamin\ B-GFP}{UAS-Lamin\ B-GFP}$; $\frac{wt}{wt}$

Chromosome 2	$\frac{UAS-Lamin\ B-GFP}{UAS-Lamin\ B-GFP}$	
If	$\frac{If}{UAS-Lamin\ B-GFP}$	$\frac{If}{UAS-Lamin\ B-GFP}$
CyO	$\frac{UAS-Lamin\ B-GFP}{CyO}$	$\frac{UAS-Lamin\ B-GFP}{CyO}$

Chromosome 3	$\frac{wt}{wt}$	
MKRS	$\frac{MKRS}{wt}$	$\frac{MKRS}{wt}$
TM6B	$\frac{wt}{TM6B}$	$\frac{wt}{TM6B}$

F1: ♀ $\frac{UAS-Lamin\ B-GFP}{CyO}$; $\frac{wt}{TM6B}$ X ♂ $\frac{UAS-Lamin\ B-GFP}{CyO}$; $\frac{MKRS}{wt}$

Chromosome 2	$\frac{UAS-Lamin\ B-GFP}{CyO}$	
UAS-Lamin B-GFP	$\frac{UAS-Lamin\ B-GFP}{UAS-Lamin\ B-GFP}$	$\frac{UAS-Lamin\ B-GFP}{CyO}$
CyO	$\frac{UAS-Lamin\ B-GFP}{CyO}$	$\frac{CyO}{CyO}$

Note: the $\frac{CyO}{CyO}$ *genotype is not viable, so it does not appear in the progeny.*

Chromosome 3	$\frac{MKRS}{wt}$	
wt	$\frac{MKRS}{wt}$	$\frac{MKRS}{wt}$
TM6B	$\frac{MKRS}{TM6B}$	$\frac{wt}{wt}$

F2: ☿ $\frac{UAS-Lamin\ B-GFP}{CyO}$; $\frac{MKRS}{TM6B}$ X ♂ $\frac{UAS-Lamin\ B-GFP}{CyO}$; $\frac{MKRS}{TM6B}$

Cross: ☿ $\frac{UAS-Lamin\ B-GFP}{CyO}$; $\frac{MKRS}{TM6B}$ X ♂ $\frac{If}{CyO}$; $\frac{UASp-RFP-KDEL}{TM6B}$

Chromosome 2	$\frac{If}{CyO}$	
UAS-Lamin B-GFP	$\frac{If}{UAS-Lamin\ B-GFP}$	$\frac{If}{CyO}$
CyO	$\frac{UAS-Lamin\ B-GFP}{CyO}$	$\frac{CyO}{CyO}$

Chromosome 3	$\frac{UASp-RFP-KDEL}{TM6B}$	
MKRS	$\frac{MKRS}{UASp-RFP-KDEL}$	$\frac{UASp-RFP-KDEL}{TM6B}$
TM6B	$\frac{MKRS}{TM6B}$	$\frac{TM6B}{TM6B}$

Note: the $\frac{TM6B}{TM6B}$ genotype is not viable, so it does not appear in the progeny.

Generation of Atlastin-GFP knock in by CRISPR/Cas9

The following description of the generation of the knock in line was performed by Leonardo Guilgur from the Fly transgenics facility at IGC Fly Transgenesis and Genome Editing Facility supported by Congento1026 Congento LISBOA-01-0145-FEDER-022170, co-financed by FCT (Portugal) and Lisboa 2020,1027 under the PORTUGAL 2020 agreement (European Regional Development Fund).

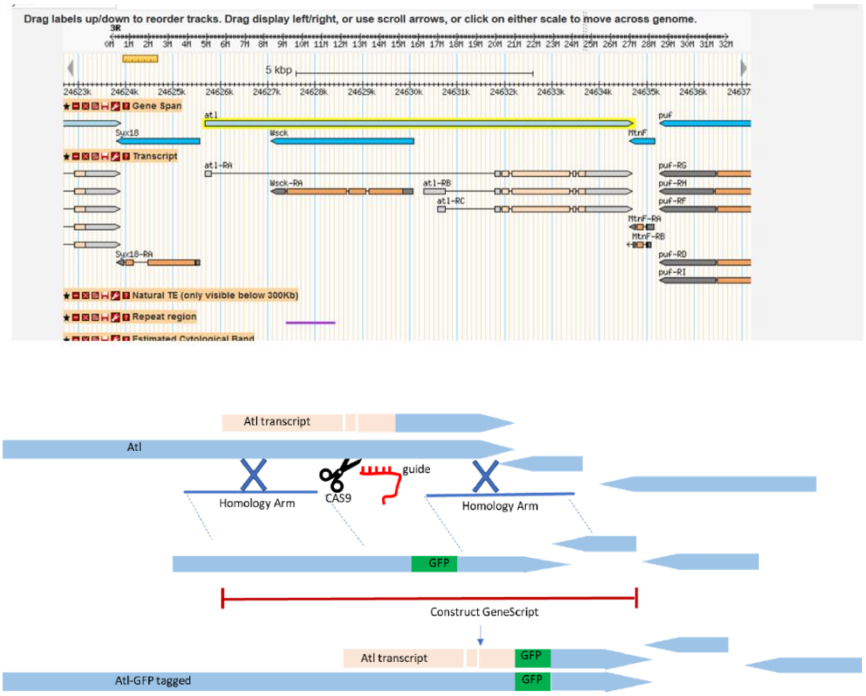

Strategy used for the knock in of GFP sequence into the C-terminal region of the atlastin locus.

CRISPR Optimal Target Finder

First Guide RNA Selected target:

GTGGGAGAAAGTAAGTAGCTGGG

5' - GTC**G**TGGGAGAAAGTAAGTAGCT - 3'

3' - ACCCTCTTTCATTCATCGACAAA - 5'

Atlas sgRNA1 TOP oligo: GTC**G**TGGGAGAAAGTAAGTAGCT

Atlas sgRNA1 Bottom oligo: AAACAGCTACTTACTTTCTCCCA

Second Guide RNA Selected target:

GCCATTGGACGCATTCACCGAGG

5' - GTC**G**CCATTGGACGCATTCACCG - 3'

3' - GGTAACCTGCGTAAGTGGCCAAA - 5'

Atlas sgRNA2 TOP oligo: GTC**G**CCATTGGACGCATTCACCG

Atlas sgRNA2 Bottom oligo: AAACCGGTGAATGCGTCCAATGG

These guides were cloned in the pCFD3 and the result was confirmed by sequencing.

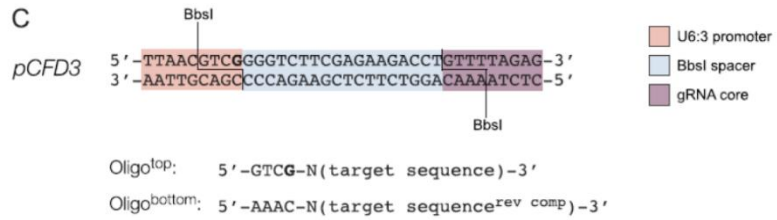

Adapted from Port et al. (2014).

The following sequence (GeneScript Synthesis) was used as donor:

GGTCGCCTCGCGCTGGCCGACACCGGCAAAAAGCCGTTCCAGCGT
CTGCAGTTCCTCGTCCGGGACTGGAGCTTTCCCTACGAGGCGGAA
TATGGTGCACTGGGCGGGGATAAGATTCTGAAACGACGTCTGGAG
GTGTCCGACAAACAGCACCCAGAACTACAGTCCCTGCGTCGCCAC
ATTTCGTCCTGTTTCACGGAGGTGGCCTGCTTCCTGATGCCCCATC
CAGGTCTCAATGTGGCCACCAATCCTAAATTTGACGGTCGGCTGCA
GGACATCACGCCCGAGTTTAAGAGTAGCCTGCGCTCCCTGGTGCC
CATGCTGCTGGCACCGGACAACCTTGTCTACAAGGAGATCAGCGG
ACAGCGGGTGCGGGCCCGCGATCTCATCCAGTACTTCCAATCGTA
CATGAACATCTACAAGGGCAACGAGCTGCCCGAGCCGAAGAGCAT
GCTGGTGGCCACCGCAGAGGCTAACCATTTGACTGCCGTGGCCGC

CGCCAAGGAGCTGTACGGACAGCTCATGGAGGAGGTGTGCGGTG
GAACGCGGCCGTACTTAAGCACCGCCCATCTCCAGACGGAGCACC
TGCGGGTGAAGGACAAGGCACTGTTCCAGTTCGCCGCCAAGCGCA
AGATGGGTGGTGAGGAGTTCACCGAGAAATTCCGCAAGCAACTGG
AAGATGATCTTGAGGAGGTCTTCACCAACTACCAAGCACACAACGA
GAGCAAGAACATCTTTAAGGCAGCACGGACACCGGCGGTGTACTT
CGCCTGCGCCGTCATCATGTACATCCTTAGCGGCATCTTTGGATTG
GTGGGTCTCTATACGTTCGCCAACTTCTGCAACCTGGTTATGGGTG
TGGCGCTTCTAACGCTGGCTCTGTGGGCCTACATTAGGTAGGTTGA
TTTAGCTTGAGCTTTTGATGATAATTTTGCCAACGATGTTTTATCAAT
TCCAGATATAGCGGAGAGCTCAGCGACTTTGGCGGCAAGTTGGAT
GACTTTGCAACGCTATTGTGGGAGAAAGTAAGTAGCTGcGAATCTA
GCGAAGATGTTCGTGTACTAACCTACGCTATGCTTGCAGTTCATGC
GACCCATCTATCACGGCTGCATGGAGAAGGGCATCCACCATGTTG
CCACTCATGCGACCGAAATGGCTGTCGGCGGAGGCGCAGCCTCCT
ACCGCTCCCAGACgTCGGTGAATGCGTCCAATGGCAAGGTGAAGC
GGTCAatggtgagcaagggcgaggagctgttcaccggggtggtgcccatcctggtcgagctgg
acggcgacgtaaacggccacaagttcagcgtgtccggcgagggcgagggcgatgccacctacg
gcaagctgaccctgaagttcatctgcaccaccggcaagctgcccgtgccctggcccaccctcgtga
ccaccctgacctacggcgtgcagtgcttcagccgctaccccgaccacatgaagcagcacgacttct
tcaagtccgccatgcccgaaggctacgtccaggagcgcaccatcttcttcaaggacgacggcaac
tacaagacccgcgccgaggtgaagttcgagggcgacaccctggtgaaccgcatcgagctgaag
ggcatcgacttcaaggaggacggcaacatcctggggcacaagctggagtacaactacaacagc
cacaacgtctatatcatggccgacaagcagaagaacggcatcaaggtgaacttcaagatccgcc
acaacatcgaggacggcagcgtgcagctcgccgaccactaccagcagaacaccccatcggc
gacggccccgtgctgctgcccgacaaccactacctgagcacccagtccgccctgagcaaagacc
ccaacgagaagcgcgatcacatggtcctgctggagttcgtgaccgccgccgggatcactctcggc
atggacgagctgtacaagtaaGAATACGCCCAAGGAGCGCAGCACAAAACG
CAGCAGCCGGTGCCGTCGCAGCCGCCGTCGGCAAGAACCAATAAC
AACAACAATAATAATAACAACAACAACAATGTGGCATACAAATCAAA
CAGGAGCAACAACATTAACGAGGCCGACGGTTTCATTCACAACATC

TGGCGCAAGTTCGGCGGCAGCAACGAAGAGAAGGGCCAAGTCAG
CACCCAAAGTCCAGCGACCCCGTCCTCTTCCTCCCAGGCGCCAAA
TAGTCGCAAGAAGCGCAAAGCGAAGCGCAATTAGGTGTCCATGGA
CCAAGTAGAATGGTTCGATTTTCGAAAGGACGACTCCCCCTCTAAT
TTGTATAAATCTAAACCCTTCTATAGTGCGTGAGAACCGGAAACACA
AACGTCTAGCTATTAATTGCCCTTAAAGGAAGTTGTTTTTATATTGC
ATTAATTGAAGTGTAGATGGTCTATATTACGTATATTTAAGAGTAAGT
GCATCATTAGTAAGTGGCTCGTGTCTGTTGAAAAGTGAAATTTTAAA
TTGTTTTTTTACAAACGATATGCGTCTGAAACGGATATATGAAATTTA
ACGCTGTAATATAAAGAAATCGCTAACGAATTTAATTTGTTTAATTTC
CATCCAAGGCGTACTCCCCCCACCTACCCGCCTCCTTTTCCATCTT
ATCTCATCTTTGGTATAGAATTCCATAAGCAATCTATGTATAAACAG
AGTGCACATTGTTGTTGGCTGGTTTGCTAAGCGCCTCATTTTGCCA
CCTTTTGTTATTTAAAATTATAAAAAAAACAAAAAAACACGAAGAAAA
TAAAATAGAAGTCATTGCCACCCATTAAAGTTCAACGCGAAGGAGC
AATGCTGGTATAGGTCATTAGTTTATCTTGTGCAGTAAAATTTATAG
AACTCTTGGTTTTGTTTCGATTAAACAATAAATGTATTTAATGATAAC
AGCTCACTAGCAGTTATGGCCATCGAAAAATAAATGGAAAAAACGT

Legend: homology arms are in blue; the EGFP sequence is in green; the target sites for CAS9 are in orange. To avoid recurrent cutting, point mutations to delete de PAM sequence, which are highlighted in yellow.

Microinjections

The stock BL#66554: y[1] M{RFP[3xP3.PB] GFP[E.3xP3]=vas-Cas9}ZH-2A was injected. Founders were crossed with the w;; MKRS/TM6B stock and 115 lines were established.

Screening

Firstly, founder flies from different lines were pooled to then extract genomic DNA. Thus, 8 groups of lines to be screened were established and pooled.

For example:

Group A: Lines 1-12

Group B: Lines 13-23

Group C: Lines 24-40….and so for.

The way to screened was by PCR using specific sets of primers annealing with the genomic region of Atlastin and GFP.

Primers

EGFP Seq Fw CAAGCAGAAGAACGGCATCAAG

EGFP Seq Rev TGCACGCCGTAGGTCAGG

Atlastin Seq Fw CGCTTCTAACGCTGGCTCTG

Atlastin Seq Rev TGTTTCCGGTTCTCACGCACTA

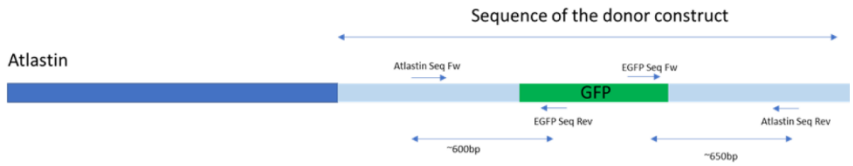

Scheme of the sequence of the donor construct.

Macro to measure area occupied by sister chromatids using Fiji software:

```
run("Clear Results");
roiManager("reset");
run("Set Measurements...", "area mean standard min centroid integrated
median limit display redirect=None decimal=4");
Stack.getDimensions(width, height, channels, slices, frames);
run("Duplicate...", "title=filtered duplicate");
selectWindow("filtered");
run("Gaussian Blur...", "sigma=1 stack");
run("Subtract Background...", "rolling=10 stack");
setAutoThreshold("Otsu dark no-reset");
setOption("BlackBackground", true);
run("Convert to Mask", "method=Otsu background=Dark black");
run("Options...", "iterations=1 count=1 black do=Open stack");
for(k=1;k<=frames;k++) {
        run("Select None");
        Stack.setFrame(k);
        //run("Find Maxima...", "noise=60 output=[Point Selection]");
        run("Create Selection");
        run("Points from Mask");
        run("Convex Hull");
        run("Fit Spline");
        roiManager("add");
        run("Measure");
        updateResults();
};
```

Output files of FRAP data analysis performed using easyFRAPweb online tool

Lys-GFP-KDEL reporter

Normalization method: Full scale

Exponential equation: Single

filename	T-half	Mobile Fraction	R square
1.xlsx	2.87	0.98	0.95
10.xlsx	4.11	1	0.81
2.xlsx	3.16	1	0.98
3.xlsx	3.07	0.96	0.94
4.xlsx	2.77	0.97	0.97
5.xlsx	3.57	0.98	0.97
6.xlsx	4.35	1	0.95
7.xlsx	5.28	1	0.95
8.xlsx	4.1	1	0.88
9.xlsx	3.21	1	0.76
Mean:	3.65	0.99	
Standard Deviation:	0.76	0.01	

Normalization method: Full scale

Exponential equation: Double

filename	T-half	Mobile Fraction	R square
1.xlsx	2.87	0.94	0.95
10.xlsx	4.11	1	0.81
2.xlsx	2.19	1	0.99
3.xlsx	2.69	0.94	0.97
4.xlsx	2.77	0.9	0.97
5.xlsx	3.53	0.95	0.97
6.xlsx	2.23	1	0.99
7.xlsx	5.28	1	0.95
8.xlsx	2.54	1	0.89
9.xlsx	3.21	1	0.76
Mean:	3.14	0.97	
Standard Deviation:	0.9	0.04	

GFP-Rtnl1 reporter – p27 (interphase) arrest, centrosome region

Normalization method: Full scale

Exponential equation: Single

filename	T-half	Mobile Fraction	R square
20220119_1.xlsx	7.31	0.79	0.9
20220119_2.xlsx	26.35	0.86	0.91
20220120_3.xlsx	5.65	0.78	0.91
20220120_4.xlsx	4.93	0.75	0.94
20220120_6.xlsx	18.92	0.91	0.87
20220120_7.xlsx	9.72	0.79	0.93
20220120_8.xlsx	16.39	0.78	0.96
20220121_10.xlsx	10.12	0.77	0.95
20220121_12.xlsx	14.29	0.87	0.98
20220121_13.xlsx	6.5	0.72	0.81
20220121_14.xlsx	7.94	0.76	0.93
20220121_9.xlsx	8.3	0.9	0.98
Mean:	11.37	0.81	
Standard Deviation:	6.16	0.06	

Normalization method: Full scale

Exponential equation: Double

filename	T-half	Mobile Fraction	R square
20220119_1.xlsx	18.26	1	0.9
20220119_2.xlsx	26.36	1	0.97
20220120_3.xlsx	12.19	1	0.93
20220120_4.xlsx	15.72	1	0.94
20220120_6.xlsx	19.1	1	0.9
20220120_7.xlsx	6.95	0.66	0.95
20220120_8.xlsx	35.46	1	0.97
20220121_10.xlsx	9.21	0.62	0.96
20220121_12.xlsx	9.71	0.83	0.99
20220121_13.xlsx	14.59	0.95	0.81
20220121_14.xlsx	7.94	0.6	0.93
20220121_9.xlsx	11.71	1	0.98
Mean:	15.6	0.89	
Standard Deviation:	7.99	0.16	

GFP-Rtnl1 reporter – p27 (interphase) arrest, equator region

Normalization method: Full scale

Exponential equation: Single

filename	T-half	Mobile Fraction	R square
20220120_1.xlsx	14.94	0.76	0.97
20220120_2.xlsx	15.6	0.9	0.98
20220120_3.xlsx	39.76	0.98	0.86
20220120_4.xlsx	14.82	0.92	0.98
20220121_5.xlsx	26.79	0.98	0.96
20220121_6.xlsx	18.62	0.81	0.98
20220121_8.xlsx	16.21	0.98	0.97
Mean:	20.96	0.9	
Standard Deviation:	8.61	0.08	

Normalization method: Full scale

Exponential equation: Double

filename	T-half	Mobile Fraction	R square
20220120_1.xlsx	34.21	1	0.98
20220120_2.xlsx	18.74	1	0.99
20220120_3.xlsx	20.33	1	0.91
20220120_4.xlsx	14.82	0.86	0.98
20220121_5.xlsx	26.79	0.97	0.96
20220121_6.xlsx	15.67	0.69	0.99
20220121_8.xlsx	14.62	0.98	0.97
Mean:	20.74	0.93	
Standard Deviation:	6.77	0.11	

GFP-Rtnl1 reporter – UbcH10^{C114S} (metaphase) arrest, centrosome region

Normalization method: Full scale

Exponential equation: Single

filename	T-half	Mobile Fraction	R square
10.xlsx	13.59	0.91	0.95
11.xlsx	12.65	0.82	0.97
12.xlsx	12.24	0.98	0.99
20211118_1.xlsx	14.32	0.87	0.99
20211118_13.xlsx	11.75	0.92	0.99
20211118_15.xlsx	19.65	0.97	0.96
20211118_16.xlsx	20.5	0.87	0.96
20211118_17.xlsx	20.69	0.99	1
20211118_2.xlsx	17.97	0.98	0.97
20211118_3.xlsx	11.25	0.89	0.93
20211118_4.xlsx	14.31	0.87	0.98
20211118_6.xlsx	14.04	1	0.92
20211213_18.xlsx	12.53	0.98	0.96
20211213_19.xlsx	12.34	0.85	0.97
20211213_20.xlsx	14.69	0.87	0.99
20211222_21.xlsx	14.22	0.9	0.97
20211222_22.xlsx	14.33	0.97	0.99
20211222_23.xlsx	14.31	0.94	0.98
7.xlsx	7.38	0.83	0.99
8.xlsx	15.68	0.92	0.95
Mean:	14.42	0.92	
Standard Deviation:	3.17	0.06	

Normalization method: Full scale

Exponential equation: Double

filename	T-half	Mobile Fraction	R square
10.xlsx	6.95	0.93	0.99
11.xlsx	17.66	0.89	0.97
12.xlsx	10.59	1	1
20211118_1.xlsx	14.13	0.88	1

20211118_13.xlsx	9.66	0.87	0.99
20211118_15.xlsx	12.12	1	0.99
20211118_16.xlsx	21.33	1	0.99
20211118_17.xlsx	18.52	0.99	1
20211118_2.xlsx	14.07	1	0.98
20211118_3.xlsx	9.63	1	0.99
20211118_4.xlsx	9.93	0.83	0.99
20211118_6.xlsx	3.99	0.88	0.69
20211213_18.xlsx	7.08	1	0.99
20211213_19.xlsx	13.94	1	0.99
20211213_20.xlsx	11.05	0.82	1
20211222_21.xlsx	13.21	1	1
20211222_22.xlsx	11.54	0.98	0.99
20211222_23.xlsx	12.83	1	1
7.xlsx	6.24	0.72	0.99
8.xlsx	10.04	1	0.99
Mean:	11.73	0.94	
Standard Deviation:	4.15	0.08	

GFP-Rtnl1 reporter – UbcH10^{C114S} (metaphase) arrest, equator region

Normalization method: Full scale

Exponential equation: Single

filename	T-half	Mobile Fraction	R square
20211118_1.xlsx	12.35	0.99	0.99
20211118_2.xlsx	9.83	1	0.96
20211118_3.xlsx	9.81	0.95	0.98
20211118_6.xlsx	16.31	0.98	0.99
20211118_7.xlsx	10.49	0.91	0.97
20211118_8.xlsx	10.18	0.93	0.98
20211213_10.xlsx	13.41	0.91	0.98
20211213_11.xlsx	13.22	0.97	0.98
20211213_12.xlsx	13.06	0.92	0.99
20211222_13.xlsx	14.08	1	0.99
20211222_14.xlsx	8.86	0.91	0.99
20211222_15.xlsx	10.28	0.92	0.98
Mean:	11.82	0.95	
Standard Deviation:	2.14	0.04	

Normalization method: Full scale

Exponential equation: Double

filename	T-half	Mobile Fraction	R square
20211118_1.xlsx	3.27	0.87	0.7
20211118_2.xlsx	9.83	1	0.96
20211118_3.xlsx	10.73	1	0.99
20211118_6.xlsx	17.5	1	0.99
20211118_7.xlsx	13.76	1	0.98
20211118_8.xlsx	8.99	0.85	0.98
20211213_10.xlsx	11.1	0.84	0.99
20211213_11.xlsx	13.98	1	0.99
20211213_12.xlsx	10.51	0.86	1
20211222_13.xlsx	14.08	1	0.99
20211222_14.xlsx	12.07	1	0.99
20211222_15.xlsx	9.55	0.89	0.99
Mean:	11.28	0.94	
Standard Deviation:	3.37	0.07	

Methods to estimate His6-Rtnl1B protein concentration

Nanodrop (A280 nm):

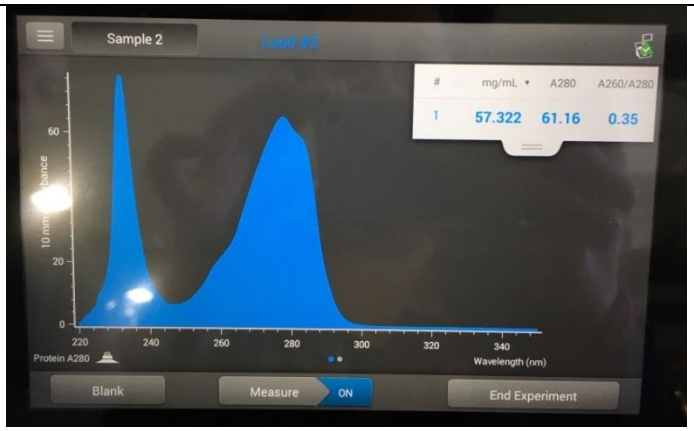

BCA protein assay kit (Milipore)

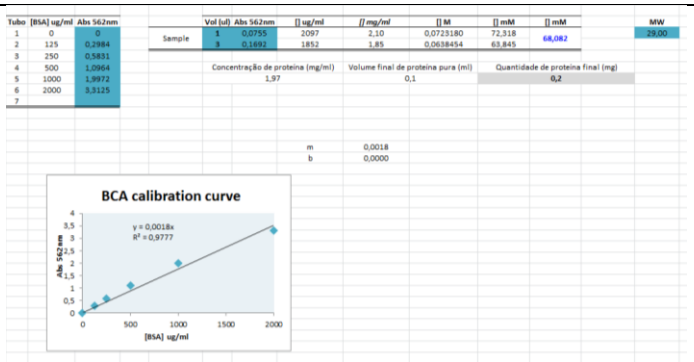

Bradford assay

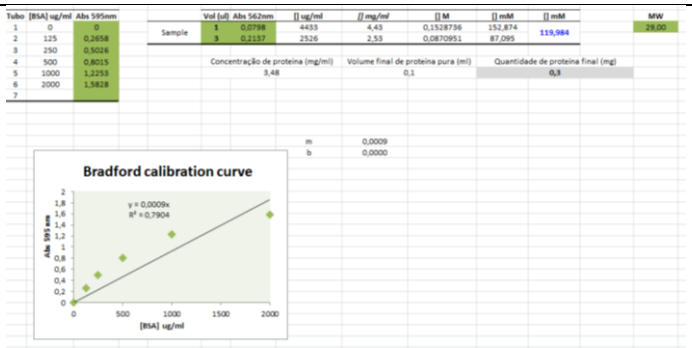

Estimation using BSA standard concentrations

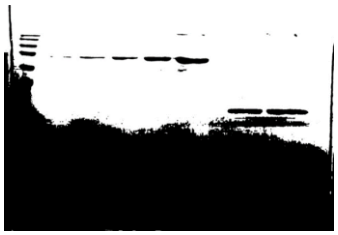

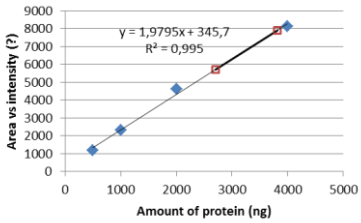

mg/ml	ng	Area	Mean	ng	Volume Total (ul)	Total mass (ug)	Conc ug/ul
0,25	500	1180	255				
0,5	1000	2299	255				
1	2000	4616	255				
2	4000	8134	255				
?	#1 (2ul)	5710	255	2709,927	100	135,4963375	1,35
?	#2 (4ul)	7894	255	3813,236		95,33089164	0,95

Scheme of His6-Rtnl1B construct

pET28a-His6-Rtnl1B

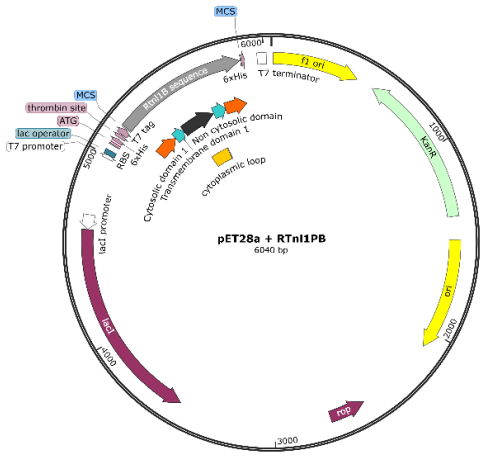

This plasmid was kindly provided by Andrea Daga (University of Padova, Italy)

Scheme of cloning of N-terminal GFP-tagged His6-Rtnl1B construct

pET28a-His6-GFP-Rtnl1B

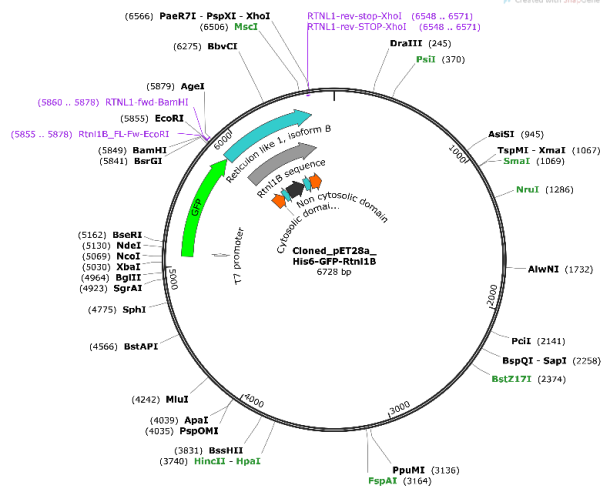

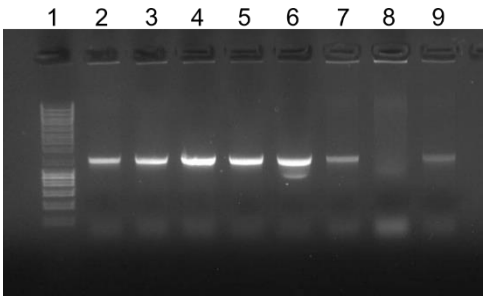

Colony PCR to screen for positive colonies for pET28a-His6-GFP-Rtnl1B. His6-GFP-Rtnl1B was cloned with EcoRI and XhoI restriction sites (see Materials and Methods). Expected PCR product size is 1455 bp. The forward primer used was designed for the GFP sequence and the reverse was designed for the insert. for the insert were used (see Materials and Methods). 1% agarose gel: 1 – GeneRuler 1 kb DNA Ladder (Thermofisher); positive colonies selected for sequencing: 2-5.

Scheme of cloning of His6-Rtnl1B and N-terminal GFP-tagged His6-Rtnl1B constructs into pRNA plasmids

pRNA-His6-Rtnl1B

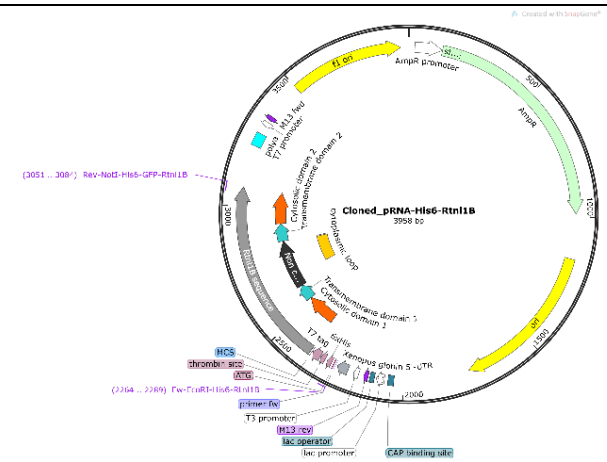

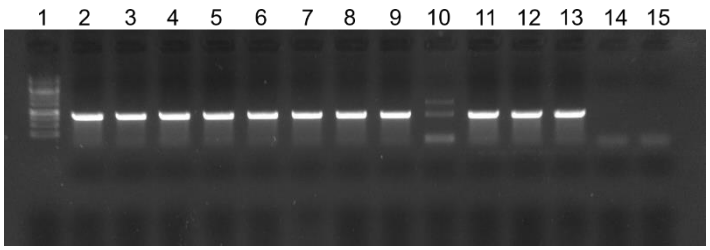

Colony PCR to screen for positive colonies for pRNA-His6-Rtnl1B. His6-Rtnl1B was cloned with EcoRI and NotI restriction sites (see Materials and Methods). Expected PCR product size is 824 bp. Primers for the insert were used (see Materials and Methods). 1% agarose gel: 1 – GeneRuler 1 kb DNA Ladder (Thermofisher); positive colonies selected for sequencing: 2-5.

pRNA-His6-GFP-Rtnl1B

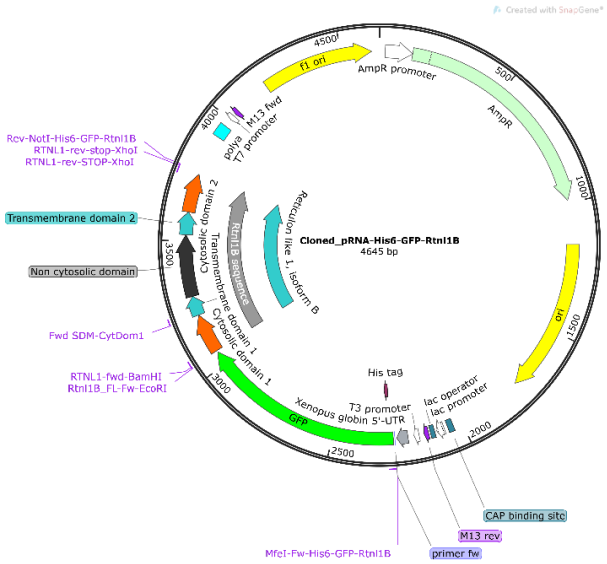

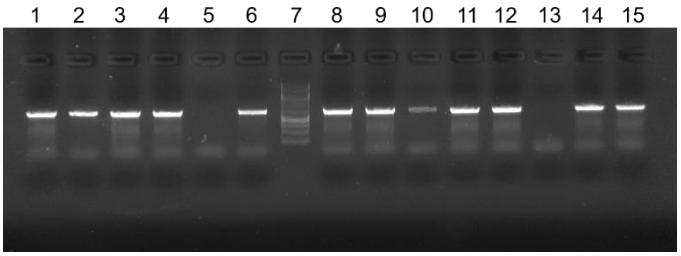

Colony PCR to screen for positive colonies for pRNA-His6-GFP-Rtnl1B. His6-GFP-Rtnl1B was cloned with MfeI and NotI restriction sites. Expected PCR product size is 1514 bp. Primers for the insert were used (see Materials and Methods). 7 – GeneRuler 1 kb DNA Ladder (Thermofisher); positive colonies selected for sequencing: 1-2, 8-9, 11-12, 14-15.

Scheme of cloning of His6-cytATL construct

pET28a-His6-cytATL

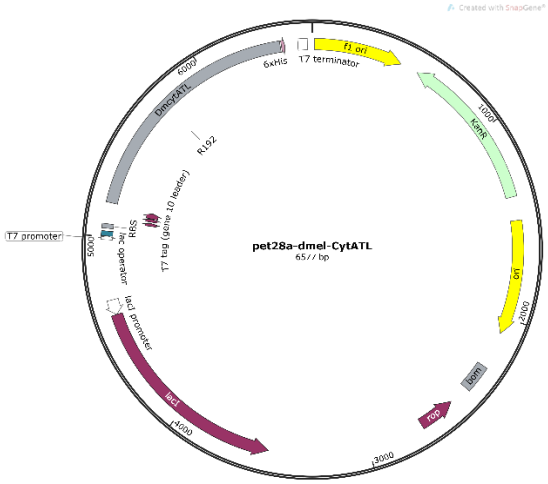

Scheme of cloning of His6-cytATL-mCherry construct

pET28a-His6-cytATL-mCherry

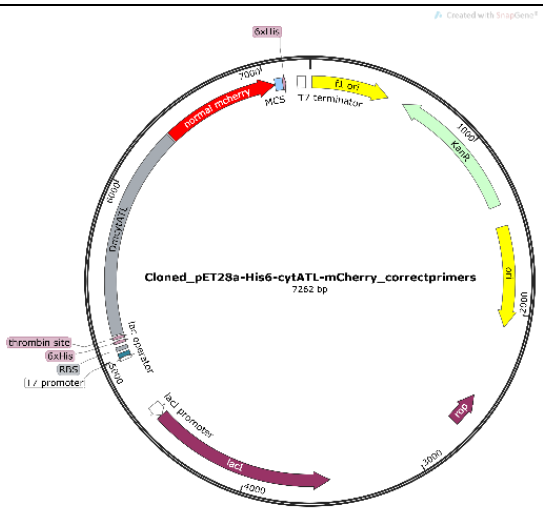

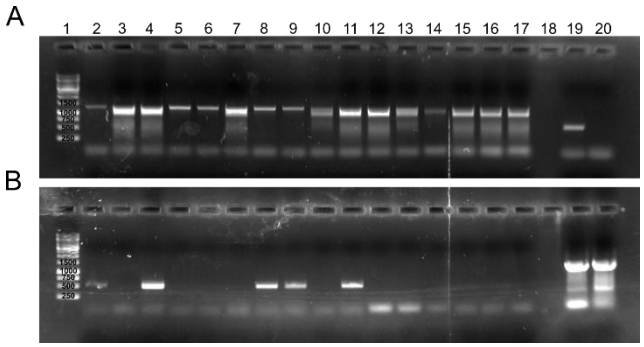

Colony PCR to screen for colonies with His6-cytATL-mCherry. (A) Forward and reverse primers for cytATL sequence (expected PCR product size is 1267 bp). (B) Forward primer in the plasmid backbone – T7 promoter – and reverse primer for cytATL sequence (expected PCR product size is 518 bp). 1 – GeneRuler 1 kb DNA Ladder (Thermofisher); positive colonies selected for sequencing: lanes 4, 8, 9, 11, 19.

Legends of the movies

Movie Fig. 2.1. Separated sister chromatids become clustered upon MT depolymerization. Embryos containing only TEV-cleavable Cohesin recombined with H2Av-mRFP1 (red) and the centromere protein CID-EGFP (green). First, a microinjection with UbcH10^{C114S} was performed to induce a metaphase-arrest, followed by microinjection with TEV protease to artificially separate sister chromatids. A third microinjection with Colchicine was used to acutely depolymerize MTs. Times are relative to microinjection with UbcH10^{C114S}. Scale bar is 10 µm. The time point used was 30 seconds. Frame rate is 3 frames per second.

Movie Fig. 2.3. Microtubule depolymerization kinetics upon microinjection with Colchicine. Embryos containing only TEV-cleavable Cohesin recombined with the centromere protein CID-EGFP (green), β-tubulin-RFP (red). Microinjection with UbcH10^{C114S} was performed to induce a metaphase-arrest, followed by microinjection with TEV protease to artificially separate sister chromatids. A third microinjection with Colchicine was used to acutely depolymerize MTs. Progressive disassembly of spindle MTs can be observed. Times are relative to microinjection with UbcH10^{C114S}. Scale bar is 10 µm. The time point used was 30 seconds. Frame rate is 3 frames per second.

Movie Fig. 2.4. Microtubule depolymerization leads to decreased distance between centrosomes. Embryos containing only TEV-cleavable Cohesin recombined with H2B-mRFP1 (red) and the PCM protein Spd2-GFP (green), Microinjection with UbcH10^{C114S} followed by microinjection with TEV protease to artificially separate sister chromatids. A third microinjection with Colchicine was used to acutely depolymerize MTs. Progressive reduction inter-centrosome distance can be observed. Times

are relative to microinjection with UbcH10^{C114S}. Scale bar is 10 µm. The time point used was 30 seconds. Frame rate is 3 frames per second.

Movie Fig. 2.6. Acentric fragments generated by laser ablation shows that centromeres are not required for the clustering of sister chromatids upon MT depolymerization. Embryos expressing solely a TEV-cleavable cohesin complex recombined with H2Av-mRFP1 (red), and the centromere marker Cid-GFP (green) were used to visualize chromosomes and centromeres upon MT depolymerization. Time is relative to microinjection with TEV protease. Scale bar is 10 µm. The time point used was 30 seconds. Frame rate is 3 frames per second.

Movie Fig. 2.10. Syncytial nuclear divisions in *Drosophila* embryos. Embryos expressing the EYFP-KDEL ER marker (left, green) or GFP-Rtnl1 ER marker (right, green) together with Histone H2B-mRFP1 (red) were microinjected with Tubulin AlexaFluor-647 (magenta) and monitored throughout the subsequent mitosis. Times are relative to injection. Scale bar is 10 µm. The time point used was 30 seconds. Frame rate is 5 frames per second.

Movie Fig. 2.11. FRAP experiment in embryos expressing GFP-Rtnl1 (black) after microinjection with 4 mg/ml of Cdk1 inhibitor p27 to induce an interphase arrest. Scale bar is 10 µm. Time in seconds is relative to pre-bleaching. Bleaching was performed at the second time point, followed by monitoring of recovery of fluorescence intensity over time. The time point used was 0.5 seconds. Frame rate is 3 frames per second.

Movie Fig. 2.12. FRAP experiment on the ER in embryos expressing GFP-Rtnl1 (left, black) or Lys-GFP-KDEL (right, black). Microinjection with 40 mg/ml UbcH10^{C114S} was performed to induce a metaphase arrest. Scale bar is 10 µm. Time in seconds is relative to pre-bleaching.

Bleaching was performed at the second time point, followed by monitoring of recovery of fluorescence intensity over time. The time point used was 0.5 seconds for GFP-Rtnl1 (left) and 0.25 seconds for Lys-GFP-KDEL (right). Frame rate is 3 frames per second.

Movie Fig. 3.18. Embryos expressing EYFP-KDEL after microinjection with 40 mg/ml of UbcH10^{C114S}, to induce a metaphase arrest, and subsequently microinjected with buffer (left) or cytATL (right, 60 mg/ml). Embryos also express H2B–mRFP1 (red). Scale bar is 10 µm. Times (minutes:seconds) are relative to the time of UbcH10^{C114S} microinjection. The time point used was 30 seconds. Frame rate is 3 frames per second.

Movie Fig. 3.19. Localization of endogenously tagged Atlastin-GFP in Drosophila syncytial embryos. Time-lapse of a representative embryo expressing Atlastin-GFP generated by CRISPR/Cas9 knock in. Scale bar is 10 µm. The time point used was 30 seconds. Frame rate is 3 frames per second.

Movie Fig. 4.2. Embryos expressing EYFP-KDEL after microinjection with 40 mg/ml of UbcH10^{C114S} together with Tubulin AlexaFluor-647, to induce a metaphase arrest, and subsequently microinjected with buffer (left) or cytATL protein (right, 60 mg/ml). Embryos also express H2B–mRFP1 (red). Scale bar is 10 µm. Times (minutes:seconds) are relative to the time of microinjection with buffer/cytATL. The time point used was 30 seconds. Frame rate is 3 frames per second.

Movie Fig. 4.3. FRAP experiment on half of the spindle. Embryos expressing β-Tubulin-GFP after microinjection with 40 mg/ml of UbcH10^{C114S}, to induce a metaphase arrest, and subsequently microinjected with buffer (left) or cytATL protein (right, 60 mg/ml). Scale

bar is 10 μm. Times (minutes:seconds) are relative to pre-bleaching. The time point used was 0.5 seconds. Frame rate is 20 frames per second.

Movie Fig. 4.4. Microtubule growth dynamics in embryos expressing EB1-GFP after microinjection with 40 mg/ml of UbcH10^{C114S}, to induce a metaphase arrest, and subsequently microinjected with buffer (top) or cytATL protein (bottom, 60 mg/ml). Scale bar is 10 μm. Times (minutes:seconds) are relative to pre-bleaching. Bleaching was performed at the second time point. The time point used was 1 second. Frame rate is 40 frames per second.

Movie Fig. 4.5. Embryos expressing solely TEV-cleavable Cohesin after microinjection with 40 mg/ml of UbcH10^{C114S}, to induce a metaphase arrest, followed by subsequent microinjection with buffer (left) or cytATL (right). A third microinjection with TEV protease was performed to induce sister chromatid separation. Embryos also express EYFP-KDEL (green) and H2B–mRFP1 (red). Scale bar is 10 μm. Times (minutes:seconds) are relative to microinjection with TEV protease. Frame rate is 3 frames per second.

Movie Fig. 4.7. Embryos expressing EYFP-KDEL (green) and H2B–mRFP1 (red) after microinjection with 40 mg/ml of UbcH10^{C114S}, to induce a metaphase arrest, followed by a subsequent microinjection with buffer (left) or cytATL (right). Then, a final microinjection with the wild-type version of UbcH10 (UbcH10 WT) was performed to induce mitotic exit. Scale bar is 10 μm. Times (minutes:seconds) are relative to the time of UbcH10 WT microinjection. Frame rate is 3 frames per second.

ITQB NOVA, Avenida da República, 2780-157 Oeiras, Portugal | Tel +351 214 469 100 | itqb.unl.pt